Separation of homogeneous hydroformylation catalysts using Organic Solvent Nanofiltration

by

Waylin Lee Peddie

Thesis presented in partial fulfilment
of the requirements for the Degree

of

MASTER OF ENGINEERING
(CHEMICAL ENGINEERING)

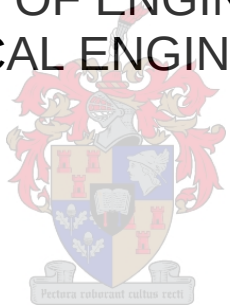

in the Faculty of Engineering
at Stellenbosch University

Supervisor
Dr. P. Van der Gryp

Co-Supervisor
Prof. H.C.M. Vosloo

March 2016

DECLARATION

By submitting this thesis electronically, I declare that the entirety of the work contained therein is my own, original work, that I am the sole author thereof (save to the extent explicitly otherwise stated), that reproduction and publication thereof by Stellenbosch University will not infringe any third party rights and that I have not previously in its entirety or in part submitted it for obtaining any qualification.

Date: March 2016

ABSTRACT

The upgrade of *inter alia* syngas and short chain olefins to high value commodities in the surfactant and detergent range, finds relevance worldwide due to the abundance of feedstock. These commodities are manufactured systematically through an innovative network of homogeneously-catalysed reactions, i.e. metathesis, hydroformylation and hydrogenation, and forms part of the overarching theme of the RSA Olefins programme of the South African Department of Science and Technology (DST) and National Research Foundation (NRF) Centre of Excellence in Catalysis (c*change). Homogeneous catalysts are generally preferred over its heterogeneous counterpart due to *inter alia* superior catalytic performance, higher product selectivity and negligible diffusional problems. However, the prevalence of homogeneous catalysts is hampered by the expensive, waste generating and destructive thermal separation methods required for the recovery of these catalysts.

The main aim of this study is therefore to demonstrate the non-destructive recovery of homogeneous catalysts, in a state allowing for their recycle and reuse, from hydroformylation post-reaction mixtures as well as the potential for further solvent purification using organic solvent nanofiltration (OSN). Furthermore, confirmation is afforded to the cost- and energy-efficiency of OSN for homogeneous catalyst recovery commonly alluded to in literature by performing an economic and energy evaluation between OSN and classical downstream recovery units, i.e. distillation.

Focus was placed on the recovery of two well-known and commercially available hydroformylation catalysts, $\mathbf{HRh(CO)(PPh_3)_3}$ and $\mathbf{Co(C_5H_7O_2)_3}$, and the solvents considered include those representative of the hydroformylation and hydrogenation reactions (1-octene, 1-decene, 1-nonanal, 1-undecanal, 1-nonanol, 1-undecanol), using the Duramem 150 (DM-150), Duramem 200 (DM-200) and STARMEM 240 (ST-240) membranes. Parameters such as applied pressure, feed concentration, solvent type and catalyst load were varied and its effects on the ST-240 membrane's performance investigated.

The main contributions and conclusions from this study were threefold regarding, 1) the capability of OSN to recover and reuse homogeneous catalysts, 2), the characterisation of OSN performance in terms of permeance and separation, and 3) the modelling of OSN performance.

1) **OSN catalyst recovery**:

It was found that the presence of the rhodium-based catalyst, **$HRh(CO)(PPh_3)_3$**, resulted in the hydroformylation reaction having a high regioselectivity toward the linear aldehyde product and produced mainly 1-nonanal with a yield of approximately 66 mol% in the case of 1-octene as substrate. Additionally, linear to branched (*n*/*iso*) product molar ratios of greater than 2 were observed. It was also found that cost and energy savings of greater than 90% can be attained upon using OSN systems for homogeneous catalyst recovery as compared to conventional distillation systems.

2) **OSN permeation and separation**:

It was found that the ST-240 membrane was able to successfully separate homogeneous catalysts from different reaction systems with catalyst recoveries up to 99%. Moreover, the recovered catalyst was found to be in a condition suitable for reuse for at least three consecutive hydroformylation reaction cycles, thereby improving upon its overall catalytic performance in excess of 30%. Flux of pure reaction species (1-octene, 1-decene, 1-nonanal, 1-undecanal, 1-nonanol and 1-undecanol) were shown to range between 1.83 $L.m^{-2}.h^{-1}$ to 135 $L.m^{-2}.h^{-1}$. Flux was also found to be highly dependent on applied pressure, solvent viscosity and interaction parameters indicative of the solvent-membrane and solute-solvent interactions. Minimal separation was attainable between binary mixtures consisting of 1-octene/1-nonanal, 1-decene/1-undecanal and 1-nonanal/1-nonanol.

3) **OSN modelling**:

The OSN separation process for the different solvents were described using literature-based transport models based on the pore-flow and solution-diffusion models with the latter performing relatively better than the former in terms of predictive capacity. Moreover, a newly postulated model which incorporated an additional solubility parameter term was found to improve predictive capacity of the solution-diffusion model by approximately 3%.

KEYWORDS: Organic Solvent Nanofiltration, Hydroformylation, Homogeneous catalyst, Catalyst separation

SAMEVATTING

Die opgradering van onder andere sintese gas en kort-ketting olefiene na hoë waarde produkte in die surfaktant en skoonmaakmiddel reeks, vind relevansie wêreldwyd as gevolg van ’n oorvloed van roumateriaal. Hierdie produkte kan sistematies vervaardig word deur ’n innoverende netwerk van homogeen-gekataliseerde reaksies, naamlik metatese, hidroformilering en hidrogenering, en vorm deel van die oorkoepelende doel van die “*RSA Olefins programme"* van die Suid-Afrikaanse Departement van Wetenskap en Tegnologie (DST) en Nasionale Stigting vir Navorsing *(NRF) “Centre of Excellence in Catalysis (c*change)*”. Homogene katalisatore word in die algemeen verkies bo sy heterogene eweknie as gevolg van onder andere beter katalitiese vermoë, hoër selektiwiteit vir produkte en weglaatbare diffusieprobleme. Die oorheersing van homogene katalisatore is egter belemmer deur duur, afval-genererende en vernietigende termiese skeidingsmetodes benodig vir die herwinning van hierdie katalisators.

Die hoofdoel van hierdie studie is om die nie-vernietigende herwinning van homogene katalisatore te demonstreer, sodat dit in ’n toestand geskik vir hergebruik is, vanaf ’n hidroformileringsreaksie produkmengsel sowel as die potensiaal vir verdere suiwering van die reaktiewe spesies deur organiese oplosmiddel nanofiltrasie (OSN). Verder, aandag is gegee aan die koste- en energie-effektiwiteit van OSN vir die herwinning van homogene katalisatore wat in die algemeen in literatuur na gewys word deur ’n ekonomiese en energie evaluering tussen OSN en klassieke stroomaf skeidings prosesse, naamlik distillasie, uit te voer.

Daar is gefokus op die herwinning, met behulp van die STARMEM 240 (ST-240) membraan, van twee welbekende en kommersieel beskikbare hidroformileringkatalisatore, **$HRh(CO)(PPh_3)_3$** en **$Co(C_5H_7O_2)_3$**, en verbindings verteenwoordigende hidroformilerings- en hidrogeneringsreaksies (1-okteen, 1-deseen, 1-nonanaal, 1-undekanaal, 1-nonanol, 1-undekanol). Parameters soos die toegepaste druk, voerkonsentrasie, oplosmiddel en katalisatorlading is gevarieer en die effek op OSN se skeidings vermoë ondersoek.

Die hoofbydraes en gevolgtrekkings van hierdie studie is drievoudig met betrekking tot, 1) die gebruik van OSN vir katalisatorherwinning, 2) die karaktarisering van OSN se skeidings vermoë en 3) die modellering van die OSN.

1) OSN katalisatorherwinning:

Daar was gevind dat die teenwoordigheid van die rodium-gebaseerde katalisator, **$HRh(CO)(PPh_3)_3$**, ’n hoë regioselektiwiteit van die hidroformileringsreaksie tot die lineêre aldehiedproduk het en gevolglik meestal 1-nonanaal vervaardig met ’n opbrengs van ongeveer 66 mol% met 1-okteen as substraat. Verder was die molêre verhouding van lineêre tot vertakte (*n*/*iso*) aldehiedprodukte van groter as 2 gemeet. Daar was gevind dat kostes- en energie-besparings van meer as 90% bereik kan word met die gebruik van OSN prosesse vir die herwinning van homogene katalisatore in vergelyking met konvensionele distillasiestelsels.

2) OSN permeasietempo en skeiding:

Daar was gevind dat die ST-240 membraan geskik was vir die suksesvolle herwinning van homogene katalisatore van die verskillende reaksie sisteme met katalisatorherwinning tot 99%. Verder was die katalisator geskei in ’n vorm geskik vir hergebruik vir ten minste drie agtereenvolgende hidroformileringsreaksiesiklusse en met dit verbeter die algehele katalitiesevermoë met meer as 30%. Permeasietempo’s van suiwer reaksiespesies (1-okteen, 1-deseen, 1-nonanaal, 1-undekanaal, 1-nonanol, 1-undekanol) wissel tussen 1.83 $L.m^{-2}.h^{-1}$ en 135 $L.m^{-2}.h^{-1}$. Permeasietempo was ook waargeneem om hoogs afhanklik te wees op toegepaste druk, spesiesviskositeit en interaksieparameters verteenwoordigend van die oplosmiddel-membraan en opgeloste stof-oplosmiddel interaksies. Minimale skeiding was bereikbaar tussen binêre mengsels van 1-okteen/1-nonanaal, 1-deseen/1-undekanaal en 1-nonanaal/1-nonanol.

3) OSN modellering:

Die OSN skeidingsproses vir die verskillende spesies was beskryf deur literatuur-gebaseerde modelle geskoei op die porie-vloei en oplossing-diffusie modelle. Verder was ’n nuut-veronderstelde model insluitend met ’n addisionele oplosbaarheidparameter gevind om voorspellende akkuraatheid met ongeveer 3% te verbeter.

SLEUTELWOORDE: Organiese oplosmiddel nanofiltrasie, Hidroformilering, Homogene katalisator, katalisatorherwinning,

ACKNOWLEDGEMENTS

Firstly, I would like to thank the Lord for all the blessings that He has bestowed upon me without which none of this would be possible.

I would like to express my deepest gratitude to Dr Percy van der Gryp and Prof. Manie Vosloo, for all their guidance, insights, support and critical feedback throughout the years and without whom I would not have been able to successfully complete this study.

I would also like to thank the DST-NRF Centre of Excellence in Catalysis (c*change) and for their financial support and for allowing me the opportunity to partake in this interesting field of study. I would also like to thank the Catalysis Society of South Africa (CATSA) for allowing me a myriad of opportunities to present my research at various academic conferences.

Upon completion of this study, I would like to acknowledge several individuals without whom this work would not have been possible:

- The analytical staff of Stellenbosch University (Mrs Hanlie Botha, Mr Jaco van Rooyen and Mrs Levine Simmers) for their aid with all things analytical, constant support and endless words of encouragement
- The technical staff of Stellenbosch University (Mr Alvin Petersen, the late Mr Vincent Carrolissen, Mr Jos Weerdenburg and Mr Anton Cordier) for their assistance and putting up with an endless barrage of technical inquiries
- The Separations Technology research group at Stellenbosch University for their assistance, support and social gatherings
- To my office companion, Mr Marvin Ngwetjana, for the late nights working in the office, all the coffees, lunches and discussions, without which completing this study would not have been as fun

Lastly, I owe a heartfelt and sincere thank you to my parents (Mr Pieter Peddie and Mrs Jennifer Peddie) and my sister (Ms Rudè Peddie) for all their love, support and patience throughout the years.

In the same breath, I would like to thank Ms Jamie Botha for all her love, encouragement, and understanding.

TABLE OF CONTENTS

NOMENCLATURE

Abbreviation	Definition
acac	Acetylacetonate
CEPCI	Chemical Engineering Plant Cost Index
DCM	Dichloromethane
DM	Duramem®
DMC	Dimethyl carbonate
DMF	Dimethyl formamide
DSPF	Donnan steric pore-flow
EA	Ethyl acetate
EPDM	Ethylene propylene diene monomer
FAAS	Flame atomic absorption spectroscopy
FID	Flame ionisation detector
GC	Gas chromatography
IL	Ionic liquid
IPA	Isopropanol
MB	Mass balance
MET	Membrane extraction technology
MF	Microfiltration
MS	Mass spectroscopy
MW	Molecular weight
MWCO	Molecular weight cut-off
NF	Nanofiltration
OSN	Organic Solvent Nanofiltration
PA	Polyamide
PDMS	Polydimethylsiloxane
PES	Polyethersulfone
PF	Pore-flow
PI	Polyimide
PPh_3	Triphenyl phosphine
RO	Reverse osmosis
RT	Room temperature
$ScCO_2$	Supercritical carbon dioxide
SD	Solution-diffusion
SFPF	Surface force pore-flow
SRNF	Solvent resistant nanofiltration
ST	STARMEM™
THF	Tetrahydrofuran
TMS	Thermomorphic multicomponent system
TOF	Turnover frequency
TON	Turnover number
TPPTS	Triphenyl phosphine trisulfonic acid
UF	Ultrafiltration

Symbol	Description	Unit
A	Molar permeance constant	mol.m^{-2}.s^{-1}.Pa^{-1}
A	Membrane active area	m^2
A, B	Kedem-Katchalsky permeance constants	-
A_c	Equipment capacity	m^2
B_o	Membrane openness	-
B_1, B_2	Bare module cost constants	-
b_f	Friction parameter between solute and solvent (Surface force pore-flow)	-
C_P	Permeate concentration	mg.L^{-1}
C_F	Feed concentration	mg.L^{-1}
C_R	Retentate concentration	mg.L^{-1}
C_{avg}	Average concentration	mol.m^{-3}
C_p^0	Purchased cost of equipment	$
c_{cat}	Cost of catalyst	$.kg^{-1}
C_{cat}	Catalyst feed concentration in reactor	kg.kg^{-1}
c_M	Cost of membrane	$.m^{-2}.a^{-1}
D	Diffusion coefficient	m^2.s^{-1}
D_c	Distillation column diameter	m
d_{pore}	Membrane pore diameter	m
d_{ij}	Effective diameter of species i in solvent j	m
$E_{coh,i}$	Cohesive energy of species i	J.mol^{-1}
F_i	Maxwell-Stefan driving force	mol.m^{-2}.s^{-1}
f_1, f_2	Parameter describing NF sublayers	m.s^{-1}
F_P	Pressure factor	-
F_M	Material factor	-
F_F	Volumetric feed flow	m^3.s^{-1}
F_r	Volumetric recycle flow	m^3.s^{-1}
H_F	Membrane pore wall correction factor	-
I_i	CEPCI for the year i	-
J_m	Mass flux	kg.m^{-2}.s^{-1}
J_V	Volume flux	m^3.m^{-2}.s^{-1}
J_n	Molar flux	mol.m^{-2}.s^{-1}
K_i	Sorption coefficient	-
K_D	Darcy's law permeance constant	s
K	Kozeny-Carmen constant	-
k_M^0, k_M^1, k_M^2	Membrane geometrical constants	m
$K_{i,d}$, $K_{i,c}$	Diffusive and convective hindrance factors (Donnan steric pore-flow)	-
K_1, K_2, K_3,	Bare module cost constants	-
l	Membrane thickness	m
L_p	Membrane permeance constant	kg.m^{-2}.h^{-1}.bar^{-1}
m	Mass	kg
MW	Molecular weight	g.mol^{-1}

Symbol	Description	Unit
$\dot{m}_{prod}$	Production capacity	kg.year^{-1}
N_{stages}	Number of cascade membrane stages	-
$P_{i,M}$	Permeanceof species i through membrane M	m^3.m^{-2}.h^{-1}.bar^{-1}
ΔP_D	Pressure drop over membrane module	Pa
ΔP	Pressure difference across membrane	Pa
P	Pressure	Pa
P^{sat}	Saturation pressure	Pa
P_o	Upstream / feed side pressure	Pa
P_z	Downstream / permeate side pressure	Pa
$\dot{Q}_M$	Heat duty of membrane	kW
$\dot{Q}_{dist}$	Heat duty of distillation	kW
$R_{cat,overall}$	Overall catalyst recovery	-
R_S^0	Surface resistance (Resistance-in-series)	Pa.s.m^{-1}
R_η^1, R_η^2	Viscous resistance (Resistance-in-series)	Pa.s.m^{-1}
R_{real}	Real rejection (Kedem-Katchalsky)	-
R_{stage}	Single stage catalyst recovery	-
R	Rejection	%
R	Universal gas constant	J.mol^{-1}.K^{-1}
r_{pore}	Membrane pore radius	m
S	Selectivity	mol product.(mol catalyst)$^{-1}$
S_F	Steric hindrance factor	-
S_P	Standard deviation of the lognormal distribution	-
s	Internal membrane surface area	m^2
t_{op}	Annual operational time	h.a^{-1}
t_c	Distillation column thickness	m
TOC_{dist}	Total operating cost of distillation column	R
TOC_M	Total operating cost of membrane	R
t	Time	s
T	Temperature	K
TON	Turnover number	mol product.(mol catalyst)$^{-1}$
TOF	Turnover frequency	s^{-1}
$\boldsymbol{u}_i$	Relative species velocity	m.s^{-1}
v	Stoichiometric coefficient	-
v	Volume fraction	-
V	Volume	m^3
V_m	Molar volume	m^3.mol^{-1}
$\bar{V}_m$	Partial molar volume	m^3.mol^{-1}
w_i	Mass fraction of species i	-

Symbol	Description	Unit
x_i	Molar fraction of species i	-
x	Conversion	mol product.(mol catalyst)$^{-1}$
x_{sm}	Friction factor between solvent molecules and membrane pore wall	-
Y	Yield	mol product.(mol catalyst)$^{-1}$
z	Direction perpendicular to membrane surface	-
z_i	Valence of solute i	-

Subscript	Description
0	Feed side
1	Solvent
2	Solute
C	Convection
D	Diffusion
dry	Dry membrane
F	Feed
i, j, k	Denotes any species
l	Permeate side
m	Mass
M	Membrane
n	Molar
P	Permeate
R	Retentate
V	Volume
wet	Wet membrane

Greek symbol	Description	Unit
α	Degree of separation	-
ε	Membrane surface porosity	-
ε_i	Dielectric constant of species i	-
σ	Reflection coefficient	-
γ_i	Activity coefficient	-
γ_c	Critical surface tension of membrane	-
γ_M	Surface tension of membrane	-
γ_l	Critical surface tension of solvent	-
δ_i	Solubility parameter of species i	$MPa^{0.5}$
δ_{SD}	Solubility fraction	-
δ_M	Solubility parameter of membrane M	$MPa^{0.5}$
δ_B	Bond polarity	-
$\emptyset$	Solvent dependent parameter	-
π	Osmotic pressure	Pa
ψ	Electric potential	-
ξ_{ij}	Friction force between species i and j	-
μ	Chemical potential	$J.mol^{-1}$
μ^0	Reference chemical potential	$J.mol^{-1}$
μ_D	Dipole moment	D
η	Solvent viscosity	Pa.s
η_{mix}	Viscosity of the binary solvent mixture	Pa.s
η_P	Pump efficiency	-
ρ	Density	$kg.m^{-3}$
τ	Membrane tortuosity	-
$\chi_{i,s}$	Friction coefficient between solute i and solvent j	-
$\chi_{i,m}$	Friction coefficient between solute i and membrane M	-
χ_P	Electronegativity	-

CHAPTER 1: Introduction

1.1 Background and motivation

Worldwide, there is an abundance of short chain olefins (C_2 – C_9) due to its low cost and ease of accessibility [1,2]. From a South African context especially, Sasol Ltd., through the well-known Fischer-Tropsch process, produces vast quantities of these short chain olefins from synthesis gas (CO/H_2) which, in turn, are manufactured from natural resources such as coal and natural gas [3–5]. On the other end of the Flory-Schulz carbon chain spectrum, long chain hydrocarbons (> C_{10}), especially functionalised aldehydes and alcohols, are low in supply but both high in cost and demand, and are used as synthesis intermediate for various high-end pharmaceutical products (i.e. face creams, fragrances, etc.) [6,7]. On a larger scale, these functionalised hydrocarbons are also used to manufacture more commonly known and commercially successful products such as detergents, surfactants and plasticisers [8–10]. The upgrading of low value short chain olefin feedstock from syngas to *inter alia* high value commodities in the surfactant and detergent range, forming part of the overall aim of the RSA Olefins programme of the South African Department of Science and Technology (DST) and National Research Foundation (NRF) Centre of Excellence in Catalysis (c*change), is achieved through a simple proposed reaction scheme, as illustrated in Figure 1.1 [11].

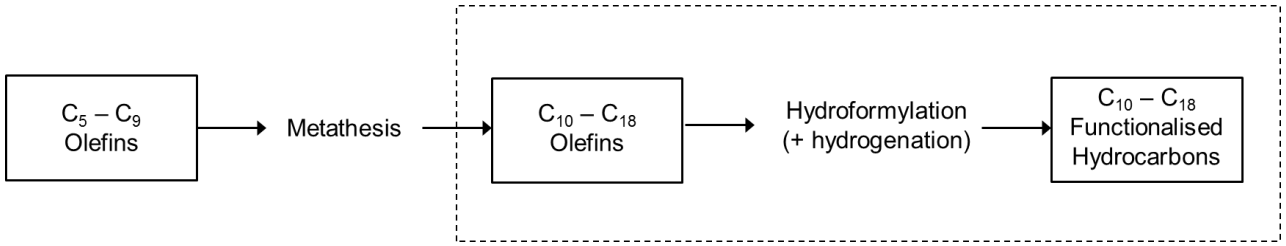

Figure 1.1: Proposed reaction scheme for the upgrading of low value olefin feedstock

The network shown in Figure 1.1 consists of three key reactions, namely: 1) metathesis of short olefins to increase its chain length, followed by the functionalization thereof through 2) hydroformylation and 3) hydrogenation reactions, producing aldehydes and alcohols, respectively. These reactions are prevalent users of transition metal based catalysts in both unmodified and modified form and of either homogeneous or heterogeneous nature. The advantages of homogeneous catalysts over its heterogeneous counterpart are widely known and well documented, including *inter alia* higher catalytic activity, higher product selectivity and little to no diffusional issues. These and more can be found in Table 1.1 which provides a direct comparison between homogeneous and heterogeneous catalysts.

Table 1.1: Homogeneous versus heterogeneous catalysts [12–15]

Homogeneous	Heterogeneous
Catalyst tailor made	Tedious synthesis
Superior catalytic activity and reactivity	Inferior catalytic activity and reactivity
Difficult catalyst separation	Ease of catalyst recovery
Mild reaction conditions	Harsh reaction conditions
Insignificant diffusional problems	Potentially significant diffusional problems
Relatively short operation life	Long operational life expectancy

It is evident from Table 1.1 that homogeneous catalysts are far superior to heterogeneous catalysts in most aspects concerning catalytic performance. However, homogeneous catalysts also have a few pitfalls when compared to its heterogeneous equivalent, namely:

a) Difficulty in recovering homogeneous catalysts from solution in a reusable form, and
b) Short operational life expectancy of homogeneous catalysts due to regular inactivation and decomposition during current recovery methods.

It is for these reasons that heterogeneous catalysts have enjoyed dominance in industrial applications. The most notable, and arguably the most damaging, inherent disadvantage of homogeneous catalysts is the difficulty in recovering the catalyst from a reaction medium in both an active and reusable form. This is due to the energy- and cost-intensive procedures necessary, i.e. distillation, evaporation, adsorption, etc., for the recovery of a homogeneous catalyst which makes the application thereof highly unfavourable from an economic point of view [16]. Furthermore, current recovery methods employed, especially distillation, use severe conditions to initiate the separation which are destructive to the integrity and efficiency of the catalyst and require additional costs to regain the catalytic activity through pretreatment before it can be recycled and reused [17]. These methods are not only destructive but generate large quantities of inactive metal waste which adds an environmental imperative to the recovery of these catalysts.

This investigation therefore addresses the aforementioned pitfalls of homogeneous catalysts and motivates the use of organic solvent nanofiltration (OSN) membranes as alternative recovery method, especially in the reaction network as illustrated in Figure 1.1. In this study, the olefin hydroformylation reaction will be used as the prototype reaction, highlighted in Figure 1.1, with all possible products as illustrated in Figure 1.2.

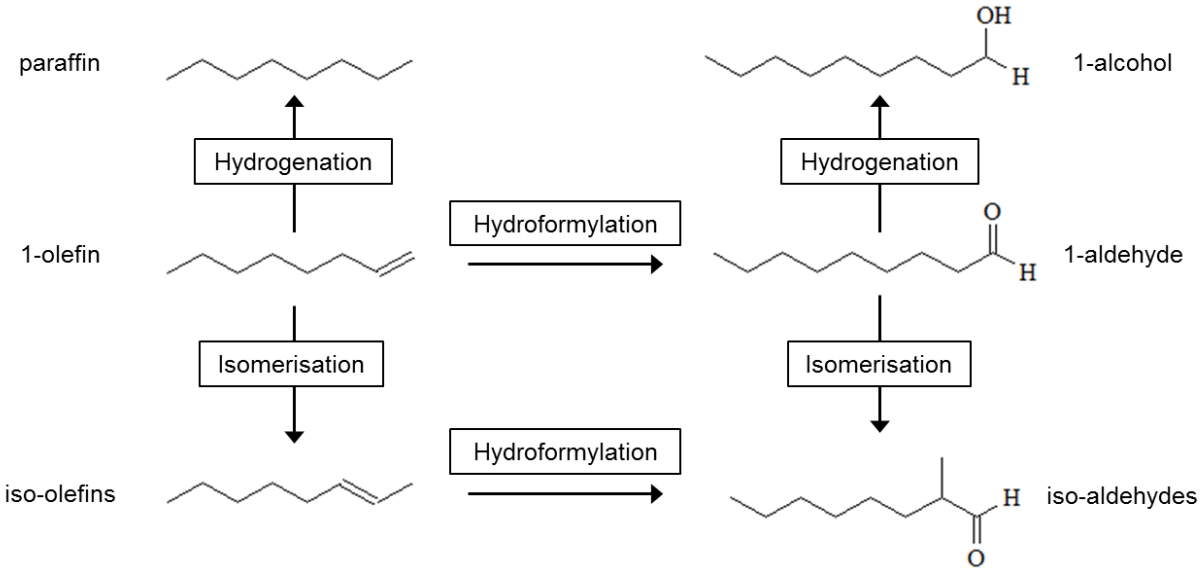

Figure 1.2: All possible reactions during the hydroformylation of olefins

Hydroformylation, as depicted in Figure 1.2, refers to the reaction of a hydrocarbon with syngas in the presence of a suitable catalyst and is considered one of the largest homogeneous processes currently applied in the chemical industry, responsible for the synthesis of more than 8 million tons of product per annum [18]. The hydroformylation of olefins has opened doors to the production of a variety of chemicals beneficial to, among others, the petrochemical, pharmaceutical and fine chemical industries [19].

Hydroformylation, formerly known as the 'oxo' process, was accidentally discovered in 1938 by a German chemist named Otto Roelen during his investigation of the Fischer-Tropsch reaction using a cobalt-based complex with the active species, cobalt tetracarbonyl hydride or **$HCo(CO)_4$**. In 1974, a major breakthrough was made, spearheaded by the Union Carbide Company, where rhodium replaced cobalt as the active species in the form of tris(triphenylphosphine) rhodium(I) carbonyl hydride, **$HRh(CO)(PPh_3)_3$** [14].

The rhodium-based catalyst, **$HRh(CO)(PPh_3)_3$**, shown in Figure 1.3, is still widely favoured in an industrial context due to its high reactivity and atom efficiency even under mild reaction conditions, has been selected for use in this investigation [20]. The cobalt-based precatalyst, **$Co(C_5H_7O_2)_3$**, also shown in Figure 1.3, is also used in this investigation as a comparative means of membrane performance in terms of catalyst flux and recovery.

The homogeneous catalysts used in this study along with other commonly used hydroformylation catalysts are summarised in Figure 1.3.

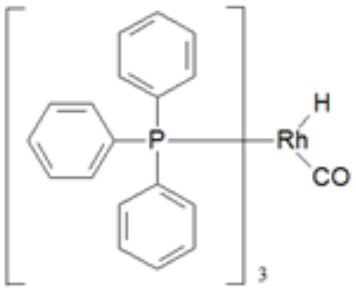

$HRh(CO)(PPh_3)_3$

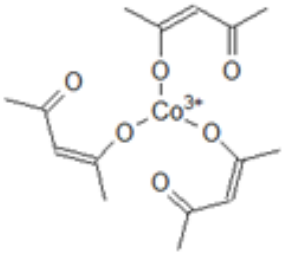

$Co(C_5H_7O_2)_3$

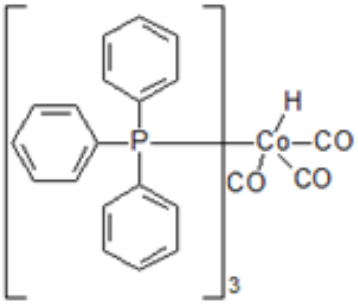

$HCo(CO)_3(PPh_3)_3$

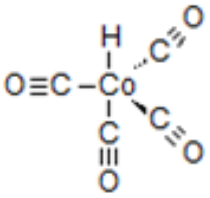

$HCo(CO)_4$

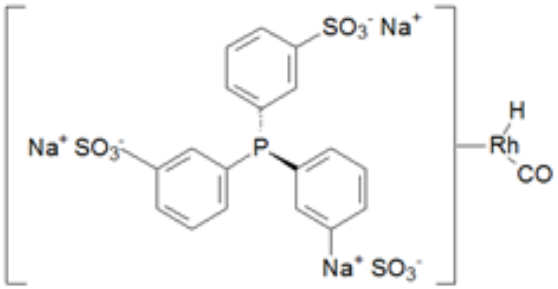

$HRh(CO)(TPPTS)_3$

Figure 1.3: Commonly used homogeneous hydroformylation catalysts

1.2 Objectives

One of the main drivers for recommending OSN as an alternative to conventional downstream catalyst recovery techniques is the overall improvements and benefits in terms of energy and cost efficiency that OSN could potentially offer. Past publications however, although revolutionary, neglected to prove this statement correct. The few papers that did perform cost analyses and comparisons focussed mainly on solvent separation [21–23]. Therefore, there is a gap in the literature which clarifies the energy benefits over that of classic homogeneous catalyst recovery methods. It is therefore the main contribution of this study to:

Demonstrate the successful recovery of homogeneous catalysts from hydroformylation post-reaction mixtures using OSN and to verify the energy- and cost-efficiency of OSN compared to distillation.

The objectives of this study are threefold and can be expressed as follows:

1) ***OSN catalyst recovery***
   - Understand the reaction network of the hydroformylation of 1-octene and 1-decene using both the rhodium-based catalyst, **$HRh(CO)(PPh_3)_3$**, and cobalt-based catalyst, **$Co(C_5H_7O_2)_3$**.
   - Experimentally determine the product distribution for the hydroformylation reaction of 1-octene and 1-decene using **$HRh(CO)(PPh_3)_3$** and **$Co(C_5H_7O_2)_3$**.
   - Evaluate the effect of pressure, solvent type and catalyst loading on the membrane's catalyst recovery performance.
   - Test the reusability of the recovered catalyst, **$HRh(CO)(PPh_3)_3$**, in terms of *n*-aldehyde product yield.
   - Perform an economic and energy evaluation to compare the cost of catalyst recovery using OSN to that of conventional separation units.
2) ***OSN permeation and separation performance***
   - Screen different membranes (STARMEM™, Duramem®) for compatibility with 1-octene, 1-decene, 1-nonanal, 1-undecanal, 1-nonanol and 1-undecanol.
   - Characterise the OSN membrane in terms of species flux, separation performance for single and binary mixtures of different species and catalyst recovery capability for the catalysts, **$HRh(CO)(PPh_3)_3$** and **$Co(C_5H_7O_2)_3$**.
   - Evaluate the effect of pressure, species concentration and catalyst loading on membrane permeation and species separation performance for single and binary mixtures of different reaction species.

3) OSN modelling

- Investigate the extent of membrane-species interaction for the different species and membrane pairings, i.e. membrane sorption.
- Verify the predictive capacity of existing literature transport models for OSN and if needed, develop a model to describe the transport of the hydroformylation reaction system across the membrane.

1.3 Scope of study and thesis layout

This thesis is submitted with the aim of investigating the use of OSN membranes for the recovery of homogeneous catalysts from different post-reaction mixtures. The scope of this investigation is presented in Figure 1.4 in the form of a flow diagram. The study at hand sets out to achieve the objectives as listed in Section 1.2 and can be divided into six chapters.

Chapter 2 offers literary support to the proposed investigation with an in-depth theoretical framework of the concepts relating to fields of hydroformylation and OSN. The purpose of this chapter is to inform and critically review pertinent literature relevant to this study. Hydroformylation principles are discussed followed by OSN concepts and modelling. A critical review of the findings of current and past publications regarding homogeneous catalyst recovery is presented. Moreover, a current state of the art is also given with regards to homogeneous catalyst recovery methods.

In **Chapter 3**, the experimental and analytical methodologies and equipment used in this investigation are described in terms of diagrammatic and photographic illustrations.

Chapter 4 provides a summary of the results, pertaining to the hydroformylation reaction, the screening of commercially available OSN membranes and the demonstration of reusability of homogeneous catalysts post OSN recovery. Moreover, a comparison is made between OSN and conventional catalyst recovery methods in terms of cost- and energy-efficiency.

In **Chapter 5**, the OSN performance with respect to permeation and separation is characterised and the effects of applied pressure, species concentration and catalyst loading on performance discussed.

Lastly, **Chapter 6** summarises the main findings and lists the conclusions drawn therefrom in a concise manner. Furthermore, recommendations for future work are also suggested and mention is briefly given to the awards and contributions gained from this investigation.

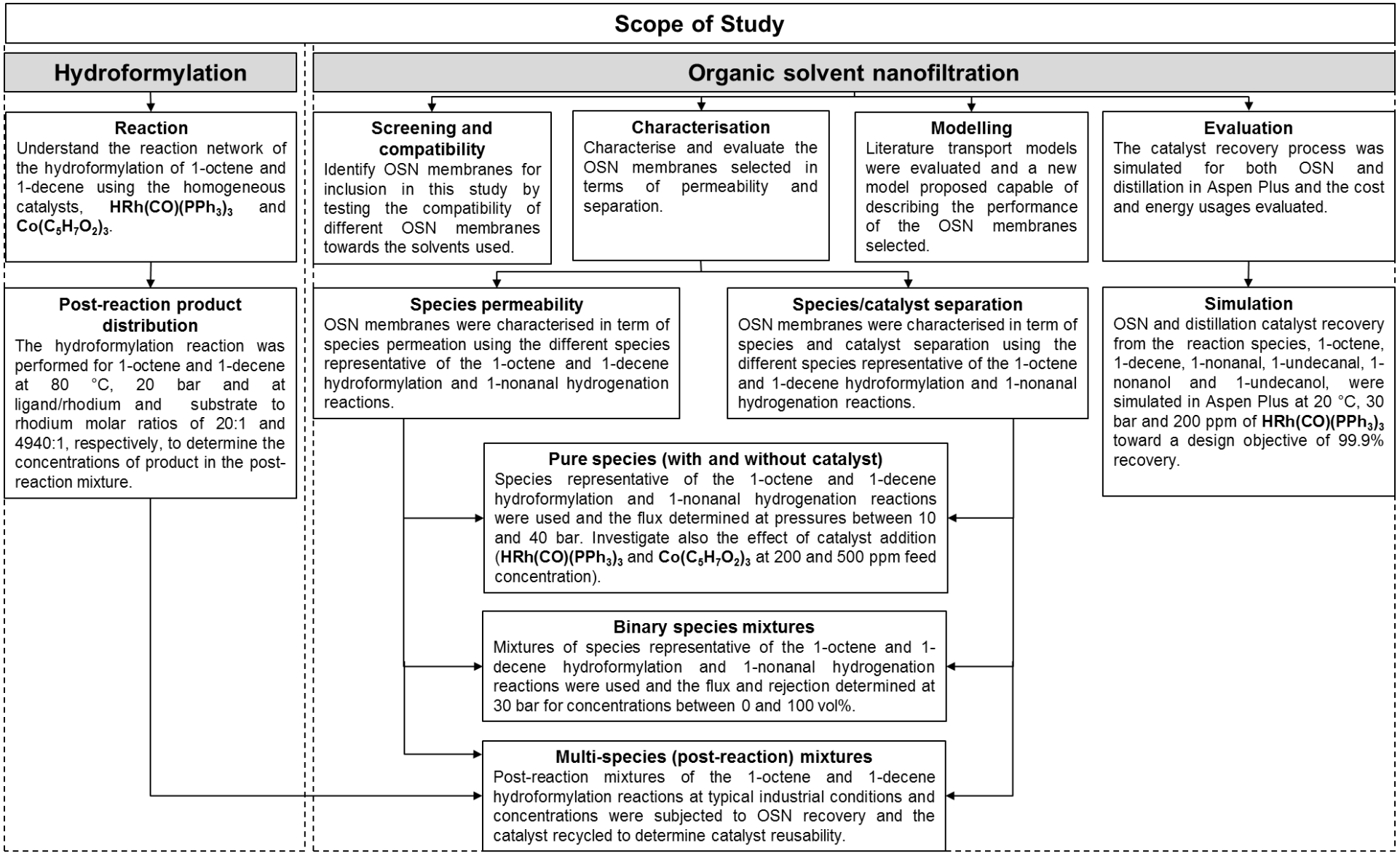

Figure 1.4: Diagrammatic depiction of the scope of this investigation

1.4 References

[1] G.J.P. Britovsek, R. Malinowski, D.S. McGuinness, J.D. Nobbs, A.K. Tomov, A.W. Wadsley, C.T. Young, *ACS Catal*. (2015) 1–15.

[2] T. Bhatelia, C. Li, Y. Sun, P. Hazewinkel, N. Burke, V. Sage, *Fuel Process. Technol*. **125** (2014) 277–289.

[3] M.E. Dry, *Catal. Today*. **71** (2002) 227–241.

[4] H. Schulz, *Appl. Catal. A Gen*. **186** (1999) 3–12.

[5] G. Henrici-Olivé, S. Olivé, *Angew. Chemie Int. Ed. English*. **15** (1976) 136–141.

[6] D. Miller, E.M. Wiener, A. Turowski, C. Thunig, H. Hoffmann, *Colloids Surfaces A Physicochem. Eng. Asp.* **152** (1999) 155–160.

[7] J.M. Behan, J.N. Ness, P.C. Traas, J.S. Vitsas, B.J. Willis, ***Aqueous Perfume Oil Microemulsions***, US5,374,614, 1994.

[8] M.C. Jensen, G.E. Culver, ***Detergent-making process using a high active surfactant paste containing mid-chain branched surfactants***, US6,294,513 B1, 2001.

[9] T.A. Cripe, D.S. Connor, P.K. Vinson, J.C.T.R. Laurent, K.W. Willman, ***Mid-Chain Branched Alkoxylated Sulfate Surfactants***, US6,008,181, 1999.

[10] B.M. Bhanage, S.S. Divekar, R.M. Deshpande, R.V. *J. Mol. Catal. A Chem.* **115** (1997) 247–257.

[11] M. Claeys, S. Harrison, H.C.M. Vosloo, B. Zeelie, R. Weber, c*change DST-NRF Centre of Excellence in Catalysis, South Africa, (2015). www.cchange.ac.za. [Date accessed: 20 October 2015].

[12] A. Behr, P. Neubert, **Applied Homogeneous Catalysis**, Wiley VCH, Germany, 2012.

[13] J. Fang, R. Jana, J.A. Tunge, B. Subramaniam, *Appl. Catal. A Gen.* **393** (2011) 294-301.

[14] P.W.N.M. Van Leeuwen, **Rhodium Catalyzed Hydroformylation: Catalysis by Metal Complexes**, Volume 22, Kluwer Academic Publishers, The Netherlands, 2000.

[15] P.F. Pruchnik, **Organometallic Chemistry of the Transition Elements**, 2nd Ed., Plenum Press, New York, 1990.

[16] D.J. Cole-Hamilton, T.P. Tooze, **Catalyst Separation, Recovery and Recycling: Chemistry and Process Design**, Springer, The Netherlands, 2006.

[17] A. Cano-Odena, P. Vandezande, D. Fournier, W. Van Camp, *Chem. A Eur. J.* **16** (2010) 1061–1067.

[18] M. Priske, K.D. Wiese, M. Kraume, C. Baumgarten, *J. Memb. Sci*. **360** (2010) 77-83.

[19] G.T. Whiteker, C.J. Cobley, *Top. Organomet. Chem*. **42** (2012) 35–46.

[20] B. Cornils, W.A. Herrmann, **Applied Homogeneous Catalysis with Organometallic Compounds**, 2nd Ed., Wiley VCH, New York, 2002.

[21] E.M. Rundquist, C.J. Pink, A.G. Livingston, *Green Chem*. **14** (2012) 2197–2205.

[22] S. Darvishmanesh, L. Firoozpour, J. Vanneste, P. Luis, J. Degrève, B. Van der Bruggen, *Green Chem.* **13** (2011) 3476–3483.

[23] J. Geens, B. De Witte, B. Van der Bruggen, *Sep. Sci. Technol.* **42** (2007) 2435-2449.

CHAPTER 2: Literature Review

2.1 Overview of chapter

In this chapter a theoretical foundation is given on which the experimental work and analysis of results are based. Initial focus is placed on the concepts and terminologies relating to the fields of hydroformylation (Section 2.2) and organic solvent nanofiltration (Section 2.4), which forms the two overarching themes of this study. This is followed by an extensive theoretical review of each field including its significance to the research at hand. Attention is then placed on narrowing the scope by performing a comprehensive literature evaluation of previous research done regarding the recovery of homogeneous catalysts using organic solvent nanofiltration as well as a current start of the art (Section 2.3) and the modelling thereof (Section 2.5).

The chapter is divided into five sections. Section 2.2 presents a contextual introduction of the hydroformylation reaction principles followed by a review of the literature published relating to the hydroformylation of olefins in the presence of homogeneous catalysts. A detailed historical overview, catalyst evolution and application of the hydroformylation reaction can be found in Section A.1 of Appendix A. In Section 2.3, a state of the art is presented regarding the conventional and alternative methods to recover homogeneous catalysts as well as literature detailed regarding these processes.

In Section 2.4, focus is placed on organic solvent nanofiltration and presents a general introduction, definition of principles and concepts and a review of related literature previously published regarding homogeneous catalysts recovery using OSN. A detailed historical overview of OSN processes can be found in Section A.2. Section 2.5 elaborates on the literature transport models available to predict the permeation of organic solvents through OSN membranes and a review of the recent studies regarding OSN modelling is presented. The origins, principles and derivations of literature transport models can be found in Section A.3.

2.2 Hydroformylation reaction

2.2.1 Introduction

The hydroformylation reaction, as shown in Figure 2.1, was discovered by Otto Roelen in 1938 and is considered a valuable industrial synthesis process, receiving widespread recognition for being responsible for the manufacture of products in excess of 8 million tons per annum [1,2].

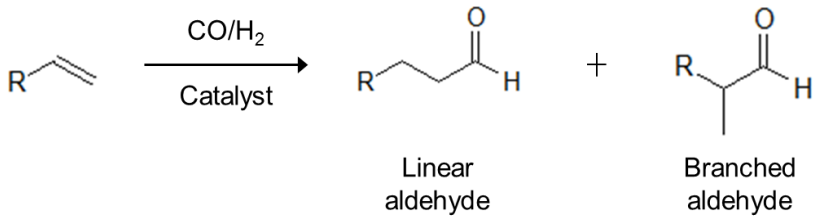

Figure 2.1: General olefin hydroformylation reaction

This investigation will focus primarily on the hydroformylation of 1-octene and 1-decene in the presence of the homogeneous catalyst, **$HRh(CO)(PPh_3)_3$** and **$Co(C_5H_7O_2)_3$**, forming preferably linear aldehydes. Hydroformylation is however not immune to side reactions as hydrogenation and isomerisation may occur. Linear aldehydes can be further hydrogenated to linear alcohols while olefins may also undergo hydrogenation, although to a lesser extent, to form paraffins. Terminal olefins can also be isomerised to internal olefins [3]. The potential reactions that 1-octene and 1-decene can undergo are presented in Figures 2.2 and 2.3.

2.2.2 Homogeneous hydroformylation catalysts

The term “homogeneous catalyst” refers to a catalyst which contacts the reactants in a single phase while in the case of a “heterogeneous catalyst”, the reaction, catalyst and its component consists of two or more phases. In the case of homogeneous catalysts, its complete dissolution in the reaction mixture allows for a superior catalyst performance in terms of activity and selectivity compared to its heterogeneous counterpart. The superior performance is due to the greater amount of catalyst surface available for reaction upon dissolution as oppose to a catalyst which remains intact. It is based on these inherent differences in catalyst behaviour, also the key to superiority of homogeneous catalysts, that heterogeneous catalysts finds itself on the forefront of industrial prominence. Since the latter remains insoluble in the reaction mixture, catalyst recovery can be easily and near completely achieved using simple separation techniques. In order to recover homogeneous catalysts, energy-, cost- and time-intensive procedures are typically being employed with the added risk of catalyst losses due to the decomposition and deposition

thereof which not only shortens catalyst lifetime but also degrades its performance [17,30]. Homogeneous catalysts used in the hydroformylation reaction are typically based on transition metals with rhodium and cobalt being the most effective. Catalysts can be modified with ligands to tailor the catalyst to suit a specific application. Cobalt-based catalysts, such as cobalt(III) acetylacetonate, **$Co(C_5H_7O_2)_3$**, are low in cost but have the inherent disadvantage of requiring relatively severe reaction conditions due to its low reactivity. Rhodium-based catalysts, the most prominent being tris(triphenylphosphine)rhodium(I) carbonyl hydride, **$HRh(CO)(PPh_3)_3$**, offer high activities therefore requiring much milder conditions and result in mainly linear aldehyde products, reportedly in excess of 80% [4–8]. **$HRh(CO)(PPh_3)_3$** has been described as one of the most established catalytic systems used in the hydroformylation reaction and is used commercially for the production of *n*-butyraldehyde from propene via the low pressure oxo synthesis process [9].

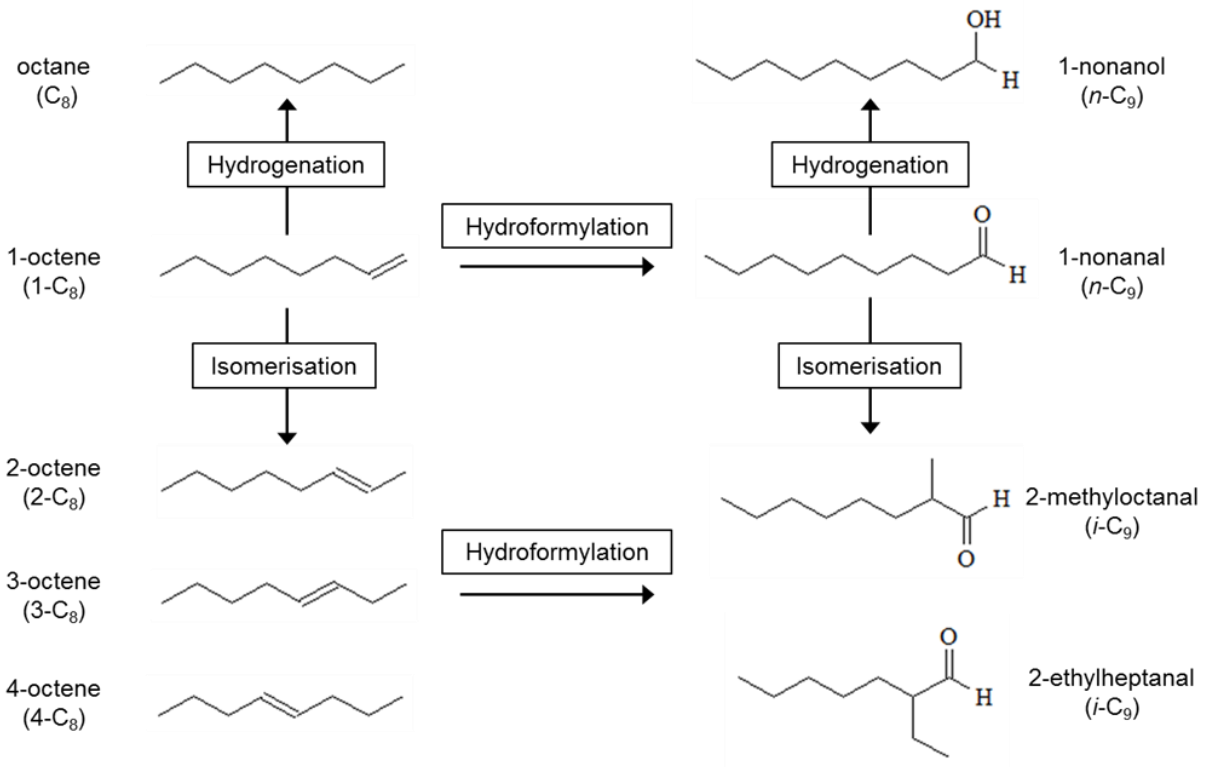

Figure 2.2: Potential reactions during the hydroformylation of 1-octene in the presence of rhodium-based catalysts

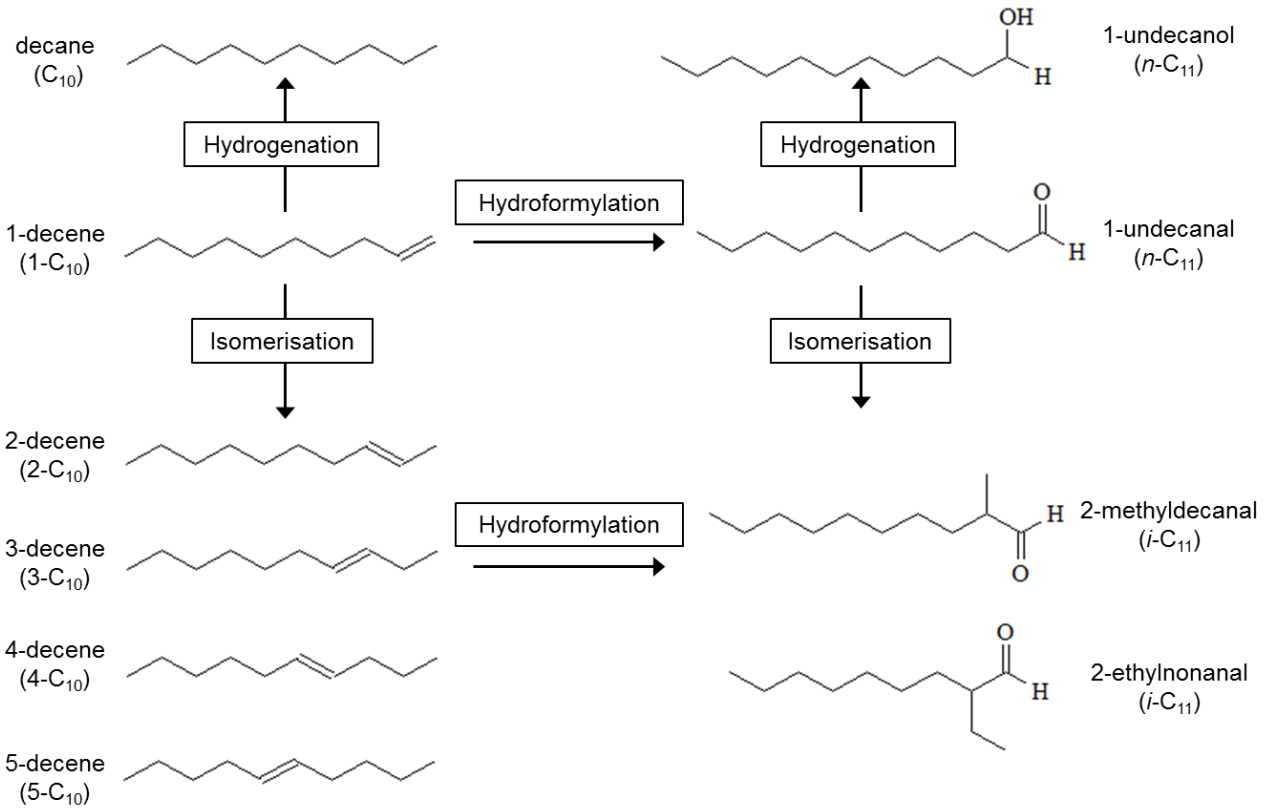

Figure 2.3: Potential reactions during the hydroformylation of 1-decene in the presence of rhodium-based catalysts

Although rhodium- and cobalt-based catalysts are mostly used, there are several studies which report on the success of other transition metals for hydroformylation including ruthenium, palladium, iridium and platinum [10–14]. Rhodium is reported to be more than 1,000 times more active than its closest rival, cobalt, and close to 100,000 times more active than ruthenium [15]. The commonly used hydroformylation catalysts are summarised in Table 2.1 and compared in terms of catalytic performance and product selectivity, specifically for 1-octene and 1-decene as substrate.

2.2.3 Principles of olefin hydroformylation

Olefin hydroformylation can be defined as the conversion of olefins in the presence of syngas to produce functionalised hydrocarbons, i.e. aldehydes. These products serve as feedstock for the synthesis of a wide range of commercially successful chemicals. Typical catalysts used in this reaction are based mainly on cobalt and rhodium and are homogeneous in nature [16]. Hydroformylation catalysts consist of a metal centre surrounded by ligands of either organic or inorganic nature. These ligands as well as the metal determine the three critical properties of a catalyst, i.e. activity, product selectivity and reaction rate [16]. Homogeneous catalysts have been widely accepted to be superior

when it comes to catalytic activity and product selectivity. However, in terms of stability under a wide range of conditions, heterogeneous catalysts have the upper hand [17].

Turnover number, TON, as defined in Equation 2.1, expresses the number of times a catalyst takes part in the catalytic cycle. In other words, it gives an indication of the extent to which reactants are converted into products. Turnover frequency, TOF, on the other hand, as defined in Equation 2.2, describes the activity of the catalyst based on the throughput of a plant or operational unit, i.e. TON as a function of time, t [18].

$$TON = \frac{moles\ of\ product}{moles\ of\ catalyst} \tag{2.1}$$

$$TOF = \frac{TON}{t} \tag{2.2}$$

Selectivity, S, refers to the fraction of the desired product k attained from a specific reactant i, as depicted in Equation 2.3 [8].

$$S_{ki} = \frac{n_k}{n_{i0} - n_i} \frac{v_i}{v_k} \tag{2.3}$$

where n is the number of moles of species (moles) and v the stoichiometric coefficient of species (-).

Table 2.1: Comparison of different homogeneous hydroformylation catalysts

Catalyst	Substrate/solvent	Conversion (%)	Yield[a] (%)	TOF (h^{-1})	Time (h)	Temperature (°C)	Pressure (bar)	Ref.
Rhodium-based								
$HRh(CO)(PPh_3)_3$	1-C_{10}/toluene	92	100 (1.6)	-	2.0	50	27.2	[7]
	1-C_8/fluorinated solvent	97	69 (4.8)	2000	1.0	70	20	[19]
	1-C_8/toluene	99	99 (2.55)	2500	1.1	100	20.4	[20]
	1-C_8/neat	-	35 (2.2)	69	-	60	20	[21]
Rh-Biphephos	4-C_8	90	75 (-)	-	4.0	125	20	[22]
	1-C_8	63	- (-)	390	3.5	50	30	[4]
Rh-BISBI	1-C_{10}/ethanol	98	85 (1.4)	-	6.0	150	27	[5]
Rh-A_4N_3	1-C_8/1,4-dioxane	100	60 (59)	-	18	120	2.5	[10]
	2-C_{10}/1,4-dioxane	99	4.0 (7.0)	-	36	120	2.5	
Rh-TPPTS	C_8/water	93	78 (-)	670	2.0	100	30	[23]
	C_{10}/water	93	75 (-)	650	2.0	100	30	
Cobalt-based								
$Co_2(CO)_8$	1-C_5/pentane	-	74 (2.9)	-	4.0	140	50	[24]
Co-TPPTS	1-C_8/water	24	55 (2.9)	-	5.0	100	50	[25]
	1-C_{10}/water	26	42 (2.7)	-	5.0	100	50	
$HCo(CO)_4$	>C_{10}/water	-	100 (-)	2.2	20	140	40	[26]
$Co_2(CO)_8$	1-C_{10}/toluene	100	77 (-)	-	22	110	40	[27]
Other								
$Fe(CO)_5(PPh_3)$	1-C_5/benzene	37	- (2.7)	-	16	110	100	[14]
(cod)Ir(PCy_3)	Silane/toluene	-	97 (1.1)	-	1.0	80	10	[28]
Ru-($C_{62}H_{42}O_6$)	1-C_{10}/toluene	100	80 (20)[b]	-	1.0	160	20	[11]

[a] Yield of *n*-aldehydes and given in brackets are the molar ratio of linear to branched aldehydes (*n*/*iso*).
[b] Alcohol yield.

Different types of selectivity exist to aid in the characterisation of a reaction towards a certain product relative to another. These include chemo-, regio-, diastereo- and enantioselectivity. Chemoselectivity describes the preference of a product to partake in a certain chemical reaction relative to another. The remaining selectivities describe the preference of product molecules to attain a certain structure or orientation relative to another. Regioselectivity describes the possibility of the product functional group attaching to a terminal or internal carbon atom resulting in either linear or branched product structures, respectively. Diastereo- and enantioselectivity gives an indication of the likelihood that diastereomer or enantiomer product orientations, respectively, will be formed [16]. Managing the different types of product selectivity is crucial for the success and efficiency of the hydroformylation reaction. The advantage of acquiring a high product selectivity of any type includes an increase in the efficient use of reagents and resources. This translates into the requirement of reagent concentrations and a reduction in waste generated [15].

Yield, Y, as defined in Equation 2.4, is the ratio of amount of product k produced to the theoretical maximum of a specific product that can be formed [8].

$$Y_{ki} = \frac{n_k v_i}{n_{i0} v_k} = S_{ki} x \tag{2.4}$$

where x is the reactant conversion (mol.mol^{-1}).Molecular structure has a significant influence on the regioselectivity of products resulting from olefin hydroformylation reactions. Studies show that linear olefins are more likely to undergo isomerisation, resulting in a higher composition of isomeric products in the post-reaction mixture. However, these same studies report that these observations can be superseded by the catalytic system selected, i.e. metal and ligand combination [18]. In terms of reactivity, linear terminal olefins have proven to be more susceptible to hydroformylation than linear internal olefins which in turn are more reactive than branched olefins. Reports show that the hydroformylation of terminal olefins are approximately 1000 times faster than internal olefins [16,29].

2.3 Recovery of hydroformylation catalysts

2.3.1 Introduction

Classical post-reaction purification methods include simple distillation, liquid-liquid extraction and pervaporation. Most of these methods are usually destructive to the catalyst and require additional costs to regain the catalytic activity prior to purification through pretreatment before it can be recycled and reused [30]. New methods have since emerged to overcome the difficulty involved in the recovery of homogeneous catalysts including heterogenisation of the catalyst, using biphasic systems and organic solvent nanofiltration (OSN). In this section, the current state of the art of homogeneous catalyst recovery is reviewed and examples are given of commonly applied and alternative recovery methods.

2.3.2 Overview of hydroformylation catalyst recovery

Desirably, the homogeneous metal catalyst, with the ligand intact, should be recycled back in a reusable form for improved productivity. Add to this the ever-increasing demand for safe and environmental friendly processing while still remaining cost-effective remains a major incentive for industries to develop and implement new and innovative strategies. In terms of homogeneous catalyst recovery, methods such as distillation have dominated the industry. However, due to its large energy and solvent demands resulting in high capital costs, the potential for improvement exists [31].

2.3.3 Conventional recovery methods

Classically, hydroformylation post-reaction mixtures are sent to a separation unit operating at different operating conditions than the reaction vessel, typically higher temperatures and/or lower pressures. In the case of distillation, which is a commonly used catalyst recovery technique, the unconverted reactants and products are separated from the catalyst by exploiting the differences in boiling point temperature. Since the separation conditions are different to that at which the reaction takes place, there is a risk that the catalyst may; 1) precipitate out of the reaction mixture potentially clogging equipment, and/or 2) decompose making recycling difficult due to its ineligibility to take part in the catalytic cycle [17]. Rhodium metal precipitation and dimer formation, associated with a distinct colour change of the reaction mixture, has been found to occur at high operating temperatures and very low pressures [1,8].

In Table 2.2, the classic catalyst recovery methods currently employed at industrial processes, such as Union Carbide and RCH/RP, are summarised.

Table 2.2: Summary of classic catalyst recovery processes [32–35]

	BASF	Union Carbide Corp.	Exxon/Shell	RHC/RP
Catalyst	**$HCo(CO)_3$**	**$HRh(CO)(PPh_3)_3$**	**$HCo(CO)_4$**	**Rh-TPPTS**
Substrate/solvent	1-Octene	Propene	1-Octene	1-Butene
Solvent	-	Toluene	Water	Water
Temperature (°C)	200	85 – 90	160 – 200	120
Pressure (bar)	25 – 100	18	250 – 300	50
Throughput (ton.year^{-1})	75,000	3,040,000	75,000 - 900,000	300,000
Catalyst concentration (wt%)	0.15	0.2	0.1 – 0.5	-
Selectivity (%)	80	93	50 – 70	99
Recovery method	Distillation		Phase separation	
Relative recovery	Very High		High	
Advantages	*(1)* High catalyst recovery *(2)* Industry proven		*(1)* Ease of separation *(2)* Low occupational hazard	
Disadvantages	*(1)* Process requires large reactor volume as activity of catalyst low *(2)* High temperatures *(3)* Catalysts prone to deactivate/decompose *(4)* Low pressures		*(1)* Restricted to short chain olefins *(2)* High pressures *(3)* Water-soluble ligands prone to decomposition *(4)* Catalyst losses due to leaching	
Relative cost	Very high		Moderately low	

Table 2.3: Summary of alternative catalyst recovery processes [1,3,19,20,35–41]

	Ionic liquid catalysts	Fluorous catalysts	Metal scavengers	Supported catalysts	Supercritical carbon dioxide	OSN
Catalyst	**$Rh\text{-}PPh_3$**	**$Rh\text{-}PPh_3$**	**$Pd(OAc)_2$**	**$Rh\text{-}SiO_2$**	**$Rh_2(OAc)_4$**	**$HRh(CO)(PPh_3)_3$**
Substrate	1-Pentene	1-Hexene	1-Hexene	1-Octene	1-Octene	1-Octene
Solvent	[bmin][PF_6]	PFMCH	Toluene	Toluene	Toluene	Toluene
Temperature (°C)	80	70	75	80	100	120
Pressure (bar)	20	20	10	180	185	35
TOF (h^{-1})	333	1150	500	35	4500	-
Selectivity[a] (%)	99 (3)	50 (-)	-	- (32)	-	-
Recovery (%)	>99.2	>97	>99	>99	>99.9%	>99
Advantages	(1) No solvation of Rh complex (2) Ease of separation	(1) Ease of separation	(1) Controllable catalyst properties	(1) Catalyst activity maintained	(1) Process well understood	(1) Low cost and energy (2) Easy scale-up and handling
Disadvantages	(1) Costly	(1) High concentrations of fluorous phase (2) High isomerisation	(1) May also incur product losses	(1) Synthesis tedious and costly (2) Loss in catalytic activity	(1) High pressures	(1) Sensitive to pH, pressure and temperature (2) Membrane fouling
Relative cost	Very high	Very high	Moderately low	Moderately low	Very high	Low

[a] Product selectivity toward linear *n*-aldehydes and given in brackets is molar ratio of linear to branched aldehydes (*n*/*iso*).

2.3.3.1 Union Carbide Corp. (UCC)

UCC, a joint venture between Union Carbide and Johnson Matthey and Co., erected its first plant in 1976 at Ponce, Puerto Rico following *ca*. 10 years of research on the development of rhodium-based catalysts [32]. It employs the gas recycle concept which utilises a multistage distillation process to evaporate off the product aldehydes from the catalyst mixture. Exact operating conditions are required to maintain adequate process volumes which lead to complex plant and equipment design [42,43].

2.3.3.2 Ruhrchemie/Rhône-Poulenc (RCH/RP)

The breakthrough of E. Kuntz, to apply water-soluble rhodium complexes as hydroformylation catalysts, was taken up and commercialised by RCH/RP in 1984 for the hydroformylation of C_3/C_4 olefins [32]. The catalyst is adsorbed in the aqueous phase and the product aldehydes in the organic phase which are separated in a decanter. The use of water as a solvent adds the benefit of lower environmental and occupational impact but limits the process to the shorter olefin range due to low solubility in water.

2.3.3.3 Exxon

Exxon employed a cobalt-based catalyst process specifically designed for the hydroformylation of olefins in the C_6 – C_{12} range. The application of the cobalt catalyst, although requiring severe operating conditions, i.e. 160 – 190 °C and 250 – 300 bar, a simple two-step catalyst recovery process can be implemented. The Exxon process employs the so-called Kuhlmann catalyst recycle technology which consists of: 1) the recovery of sodium cobalt carbonylate ($NaCo(CO_4)$) following the treatment of the product mixture with aqueous alkali, and 2) the regenerative conversion into the active complex, $HCo(CO)_4$, by the addition of sulphuric acid, H_2SO_4 [16,32].

2.3.4 Alternative recovery methods

Various alternative catalyst recovery methods have been investigated and although not achieving industrial dominance as of yet, significant research effort has been made to drive this concept. In Table 2.3, the various alternative methods for recovering homogeneous catalysts, specifically those used for hydroformylation, are summarised.

2.3.4.1 Supported catalysts

The research field of supported catalysts is vast with several reviews published [44]. Although many patents and publications have come out of this field, only a few commercial processes have been adopted. This is due to the drawbacks of 1) metal leaching from the support (0.1 – 10 ppm), and 2) reduced catalytic activity and selectivity upon

immobilisation. For expensive rhodium-based complexes, metal losses typical to supported catalysts (0.1 – 10 ppm) would be economically unacceptable [17].

2.3.4.2 Biphasic catalysts: ionic liquids

Ionic liquids, first recognised for its applicability to hydroformylation by Chauvin *et al*. [37] in 1995, are similar to aqueous biphasic systems in that it requires intense mixing to create a single homogeneous phase and offer ease of recovery, i.e. phase decantation [17,45]. Although ionic liquids offer additional advantages of good thermal stability and tuneable solubility, Chauvin initially reported poor selectivity toward the linear aldehyde product.

2.3.4.3 Biphasic catalysts: fluorous solvents

Similar to aqueous biphasic catalysts as employed by RCH/RP, the catalyst is dissolved in a second immiscible phase, i.e. fluorinated solvent, while the products are dissolved in the organic phase. The difference is that for aqueous systems, vigorous mixing is required while for fluorinated solvents, a single homogeneous phase can be created upon heating [17]. This allows for ease of recovery while maintaining minimal catalyst losses. Commercialisation of these fluorinated catalysts, first suggested by Horvàth and Rabai in 1994 [46], are hindered due to the high cost of these catalysts and the reduced hydroformylation activity that follows [47,48].

2.3.4.4 Supercritical carbon dioxide

Supercritical fluids, with supercritical ($scCO_2$) being the most widely in the application of catalysis used by far, are substances which are heated and compressed above its critical temperature and pressure, i.e. 31 °C and 73.8 bar for CO_2 [49–51]. Recovery of the catalyst is achieved through simple phase decantation after changing the temperature and pressure. $ScCO_2$ is non-toxic, non-flammable and low in cost with minimal catalyst leaching during operation. Rathke *et al.* [52] were the first to perform a hydroformylation in $scCO_2$ and found relatively high selectivity toward the linear aldehyde product (88 mol%). Although no industrial process using $scCO_2$ for hydroformylation has been implemented, there is no technological or economic barrier which prevents its future application [17].

2.3.4.5 OSN

Section 2.4.3 addresses the use of OSN for catalyst recovery from post-reaction mixtures and provides a critical review of past and recent publications, with emphasis specifically placed on the reaction network of converting short chain olefins to longer chain functionalised hydrocarbons, i.e. metathesis, hydroformylation and hydrogenation.

2.4 Organic solvent nanofiltration

2.4.1 Introduction

The definition of a membrane phrased by Mulder [53] captures the versatility of membranes:

"*A membrane can be thick or thin, its structure can be homogeneous or heterogeneous, transport can be active or passive and it can be driven by means of a pressure, concentration or a temperature difference, membranes can be natural or synthesized and can be neutral or charged*."

A membrane can be viewed as a semi-permeable barrier separating two phases, i.e. the feed phase or upstream side and the permeate phase or downstream side, as shown in Figure 2.4. Permeation is instigated by the application of a driving force based on either a difference in pressure, concentration or electric potential between these phases. Membranes have the ability to manipulate the motion of species through itself, thus achieving separation, by controlling their rate of permeation based on distinct differences in various physical and chemical properties. These properties include molecular size, geometry, polarity, viscosity, and many more [53].

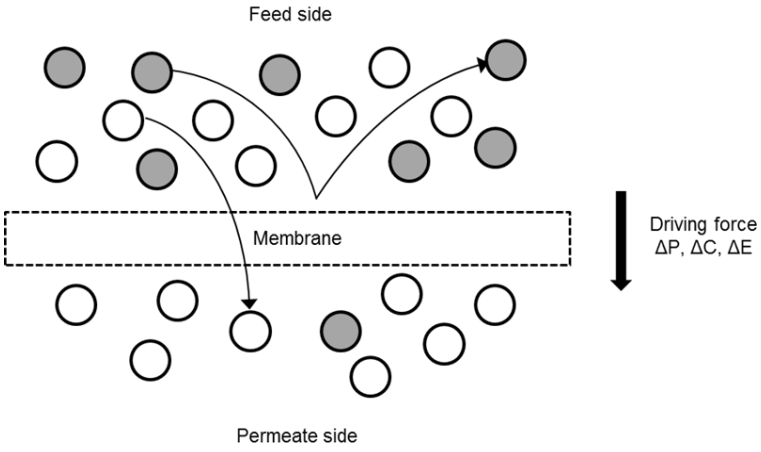

Figure 2.4: Schematic representation of a basic membrane process (adapted from [54])

Despite the large amount of research being conducted in this field over the last *ca.* 20 years, it would seem that Mulder's definition still remains relevant. Further extensive research is still however needed to characterise different membranes for a wide range of systems in order to build-up a database of membrane performance and application. Vandezande and co-writers [55] have noted that literature available of OSN is very application specific. For this reason, literature data is usually non-comparable and rigorous membrane screening is required to match the correct membrane with a certain application.

Ideally, this database should be able to be used as reference in order to determine which type of membrane is applicable to which systems. The work in this study, although relatively small in scope, aims to add to this database.

Conventional filters share similarities with membranes only in its definition which states that separation occur based on differences in size. However, filters are only capable of separating particulate larger than 10 µm while some membranes can separate on a nanoscale. With this in mind, membranes are unique in their ability to selectively control the flux of different species depending on their physical and chemical properties, such as shape, solubility, viscosity, surface tension, etc. [56]. It is easy to understand when considering a barrier consisting of holes and that everything larger than these holes will not pass through. However, this process gets more complicated when separation occurs on a molecular level and properties such as diffusion start to play a significant role [55].

In summary, the advantages and disadvantages of membranes are given in Table 2.4 [53,54].

Table 2.4: Advantages and disadvantages of membrane processes

Advantages	Disadvantages
Minimal energy usage	Membrane material may be chemically incompatible if not properly selected
Operator friendly	Limitations in terms of temperature and pH
Easy scale-up	Fouling and/or concentration polarisation

Humphrey and Keller [54] defines fouling as the process by which a membrane's performance degrades as a result of suspended and/or dissolved solids deposition or growth of biological films on the membrane's external surface or within its pores, subsequently blocking pores and creating a barrier which resists the permeation of molecules through the membrane. Concentration polarisation refers to the mechanism by which fouling takes place and is the accumulation of solutes on the membrane such that there is a higher concentration of solutes at the membrane boundary layer than in the bulk solution, creating additional resistance to permeating species [55]. These phenomena are exacerbated by improper membrane cleaning and pretreatment, excessive flux and unsuitable membrane-solvent pairing [57].

OSN membranes offer the same advantages as conventional nanofiltration membranes such as requiring no additives, phase transition or thermal input to initiate separation as well as the relative ease of installation and upscaling. In addition, it brings to the table the added benefit of being stable in non-aqueous environments. However, despite the long list of advantages these membranes have to offer, only a few have found its way into large scale application. This is due not only to industry's reluctance to adopt newer technologies but also to the lack of long-term reproducibility in terms of flux and selectivity of the membrane technology [55].

Membranes can be classified according to its capacity to separate specific molecular size ranges. These classifications include microfiltration (MF), ultrafiltration (UF), nanofiltration (NF) and reverse osmosis (RO). Figure 2.5 shows that membranes have the ability to separate relatively large particulate matter from fluids as well as distinguish between ions or molecules less than 100 g.mol^{-1} or 1 nm in size while Table 2.5 classify the different membranes in terms of permeance [53].

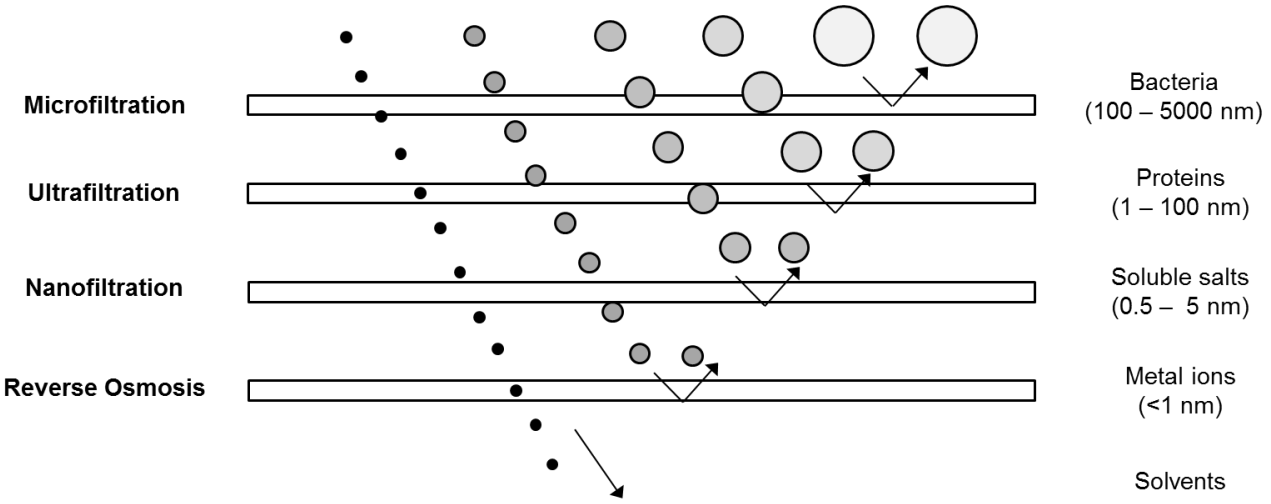

Figure 2.5: Membrane classifications in terms of molecular size (adapted from [17])

Table 2.5: Membrane classification in terms of permeance [53]

Membrane type	Operating pressure range (bar)	Permeance (x10^{-3} m^3.m^{-2}.h^{-1}.bar^{-1})
MF	0.1 – 2	> 50
UF	1 – 5	10 – 50
NF	5 – 15	1 – 15
RO	10 – 100	<1

Nanofiltration is a pressure-driven membrane process capable of separating molecules in the lower size (0.5 – 5 nm) and weight range (200 – 1000 $g.mol^{-1}$) with moderate permeance, as shown in Table 2.5. It allows for greater rejections than UF and higher fluxes than RO processes [58]. Nanofiltration is an established water treatment method used for the removal of multivalent ions [59–61].

There are two modes in which membrane processes can be operated and are classified by the flow pattern associated with the permeation of molecules. These include dead-end flow mode and cross-flow mode which are illustrated in Figure 2.6.

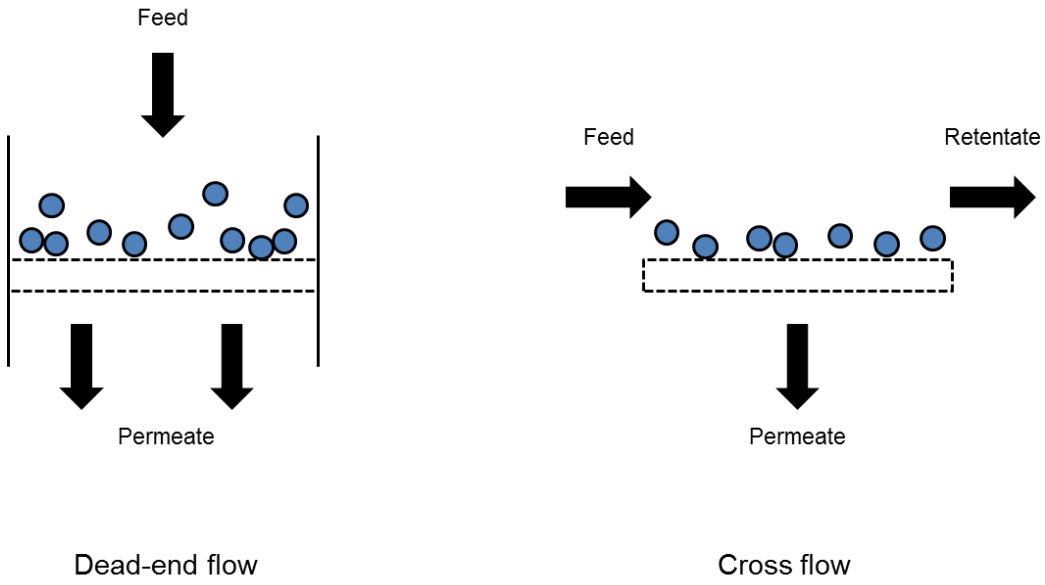

Figure 2.6: Comparison between dead-end and cross flow (adapted from [54])

Dead-end mode is characterised by a feed flow perpendicular to the membrane surface. All flow capable of permeating through the membrane will pass through with no retentate stream. The feed is forced through the membrane by means of a pressure difference created between the feed and permeate sides. This mode is advantageous in terms of cost efficiency, ease of construction and simple installation and use but has the inherent disadvantage of being more susceptible to fouling due to the build-up residue on the membrane surface which confines its use to small-scale laboratories. This built-up layer of residue results in reduced performance and requires operation to be halted, the membrane cleaned and process restarted, indicative of a typical batch process [62].

In the case of cross-flow filtration, the feed is circulated parallel to the membrane surface via a pump. Due to this action, excessive build-up of solids on the membrane surface is prevented and the risk of membrane fouling is reduced as residue is continuously washed

of the surface. The feed stream is split into a permeate and retentate stream. Cross-flow filtration is characterised by complex operational procedures [63].

Membranes can be manufactured from different materials which can be classified as either organic or inorganic. Organic membranes, commonly preferred due to its low cost and greater flux capacities, are made from polymer- or cellulose-based materials. However, polymeric membranes have the inherent disadvantage of being limited by operating conditions such as solvent type, temperature, pressure and operational lifetime [64]. Inorganic membranes are ceramic in nature and are considered less conventional due to its high cost and uncompromising structure [65]. The development of asymmetric membranes was a significant breakthrough in the field of membrane technology. These membranes consist of an active very dense thin top layer (thickness < 0.5 µm) supported on a porous sublayer (thickness 50 – 200 µm) [53]. For the active layer, polyimides (PI), polydimethylsiloxanes (PDMS) or polyamides (PA) are typically selected as the material of construction due to their excellent chemical and thermal stability while for the support layer, polyacrylonitrile or polypropylene or polyimide are used [66,67].

2.4.2 Principles of organic solvent nanofiltration

An important parameter to consider when selecting a membrane is its molecular weight cut-off (MWCO) referring to the molecular weight for which the membrane will achieve a 90% rejection [68]. However, for organic solvents, this value can be misconstrued due to interactions between the solute, solvent and the membrane. In addition to MWCO, other properties which should be considered to attain a more reasonable assessment of a membrane's capabilities are solvent properties (solubility, size, polarity, viscosity, etc.), solute properties (solubility, size, shape, etc.) and membrane properties (polarity, surface tension, pore size and pore size distribution) [69,70]. These properties are necessary, not only in its selection, but also for the approximation of membrane performance. Researchers have previously studied the effects of size on membrane permeance, reporting contrasting observations regarding its influence [71–73]. Robinson *et al.* [74], and Van der Bruggen *et al.* [75], reported on the importance of polarity on flux and how its influence varies for hydrophilic and hydrophobic membranes while Darvishmanesh *et al.* [70], and Stamatialis *et al.* [76], focussed on the effects of viscosity.

The performance of membrane processes are evaluated by two parameters, namely flux and rejection. Flux, J, as shown in Equation 2.5, is defined as the amount of fluid, i.e. volumetric, molar or mass, that passes through the membrane per unit time and surface area, A.

$$J = \frac{V \text{ or } m}{A \times t} \tag{2.5}$$

where

V volume of fluid that has permeated through membrane (L)

m mass of fluid that has permeated through membrane (kg)

A effective membrane surface area (m^2)

t time required to permeate volume V of fluid through the membrane (s)

Rejection, R, as shown in Equation 2.6, is defined as the ability of a membrane to reject a solute and is a function of feed and permeate concentration.

$$R = \left(1 - \frac{C_P}{C_F}\right) \times 100\% \tag{2.6}$$

where

C_P concentration of solute in the permeate stream ($mL.mL^{-1}$ or $mg.L^{-1}$)

C_F concentration of solute in the feed stream ($mL.mL^{-1}$ or $mg.L^{-1}$)

The separation coefficient, α_{ij}, ability of a membrane to separation a binary mixture of i and j can be determined based on the concentrations of i in the permeate stream relative to the feed and is defined in analogy to distillation as shown in Equation 2.7:

$$\alpha_{ij} = \frac{C_{P,i}}{C_{F,i}} \tag{2.7}$$

2.4.3 Review of homogeneous catalyst recovery using OSN

Goldup [77] and Gosser *et al.* [78,79], during the 1970's, were one of the firsts to allude to the potential of OSN as an alternative to current separation methods and to successfully recover homogeneous catalysts which was later recognised through the pioneering work done by the groups of Livingston [80–90] and Vankelecom [30,91–97] thereby cementing the foothold of OSN in this field. In this section, a literature review is presented regarding the separation of different homogeneous catalysts using OSN with a summary of recent publications given in Table 2.6.

Table 2.6: Summary of previous publications regarding the separation of different homogeneous catalysts using OSN

Year	Homogeneous catalyst (MW)	Catalyst weight ($g.mol^{-1}$)	Solvent	Membrane	Rejection	Ref.
Metathesis						
2008	Hoveyda-Grubbs 2	627	Toluene	STARMEM-228	0.7	[98]
	Enlarged Hoveyda-Grubbs 2	2200	Toluene	STARMEM-228	0.9	
2009	Hoveyda-Grubbs	1380	Toluene	PAN/PDMS	>0.998	[99]
2010	Grubbs 1	823	1-Octene	STARMEM-120	>0.99	[100]
				STARMEM-122	>0.99	
				STARMEM-228	>0.99	
				STARMEM-240	86	
	Chelated Grubbs-type	794	1-Octene	STARMEM-120	>0.994	
				STARMEM-122	>0.994	
				STARMEM-228	>0.994	
				STARMEM-240	0.85	
2011	Hoveyda-Grubbs 2	627	Toluene	STARMEM-122	>0.96	[101]
				Duramem-300	>0.46	
2013	Hoveyda-Grubbs 1	601	DCM	0.9 nm TiO_2	>0.9995	[102]
				Duramem-200	>0.9995	
			Acetone	0.9 nm TiO_2	>0.88	
	Umicore M2	949	DCM	0.9 nm TiO_2	>0.9995	
				Duramem-200	>0.6	
			Acetone	0.9 nm TiO_2	>0.93	
				Duramem-200	0.91	
	Umicore M41	888	DCM	0.9 nm TiO_2	>0.99	
	Umicore M51	655	DCM	0.9 nm TiO_2	>0.94	
Hydroformylation						
1977	$HRh(CO)(PPh_3)_3$	920	Benzene	Polyimide-based	0.91	[78]
2010	Rhodium-based	850	Toluene	STARMEM	>0.99	[1]
2011	Rhodium-based	200 – 400	Toluene	STARMEM	>0.94	[4]
2013	$HRh(CO)(PPh_3)_3$	920	Toluene	STARMEM 122	0.810	[103]
				STARMEM 240	0.950	
	$HRh(CO)(PPh_3)_3$	920	EA	STARMEM 122	0.745	
				STARMEM 240	0.810	
2014	Triphenylphosphine	262	Toluene	Puramem 280	0.967	[104]
				GMT-oNF-2	0.905	
			n-Hexane	Puramem 280	0.734	
				GMT-oNF-2	0.389	
			2-Propanol	Puramem 280	0.828	
				GMT-oNF-2	0.663	
			n-Hexanal	Puramem 280	0.734	
				GMT-oNF-2	0.389	
			DCM	Puramem 280	0.884	
				GMT-oNF-2	0.581	
			o-Xylene	Puramem 280	0.900	
				GMT-oNF-2	0.900	
			1-Pentanol	Puramem 280	0.490	
				GMT-oNF-2	0.510	

Table 2.6: Summary of previous publications regarding the separation of different homogeneous catalysts using OSN (*cont.*)

Year	Homogeneous catalyst (MW)	Catalyst weight ($g.mol^{-1}$)	Solvent	Membrane	Rejection	Ref.
			n-Decane	STARMEM 122	0.415	
2015	Rh-BIPHEPHOS	900	*n*-Nonanal/ toluene	MET-oNF2	0.850	[105]
			n-Nonanal/ toluene	MET-oNF2	0.999	
			Tridecanal/ toluene	MET-oNF2	0.950	
	Rh-XANTPHOS	680	*n*-Nonanal/ toluene	MET-oNF2	0.999	[105]
			Tridecanal/ toluene	MET-oNF2	0.960	
			n-Nonanal/ toluene	MET-oNF2	0.999	
			Tridecanal/ toluene	MET-oNF2	0.960	
Hydrogenation						
1977	Wilkinson's catalyst	925	Neat	Polyimide-based	0.88	[78]
2001	Ru-BINAP	929	Methanol	MPF-60	>0.98	[97]
	Rh-EtDUPHOS	723	Methanol	MPF-60	0.97	
2002	Wilkinson catalyst	925	EA	STARMEM-120	0.994	[87]
				STARMEM-122	0.985	
				STARMEM-240	0.787	
				MPF-50	0.864	
			DCM	MPF-50	0.976	
				Desal-5	0.930	
			THF	STARMEM-122	0.981	
				MPF-50	0.578	
2003	Wilkinson's catalyst	925	$ScCO_2$	Silica-based	>0.999	[106]
Other						
1977	$Co_2(CO)_8$	930	Benzene	Polyimide-based	0.84	[78]
1996	α,α-diphenyl-prolinol	96,000	Hexane	PAH20	0.998	[107]
1998	Oxazaborolidines	13,800	Toluene	MPF-50	0.98	[108]
1999	Pd-	10,200	DCM	MPF-50	0.999	[109]
	Pd complex	Undisclosed	THF	MPF-60	0.981	[110]
2001	Heck catalyst	749	EA/Acetone	STARMEM-122	0.96	[90]
2002	TOABr	549	Toluene	STARMEM-122	>0.99	[111]
	Jacobsen catalyst	622	EA	STARMEM-120	0.996	[87]
				STARMEM-122	0.994	
				STARMEM-240	0.954	
				MPF-50	0.930	
			DCM	MPF-50	0.814	
				Desal-5	0.841	
			THF	STARMEM-122	0.958	
				MPF-50	0.942	
				Desal-5	0.779	

Table 2.6: Summary of previous publications regarding the separation of different homogeneous catalysts using OSN (*cont.*)

Year	Homogeneous catalyst (MW)	Catalyst weight ($g.mol^{-1}$)	Solvent	Membrane	Rejection	Ref.
2002	Pd-BINAP	849	EA	STARMEM-120	1	[87]
				STARMEM-122	1	
				STARMEM-240	>0.949	
				MPF-50	>0.957	
			DCM	MPF-50	0.934	
				Desal-5	>0.886	
			THF	STARMEM-122	1	
				MPF-50	>0.947	
	TOABr	546	Toluene	STARMEM-120	>0.99	[88]
				STARMEM-122	>0.99	
				STARMEM-240	>0.99	
				MPF-50	0.48	
				MPF-60	0.86	
				Desal-5	0.62	
				Silicone rubber	>0.99	
				EPDM rubber	>0.99	
	TBABr	322	Toluene	STARMEM-120	>0.99	[88]
				STARMEM-122	>0.99	
				STARMEM-240	0.8	
				MPF-50	0.61	
				MPF-60	0.89	
				Desal-5	0.55	
				Silicone rubber	>0.99	
				EPDM rubber	>0.99	
2003	Pd-based	5,000	Toluene	PDMS	0.9995	[112]
2004	Co-Jacobsen catalyst	622	Diethyl ether	MPF-50	0.16	[95]
				Desal DL	<0.05	
				Desal GE	0.2	
				N30F	0.4	
				NF-PES-10	0.08	
				PDMS	0.79	
2004	Pd-based	1,440	DCM	Silica-based1	0.98	[64]
				Silica-based2	0.994	
	TOABr	546	Toluene	STARMEM-122	1	[86]
2005	Gold nanosols	13,000 – 23,000	2-Propanol	PDMS	1	
2005	Polyoxometalate	Undisclosed	Toluene	Alumina supported membrane	>0.999	[113]
	TOABr	546	Toluene	STARMEM-122	>0.99	[85]
				MPF-50	>0.79	
	TOABr	546	Methanol	STARMEM-122	>0.98	
				MPF-50	>0.92	
	TOABr	546	EA	STARMEM-122	>0.99	
	Prophyrin-functionalised dendrimers	2,120 – 4,390	$CHCl_3$/IPA	MPF-50	>0.05	[93]
2006	Co-Jacobsen catalyst	622	IPA	MPF-44	0.8	[92]
				N30F	0.9	
				PDMS	0.84	

Table 2.6: Summary of previous publications regarding the separation of different homogeneous catalysts using OSN (*cont.*)

Year	Homogeneous catalyst (MW)	Catalyst weight ($g.mol^{-1}$)	Solvent	Membrane	Rejection	Ref.
	TOABr	546	Toluene	PAN/PDMS membrane	1	[76]
	Ru-cymene	612	Toluene	STARMEM-122	0.996	[83]
	Ru-BINAP	623	Methanol	STARMEM-122	0.999	[84]
2008	Pd-based	916	EA	STARMEM-122		[114]
2009	Ru-BINAP	623	Methanol	STARMEM-122	>0.99	[115]
2010	Copper-based	317	DMF	Polyimide membrane	>0.52	[30]
2011	BINOL ligand	286	Toluene	PDCPD	0.72	[116]
2013	Quinidine	324	THF	Duramem-300	>0.65	[81]
				Duramem-500	>0.2	
	Enlarged Quinidine	1,330	THF	Duramem-300	>0.99	
				Duramem-500	>0.99	

Recent reviews published by Cheng *et al*. [66], Marchetti *et al*. [117] and Janssen *et al*. [68] provides a critical demonstration of the use of OSN in catalyst recycling and a comprehensive state of the art of OSN.

In the 1970's, Gosser *et al.* [78] confirmed the technical applicability of OSN for catalyst recovery from rhodium-catalysed hydroformylation reaction mixtures and set the standard for the publications thereafter. Priske *et al.* [1] considered the possibility of an integrated reaction and separation step using the rhodium-catalysed hydroformylation of 1-octene and 1-dodecene as prototype reactions while Fang *et al.* [4] focussed on improving the continuity of OSN systems for the recovery of homogeneous rhodium-catalysts from 1-octene hydroformylation reaction mixtures. Both researchers reported successful findings with catalyst recoveries up to 99% using the STARMEM^{TM} series of membranes (Evonik MET). More importantly, Priske *et al.* [1] further reported that no significant difference in catalytic activity before and after recovery by means of OSN was observed. Thereby proving that successful recycling of homogeneous catalysts can be achieved using OSN. Recently, Dreimann *et al*. [105] successfully combined a thermomorphic multicomponent solvent system (TMS) with OSN and reported rhodium recoveries >90%.

Perhaps the most promising work was done by the group of Lutze who were able to successfully confirm the technical and economic viability of OSN integration with the hydroformylation reaction. As a follow-up to their previous work, they investigated the effect of targeted solvent additions on OSN performance and used the rhodium-catalysed

hydroformylation reaction as a case study. They reported successful catalyst recoveries for the Puramem® 280 (Evonik MET) and GMT-oNF-2 (Borsig) membranes and also performed a brief short-cut analysis to determine the total cost of operation for an optimised OSN process [104,118].

The applicability of OSN for catalyst recovery has been greatly emphasised for various homogeneous reactions over the years, including addition, substitution, alkylation and epoxidation reactions. Kragl *et al.* [107] and Giffels *et al.* [108] were the first to demonstrate the successful use of OSN for homogeneous catalyst recovery from addition and reduction reaction mixtures. These authors did not consider rhodium-based catalysts, as in the case of Priske *et al.* [1] and Fang *et al.* [4], instead focussed their attention on the recovery of soluble polymer enlarged catalysts, with molecular weights of 96000 $g.mol^{-1}$ and 13800 $g.mol^{-1}$, respectively. Both Kragl *et al*. and Giffels *et al.* reported recoveries of >98% using a polyaramide UF PAH20 membrane (Nadir) and MPF-50 membrane (Koch), respectively. Moreover, Giffels *et al.* [108] reported an increase in the total turnover number from 10 to 560 as a direct result of the continuous membrane reactor implemented.

Later, Cano-Odena *et al.* [30] and Siew *et al.* [81] attempted to continue the work previously demonstrated by Kragl *et al.* [107] and Giffels *et al.* [108] on the application of OSN in catalytic addition reactions. However, both Cano-Odena *et al.* and Siew *et al.* reported less than favourable results for polyimide membranes and required catalyst enlargement, in the case of Siew *et al.* [81], in order to improve recovery to >99% and enantioselectivities to >92% *ee*.

Around the same time, Brinkmann *et al.* [109] and de Groot *et al.* [110] followed the example set by Giffels *et al.* [108] and tested the possibility of using continuously operated membrane reactors to carry out homogeneous allylic reactions catalysed by dendritic catalysts. Both Brinkmann *et al.* and de Groot *et al.* reported successful results with recoveries reaching 99.9% using the MPF series membranes. Moreover, Brinkmann *et al.* [109] reported the use of OSN membranes to result in a six-fold increase of the total turnover number of the palladium-based catalyst employed.

Publications by Nair *et al.* [90], Luthra *et al.* [88], Peeva *et al.* [86], Silva *et al.* [85], and Stamatialis *et al.* [76], investigated the application of OSN in the phase transfer catalytic conversion of bromoheptane into iodoheptane with toluene as solvent. This system used an aqueous solution of potassium iodide and was catalysed by the phase transfer catalyst,

tetraoctylammonium bromide (TOABr). Luthra *et al.* performed the most comprehensive study, considering different commercially available OSN membranes (MPF-50, MPF-60, Desal-5, STARMEM^{TM} 120, 122, 240). The STARMEM^{TM} series membranes have been shown to provide the best performance in terms of catalyst recoveries (100% in some cases) and permeate flux. Luthra *et al.* [88] further reported that the recovered catalyst experienced no loss in catalytic activity and was 100% recyclable and reusable for at least three consecutive reactions.

Nair et al. [111], along with Datta et al. [112], also studied the use of OSN for the recovery of the homogeneous palladium-based Heck catalysts from the Heck coupling reactions. Both Nair *et al.* and Datta *et al.* successfully demonstrated the recycle potential of OSN using a STARMEM^{TM} 122 and PDMS membrane, respectively, achieving catalyst recoveries of up to 99.95% and observed the catalyst maintaining its activity for up to four reaction cycles.

In 2002, Scarpello *et al.* [87] published a comprehensive study based on the non-destructive separation of different homogeneous organometallic catalysts typically used for commercial organic synthesis processes, namely the Jacobsen catalyst, the Wilkinson catalyst and a Pd-BINAP catalyst. A wide range of commercial OSN membranes were considered (MPF-50, Desal-5, STARMEM^{TM} 120, 122, 240) in various organic solvents (EA, THF and DCM). Catalyst rejections of >95% were reported coupled with good permeate fluxes (>50 $L.m^{-2}.h^{-1}$ at 20 bar operating pressure) for the majority of the systems tested. Aerts *et al.* [92,95] continued the consideration of the recycling of the organometallic Jacobsen catalyst, as used by Scarpello *et al*. [87], for the hydrolytic kinetic resolution of epoxidation in two separate publications. They were unsuccessful in their first attempt in 2004 and reported a catalyst recovery of *ca.* 16% for the MPF-50 membrane and even less (~5%) for the Desal-5 membrane. Better recoveries of >83% were achievable using their laboratory prepared COK M2 membrane but at the expense of permeance (<0.02 $g.cm^{-2}.h^{-1}.bar^{-1}$). In 2006, they published better results using the same prototype reaction, reaching recoveries >80% for the MPF-44 and N30F membranes.

Recently, increasing focus has been placed on OSN application for recovery of homogeneous catalysts from metathesis reactions, spurred on by the economic and environmental interests of various industries, especially petrochemical.

To author's knowledge, the first documented use of OSN in the field of metathesis was done in 2000 by Wijkens *et al.* [119]. They performed an investigation on the recovery of a

ruthenium-based catalyst functionalised onto a carbosilane dendrimer support and considered the ring close metathesis reaction of diethyl diallyl malonate into diethyl-3-cyclopentene dicarboxylate as prototype reaction. Wijkens *et al.* [119] were, however, unsuccessful in their attempt at catalyst recovery using the MPS-60 membrane (SelRO) and suggested future success may be achievable if membrane compatibility were improved. In the decade succeeding the paper by Wijkens *et al.* [119], significant strides were indeed made in terms of OSN compatibility and Keraani *et al.* [98] took full advantage by performing a study to test the recoverability of the homogeneous second-generation Hoveyda-Grubbs catalyst using the STARMEM^{TM} 228 membrane. They observed recoveries of up to 90% and confirmed that the catalyst activity remains intact for at least five reaction cycles.

Later studies by Schoeps *et al.* [99], Van der Gryp *et al.* [100], Rabiller-Baudry *et al.* [101], and Ormerod *et al.* [120], further demonstrated the successful synergy between OSN as catalyst recovery method and the metathesis reaction. Reports once again favour the STARMEM^{TM} series of membranes for the recovery of different Grubbs-type catalysts, achieving recoveries in the order of 99%.

2.5 Modelling of species transport in OSN

2.5.1 Introduction

Having membranes which are applicable on an industrial scale in terms of solvent stability and operation robustness are essential but equally so is having an accurate mathematical description of the transport of species across the membrane. With such a description, knowledge-based development can occur to tailor membranes to meet specific objectives, thus furthering its relevance in industrial applications. Various mathematical models are currently available to estimate the transport of species through nanofiltration membranes in non-aqueous media. However, at present, there is no one model which can fully describe the transport of all species through different OSN membranes. The models that are available are rather application specific, with performance being non-relatable across different membranes. This is, in part, due to the vast differences in solvent properties, membrane synthesis techniques and membrane material properties which make it nearly impossible to account in a single model [72]. Moreover, the occurrence of membrane swelling in the presence of organic solvents, creating so-called channels through which species can easily pass, complicates the model development process as membrane performance is influenced greatly by swelling [74]. Currently, three kinds of transport models exists which enable the description of species transport under specific conditions,

relating to the assumptions made in the model, and include the solution-diffusion, pore-flow and phenomenological (or irreversible thermodynamic) model [85].

This section reviews the applicability of these three commonly used literature transport models, i.e. solution-diffusion, pore-flow and phenomenological models, in the description of solvent transport across OSN membranes. The theory of mass transport through membranes on which the abovementioned models are built as well as their origins and derivations are presented in Section A.3 of Appendix A.

2.5.2 Review of OSN transport models

Many contradicting suggestions have been observed in literature with some recommending the pore-flow model while others suggest the solution-diffusion model to be all encompassing. This highlights the fact that, although OSN systems have been under investigation for several years, molecular transport through OSN membrane remains misunderstood.

Despite the prevalence of several membrane process modelling publications, the literature available is riddled with inconsistencies and lack of consensus regarding the OSN performance for some membrane and solvent systems. Gibbins *et al.* [96] noted that Machado *et al.* [121] and Whu *et al.* [122], who studied the same conditions using the MPF50 membrane at 30 bar, reported different methanol fluxes, 172 $L.m^{-2}.h^{-1}$ and 38 $L.m^{-2}.h^{-1}$. Gibbins and team further suggested that this inconsistency may be due to different pretreatment methods employed which produced non-reproducible results.

Excellent general reviews have been published by Soltanieh and Gill [123], Mason and Lonsdale [124], Vrentas and Vrentas [125], Bhanushali and Bhattacharyya [126] as well as the Livingston group [117,127] with the aim of consolidating the various models available and to elucidate on the misconceptions regarding transport modelling of solvents through dense polymeric membranes. In 2001, George and Thomas [128] took a different approach, recognising the importance of understanding of transport phenomena in polymeric membranes, rather than being application specific, reviewed the transport mechanisms taking place in different polymeric materials, i.e. rubbery, glassy and polymer blends, for different fluid phases. They placed focus on relating the membrane characteristics and polymer structure to membrane performance. Similar investigations were done by the Livingston group [129].

As mentioned previously, the transport models available remain application specific, with performance being non-transferrable between membranes of different types. In this section, further clarity is provided to the three main transport models, i.e., solution-diffusion, pore-flow and phenomenological, considered in this study regarding application and relevance.

The classic solution-diffusion and Hagen-Poiseuille pore-flow models, as shown in Equations 2.8 and 2.9 respectively, are well reviewed in literature and have maintained prominence in their application throughout the years [74,130,131]. These solution-diffusion and pore-flow models are derived based on the fundamental principle, as well as assumptions as illustrated in Figures 2.8 and 2.9 respectively, that a driving force is exerted based on a gradient in chemical potential across the membrane and is widely accepted. Refer to Sections A.3.2 and A.3.3 in Appendix A for additional literature regarding the origins and derivations of the solution-diffusion and pore-flow models.

$$J_{n,i} = \frac{D_i K_i}{l}\left[c_{i,FM} - c_{i,P}\frac{\gamma_{i,P}}{\gamma_{i,MP}}\exp\left(-\frac{V_{m,i}\times(P_{MP}-P_P)}{RT}\right)\right] \tag{2.8}$$

$$J_V = \frac{\varepsilon {d_{pore}}^2}{32l\tau}\times\frac{P_o-P_z}{\eta} \tag{2.9}$$

where $J_{n,i}$ is the partial molar flux of species i, J_V the volume flux, D_i the diffusion coefficient of species i, K_i the sorption coefficient, γ_i the surface tension and $V_{m,i}$ the molar volume of species i, ε the membrane porosity, τ the membrane tortuosity, d_{pore} the membrane pore diameter, l the membrane thickness and η is the species viscosity.

The models given in Equations 2.8 and 2.9 have given rise to many other variations, each intended to extend model applicability and predictive accuracy. The Hagen-Poiseuille pore-flow model describes the transport of species through a membrane assumed to consist of cylindrical pores fixed in size and position. When the assumption is made that the membrane consists of closely packed spheres, the Kozeny-Carmen equation, as shown in Equation 2.10, can be used to describe the transport of species [53]:

$$J_V = \frac{\varepsilon^3}{Kls^2(1-\varepsilon)^2}\times\frac{P_o-P_z}{\eta} \tag{2.10}$$

where K refers to the Kozeny-Carmen constant and s is the internal membrane surface area.

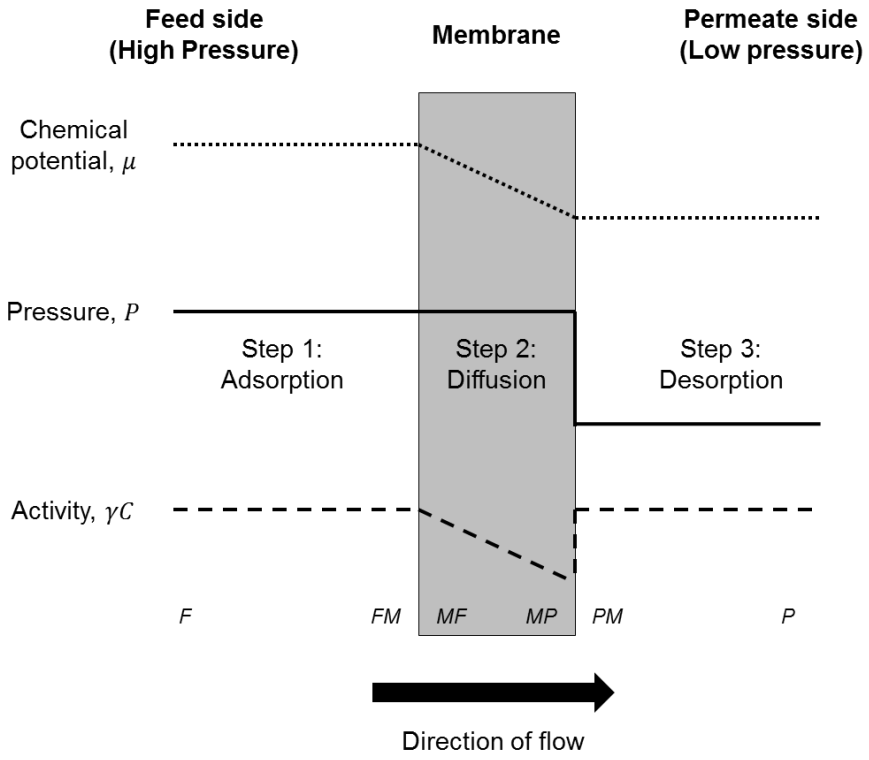

Figure 2.7: Schematic illustration of solution-diffusion model (adapted from [132])

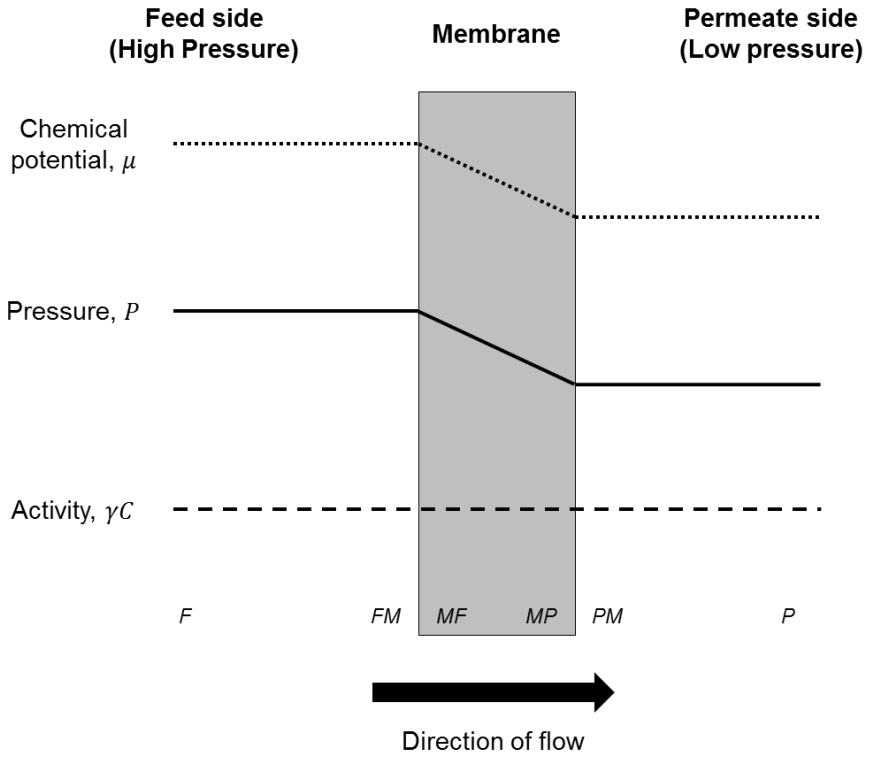

Figure 2.8: Schematic illustration of pore-flow model (adapted from [132])

The Hagen-Poiseuille and Kozeny-Carmen models encapsulate solvent flux in terms of one physical parameter of the solvent. However, the research group of Vandecasteele proved that this approach is insufficient to describe the transport of organic solvents through dense nanofiltration and reverse osmosis membranes [71]. Jonsson and Boesen was able to modify the Hagen-Poiseuille model to describe solute flux in RO membranes by including molecular weight, MW, as a second parameter representative of the solute size as presented in Equation 2.11 [133]:

$$J_V = \frac{\varepsilon d_{pore}^2}{32\eta\tau}\left[\frac{1}{1+\frac{d_{pore}^2 x_{sm} C}{32\eta \quad MW}}\right]\times\frac{\Delta P}{\Delta z} \tag{2.11}$$

where x_{sm} friction factor between solvent molecules and membrane pore wall.

Although the inclusion of molecular sizes allows for the coverage of all four membrane classifications ranging from MF to RO, the model remains incapable of representing a wide range of organic solvents. The resistance-in-series model presented by Machado *et al*. as shown in Equation 2.12, accounts for organic solvents and therefore, although lacking robustness as it was developed for hydrophobic membranes specifically, is able to provide a much better description of the convective transport of pure solvents and solvent mixtures through hydrophobic membranes [57,134].

$$J_V = \frac{\Delta P}{\emptyset[(\gamma_c-\gamma_l)+f_{1,n}]+f_{2,n}} \tag{2.12a}$$

with

$$f_1 = \frac{k_M^1}{k_M^0} \tag{2.12b}$$

$$f_2 = \frac{k_M^2}{\left(d_{pore}^2\right)^2} \tag{2.12c}$$

$$\emptyset = \frac{k_M^0}{\left(d_{pore}^1\right)^2} \tag{2.12d}$$

where f is the parameter describing the nanofiltration sublayers independent of the solvent, $\emptyset$ the solvent dependent parameter, γ_c the critical surface tension of membrane material, and γ_l the critical surface tension of solvent.

Machado *et al.* proposed that each permeant encounters three types of resistance: 1) surface resistance, R_S^0, at the pore entrance, 2) viscous resistance, R_μ^1, during permeation

through the NF portion of the membrane, and 3) another viscous resistance, R_{μ}^{2}, as the permeant passes through the UF portion of the membrane, and relates these resistances to flux as shown in Equations 2.13 through 2.16 [135].

$$J_V = \frac{\Delta P}{R_S^0 + R_\eta^1 + R_\eta^2} \tag{2.13}$$

The three resistances are expressed as:

$$R_S^0 = \frac{k_M^0}{\left(d_{pore}^1\right)^2}(\gamma_c - \gamma_L) \tag{2.14}$$

where k_M^0 is constant representative of the membrane characteristics, d_p^1 the mean pore diameter of the first layer, γ_c the critical surface tension of the membrane, and γ_L the surface tension of the solvent.

$$R_\eta^1 = k_M^1 \frac{\eta}{\left(d_{pore}^1\right)^2} \tag{2.15}$$

where k_M^1 is a membrane geometrical constant taking representative of its tortuosity and porosity.

$$R_\eta^2 = k_M^2 \frac{\eta}{\left(d_{pore}^2\right)^2} \tag{2.16}$$

As a variation to the pore-flow model, Matsuura and Sourirajan proposed a two-dimensional extension of the basic pore-flow model, as shown in Equation 2.17, named the surface force pore-flow model (SFPF), which accounts for the effects of solute-membrane interactions. This model accounts for solute-membrane interactions by considering the distribution of solutes on the membrane surface through interfacial forces between the solute and membrane material [136]. The SFPF model derivation was based on four assumptions: 1) the membrane is microporous with straight cylindrical pores, 2) water or solvent transport through the membrane is dominated by viscous flow, 3) solute transport is governed by both convective and diffusive transport, and 4) the driving force for transport is determined by the interaction forces, friction forces and chemical potential gradients [137]. Bhanushali *et al.* [138] as well as Farnard and Talbot [139] used the SFPF model to describe the transport of organic solutes in organic solvents.

$$J_{n,i} = -\frac{RT}{\chi_{i,j} b_f}\frac{dc_i}{dx} + \frac{V_{m,i} c_i}{b_f} \tag{2.17}$$

where b_f is the friction parameter which relates the friction coefficient between the solute and the solvent, $\chi_{i,j}$, and the solute and the membrane, $\chi_{i,M}$ and is defined as $\frac{\chi_{i,s}+\chi_{i,M}}{\chi_{i,s}}$.

However, a few years later, a publication by Mehdizadeh and Dickson disproved the SFPF model, stating that it will predict physically unacceptable results as it was fundamentally flawed due to an error in the material balance and an inconsistent potential function within the cylindrical pore geometry. They corrected the principle errors and proposed a new model, amply named as the modified surface fore pore-flow model (MD-SFPF) [140]. Mehdizadeh and Dickson later also proposed a modified version of the pore-flow model, named the finely porous model, in which focus is placed on the friction between the species and the pore wall, of which details can be found in literature [141].

The Hagen-Poiseuille pore-flow model was developed to determine solvent flux. For solute flux, several empirical pore-flow models have been developed stemming from the Nernst-Planck equation to describe the transport of solutes through narrow distinguishable channels within the membrane. Bowen and Welfoot as well as Bowen and Mukthar developed the Donnan Steric pore-flow model (DSPF), based on the extended Nernst-Planck equation which couples steric hindrance and Donnan exclusion effects for a general solute i. The DSPF model expresses solute flux as [142,143]:

$$J_{n,i} = -K_{i,d} D_i \frac{dc_i}{dx} - \frac{z_i c_i K_{i,d} D_i}{RT} F \frac{d\psi}{dx} + K_{i,c} c_i J_V \tag{2.18}$$

where $K_{i,d}$ and $K_{i,c}$ refer to the diffusion and convective hindrance factors, respectively, z_i the solute valence and ψ the electric potential.

In the case of the classic solution-diffusion model, Bhanushali *et al.* [73] used this model to propose a new diffusion-based model, as shown in Figure 2.19, which utilises four different parameters including solvent viscosity, η, molar volume, V_m (representing hindrance effects caused by molecular size), the surface energy of the membrane material, γ_M, and the sorption value, $\emptyset^n$ (representing the affinity or interaction between the membrane and the solvent) [73]:

$$J \sim \left(\frac{V_m}{\eta}\right)\left(\frac{1}{\emptyset^n \gamma_M}\right) \tag{2.19}$$

This model has been revised by other researchers including White [144], Peeva *et al*. [86], Gibbins *et al.* [96], each playing around with different combinations of measurable physical properties and has been observed to provide a high correlation with their experimental

data and, at the time, proved to be the best model to describe the transport through relatively dense membranes. However, researchers have recently started to question the model proposed by Bhanushali *et al* [73]. In the article published by Geens *et al*. [71] for example, they pointed out the inaccurate representation of the relationship between the membrane sorption value and solvent flux. Bhanushali's model suggests that a high $\emptyset$ value, indicating a high affinity of the solvent towards the membrane, will result in low flux. Realistically, this is not true for hydrophobic membranes where greater solvent-membrane interactions, i.e. high degree of swelling, results in higher solvent fluxes. This model further predicts that a decrease in the surface tension, γ_M, or hydrophilicity, of the membrane will lead to high solvent fluxes. As Geens *et al*. [71] noted, this is once again not true for hydrophobic membranes were lower fluxes are expected. Darvishmanesh *et al.* [145] supported the arguments made by Geens *et al*. Therefore, Geens *et al*. [71] suggested a new model, shown in Equation 2.20, where the interaction parameters, $\emptyset^n$ and γ_M, is replaced by a single parameter describing solvent-membrane affinity:

$$J \sim \left(\frac{V_m}{\eta \Delta\gamma}\right) \tag{2.20}$$

where the parameter referring to the difference in surface tension between the membrane and the solvent, $\Delta\gamma$, is similar to that used by Machado *et al*. in resistance-in-series model, $\gamma_c - \gamma_l$, as given in Equation 2.12.

Although differing in structure, Bhanushali *et al.* [73] and Geens *et al.* [71] followed the same approach to propose their respective models, concluding that the transport of solutes, although balanced by convective and viscous flow contributions, is directed more toward convective transport.

Bhanushali's model was also questioned by Li *et al.* [146], stating that: 1) high sorption value should indicate higher flux due to greater solvent-membrane affinity, and 2) high surface energies should lead to greater fluxes due to improved solvent-membrane interactions. However, both these parameters are present in the denominator of Bhanushali's model, indicating an inverse relationship between flux and sorption value and surface tension, which is not the case. Li *et al.* [146] then also presented a new model, as given in Equation 2.21, based solely on differences in solubility parameter and polarity, which they classified as being the most important parameters for describing membrane flux and solvent separation.

$$J = \frac{1}{\Delta\delta_{iM} - \Delta\varepsilon_{iM}} \tag{2.21a}$$

with

$$\Delta\delta_{iM} = \left|{\delta_i}^2 - {\delta_M}^2\right|^{\frac{1}{2}} \tag{2.21b}$$

$$\Delta\varepsilon_{iM} = \left|{\varepsilon_i}^2 - {\varepsilon_M}^2\right|^{\frac{1}{2}} \tag{2.21c}$$

where $\Delta\delta_{im}$ is the difference between the solubility parameter of species σ_i and the membrane δ_M and $\Delta\varepsilon_{iM}$ is the difference between the dielectric constant of species ε_i and the membrane ε_M.

However, Li *et al.* [146] found that this model has a poor fit for the STARMEM™ series as the exact properties of these membranes are patent-protected which leads to an invalidation of the model. Good fit was however reported for Duramem® and MPF membranes.

For a binary system consisting of species i and j, Peeva *et al*. proposed a model, shown in Equation 2.22, requiring only measurable data and is similar to that of the classical solution-diffusion model presented in Equation 2.8.

$$J_{n,i} = P_{i,M}\left[C_{i,FM} - \frac{J_i}{J_i + J_j}.\frac{\gamma_{i,P}}{\gamma_{i,FM}}\exp\left(-\frac{V_{m,i}P}{RT}\right)\right] \tag{2.22}$$

where $P_{i,M}$ refers the permeance of species i through membrane M.

The Maxwell-Stefan equations were originally derived from kinetic theory to describe gas diffusion at low density but have been extended to be applicable to dense gases, liquids and polymers [147,148]. These equations have previously been used to successfully describe the transport of organic solvents across polymeric membranes [149–151].

The biggest advantage of using the Maxwell-Stefan equations over the Fickian law is its consideration of diffusional coupling effects between all species, i.e. membrane, solute and solvent [67]. This advantage was recognised by Silva *et al.* who derived a two-term Hagen-Poiseullie model, as shown in Equation 2.23, using the Maxwell-Stefan equations as a starting point for derivation and making two additional assumptions, namely: 1) friction between a species and the membrane is much higher than the friction between species, and 2) partial molar volumes of species are negligibly small [85].

$$J_V = \frac{\Delta P}{\eta_{mix}}\left[\bar{V}_{m,1}C_1\left(\frac{\varepsilon d_{pore}^2}{32l\tau}\right)_1 + \bar{V}_{m,2}C_2\left(\frac{\varepsilon d_{pore}^2}{32l\tau}\right)_2\right] \quad (2.23)$$

where η_{mix} refers to the viscosity of the binary solvent mixture.

Moreover, Paul [152] used the Maxwell-Stefan equations to make provision for the inherent limitation of the classic solution-diffusion model to describe solute-solvent coupling. Paul [152] went on to discuss these limitations which included limiting solute rejection to positive values, concentration difference within membrane approximated to be linear and unbounded to pressure driving force and the independent transport of solute and solvent. These limitations were negligible for desalination applications for which the solution-diffusion model was originally developed. Paul revisited the derivation of the solution-diffusion model and instead used the Maxwell-Stefan equations, resulting in the expression for solute (1) mass flux, $J_{m,1}$, coupled by solvent (2) transport through the frictional coupling coefficient, ε. He then adapted the classic solution-diffusion model to consider the effects of convective or frictional coupling between solute and solvent permeation through the membrane. Specifically, he derived the solution-diffusion model using Maxwell-Stefan equations as a starting point. Since the Maxwell-Stefan equations rely on inter-species force balances, i.e. thermodynamic driving force of a specie, df_i, is in equilibrium with the total friction force, it can predict diffusive coupling in multicomponent systems. In this case, the driving force, under isothermal conditions, becomes [117,127]:

$$df_i = \frac{x_i}{RT}\nabla\mu_i \quad (2.24)$$

With chemical potential as previously defined, the expression becomes:

$$\boldsymbol{df}_i = -\sum_{j\neq i} f_{ij}x_i x_j \times \left(\boldsymbol{u}_i - \boldsymbol{u}_j\right) \quad (2.25)$$

where f_{ij} is the drag coefficient and the mutual friction force between i and j are assumed proportional to the relative velocity, $\left(\boldsymbol{u}_i - \boldsymbol{u}_j\right)$ and the molar mass.

Introducing the Maxwell-Stefan diffusivity, $D_{ij} = \frac{1}{f_{ij}}$, the expression for a binary system becomes:

$$J_{m,1} = \frac{\rho D_{1,m}}{\bar{w}_{ml}\left(1+\varepsilon_1\frac{\bar{w}_2}{\bar{w}_m}\right)}\left(w_{1,0} - w_{1,l}\right) + \frac{\rho D_{2,m}}{\bar{w}_{ml}\left(1+\varepsilon_1\frac{\bar{w}_2}{\bar{w}_m}\right)}\left(w_{2,0} - w_{2,l}\right) \quad (2.26a)$$

with

$$\varepsilon_1 = \frac{MW_1}{MW_2}\frac{D_{1,m}}{D_{1,2}} \tag{2.26b}$$

$$\bar{w}_m = \frac{w_{2,0} - w_{2,l}}{\ln\left(\frac{1-w_{2,l}}{1-w_{2,0}}\right)} \tag{2.26c}$$

where w_i is the mass fractions and ρ the mass density of the mixture.

The Wessling group [153] later proved that the Maxwell-Stefan equations indeed take membrane-solvent-solute interactions into account and successfully used it to describe solvent fluxes for binary mixtures of methanol and isopropanol.

The phenomenological models, the Spiegler-Kedem and Kedem-Katchalsky models, existed prior to the solution-diffusion and pore-flow models and are derived based on irreversible thermodynamics theory which approximates the membrane as a black-box. These phenomenological models however provide no insight into mechanistic transport and are often limited to aqueous systems for RO membranes [146,154,155]. The Spiegler-Kedem and Kedem-Katchalsky models describe the solute flux, J_s, as given in Equations 2.27 and 2.28, respectively, while solvent flux, J_w, is described as given in Equation 2.29 [156,157]:

$$J_s = B\Delta\pi + (1-\sigma)C_{avg}J_w \tag{2.27}$$

$$J_s = B\Delta x\frac{dC}{dx} + (1-\sigma)J_w C_{avg} \tag{2.28}$$

with

$$J_w = A(\Delta P - \sigma\Delta\pi) \tag{2.29}$$

where C_{avg} is the average solute concentration and other key parameters are defined as,

$$A = \left(\frac{J_w}{\Delta P}\right)_{\Delta\pi=0} \tag{2.30}$$

$$B = \left(\frac{J_s}{\Delta\pi}\right)_{J_w=0} \tag{2.31}$$

$$\sigma = \left(\frac{\Delta P}{\Delta\pi}\right)_{J_w=0} \tag{2.32}$$

These phenomenological models were often used to describe the transport of charged solutes in aqueous media through RO membranes and have been proven successful in this application [158–160]. The Spiegler-Kedem and Kedem-Katchalsky models have also been attempted for application in organic solvents with contrasting observations. Refer to Section A.3.5 in Appendix A for additional literature regarding the origins and derivations of the Spiegler-Kedem and Kedem-Katchalsky models.

Geens *et al.* [154] found a high correlation between various reflection coefficient models in the Spiegler-Kedem equations and experimental values of organic solute rejection from methanol, ethanol, acetate and EA. Similar success was achieved by Labanda *et al.* [161] for describing the permeation of NaCl-water solutions through the polymer nanofiltration membranes, Desal-5 DK, UTC-70UB, SE and SW30HR320. However, Van der Bruggen *et al.* [162] reviewed the applicability of the Spiegler-Kedem model to describe the behaviour of organic solvents (including methanol, ethanol, isopropanol, EA, toluene, etc.) through polymer nanofiltration membranes (NF270, NTR 7450 and UTC20) but found deviations from experimental data which were attributed to deviations in the calculation of the reflection coefficients. They claimed that the reflection correlations, as listed in Section A.3.5 of Appendix A, are based on an “idealized view of the membrane structure” and can be considered as a theoretical approximation at best, especially the steric hindrance and Zeman and Wales model. Furthermore, it was noted by Bhanushali *et al.* [138] that the Spiegler-Kedem model also disregards solvent-membrane interactions. Due to these inconsistencies, the application of solution-diffusion and pore-flow models has enjoyed prevalence for application in organic media.

In summary, Table 2.7 provides a collection of the transport models reviewed.

Table 2.7: Collection of literature-based transport models

Model name	Expression
Solution-diffusion	
Classic solution-diffusion	$J_{n,i} = \frac{D_i K_i}{l}\left[C_{i,FM} - C_{i,P}\frac{\gamma_{i,P}}{\gamma_{i,MP}}\exp\left(-\frac{V_{m,i}\times(P_{MP}-P_P)}{RT}\right)\right]$
Peeva *et al*.	$J_{n,i} = P_{i,M}\left[C_{i,FM} - \frac{J_{n,i}}{J_{n,i}+J_{n,j}}.\frac{\gamma_{i,P}}{\gamma_{i,FM}}\exp\left(-\frac{V_{m,i}P}{RT}\right)\right]$
Bhanushali *et al.* model	$J \sim \left(\frac{V_m}{\eta}\right)\left(\frac{1}{\emptyset^n \gamma_m}\right)$
Geens *et al*. model	$J \sim \left(\frac{V_m}{\eta \Delta\gamma}\right)$
Pore-flow	
One-term Hagen-Poiseuille	$J_V = \frac{\varepsilon {d_{pore}}^2}{32l\tau}\times\frac{P_o - P_z}{\eta}$
Silva *et al*. (two-term Hagen-Poiseuille)	$J_V = \frac{\Delta P}{\eta_{mix}}\left[\bar{V}_{m,1}C_1\left(\frac{\varepsilon d_{pore}^2}{32l\tau}\right)_1 + \bar{V}_{m,2}C_2\left(\frac{\varepsilon d_{pore}^2}{32l\tau}\right)_2\right]$
Kozeny-Carmen	$J_V = \frac{\varepsilon^3}{Kls^2(1-\varepsilon)^2}\times\frac{P_o - P_z}{\eta}$
Combinations of solution-diffusion and pore-flow	
Solution-diffusion-with-imperfections	$J_V = \frac{C_{i,M}D_{i,M}V_{m,i}}{RTl}\Delta P + \frac{C_{i,M}B_o}{\eta l}\Delta P$
Machado *et al*. (resistance-in-series)	$J_V = \frac{\Delta P}{\emptyset\left[(\gamma_c - \gamma_l) + f_{1,n}\right] + f_{2,n}}$
Phenomenological	
Kedem-Katchalsky	$J_s = B\Delta\pi + (1-\sigma)C_{avg}J_w$
Spiegler-Kedem	$J_s = B\Delta x\frac{dC}{dx} + (1-\sigma)J_w C_{avg}$

2.6 Concluding Remarks

Hydroformylation, a reaction of considerable value within an industrial context, often utilizes expensive homogeneous catalysts. Literature verified that conventional homogeneous catalyst recovery methods, such as those employed by BASF, Union Carbide, RHC/RP, etc., although offering high relative recoveries, are cost-intensive and often require high temperatures (*ca*. 100 – 300 °C). Therefore, over the years, efforts have been directed to the research and implementation of "alternative" recovery methods, such as the use of supported catalysts, metal scavengers, ionic liquids, etc. Of these "alternative" methods, this study finds membrane technology to be most suited for homogeneous catalyst reaction within the context of the hydroformylation reaction.

OSN, referring to membranes that have been enhanced in terms of solvent resistance, has been proposed for catalyst recovery since the 1970's where it was first highlighted by Goldup and Gosser, then later established through the pioneering work by the research groups of Livingston and Vankelecom. Recently, research efforts have been directed to validate the economic benefits of using OSN for catalyst recovery compared to conventional methods.

In terms of OSN species transport modelling, its importance was emphasised but various contradictions in researcher findings were identified. Literature highlights two main principle models, namely the pore-flow model and the solution-diffusion model, each based on their own set of assumptions. Throughout the years, researchers have proposed new models based on these two principle models with the intention of adding complexity pr improving model predictive accuracy. However, these newly proposed model variations tend to be rather application specific and therefore are non-relatable across membranes and operating conditions. Based on the classic pore-flow model, the Kozeny-Carmen, resistance-in-series and surface force pore-flow models were proposed. In the case of the classic solution-diffusion model, Bhanushali *et al.* and Geens *et al*. proposed simplified variations of this model using easily measurable parameters,namely solvent viscosity, molar volume and solvent-membrane affinity, i.e. the surface energy of the membrane material, membrane sorption, etc. Peeva *et al*. then proceeded to further improve on the classic solution-diffusion model by improving the description of flow coupling effects, i.e. solvent-solvent interactions, by incorporating the partial fluxes of each solvent passing through the membrane.

2.7 References

[1] M. Priske, K.D. Wiese, M. Kraume, C. Baumgarten, *J. Memb. Sci*. **360** (2010) 77-83.

[2] G.D. Frey, *J. Organomet. Chem*. **754** (2014) 5–7.

[3] A.C.J. Koeken, L.J.P. Van den Broeke, B. Deelman, J.T.F. Keurentjes, *J. Mol. Catal. A Chem.* **346** (2011) 1–11.

[4] J. Fang, R. Jana, J.A. Tunge, B. Subramaniam, *Appl. Catal. A Gen.* **393** (2011) 294-301.

[5] T. Ichihara, K. Nakano, M. Katayama, K. Nozaki, *Chem. Asian J.* **3** (2008) 1722-1728.

[6] H.S. Ahn, S.H. Han, S.J. Uhm, W.K. Seok, H.N. Lee, G.A. Korneeva, *J. Mol. Catal. A Chem*. **144** (1999) 295–306.

[7] S.S. Divekar, R.M. Bhanage, R.M. Deshpande, R. V. Gholap, R. V. Chaudhari, *J. Mol. Catal.* **91** (1994) L1–L6.

[8] R.M. Deshpande, S.S. Divekar, *J. Mol. Catal.* **67** (1991) 333–338.

[9] B.M. Bhanage, S.S. Divekar, R.M. Deshpande, R.V. Chaudhari, *J. Mol. Catal. A Chem.* **115** (1997) 247–257.

[10] Y. Yuki, K. Takahashi, Y. Tanaka, K. Nozaki, *J. Am. Chem. Soc.* **135** (2013) 17393–17400.

[11] K. Takahashi, M. Yamashita, K. Nozaki, *J. Am. Chem. Soc*. **134** (2012) 18746–18757.

[12] F. Ungvary, *Coord. Chem. Rev.* **251** (2007) 2072–2086.

[13] M. Englisch, V.S. Ranade, J.A. Lercher, *Appl. Catal. A Gen*. **163** (1997) 111–122.

[14] D. Evans, T.A. Osborn, G. Wilkinson, *J. Chem. Soc*. **11** (1968) 3133–3142.

[15] P.W.N.M. Van Leeuwen, **Rhodium Catalyzed Hydroformylation: Catalysis by Metal Complexes**, Volume 22, Kluwer Academic Publishers, The Netherlands, 2000.

[16] P.W.N.M. Van Leeuwen, **Homogeneous Catalysis - Understanding the art**, Kluwer Academic Publishers, The Netherlands, 2004.

[17] D.J. Cole-Hamilton, T.P. Tooze, **Catalyst Separation, Recovery and Recycling: Chemistry and Process Design**, Springer, The Netherlands, 2006.

[18] A. Behr, P. Neubert, **Applied Homogeneous Catalysis**, Wiley VCH, Germany, 2012.

[19] D.F. Foster, D. Gudmunsen, D.J. Adams, A.M. Stuart, E.G. Hope, D.J. Cole-Hamilton, P. Schwarz, P. Pogorzelec, *Tetrahedron.* **58** (2002) 3901–3910.

[20] K. Mukhopadhyay, A.B. Mandale, R. V. Chaudhari, *Chem. Mater*. **15** (2003) 1766-1777.

[21] D. Guha, H. Jin, M.P. Dudukovic, P.A. Ramachandran, B. Subramaniam, *Chem. Eng. Sci.* **62** (2007) 4967–4975.

[22] A. Behr, D. Obst, C. Schulte, T. Schosser, *J. Mol. Catal. A Chem*. **206** (2003) 179-184.

[23] S.K. Sharma, R. V. Jasra, *Catal. Today.* **247** (2015) 70–81.

[24] R. Meijboom, M. Haumann, A. Roodt, L. Damoense, *Helv. Chim. Acta*. **88** (2005) 676–693.

[25] A. Dabbawala, **Cobalt catalyzed hydroformylation of higher olefins in the presence of various mass transfer promoters under aqueous biphasic conditions**, 2010.

[26] D. Wu, Y. Wang, G. Li, J. Jiang, Z. Jin, *Catal. Commun.* **44** (2014) 54–56.

[27] G. Achonduh, Q. Yang, H. Alper, *Tetrahedron.* **71** (2015) 1241–1246.

[28] E. Mieczynska, A.M. Trzeciak, J.J. Ziolkowski, I. Kownacki, B. Marciniec, *J. Mol. Catal. A Chem*. **237** (2005) 246–253.

[29] J.K. MacDougall, D.J. Cole-Hamilton, *J. Chem. Soc.* (1990) 165–167.

[30] A. Cano-Odena, P. Vandezande, D. Fournier, W. Van Camp, *Chem. A Eur. J.* **16** (2010) 1061–1067.

[31] S. Darvishmanesh, L. Firoozpour, J. Vanneste, P. Luis, J. Degrève, B. Van der Bruggen, *Green Chem*. **13** (2011) 3476–3483.

[32] M. Beller, B. Cornils, C.D. Frohning, C.W. Kohlpainter, *J. Mol. Catal. A Chem.* **104** (1995) 17–85.

[33] B. Cornils, E.G. Kuntz, *J. Organomet. Chem*. **502** (1995) 177–186.

[34] J. Fang, **Towards a Benign and Viable Rhodium Catalyzed Hydroformylation of Higher Olefins: Economic and Environmental Impact Analyses, Solvent Effects and Membrane-based Catalyst Separation**, 2009.

[35] A. Sharma, **Catalytic Reaction Engineering using Ionic Liquids: Hydroformylation of 1-Octene**, Toulouse, 2009.

[36] T. Schäfer, C.M. Rodriques, C.A.M. Afonso, J.G. Crespo, *Chem. Commun*. (2001) 1622–1623.

[37] Y. Chauvin, L. Mussmann, H. Olivier, *Angew. Chemie*. **107** (1995) 2915–2917.

[38] E. Perperi, Y. Huang, P. Angeli, G. Manos, D.J. Cole-Hamilton, *J. Mol. Catal. A Chem.* **221** (2004) 19–27.

[39] Y. Huang, E. Perperi, G. Manos, D.J. Cole-Hamilton, *J. Mol. Catal. A Chem*. **210** (2004) 17–21.

[40] L.M. Rossi, L.L.R. Vono, F.P. Silva, P.K. Kiyohara, E.L. Duarte, J.R. Matos, *Appl. Catal. A Gen.* **330** (2007) 139–144.

[41] M.F. Sellin, P.B. Webb, D.J. Cole-Hamilton, *Chem. Commun*. (2001) 781–782.

[42] R.L. Pruett, J.A. Smith, **Hydroformylation Process**, US3,527,809, 1970.

[43] R.L. Pruett, J.A. Smith, **Hydroformylation of olefins**, US4,148,830, 1979.

[44] Â.C.B. Neves, M.F. Calvete, M.V.D. Pinho, M.M. Pereira, *European J. Org. Chem*. (2012) 6309–6320.

[45] C.P. Mehnert, R.A. Cook, N.C. Dispenziere, M. Afeworki, *J. Am. Chem. Soc*. **124** (2002) 12932–12933.

[46] I.T. Horvàth, J. Ràbai, *Science.* **266** (1994) 72–75.

[47] T. Mathivet, E. Monflier, Y. Castanet, A. Mortreux, J. Couturier, *Tetrahedron*. (2002) 3877–3888.

[48] I.T. Horvàth, G. Kiss, R.A. Cook, J.E. Bond, P.A. Stevens, J. Ràbai, E.J. Mozeleski, *J. Am. Chem. Soc.* **120** (1998) 3133–3143.

[49] W. Leitner, *Acc. Chem. Res*. **35** (2002) 746–756.

[50] P.G. Jessop, W. Leitner, **Chemical Synthesis Using Supercritical Fluids**, Wiley VCH, Weinheim, 1999.

[51] P.G. Jessop, T. Ikariya, R. Noyori, *Chem. Rev*. **99** (1999) 475–493.

[52] J.W. Rathke, R.J. Klinger, T.R. Krause, *Am. Chem. Soc.* **10** (1991) 1350–1355.

[53] M. Mulder, **Basic Principles of Membrane Technology**, Kluwer Academic Publishers, The Netherlands, 1991.

[54] J.L. Humphrey, G.E. Keller, Separation Process Technology, McGraw-Hill & Hall, New York, 1997.

[55] P. Vandezande, L.E.M. Gevers, I.F.J. Vankelecom, *Chem. Soc. Rev*. **37** (2008) 365–405.

[56] R.W. Baker, **Membrane Technology and Applications**, 2nd Ed., John Wiley & Sons, Ltd., England, 2004.

[57] E. Drioli, L. Giorno, **Membrane Operations: Innovative Separations and Transformations**, Wiley VCH, Weinheim, 2009.

[58] Y. Zhao, Q. Yuan, *J. Memb. Sc*i. **279** (2006) 453–458.

[59] J. Dasgupta, D. Mondal, S. Chakraborty, J. Sikder, S. Curcio, H.A. Arafat, *Ecotoxicol. Environ. Saf.* **121** (2015) 22–30.

[60] C. Gherasim, K. Hancková, P. Mikulá, *J. Memb. Sci*. **490** (2015) 46–56.

[61] S. Sun, L. Cai, X. Nie, X. Song, J. Yu, *J. Water Process Eng*. **7** (2015) 210–217.

[62] A. Munir, **Dead End Membrane Filtration**, 2006.

[63] W. Stolp, **Nickel Recovery From Spent Electrolyte By Nanofiltration**, Potchefstroom, 2007.

[64] I. Gàllego, R. Mallada, E.P. Urriolabeitia, R. Navarro, M. Menèndez, J. Santamarìa, *Inorganica Chim. Acta*. 357 (2004) 4577-4581.

[65] R. Hughes, K. Scott, **Industrial Membrane Separation Technology**, Chapman & Hall, Glasgow, 1996.

[66] X.Q. Cheng, Y.L. Zhang, Z.X. Wang, Z.H. Guo, Y.P. Bai, L. Shao, *Adv. Polym. Technol.* (2014) 1–24.

[67] L. Hesse, J. Mićović, P. Schmidt, A. Górak, G. Sadowski, *J. Memb. Sci*. **428** (2013) 554–561.

[68] M. Janssen, C. Müller, D. Vogt, *Green Chem.* **13** (2011) 2247.

[69] P. Lutze, A. Gorak, *Chem. Eng. Res. Des*. **91** (2013) 1978–1997.

[70] S. Darvishmanesh, J. Degrève, B. Van der Bruggen, *Phys. Chem. Chem. Phys*. **12** (2010) 13333–13342.

[71] J. Geens, B. Van der Bruggen, C. Vandecasteele, *Sep. Purif. Technol.* **48** (2006) 255–263.

[72] I.F.J. Vankelecom, K. De Smet, L.E.M. Gevers, A. Livingston, D. Nair, S. Aerts, S. Kuypers, P.A. Jacobs, *J. Memb. Sci.* **231** (2004) 99–108.

[73] D. Bhanushali, S. Kloos, C. Kurth, D. Bhattacharyya, *J. Memb. Sci.* **189** (2001) 1–21.

[74] J.P. Robinson, E.S. Tarleton, C.. R. Millington, A. Nijmeijer, *J. Memb. Sci*. **230** (2004) 29–37.

[75] B. Van der Bruggen, J. Geens, C. Vandecasteele, *Chem. Eng. Sci.* **57** (2002) 2511-2518.

[76] D.F. Stamatialis, N. Stafie, K. Buadu, M. Hempenius, M. Wessling, *J. Memb. Sci.* **279** (2006) 424–433.

[77] A. Goldup, M.T. Westaway, G. Walker, **Separation of Metal Compounds**, US3,645,891, 1972.

[78] L.W. Gosser, W.H. Knoth, G.W. Parshall, **Reverse Osmosis in Homogeneous Catalysis**, J. Mol. Catal. 2 (1977) 253–263.

[79] L.W. Gosser, **Membrane separation of homogeneous catalysts from nitrile solutions**, US3,853,754, 1974.

[80] L. Peeva, J.D.S. Burgal, I. Valtcheva, A.G. Livingston, *Chem. Eng. Sci*. **116** (2014) 183–194.

[81] W.E. Siew, C. Ates, A. Merschaert, A.G. Livingston, *Green Chem*. **15** (2013) 663-674.

[82] A. Tsoukala, L. Peeva, A.G. Livingston, H. Bjòrsvik, *ChemSusChem*. **5** (2012) 188–193.

[83] C. Roengpithya, D.A. Patterson, P.C. Taylor, A.G. Livingston, *Desalination*. **199** (2006) 195–197.

[84] H. Wong, Y.H. See-Toh, F.C. Ferreira, R. Crook, A.G. Livingston, *Chem*. *Commun*. *(Camb).* (2006) 2063–2065.

[85] P. Silva, S. Han, A.G. Livingston, *J. Memb. Sci.* **262** (2005) 49–59.

[86] L.G. Peeva, E. Gibbins, S.S. Luthra, L.S. White, R.P. Stateva, A.G. Livingston, *J. Memb. Sci.* **236** (2004) 121–136.

[87] J.T. Scarpello, D. Nair, L.M. Freitas Dos Santos, L.S. White, A.G. Livingston, *J. Memb. Sci.* **203** (2002) 71–85.

[88] S.S. Luthra, X. Yang, L.M. Freitas Dos Santos, L.S. White, A.G. Livingston, *J. Memb. Sci*. **201** (2002) 65–75.

[89] D. Nair, J.T. Scarpello, I.F.J. Vankelecom, L.M. Freitas Dos Santos, L.S. White, R.J. Kloetzing, T. Welton, A.G. Livingston, *Green Chem*. **4** (2002) 319–324.

[90] D. Nair, J.T. Scarpello, L.S. White, L.M. Freitas Dos Santos, I.F.J. Vankelecom, A.G. Livingston, *Tetrahedron Lett*. **42** (2001) 8219–8222.

[91] K. Vanherck, G. Koeckelberghs, I.F.J. Vankelecom, *Prog. Polym. Sci.* **38** (2013) 874–896.

[92] S. Aerts, A. Buekenhoudt, H. Weyten, L.E.M. Gevers, I.F.J. Vankelecom, P.A. Jacobs, *J. Memb. Sci*. **280** (2006) 245–252.

[93] S.A. Chavan, W. Maes, L.E.M. Gevers, J. Wahlen, I.F.J. Vankelecom, P.A. Jacobs, W. Dehaen, D.E. De Vos, *Chem. - A Eur. J*. **11** (2005) 6754–6762.

[94] P.G.N. Mertens, M. Bulut, L.E.M. Gevers, I.F.J. Vankelecom, P.A. Jacobs, D.E. De Vos, *Catal. Letters.* **102** (2005) 57–61.

[95] S. Aerts, H. Weyten, A. Buekenhoudt, L.E.M. Gevers, I.F.J. Vankelecom, P.A. Jacobs, *Chem. Commun. (Camb).* (2004) 710–711.

[96] E. Gibbins, M. D'Antonio, D. Nair, L.S. White, L.M. Freitas dos Santos, I.F.J. Vankelecom, A.G. Livingston, *Desalination*. **147** (2002) 307–313.

[97] K. De Smet, S. Aerts, E. Ceulemans, I.F.J. Vankelecom, P.A. Jacobs, *Chem. Commun.* (2001) 597–598.

[98] A. Keraani, T. Renouard, C. Fischmeister, C. Bruneau, *ChemSusChem*. **11** (2008) 927–933.

[99] D. Schoeps, K. Buhr, M. Dijkstra, K. Ebert, H. Plenio, *Chem. - A Eur. J.* (2009) 3922–3927.

[100] P. Van der Gryp, A. Barnard, J.P. Cronje, D. de Vlieger, S. Marx, H.C.M. Vosloo, *J. Memb. Sci.* **353** (2010) 70–77.

[101] M. Rabiller-Baudry, G. Nasser, T. Renouard, D. Delaunay, M. Camus, *Sep. Purif. Technol.* **116** (2013) 46–60.

[102] D. Ormerod, B. Sledsens, G. Vercammen, D. Van Gool, T. Linsen, A. Buekenhoudt, B. Bongers, *Sep. Purif. Technol.* **115** (2013) 158–162.

[103] N.S.A. Razak, M.S. Shaharun, H. Mukhtar, M.F. Taha, *Sains Malaysiana.* **42** (2013) 515–520.

[104] P. Schmidt, E.L. Bednarz, P. Lutze, A. Górak, *Chem. Eng. Sci.* **115** (2014) 115–126.

[105] J. Dreimann, P. Lutze, M. Zagajewski, A. Behr, A. Gòrak, A.J. Vorholt, *Chem. Eng. Process.* (2015) 1–26.

[106] E.L. V. Goetheer, A.W. Vekerk, L.J.P. van den Broeke, E. de Wolf, B. Deelman, G. van Koten, J.T.F. Keurentjies, *J. Catal*. **219** (2003) 126–133.

[107] U. Kragl, C. Dreisbach, *Angew. Chemie Int. Ed. English*. **35** (1996) 642–644.

[108] G. Giffels, J. Beliczey, M. Felder, U. Kragl, *Tetrahedron*. **9** (1998) 691–696.

[109] N. Brinkmann, D. Giebel, G. Lohmer, M.T. Reetz, U. Kragl, *J. Catal*. **183** (1999) 163–168.

[110] D. de Groot, E.B. Eggeling, J.C. de Wilde, H. Kooijman, R.J. van Haaren, A. van de Made, A.L. Spek, D. Vogt, J.N.H. Reek, P.C.J. Kramer, P.W.N.M. Van Leeuwen, *Chem. Commun*. (1999) 1623–1624.

[111] D. Nair, S.S. Luthra, J.T. Scarpello, L.S. White, L.M. Freitas Dos Santos, A.G. Livingston, *Desalination*. **147** (2002) 301–306.

[112] A. Datta, K. Ebert, H. Plenio, *Organometallics*. **22** (2003) 4685–4691.

[113] P.T. Witte, S.R. Chowdhury, J.E. ten Elshof, D. Sloboda-Rozner, R. Neumann, P.L. Alsters, *Chem. Commun*. (2005) 1206–1208.

[114] C.J. Pink, H. Wong, F.C. Ferreira, A.G. Livingston, *Org. Process Res. Dev.* **12** (2008) 589–595.

[115] D. Nair, H. Wong, S. Han, I.F.J. Vankelecom, L.S. White, A.G. Livingston, A.T. Boam, *Org. Process Res. Dev.* **13** (2009) 1471–1477.

[116] T.R. Long, A. Gupta, A.L. Miller II, D.G. Rethwisch, N.B. Bowden, *J. Mater. Chem*. **21** (2011) 14265–14276.

[117] P. Marchetti, M.F.J. Solomon, G. Szekely, A.G. Livingston, *Chem. Rev.* **114** (2014) 10735–10806.

[118] P. Schmidt, P. Lutze, *J. Memb. Sci*. **429** (2013) 103–120.

[119] P. Wijkens, J.T.B.H. Jastrzebski, P.A. Van der Schaaf, R. Kolly, A. Hafner, G. Van Koten, *Org. Lett.* **7** (2000) 10–13.

[120] D. Ormerod, B. Bongers, W. Porto-carrero, S. Giegas, G. Vijt, Y. Chauvin, R.H. Grubbs, R.H. Schrock, *RSC Adv.* **3** (2013) 21501–21510.

[121] R. Machado, D. Hasson, R. Semiat, *J. Memb. Sci.* **163** (1999) 93–102.

[122] J.A. Whu, B.C. Baltzis, K.K. Sirkar, *J. Memb. Sci*. **170** (2000) 159–172.

[123] M. Soltanieh, W.N. Gill, *Chem. Eng. Commun*. **12** (1981) 279.

[124] E.A. Mason, H.K. Lonsdale, *J. Memb. Sci.* (1990) 1–81.

[125] J.S. Vrentas, C.M. Vrentas, *Chem. Eng. Sci.* **57** (2002) 4199–4208.

[126] D. Bhanushali, D. Bhattacharyya, *Ann. New York Acad. Sci.* **177** (2003) 159–177.

[127] P. Marchetti, A.G. Livingston, *J. Memb. Sci*. **476** (2015) 530–553.

[128] S.C. George, S. Thomas, *Prog. Polym. Sci*. **26** (2001) 985–1017.

[129] R. Valadez-blanco, A.G. Livingston, *J. Memb. Sci.* **326** (2009) 332–342.

[130] A. Miyagi, H. Nabetani, M. Nakajima, *Sep. Purif. Technol*. **88** (2012) 216–226.

[131] N. Stafie, D.F. Stamatialis, M. Wessling, *J. Memb. Sci.* **228** (2004) 103–116.

[132] J.G. Wijmans, R.W. Baker, *J. Memb. Sci*. **107** (1995) 1–21.

[133] G. Jonsson, C.E. Boesen, *Desalination*. **17** (1975) 145–165.

[134] X.J. Yang, A.G. Livingston, L. Freitas Dos Santos, *J. Memb. Sci*. **190** (2001) 45–55.

[135] R. Machado, D. Hasson, R. Semiat, *J. Memb. Sci.* **166** (2000) 63–69.

[136] T. Matsuura, S. Sourirajan, *Ind. Eng. Chem. Process Des. Dev*. **20** (1981) 273–282.

[137] S. Jain, S.K. Gupta, *J. Memb. Sci.* **232** (2004) 45–61.

[138] D. Bhanushali, S. Kloos, D. Bhattacharyya, *J. Memb. Sci*. **208** (2002) 343–359.

[139] B.A. Farnard, F.D.F. Talbot, *Ind. Eng. Chem. Process Des. Dev.* **22** (1983) 179–187.

[140] H. Mehdizadeh, J.M. Dickson, *J. Memb. Sci.* **42** (1989) 119–145.

[141] H. Mehdizadeh, J.M. Dickson, *J. Appl. Polym. Sci.* **42** (1991) 1143–1154.

[142] W.R. Bowen, J.S. Welfoot, *Desalination*. **147** (2002) 197–203.

[143] W.B. Richard, H. Mukhtar, *J. Memb. Sci*. **112** (1996) 263–274.

[144] L.S. White, *J. Memb. Sci.* **205** (2002) 191–202.

[145] S. Darvishmanesh, A. Buekenhoudt, J. Degrève, B. Van der Bruggen, *J. Memb. Sci*. **334** (2009) 43–49.

[146] J. Li, M. Wang, Y. Huang, B. Luo, *RSC Adv.* **4** (2014) 37375–37380.

[147] R.B. Bird, W.E. Stewart, E.N. Lightfoot, **Transport Phenomena**, 2nd Ed., John Wiley & Sons, Ltd., Danvers, MA, 2002.

[148] C.F. Curtiss, R.B. Bird, *Ind. Eng. Chem. Res*. **38** (1999) 2515–2522.

[149] L.E.M. Gevers, G. Meyen, K. De Smet, P. Van de Velde, F. Du, I.F.J. Vankelecom, P.A. Jacobs, *J. Memb. Sci.* **274** (2006) 173–182.

[150] P. Izák, L. Bartovská, K. Friess, P. Uchytil, *J. Memb. Sci.* **214** (2003) 293–309.

[151] T.R. Noordman, J.A. Wesselingh*, J. Memb. Sci.* **210** (2002) 227–243.

[152] D.R. Paul, *J. Memb. Sci.* **241** (2004) 371–386.

[153] S. Postel, S. Wessel, T. Keil, P. Eiselt, M. Wessling, *J. Memb. Sci.* **466** (2014) 361-369.

[154] J. Geens, K. Boussu, C. Vandecasteele, B. Van Der Bruggen, *J. Memb. Sci.* **281** (2006) 139–148.

[155] O. Kedem, A. Katchalsky, *J. Gen. Physiol.* **45** (1961) 143–179.

[156] G.H. Koops, S. Yamada, S.I. Nakao, *J. Memb. Sci*. **189** (2001) 241–254.

[157] K.S. Spiegler, O. Kedem, *Desalination*. **1** (1966) 311–326.

[158] A.M. Hidalgo, G. Leòn, M. Gòmez, M.D. Murcia, E. Gòmez, J.L. Gòmez, *Desalination*. **315** (2013) 70–75.

[159] A.L. Ahmad, M.F. Chong, S. Bhatia, *J. Memb. Sci.* **253** (2005) 103–115.

[160] T. Fukuda, W. Yang, A. Yamauchi, *J. Memb. Sci.* **212** (2003) 255–261.

[161] J. Labanda, J. Sabaté, J. Llorens, *Desalination*. **315** (2013) 83–90.

[162] B. Van der Bruggen, J. Schaep, D. Wilms, C. Vandecasteele, *Sep. Sci. Technol*. **35** (2000) 169–182.

CHAPTER 3: Materials and Methods

3.1 Overview

This chapter provides a detailed description of the experimental procedures followed in this investigation and is subdivided into seven sections, starting with Section 3.2 which gives details on the different membranes, catalysts and chemicals used. Sections 3.3 and 3.4 highlights the procedures used to perform the hydroformylation reaction and OSN experiments, respectively and Section 3.5 includes details regarding the analytical equipment used. Details regarding the membrane sorption tests are discussed in Section 3.6. This chapter is then concluded with Section 3.7 which presents the experimental design in terms of manipulated, response and constant parameters selected for this investigation.

3.2 Materials

3.2.1 Membranes used

Commercially available organic solvent nanofiltration (OSN) membranes from the STARMEM^{TM} and Duramem® series were considered for this investigation and were all purchased from Membrane Extraction Technology (MET) Ltd. which forms part of Evonik Industries since 2010 [1]. All membranes used were supplied in dry form and were soaked in preservation oil during manufacture as a measure of protection against drying out and contamination. Details of the membrane manufacturer and its specifications are summarised in Table 3.1.

Table 3.1: Summary of the specifications for the STARMEM^{TM} and Duramem® series membranes used

	STARMEM^{TM} 240	**Duramem® 150**	**Duramem® 200**
MWCO[a]	400	150	200
Membrane material	Polyimide	Polyimide	Polyimide
Membrane type	Hydrophobic	Hydrophilic	Hydrophilic
Solubility parameter[b]	23.2 $MPa^{0.5}$	23.2 $MPa^{0.5}$	23.2 $MPa^{0.5}$
Flux[c]	50 $L.m^{-2}.h^{-1}$	7.5 $L.m^{-2}.h^{-1}$	13 $L.m^{-2}.h^{-1}$

[a] Molecular weight cut-off, defined as the molecular weight for which a membrane will achieve a 90% rejection; MWCO values were determined according to procedures previously described [2,3].
[b] Solubility parameter approximated based on Matrimid 5218 [4,5].
[c] Experimentally determined based on pure toluene (membrane pretreatment and hydroformylation reaction solvent) at 30 bar transmembrane pressure.

These membranes are specifically designed to offer compatibility with organic solvents and are manufactured using polyimides such as Matrimid 5218 and Lenzing P84 with molecular structures as shown in Figure 3.1.

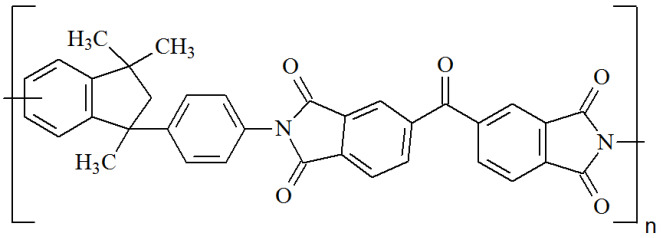

Matrimid 5218

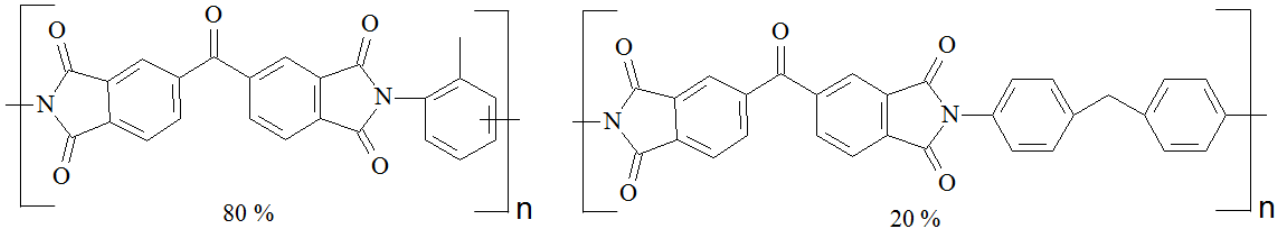

Lenzing P84

Figure 3.1: Chemical structures of typical membrane polyimides Matrimid 5218 and Lenzing P84 (redrawn from [6,7])

Previous studies have shown that these membranes have been successfully used for the recovery of homogeneous catalysts based on palladium, rhodium, manganese and ruthenium from organic solvent reaction systems including addition [8–10], coupling [11–13], epoxidation [14] and substitution [15–17] reactions with most cases reporting catalyst recoveries in excess of 99%. Considering the hydroformylation reaction using rhodium- and cobalt-based complexes, as investigated in this study, Gosser *et al.,* in 1977, was the earliest recorded publication, to the best knowledge of the author, documenting the success of using reverse osmosis membranes for homogeneous catalyst recovery [18]. More recently, Priske *et al.* [19] and Fang *et al.* [20] conducted detailed studies of a proposed integrated hydroformylation-OSN system and using the STARMEM^{TM} series membranes for catalyst recovery. Both these publications reported catalyst recovery values in excess of 85% with Priske and co-workers consistently achieving >99%.

3.2.2 Catalysts used

Two well-known and commercially available catalysts, tris(triphenylphosphine)rhodium(I) carbonyl hydride (98 wt%) and cobalt(III) acetylacetonate (98 vol%), as illustrated in Figure 3.2, were used in this study. Previous studies have confirmed the success of the rhodium-based [21–26] and cobalt-based catalysts [27–30] in the hydroformylation of olefins.

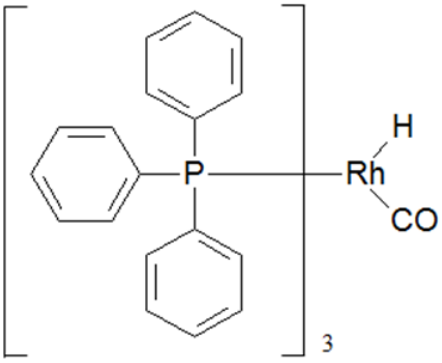

Commercially available from Sigma Aldrich

$HRh(CO)(PPh_3)_3$

Tris(triphenylphosphine)rhodium(I) carbonyl hydride (98 wt%)

MW = 920 $g.mol^{-1}$

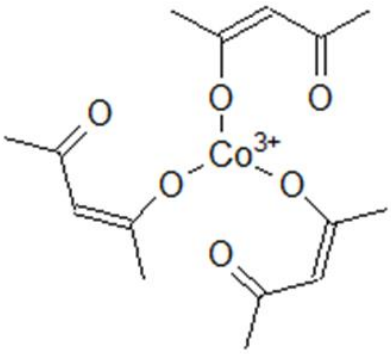

Commercially available from Sigma Aldrich

$Co(C_5H_7O_2)_3$

Cobalt(III) acetylacetonate (98 wt%)

MW = 356 $g.mol^{-1}$

Figure 3.2: Homogeneous hydroformylation catalysts used in this study

3.2.3 Chemicals used

1-Octene (98 vol%), 1-decene (94 vol%), 1-nonanal (>95 wt%), 1-undecanal (>96 wt%), 1-nonanol (98 vol%), 1-undecanol (>96 wt%), *n*-dodecane (>99 vol%) and toluene (99.8 vol%) were all purchased from Sigma Aldrich and were used for both hydroformylation and OSN experiments. Toluene was also used to perform the membrane pretreatment and as solvent for gas chromatography (GC) analyses while *n*-dodecane was used as the internal standard. High purity nitrogen and synthesis gases ($CO:H_2$, 1:1) were supplied by Afrox.

All the aforementioned chemicals were used as is with no further purification. Table 3.2 presents a few relevant literature and calculated properties of the chemicals used.

Table 3.2: List of relevant chemical properties[a] [31–33]

	MW ($g.mol^{-1}$)	V_m ($cm^3.mol^{-1}$)	η ($mPa.s^{-1}$)	μ_D (D)	δ[b] ($MPa^{0.5}$)
Toluene	92.1	107	0.551	0.375	18.7
1-Octene	112	157	0.452	0.340	15.6
1-Decene	140	187	0.748	0.420	16.0
1-Nonanal	142	172	1.35	2.84	19.0
1-Undecanal	170	206	1.73	2.50	18.7
1-Nonanol	144	174	9.32	1.61	20.7
1-Undecanol	172	208	15.5	1.62	20.3

[a] All properties obtained at 25 °C and 1 atm.
[b] Solubility parameters of species were calculated using the Group contribution method demonstrated by Van Krevelen and te Nijenhuis [34] as well as Fedors [35].

3.3 Hydroformylation experiments

3.3.1 Equipment used

A standard reaction setup, as shown is Figure 3.3, was used to generate the hydroformylation data and is well described in literature [36].

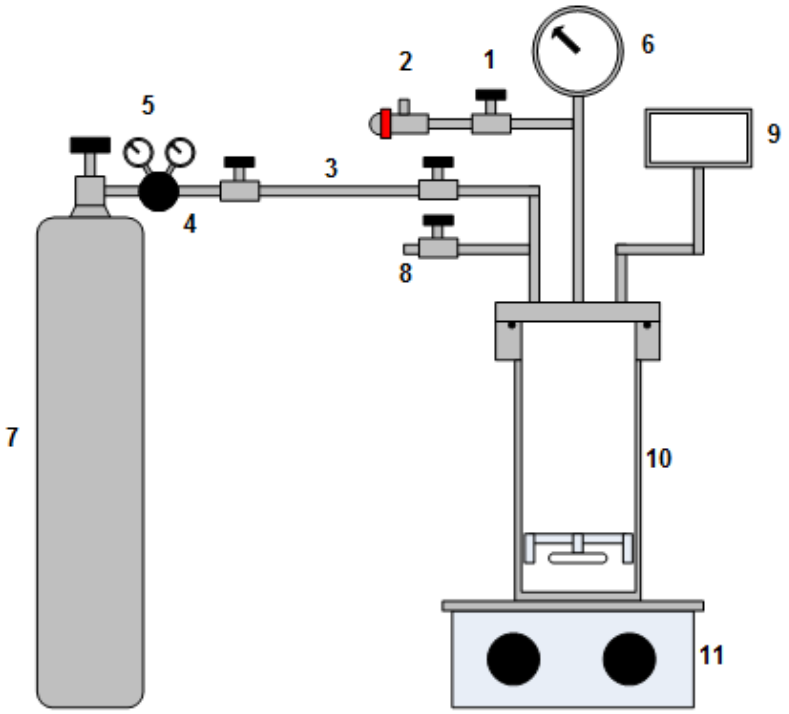

(1: Cell pressure release valve; 2: Safety pressure relief valve; 3: N_2 gas line; 4: Regulator; 5: N_2 cylinder pressure gauge (bar); 6: Reactor pressure gauge (MPa); 7: N_2 gas cylinder; 8: Sample port; 9: Temperature indicator; 10: Reactor; 11: Magnetic stirrer)

Figure 3.3: Standard hydroformylation experimental setup used in this study

3.3.2 General experimental methodology

A standard reaction methodology was used in this investigation as previously described in literature [21,37–40].

Hydroformylation reactions were carried out in a 75 mL stainless steel Teflon-coated pipe reactor. For 1-octene as substrate: The reactor was charged with a 200 ppm solution of **$HRh(CO)(PPh_3)_3$** (4 mg, 0.00435 mmol) in toluene (21 mL) and *n*-dodecane (0.7 mL) which remains unreactive and acts as internal standard. The 1-octene (3.3 mL, 21 mmol) was then introduced into the reactor resulting in a substrate to rhodium molar ratio of 4940:1. Literature suggested that additional amounts of the **PPh_3** ligand (22 mg, 0.085 mmol) be added, at a ligand to rhodium molar ratio of 20:1 [41], to maintain a high catalytic activity by preventing catalyst decomposition and to promote aldehyde formation [39]. For 1-decene as substrate: The reactor was charged with a 6850 ppm solution of **$Co(C_5H_7O_2)_3$** (151 mg, 0.423 mmol) in toluene (20 mL) and n-dodecane (0.2 mL) which remains unreactive and acts as internal standard. The 1-decene (1.6 mL, 8.46 mmol) was then introduced into the reactor resulting in a substrate to rhodium molar ratio of 121:1. No ligands were added. The reactor was then sealed and flushed three times with syngas in order to purge the system.

After purging, the reactor was pressurised and heated to the desired syngas pressure (20 bar) and temperature (80 °C), respectively. The reactor was heated by submerging the reactor into a container filled with preheated glycerol fluid which was heated by means of a heating plate. The fluid ensured a uniform temperature throughout the reactor. The reaction mixture was stirred continuously at a stirrer speed of 500 rpm until the conclusion of the reaction. Based on literature, the reaction was assumed to reach completion after 120 minutes (300 minutes in the case of the cobalt precatalyst) [41]. Samples were withdrawn (3 x 1.5 mL) after reaction completion and analysed using gas-chromatography (GC) to identify the products formed at the time of sampling. At the end of the reaction, the reactor was allowed to cool until room temperature and the gas slowly vented prior to opening.

3.4 OSN permeation experiments

3.4.1 Equipment used

A standard OSN setup, as shown in Figure 3.4, was used to perform the permeation experiments and has previously been described in literature [42–44]. A stainless steel dead-end bench-scale pressure cell along with all the necessary ancillary equipment, as presented in Figure 3.5, were used to perform all OSN permeation experiments.

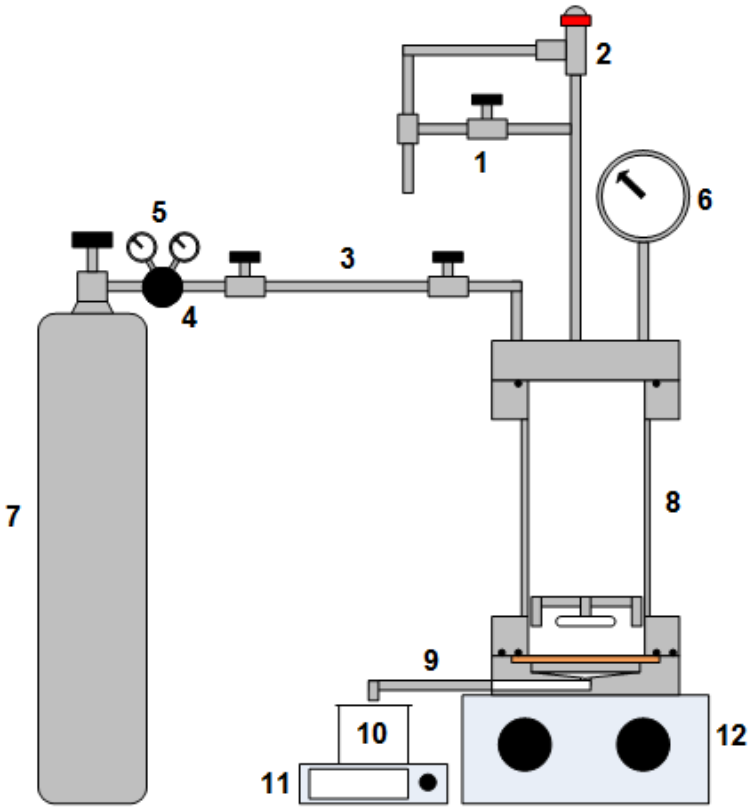

(1: Cell pressure release valve; 2: Safety pressure relief valve; 3: N_2 gas line; 4: Regulator; 5: N_2 cylinder pressure gauge (bar); 6: Membrane cell pressure gauge (MPa); 7: N_2 gas cylinder; 8: Stirred pressure cell with membrane; 9: Permeate drain pipe; 10: Permeate collection flask; 11: Electronic balance; 12: Magnetic stirrer)

Figure 3.4: Standard OSN permeation setup used in this study

The pressure cell (**8**), consisting of a chamber with an inner diameter of 46 mm and a maximum volume capacity of 300 mL, houses the membrane at the bottom supported on a stainless steel porous circular plate. The cell is securely assembled with removable end plates at both ends fitted with all the necessary inlet and outlet ports, i.e. pressure release (**1**) and pressure control valves (**2**), a pressure gas inlet (**3**), a pressure gauge (**6**) and a permeate exit pipe (**9**), as portrayed in Figure 3.4.

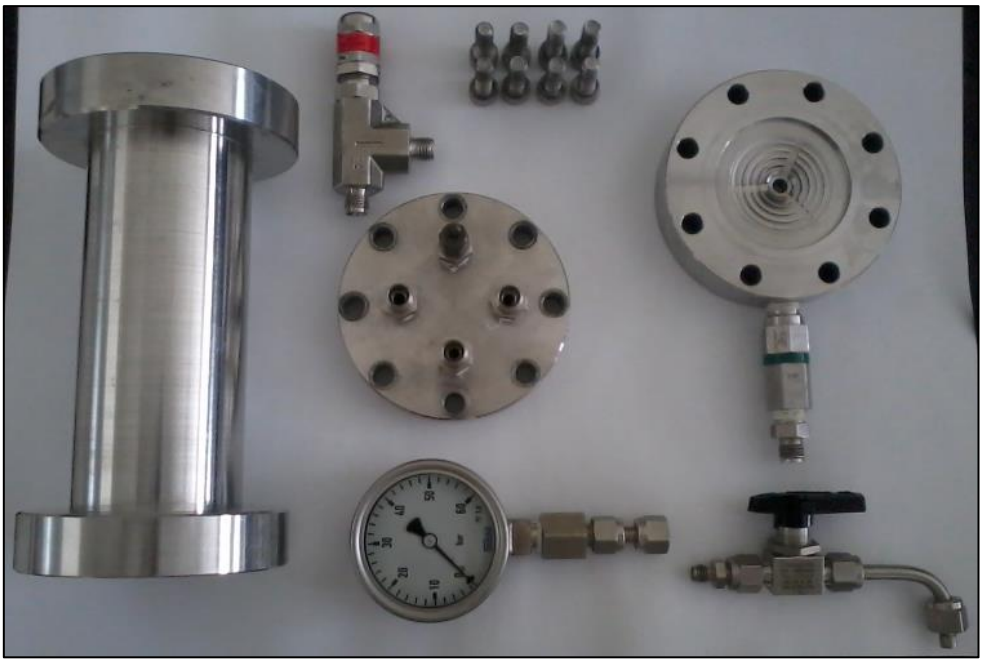

Figure 3.5: Membrane pressure cell

The selected membrane discs were cut from A4 sheets of membrane, as provided by the supplier, to give an active membrane surface area of 16.6 cm^2. The active membrane surface refers to the membrane surface in direct contact with the feed. The membrane was then placed in the cell, tightly fixed sealed between an O-ring and the support plate, with its active layer, typically characterised by a glossy smooth surface, directed to the feed.

The membrane pressure cell was fitted with a Teflon-coated stirrer bar located about 3 mm above the membrane surface which was put into effect by placing the cell on a magnetic stirrer (**12**). A stirrer speed of 500 rpm was used for all permeation experiments throughout this investigation. This was done so as to create a homogeneous mixture, minimise the effects of concentration polarisation and to subsequently prolong the effective operational lifetime of the membrane. High purity nitrogen gas (**7**) was used to pressurise the cell and create a transmembrane pressure in order to initiate permeation process. The cylinder was fitted with a regulator (**4**) and pressure gauge (**5**).

Vandezande *et al.* [45] defined concentration polarization as the accumulation of solids on the membrane surface. This solids layer increases the solute concentration at the membrane surface boundary, resulting in an increase in osmotic pressure and ultimately leading to a reduction in permeate flux. This finding was supported by Stamatialis *et al.* [46] and Peeva *et al.* [16]. The authors suggested the use of cross-flow conditions to minimise the build-up of solids. In this investigation, stirring was used to simulate cross-flow conditions in the dead-end membrane cell.

The outlet pipe, through which permeate was continuously drained, was directed toward a measuring cylinder for permeate collection (**10**). This measuring cylinder was placed on an electronic scale (**11**) to continuously weigh the permeate as it was being collected. Once the pressure cell had been properly sealed and it and its contents have been pressurised, the feed solution was allowed to permeate through the membrane to commence the flux and rejection characterisation of the membrane at hand. The cell was placed inside a fume cupboard to extract and remove and hazardous vapours.

3.4.2 Membrane screening

3.4.2.1 Introduction

In this section, commercially available OSN membranes are assessed based on stability, solvent compatibility, permeance and rejection for suitability for the recovery of homogeneous catalysts from different post-reaction solvent mixtures. Membranes deemed fit based on the highest possible combination of permeance and rejection values were selected for inclusion in this study.

3.4.2.2 Screening criterion and experimental methodology

From literature, it is evident that polymeric membranes are preferred for OSN applications due to their strong tolerance to organic solvents. Although the use of these OSN membranes dates back many years, only a few successful commercially available OSN membranes exist, including the STARMEM^{TM} series, the SolSep series as well as the Duramem® and Puramem® series and to some extent the MPF, Nadir and Desal series. Therefore, the aforementioned OSN membranes were first validated from a literature perspective by comparing and reviewing the observations of previously published works for similar conditions and systems. A complete literature revision of commercial OSN membranes can be found in Appendix C.

Following the literature validation, the commercially available membranes were reduced to three suitable candidates, namely the STARMEM^{TM} (ST-240) and Duramem® (DM-150 and DM-200) membranes, as these membranes were found to provide the highest flux and recovery values for the systems considered in this study. Thereafter, membrane compatibility tests were performed using these selected membranes to determine which of these three membranes would be best suited for further participation in this study. These membranes were subjected to the different organic species used in this study, namely 1-octene, 1-decene, 1-nonanal, 1-undecanal, 1-nonanol and 1-undecanol.

The physical and permeation compatibility of the membrane with the species were then evaluated by observing any change to the active layer of the membrane and measuring the solvent fluxes, respectively. Prior to the permeation compatibility tests, the membranes used were first conditioned using a predetermined pretreatment solvent. A membrane was classified as unstable if any discoloration or disintegration occurs on the top active layer during prolonged exposure to the reaction species. Moreover, it was desired that a flux of >1 $L.m^{-2}.h^{-1}$ be achievable at a pressure of 30 bar. However, the membrane was considered incompatible if fluxes below 1 $L.m^{-2}.h^{-1}$ were achieved after a minimum of 8 hours and subsequently rejected from the study.

Hereafter, tests were conducted to determine the compatibility of a membrane with a given solvent. These compatibility tests were performed visually, to attain a sense of the physical stability of a membrane in a solvent environment. For a visual representation of the membrane-solvent compatibility, a piece of membrane was placed in a petri dish filled with a given solvent for four weeks. Throughout this period, the membrane was visually inspected at regular intervals for any damage or dissolution. All observations were documented.

For the visual tests, no discoloration or damage to the top active layer was observed which correlates well with the specifications provided by the manufacturer. However, the absence of any visual defects does not mean the membrane's properties remain intact. Van der Bruggen *et al.* [47] recently did a study to determine the effects of membrane exposure to organic solvents and found that the characteristics of the membrane changes after contact, ranging from slight (small change in flux) to significant (complete loss of selectivity). In this study, the STARMEM™ and Duramem® membranes curled when exposed to the organic solvents, caused by the shrinkage and swelling of different surfaces of a membrane, which can result in significant changes in solvent flux.

Based on the membrane screening results, given and discussed in Appendix C, the ST-240 membrane was selected for inclusion in this investigation and was used for further testing.

3.4.3 General experimental methodology

3.4.3.1 Introduction

This study required several experiments to be performed in order to fully assess the performance of the membranes, each with its own focus and purpose with regard to solvent permeation, solvent separation, catalyst rejection and membrane and solvent

interaction. Different pure components, and component mixtures, were considered using reaction species varying in molecular weight, polarity, carbon chain length and functional group. A typical experiment consisted of four steps: 1) membrane pretreatment tests, 2) membrane conditioning procedures and steady-state verification, 3) reaction species permeation and separation and 4) catalyst recovery.

3.4.3.2 Membrane pretreatment

The hydrophilic polyimide Duramem® series and hydrophobic polyimide STARMEM™ series membranes were supplied in dry form. These membranes were soaked in preservation oil during manufacture as a measure of protection against drying out and contamination. For this reason, a standardised method of membrane pretreatment is required in order to alleviate the presence of any oils to create, in essence, a homogeneous membrane surface and to level the playing field for all membranes to be compared. Jezowska *et al*. [48] has reported that by subjecting the membrane to pretreatment, the homogeneity of the membrane material's properties can be increased. Toluene was chosen as the pretreatment solvent for the Duramem® and STARMEM™ series membranes as it is also commonly used as a solvent for the hydroformylation reaction.

During pretreatment, toluene was allowed to permeate through the membrane at a constant transmembrane pressure until no sign of the preservation oil was present. This could be confirmed by the attainment of a steady solvent flux and for some membranes, e.g. the Duramem® series, by observing any discoloration of the permeate due to the oil. The permeate containing the oil was then discarded and prior to starting the succeeding the experiment, the cell chamber thoroughly rinsed with 5 mL of the solvent to be used, i.e. 1-octene, 1-decene, 1-nonanal, etc.

The cell was loaded with 250 mL toluene and was allowed to permeate through the membrane in a semi-batch manner for 6 to 8 hours at 30 bar until a steady flux was achieved. A maximum of two thirds of the initial feed volume was allowed to permeate at any given time. Once 150 mL of toluene had permeated, the experiment was temporarily stopped by depressurising the cell and 150 mL of fresh toluene was added to the cell. The cell was then pressurised to 30 bar and the pretreatment process continued. Note that membrane pretreatment with toluene was performed only once for a given membrane. Once the preservation oil has been completely removed from the membrane surface, no further pretreatment was required.

3.4.3.3 Membrane conditioning procedure and steady-state characterisation

In order to minimise the effect of membrane compaction and to prepare the membrane for the establishment of steady-state conditions, literature shows that the membrane has to be broken-in prior to characterisation. It was noted by Vandezande *et al*. [45] that incorrect membrane preparation can result in significant performance degradation.

The conditioning procedure was characterised by a gradual increase or decrease in flux and was completed when a steady flux was achieved. The initial flux change, found to be a common phenomenon in membrane operations, can be ascribed to membrane compaction where it can be seen as the membrane acclimatising to its conditions. Yang *et al.* classified this flux change as a decrease. However, this change depends on the effect of swelling on the membrane effective contact area. In some cases, the membrane effective area increases in size during swelling which may lead to an increase in flux. Several researchers have observed this initial increase in flux caused by compaction [49,50]. The degree of this initial change depends on the membrane, solvent and operating conditions selected which indicates that the resulting OSN performance, i.e. flux and rejection, is characteristic of a specific system. The effects of compaction have been noted in previous publications [51].

The membrane conditioning procedure was implemented by allowing the feed solution, whether it was a pure or solvent mixture, to permeate through the membrane at the desired pressure until steady-state was achieved. Prior to the conditioning procedure, the cell was thoroughly rinsed with 5 mL of the solvent to be used. Thereafter, the solvent was loaded into the cell, the cell was sealed and pressurised and the conditioning procedure initiated. The feed solution was allowed to permeate through the membrane until a maximum of two thirds of the initial feed volume has permeated. At this point, the cell was depressurised, the permeate was recycled back to the cell as feed and the process continued. This was repeated for a minimum of 8 hours or until steady-state conditions, characterized by a steady permeate flux, can be confirmed. Some researchers observed that the attainment of steady-state or equilibrium conditions may take up to several days [45].

Permeate flux, J, was calculated by measuring the time intervals, Δt, necessary to obtain a certain predetermined volume or mass of permeate, ΔV or Δm, for a given active membrane surface area, A, as shown in Equation 3.1.

$$J = \frac{\Delta V \text{ or } \Delta m}{A \times \Delta t} \tag{3.1}$$

3.4.4 Reaction species separation methodology

Apart from characterising the membrane for pure solvent permeability, binary solvent mixtures were considered which consisted of olefins, aldehydes and alcohols, representative of typical rhodium-catalysed hydroformylation and hydrogenation post-reaction mixtures. Therefore, focus was not exclusively placed on the membranes ability towards catalyst recovery but also on solvent separation and as a result, broadens the scope and relevancy of this study. It is evident from literature that a large amount of effort is directed to applicability of OSN to solvent separation which emphasises its industrial importance [52–55]. Therefore, this study launched an investigation into the possibility and efficiency of OSN membranes for solvent separation in the context of the homogeneous reactions.

Binary mixtures consisted of 1-octene/1-nonanal, 1-decene/1-undecanal and 1-nonanal/1-nonanol, exemplary of the hydroformylation and hydrogenation reaction systems and concentrations ranging from 0 vol% to 100 vol% were used.

A similar procedure outlined in Section 3.4.2 was used and only membranes that have been successfully pretreated were used. In contrast to pure solvents, the pressure cell was loaded with a total feed volume of 150 mL for solvent mixtures so as to minimise the rate of waste generation. After the loading of the feed, the cell was pressurised and the feed allowed to permeate. Care was taken to only permeate roughly 40 vol% (60 mL) of the initial feed volume in order to maintain consistency of results and to ensure that these results were representative of the concentrations under consideration. Permeating more than 40 vol% would provide data that was uncharacteristic of the experimental conditions at hand. Once 40 vol% has permeated, the cell was depressurised, the permeate recycled back to the cell and the process reinitialised. This was repeated until a steady permeate flux was confirmed after which the process was repeated and allowed to proceed until roughly 10 vol% (15 mL) of the initial feed volume has permeated. At this point, a permeate sample of approximately 4 mL (3 x 4 mL) was withdrawn into a 4 mL vial. The sample was then subjected to GC analysis to determine the concentration of the organic solvents which were then used to calculate the degree of solvent separation, α, achieved by the membrane using Equation 3.2.

$$\alpha = \frac{C_P}{C_F} \tag{3.2}$$

Where C_P and C_F refers to the concentration of an organic solvent in the permeate and feed, respectively.

3.4.5 Catalyst rejection methodology

OSN membranes were not just characterised by solvent flux but also with regard to catalyst rejection in the presence of single solvents and utilises similar procedures as described in Sections 3.4.3. The primary objective of this investigation, which was to facilitate the homogeneous catalyst rejection process, stems from the necessity of recovering expensive and often toxic transition metal based catalysts.

The performance of the OSN membranes selected in terms of catalyst rejection was put to the test using different pure solvents (i.e. 1-octene, 1-decene, 1-nonanal, 1-undecanal, 1-nonanol, 1-undecanol) at varying pressures of between 10 and 40 bar and at catalyst concentrations of 200 ppm and 500 ppm. As the catalyst of interest, **$HRh(CO)(PPh_3)_3$** was selected due to its prominence, and superiority compared to other catalysts in the hydroformylation reactions. The catalyst concentration was chosen to be representative of the typical conditions as reported by literature [41]. However, this concentration was also limited by the solubility of the different organic solvents used in this investigation. The cobalt-based catalyst, **$Co(C_5H_7O_2)_3$**, another prominent hydroformylation catalyst based on its catalytic activity, was used as a comparative measure of the OSN capacity for flux and catalyst recovery.

Similar to the solvent separation experiments, only membranes that have adequately undergone pretreatment were used. A feed solution with a total volume of 150 mL was made up of the desired catalyst concentration and loaded into the pressure cell. Note that no reaction occurred as inert nitrogen gas was used to pressurise the cell instead of syngas which was required for reaction initialisation. Care should be taken to only permeate 40 vol% (60 mL) of the initial feed volume. After 40 vol% has permeated, the cell was depressurised, the permeate recycled and the process continued. This was repeated until a steady permeate flux was achieved. After the confirmation of steady-state flux, the experiment was restarted and once again allowed until 40 vol% of the feed has permeated. At this point, a 5 mL sample (3 x 5 mL) of the bulk permeate solution was withdrawn as well as a sample (3 x 5 mL) of the retentate, each into a 40 mL vial. With some preparation, the samples were then tested for catalyst concentration using flame atomic absorption spectrometry (FAAS) which can then be used to calculate catalyst rejection, R, based on the catalyst concentration in the permeate, C_P,and the feed, C_F, using Equation 3.3 [17].

$$R = \left(1 - \frac{C_P}{C_F}\right) \times 100\% \qquad (3.3)$$

At the completion of an experiment, the cell chamber was thoroughly rinsed with approximately 5 mL of the solvent to be used in the succeeding run.

3.5 Analytical equipment and procedures

3.5.1 Gas chromatography (GC)

A Varian 3600 gas chromatograph consisting of a HP5 capillary column with dimension 60 m x 0.35 mm x 0.25 µm along with a flame ionisation detector (FID) was used to measure the concentration of the organic solvents in the sample solutions. In summary, the temperature programming employed for the chromatograph consisted of an initial oven temperature of 50 °C for 1 minute, heated from 50 to 250 °C at 15 °C.min^{-1} and held at 250 °C for 10 minutes. The hydrogen, air and a helium make-up gas flowrates were 30 mL.min^{-1}, 300 mL.min^{-1} and 20 mL.min^{-1} with a split ratio of 70:1.

Standard solutions were used to generate a calibration curve which in turn provided a GC response factor for each of the solvents. Five standard solutions were prepared with each containing 10, 20, 40, 80 and 100 µL of each solvent to be used in this study. These solutions also contained 30 µL of *n*-dodecane which was used as internal standard, followed by the addition of toluene to increase the sample volume to roughly 2 mL. From each of these standard solutions, 0.3 µL was then manually injected into the chromatograph to determine the solvent peak areas and retention times. The resulting peak areas are then plotted against the volumes, where the gradient of the resulting curve was the response factor for a given solvent. Table 3.3 summarises the retention times and response factors determined for each solvent used.

Table 3.3: Summary of solvent retention times and response factors

Solvent	Retention time (min)	Response factor (-)
Toluene	7.74	-
1-Octene	8.12	1.06
Octane	8.32	1.33
1-Decene	13.88	1.08
1-Nonanal	17.55	1.18
iso-Nonanal	19.62	-
1-Nonanol	19.62	1.13
1-Undecanal	23.80	1.18
1-Undecanol	25.65	1.16

Once the gas chromatograph has been calibrated and the respective solvent response factors were known, the organic concentrations of the samples were determined. The GC calibration curve and response factor for 1-octene is shown in Figure 3.6.

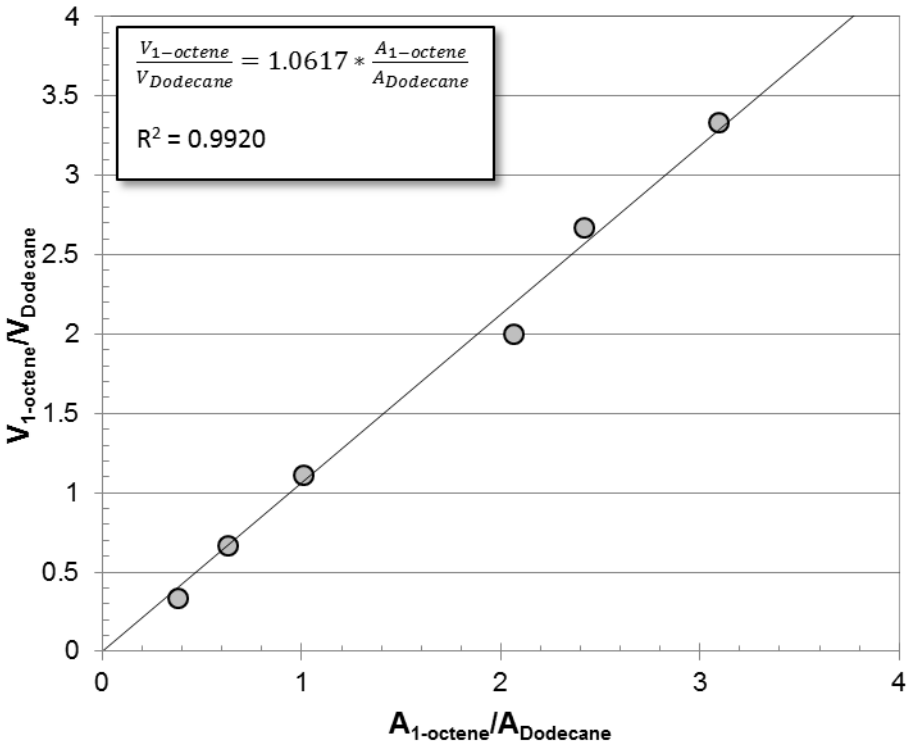

Figure 3.6: GC calibration curve and response factor for 1-octene

The sample vial was stirred to ensure sample homogeneity. From the initial sample, 200 µL was added to a 4 mL vial using a pipette along with 30 µL of the internal standard, i.e. n-dodecane. Toluene was then added to increase the sample volume to 2 mL. From this vial, 200 µL was added to another 4 mL vial and similarly topped up with toluene. After stirring, 0.3 µL of the resulting solution was manually injected into the chromatograph to proceed with GC analysis. The Volume, V_i, of any given solvent can then be determined by using the known response factors, RF, internal standard volume, $V_{Dodecane}$ and peak areas relative to that of the standard, $\frac{A_i}{A_{Dodecane}}$, in combination with Equation 3.4.

$$V_i = V_{Dodecane}\left(\frac{A_i}{A_{Dodecane}}\right) * RF \tag{3.4}$$

For further details regarding the gas chromatograph start-up, operation and shutdown procedures, the temperature programming and the preparation of standards used for calibration, refer to Appendix E. The calibration curves for each of the species used are also given.

3.5.2 Flame atomic absorption spectroscopy (FAAS)

FAAS was used to determine the concentration of the rhodium-based and cobalt-based catalysts in the sample solutions. Pretreatment of the samples prior to FAAS analysis was however required due to the incompatibility of the FAAS instrument with organic solvents. Therefore, it was necessary to remove the catalysts from its organic matrix and transfer it into an aqueous acidic solution more suitable to the spectrometer. Balcerzak [56] recommended the use of acid digestion using aqua regia, i.e. a 1:3 mixture of HNO_3 and HCl, as it is effective in the dissolution of rhodium and cobalt metals. The original sample, contained in a 40 mL vial, is placed inside a vacuum oven with the cap off to prevent pressure build up. All of the organic solution was then allowed to evaporate at 0.2 bar until only the dry residue remains. The catalyst residue was allowed to cool to room temperature and 3 mL aqua regia was added to dissolve the residue. The vial was then heated to 70 °C for 2 hours in order to ensure that the catalyst that has adhered to the vial during evaporation was also dissolved. After this, the vial was allowed to cool to room temperature and 27 mL distilled water was added to the vial while being thoroughly shaken until a homogeneous mixture was ensured. The resulting mixture was then analysed with FAAS.

Similar to the chromatograph, the FAAS instrument requires calibration in order to provide accurate and reliable results. Standard solutions with known catalyst concentrations in an aqueous acidic medium (aqua regia) were prepared using the catalysts. A concentration range of 5 – 100 ppm was selected to reflect the estimated catalyst concentration used in this study. Once prepared, the standards were then manually injected into the spectrometer and analysed for rhodium and cobalt absorbance, respectively. These absorbance values were then plotted against the known standard solution catalyst concentrations to obtain a calibration curve for the rhodium-based and cobalt-based catalysts. The calibration data for the catalysts used are presented in Table 3.4 and Figure 3.7.

The lower detection limit of the FAAS for the rhodium-based and cobalt-based catalyst content was 5 ppm and 3 ppm, respectively. Further details regarding the FAAS start-up, operation and shutdown procedures, the preparation of standards used for calibration and the calibration data themselves can be found in Appendix E.

Table 3.4: Standards of catalysts used for FAAS calibration

Catalyst concentration (ppm)	RSD (%)	Mean absorption (-)
$HRh(CO)(PPh_3)_3$		
45	1.4	0.048
89	0.9	0.099
134	1.1	0.150
179	1.6	0.201
223	2.0	0.243
335	0.8	0.383
446	0.9	0.523
$Co(C_5H_7O_2)_3$		
50	1.1	0.096
75	1.8	0.145
100	1.2	0.191
150	1.0	0.281
200	0.5	0.367

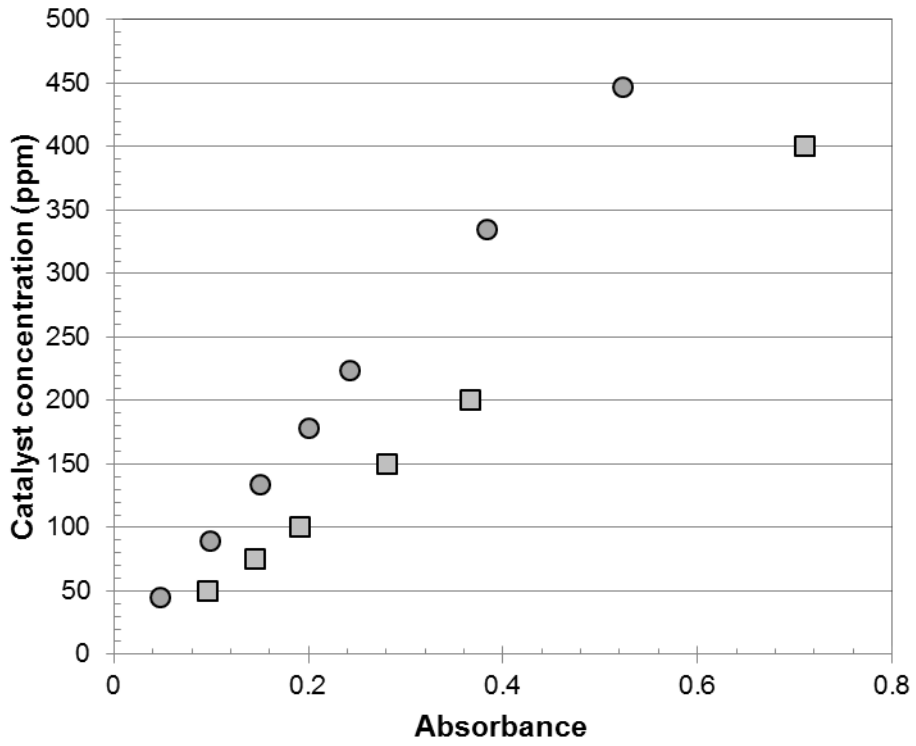

Figure 3.7: FAAS calibration curve for **$HRh(CO)(PPh_3)_3$** (○) and **$Co(C_5H_7O_2)_3$** (□)

3.6 OSN sorption studies

3.6.1 Introduction

Nearly all polymeric membranes have the tendency to swell with the degree of swelling being dependent on the solvent and operating conditions. Furthermore, different membranes swell at varying degrees. Therefore, its effect on separation performance differs among membranes. For this reason, swelling or sorption experiments were performed in order to characterise the thermodynamic interaction between the different solvent-membrane pairings.

3.6.2 General experimental methodology

The ST-240 membranes were cut into small pieces, weighed for an initial dry weight, M_{dry}, and soaked in different pure solvents for 48 hours. During this period, the membrane samples were weighed, M_{wet}, at different time intervals and the weight recorded along with the time. During the weighing of the membrane, care was taken to do so in the shortest time possible (maximum of 30 seconds) to avoid drying out the membrane which may damage the membrane integrity. Upon weighing, the membrane was gently pressed between two layers of tissue paper to remove the excess fluid on the membrane surface. This process was repeated until sorption equilibrium is confirmed, i.e. until no further increase in membrane weight was observed. The swelling degree, SD, which is a parameter describing the membrane-solvent interaction was then calculated using Equation 3.5.

$$SD = \frac{M_{wet} - M_{dry}}{M_{wet}} \tag{3.5}$$

3.7 Experimental design

The main objective of this investigation is to determine the feasibility of recovering a catalyst from a hydroformylation post-reaction medium using OSN. The performance of the OSN membrane were characterised for a wide range of operating parameters in order to confirm process feasibility. This was achieved by performing various experiments at predetermined manipulated parameter combinations, measuring the resulting response parameters and observing as well as analysing the values obtained. In this section, an overview of the experimental design used in this investigation will be presented, as shown in Figure 3.8.

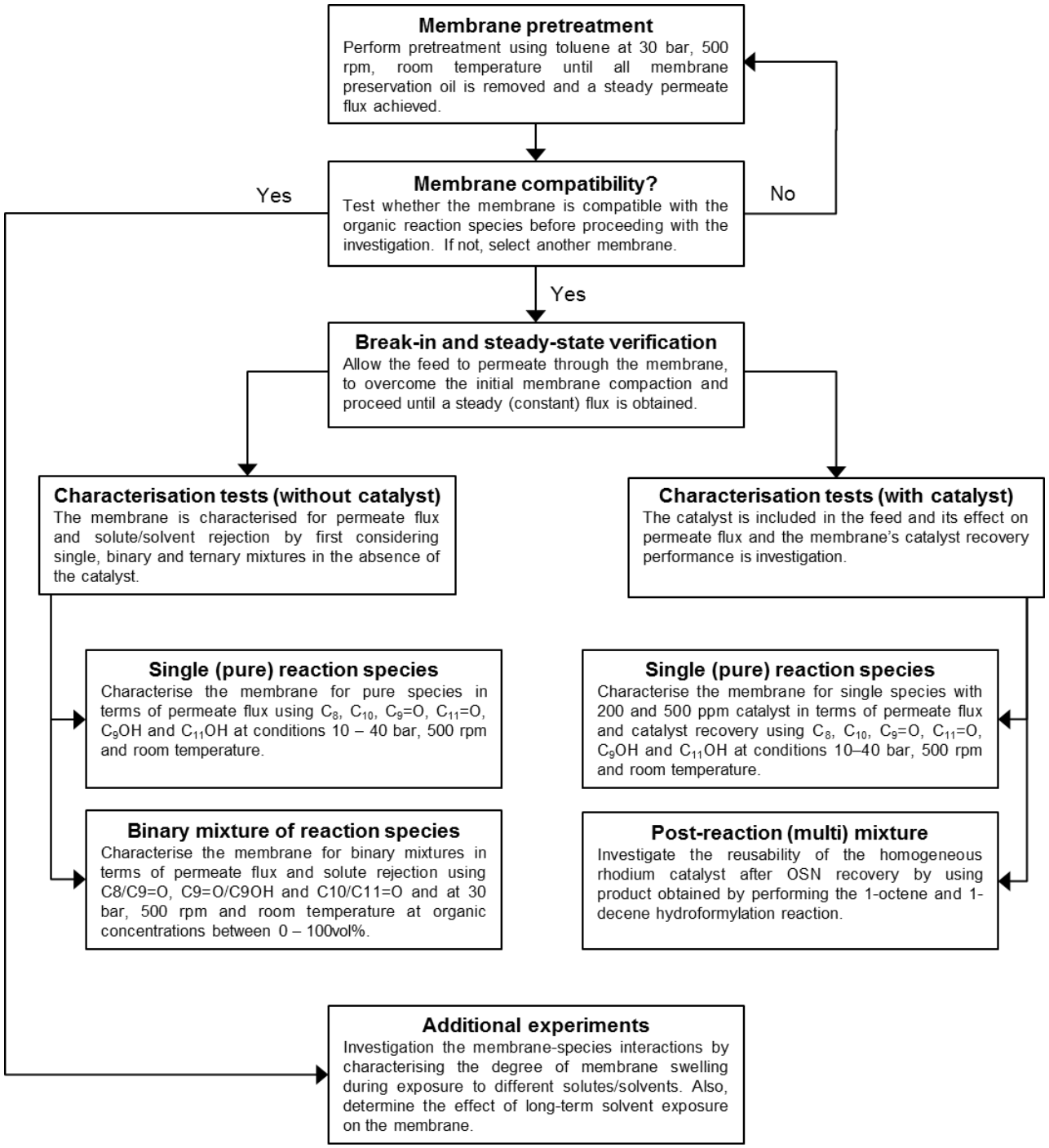

Figure 3.8: Overview of OSN experimental design used in this investigation

3.7.1 Response and manipulated variables

The response parameters for this investigation are permeate flux and separation which were measured according to the methods described Section 3.4 and calculated according to Equations 3.1 through 3.3, respectively. The manipulated parameters include applied pressure, solute species, binary solute concentration, catalyst species and catalyst concentration. The validation and description of the selected variables and ranges are summarised in Table 3.5.

Table 3.5: Summary of manipulated variables used in experimental design

Variable	Range	Validation
Feed pressure	10 – 40 bar	Typical hydroformylation reaction pressures were used in order to quantify the effect of pressure of OSN performance in terms of solvent flux and catalyst rejection.
Olefin species	C_8 and C_{10}	1-Octene (C_8) and 1-decene (C_{10}) were used as these olefins are widely used as reagents in the hydroformylation reaction to produce aldehydes.
Aldehyde species	C_9=O and C_{11}=O	1-Nonanal (C_9=O) and 1-undecanal (C_{11}=O) were used as these aldehydes represent the respective hydroformylation products of 1-octene and 1-decene.
Alcohol species	C_9OH and C_{11}OH	1-Nonanol (C_9OH) and 1-undecanol (C_{11}OH) were used as these alcohols represent the respective hydrogenation products of 1-nonanol and 1-undecanol.
Organic concentration	0 – 100 vol%	For binary mixtures of olefins, aldehydes and alcohols, the concentrations were ranged between 0 and 100 vol% to investigate the effect of binary concentration on OSN performance in terms of flux and rejection.

Table 3.5: Summary of manipulated variables used in experimental design (*cont.*)

Variable	Range	Validation
Catalyst species	**$HRh(CO)(PPh_3)_3$** and **$Co(C_5H_7O_2)_3$**	The two most prominent transition metal-based catalysts used in industry for the hydroformylation reaction were used to characterise the OSN separation performance.
Catalyst concentration	200 and 500 ppm	Typical catalyst concentrations found in literature applications of the hydroformylation reaction was used and held constant to determine the effect of catalyst addition on membrane permeability and characterise the OSN performance in terms of catalyst recovery.
Membrane	Duramem® and STARMEM^{TM} series	Two well-known and commercially available membranes were used in this study so as to characterise the performance of each.

Although Scarpello *et al.* [14] reported that temperature influences the membrane performance in terms of permeate flux and rejection, attributed to increased polymer chain mobility and decreased solvent viscosity, the effect of temperature is not within the scope of this investigation and is maintained constant at ambient temperature (20 ± 2 °C). It was shown by Scarpello *et al.* [14], that when the temperature is varied, catalyst recovery and permeate flux exhibited contrasting behaviour. They found that flux increased and rejection decreased and the extents to which these parameters are affected are highly system dependent. This finding was corroborated previously by researchers who attributed this observation to three possible reasons: 1) reduction in solvent viscosity, 2) increase in species diffusivity, and 3) increase in the mobility of the polymer matrix [55,57,58]. The stirrer speed was also maintained constant at 500 rpm throughout the investigation.

3.8 References

[1] Evonik Industries AG, Germany. [Online], (2015). http://corporate.evonik.com/.

[2] X. Li, F. Monsuur, B. Denoulet, P. Vandezande, I.F.J. Vankelecom, A. Dobrak, *Anal. Chem.* **81** (2009) 1801.

[3] Y.H. See Toh, X.X. Loh, K. Li, A. Bismarck, A.G. Livingston, *J. Memb. Sci*. **291** (2007) 120–125.

[4] J. Li, M. Wang, Y. Huang, B. Luo, *RSC Adv*. **4** (2014) 37375–37380.

[5] Y.H. See Toh, F.W. Lim, A.G. Livingston, *J. Memb. Sci.* **301** (2007) 3–10.

[6] D.Q. Vu, W.J. Koros, S.J. Miller, *J. Memb. Sci.* **211** (2003) 311–334.

[7] D.A. Patterson, A. Havill, S. Costello, Y.H. See-Toh, A.G. Livingston, A. Turner, *Sep. Purif. Technol.* **66** (2009) 90–97.

[8] W.E. Siew, C. Ates, A. Merschaert, A.G. Livingston, *Green Chem*. **15** (2013) 663–674.

[9] T.R. Long, A. Gupta, A.L. Miller II, D.G. Rethwisch, N.B. Bowden, *J. Mater. Chem.* **21** (2011) 14265–14276.

[10] A. Cano-Odena, P. Vandezande, D. Fournier, W. Van Camp, *Chem. A Eur. J.* **16** (2010) 1061–1067.

[11] C.J. Pink, H. Wong, F.C. Ferreira, A.G. Livingston, *Org. Process Res. Dev.* **12** (2008) 589–595.

[12] D. Nair, J.T. Scarpello, I.F.J. Vankelecom, L.M. Freitas Dos Santos, L.S. White, R.J. Kloetzing, T. Whelton, A.G. Livingston, *Green Chem.* **4** (2002) 319–324.

[13] D. Nair, J.T. Scarpello, L.S. White, L.M. Freitas Dos Santos, I.F.J. Vankelecom, A.G. Livingston, *Tetrahedron Lett*. **42** (2001) 8219–8222.

[14] J.T. Scarpello, D. Nair, L.M. Freitas Dos Santos, L.S. White, A.G. Livingston, *J. Memb. Sci.* **203** (2002) 71–85.

[15] P. Silva, S. Han, A.G. Livingston, *J. Memb. Sci*. **262** (2005) 49–59.

[16] L.G. Peeva, E. Gibbins, S.S. Luthra, L.S. White, R.P. Stateva, A.G. Livingston, *J. Memb. Sci*. **236** (2004) 121–136.

[17] S.S. Luthra, X. Yang, L.M. Freitas Dos Santos, L.S. White, A.G. Livingston, *J. Memb. Sci.* **201** (2002) 65–75.

[18] L.W. Gosser, W.H. Knoth, G.W. Parshall, *J. Mol. Catal*. **2** (1977) 253–263.

[19] M. Priske, K.D. Wiese, M. Kraume, C. Baumgarten, *J. Memb. Sci*. **360** (2010) 77–83.

[20] J. Fang, R. Jana, J.A. Tunge, B. Subramaniam, *Appl. Catal. A Gen*. **393** (2011) 294–301.

[21] P.J. Baricelli, E. Lujano, M. Modrona, A.C. Marrero, Y.M. Garcia, A. Fuentes, R.A. Sanchèz-Delgado, *J. Organomet. Chem.* **689** (2004) 3782–3792.

[22] D. He, D. Pang, T. Wang, Y. Chen, Y. Lui, J. Lui, Q. Zhu, *J. Mol. Catal. A Chem*. **17**4 (2001) 21–28.

[23] B.M. Bhanage, S.S. Divekar, R.M. Deshpande, R.V. Chaudhari, *J. Mol. Catal. A Chem.* **115** (1997) 247–257.

[24] S.S. Divekar, R.M. Bhanage, R.M. Deshpande, R. V. Gholap, R. V. Chaudhari, *J. Mol. Catal.* **91** (1994) L1–L6.

[25] R.M. Deshpande, B.M. Bhanage, S.S. Divekar, R. V. Chaudhari, *J. Mol. Catal*. **78** (1993).

[26] C.K. Brown, G. Wilkinson, *J. Chem. Soc*. (1970).

[27] G. Achonduh, Q. Yang, H. Alper, *Tetrahedron*. **71** (2015) 1241–1246.

[28] F. Hebrard, P. Kalck, *Chem. Rev*. **109** (2009) 4272–4282.

[29] T. Zeelie, **Rhodium and Cobalt Catalysts in the Heterogeneous Hydroformylation of Ethene, Propene and 1-Hexene**, Helsinki, 2007.

[30] L.B. Backman, A. Rautiainen, A.O.I. Krause, M. Lindblad, *Catal. Today.* **43** (1998) 11–19.

[31] C.L. Yaws, **Thermophysical Properties of Chemicals and Hydrocarbons**, 2nd Ed., Elsevier, Oxford, 2014.

[32] H. Djojoputro, S. Ismadji, *J. Chem. Eng. Data.* **50** (2005) 2003–2007.

[33] R.H. Perry, D.W. **Green, Perry's Chemical Engineers' Handbook**, 7th Ed., McGraw-Hill, Kansas, 1999.

[34] D. Van Krevelen, K. te Nijenhuis, **Properties of Polymers: their correlation with chemical structure; their numerical estimation and prediction from additive group contributions**, Elsevier, 2009.

[35] R.F. Fedors, *Polym. Eng. Sci*. **14** (2004) 147–154.

[36] E.B. Hager, C.E. Banothile, B.C.E. Makhubela, G.S. Smith, *Dalt. Trans.* **41** (2012) 13927–13935.

[37] B.C.E. Makhubela, A.M. Jardine, G. Westman, G.S. Smith, *Dalt. Trans*. **41** (2012) 10715–10723.

[38] N.C. Antonels, J.R. Moss, G.S. Smith, *J. Organomet. Chem.* **696** (2011) 2003–2007.

[39] J.K. MacDougall, M.C. Simpson, M.J. Green, D.J. Cole-Hamilton, *J. Chem. Soc.* (1996) 1161–1172.

[40] D. Evans, T.A. Osborn, G. Wilkinson, *J. Chem. Soc*. **11** (1968) 3133–3142.

[41] A. Buhling, P.C.J. Kamer, P.W.N.M. Van Leeuwen, *J. Mol. Catal. A Chem*. **98** (1995) 69–80.

[42] K. Xiao, Y. Shen, X. Huang, *J. Memb. Sci*. **427** (2013) 139–149.

[43] B.M. Xaba, **Separation and Recovery of Selected Transition-Metal Catalyst Systems Using Membrane Processes**, 2010.

[44] P. Van der Gryp, A. Barnard, J.P. Cronje, D. de Vlieger, S. Marx, H.C.M. Vosloo, *J. Memb. Sci.* **353** (2010) 70–77.

[45] P. Vandezande, L.E.M. Gevers, I.F.J. Vankelecom, *Chem. Soc. Rev*. **37** (2008) 365–405.

[46] D.F. Stamatialis, N. Stafie, K. Buadu, M. Hempenius, M. Wessling, *J. Memb. Sci.* **279** (2006) 424–433.

[47] B. Van der Bruggen, J. Geens, C. Vandecasteele, *Sep. Sci. Technol.* **37** (2007) 783–797.

[48] A. Jezowska, T. Schipolowski, G. Wozny, *Desalination.* **189** (2006) 43–52.

[49] P. Van der Gryp, H.C.M. Vosloo, S. Marx, **Separation of Grubbs-based catalysts with nanofiltration**, Potchefstroom, 2008.

[50] X.J. Yang, A.G. Livingston, L. Freitas Dos Santos, *J. Memb. Sci*. **190** (2001) 45–55.

[51] J.A. Whu, B.C. Baltzis, K.K. Sirkar, *J. Memb. Sci.* **170** (2000) 159–172.

[52] S. Postel, S. Wessel, T. Keil, P. Eiselt, M. Wessling, *J. Memb. Sci*. **466** (2014) 361–369.

[53] B. Bawareth, *J. Teknol.* **69** (2014) 29–39.

[54] G.H. Koops, S. Yamada, S.I. Nakao, *J. Memb. Sci*. **189** (2001) 241–254.

[55] W.J. Adam, B. Luke, P. Meares, *J. Memb. Sci.* **13** (1983) 127–149.

[56] M. Balcerzak, *Anal. Sci*. **18** (2002) 737–750.

[57] R. Othman, A. Wahab, M. Ismail, J. Salimon, *J. Memb. Sci*. **348** (2010) 287–297.

[58] S. Aerts, A. Buekenhoudt, H. Weyten, L.E.M. Gevers, I.F.J. Vankelecom, P.A. Jacobs, *J. Memb. Sci.* **280** (2006) 245–252.

CHAPTER 4: Results and Discussion – Catalyst Recovery

4.1 Overview

The numerous benefits of homogeneous catalysts are squandered as industries favour its heterogeneous counterpart due to the difficulty in recovering homogeneous catalysts, such as the transition metal-based catalysts depicted in Figure 4.1, from their post-reaction mixture. Currently, homogeneous catalyst recovery necessitates the use of conventional methods which often are highly energy-intensive and waste generating. The potentially destructive nature of conventional methods highlights both the economic and environmental imperative for the development of alternative homogeneous catalyst recovery techniques in the field of hydroformylation.

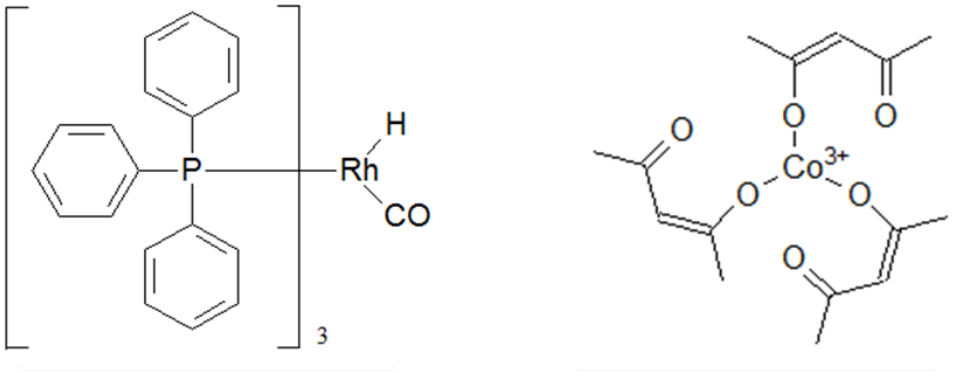

$HRh(CO)(PPh_3)_3$

MW = 920 $g.mol^{-1}$

$Co(C_5H_7O_2)_3$

MW = 356 $g.mol^{-1}$

Figure 4.1: Transition metal-based catalysts used in this investigation

The aim of this chapter is therefore to demonstrate the use of OSN membranes to successfully separate homogeneous catalysts from post-reaction mixtures for reuse. A key disadvantage in the field of homogeneous catalysis is therefore addressed and a solution presented.

This chapter can be divided into six sections. Section 4.2 discusses the hydroformylation reactions performed and presents the results obtained therefrom. Thereafter, the selected membrane is characterised in Section 4.3 with respect to catalyst rejection performance and in Section 4.4, these recovered catalysts are tested for usability. In Section 4.5, a cost and energy evaluation is performed for OSN catalyst recovery. Section 4.6 then provides a summary of the major results obtained as well as the importance of this work.

4.2 Hydroformylation of olefins

4.2.1 Introduction

In order to determine the product species that should be involved in the OSN permeation experiments, the hydroformylation reaction of olefins in the presence of **$HRh(CO)(PPh_3)_3$** and **$Co(C_5H_7O2)_3$** was carried out to obtain the product distribution. Figure 4.2 illustrates the homogeneous reaction network employed to upgrade low value short chain olefin feedstock to longer chain functionalized hydrocarbons, i.e. aldehydes and alcohols, in the surfactant and detergent range.

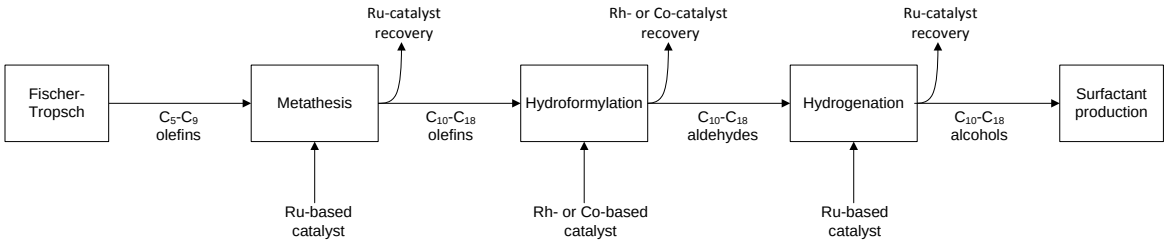

Figure 4.2: Reaction network for the upgrading of olefins to functionalised hydrocarbons

It was previously shown by Van der Gryp *et al.* [1] that the application of OSN can be successfully applied for the recovery of homogeneous ruthenium-based (Grubbs-type) catalysts, achieving a recovery of >99.0% with the STARMEM^{TM} 228 membrane. Therefore, the focus of this investigation will shift further down the reaction network to the hydroformylation reaction. Figure 4.3 demonstrates the hydroformylation reaction scheme with all possible species in the presence of both rhodium- and cobalt-based catalysts.

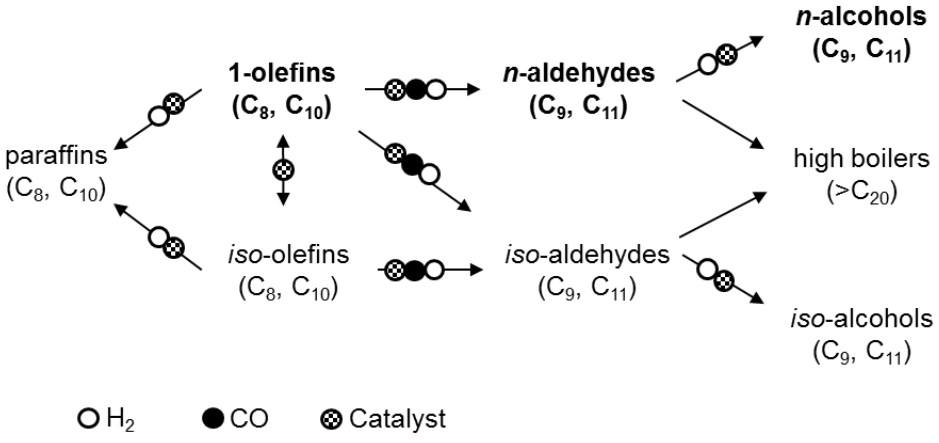

Figure 4.3: Hydroformylation reaction scheme (adapted from [2])

It can be observed from Figure 4.3 that the desired end-products for the hydroformylation and hydrogenation reactions are two-fold, namely aldehydes and alcohols, both linear and branched. However, other by-products may also form, although to a small extent, including isomeric olefins and paraffins as well as high boilers [3,4].

The purpose of this section is to determine the approximate product distributions of the 1-octene and 1-decene hydroformylation reactions using both homogeneous catalysts used in this study, i.e. **$HRh(CO)(PPh_3)_3$** and **$Co(C_5H_7O_2)_3$**, and to validate the synthetic post-reaction mixture to be used as feed stream in the succeeding OSN experiments through literature and experimental observations

4.2.2 Literature validation of typical product distributions

Literature has shown that the use of **$HRh(CO)(PPh_3)_3$** as catalyst, ensures that reactions are highly stereoselective towards the linear products being formed, including as far back as Evans *et al.* [5] in 1968 who obtained linear to branched ratio of approximately 3 at high olefin conversions. Buhling *et al.* [6] reported a selectivity of close to 73% towards linear aldehydes with a 1-octene conversion of 81.2%. MacDougall and Cole-Hamilton [3] reported that in the presence of **$HRh(CO)(PPh_3)_3$**, the rate at which internal olefins undergo conversion to branched aldehydes are approximately 3% that of the rate at which linear aldehydes are formed.

Furthermore, the abovementioned complex hinders the isomerisation and hydrogenation of olefins resulting in much less isomeric olefins and paraffins in the post-reaction mixture. Buhling *et al.* [6] showed that a mere 1.5% was dedicated to the isomerisation of 1-octene during the reaction. Therefore, the approximation can be made, based on literature findings, that only linear aldehydes and alcohols are formed during the hydroformylation and subsequent hydrogenation of 1-octene and 1-decene feedstock, as illustrated in Figure 4.4, and these solvents will be used as representative of post-reaction mixtures.

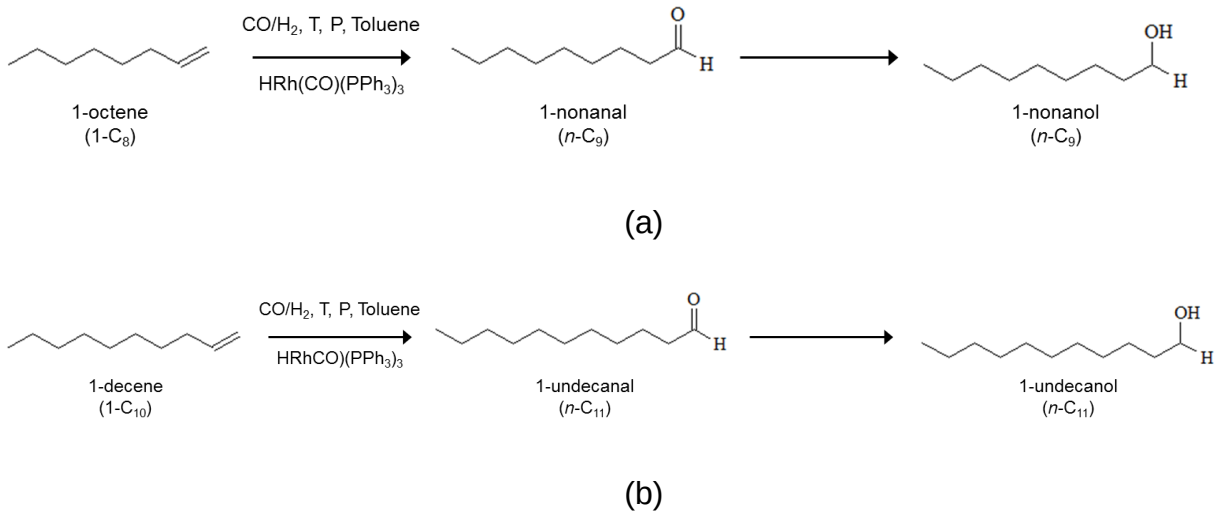

Figure 4.4: Reaction network for the upgrading of (a) 1-octene and (b) 1-decene

4.2.3 Experimental validation of typical product distributions

The approximations illustrated in Figure 4.3 were experimentally verified by performing the hydroformylation reaction of 1-octene and 1-decene with both homogeneous catalysts considered in this study, i.e. **$HRh(CO)(PPh_3)_3$** and **$Co(C_5H_7O_2)_3$**.

Firstly, reactions were performed using 1-octene as substrate, toluene as solvent and **$HRh(CO)(PPh_3)_3$** as active catalyst at a ligand to rhodium and substrate to rhodium molar ratio of 20:1 and 4940:1, respectively, at 20 bar syngas pressure ($CO:H_2$, 1:1) and 80 °C for a total reaction time of 2 hours (120 minutes). These tests were repeated at least three times under the same conditions to ensure repeatability.

Reactions were also performed with 1-decene as substrate and **$Co(C_5H_7O_2)_3$** as catalyst. The reaction was done at a substrate to cobalt molar ratio of 120:1, 20 bar syngas pressure (CO:H2, 1:1) and 110 °C for a total reaction time of 5 hours (300 minutes). The results from the 1-octene and 1-decene hydroformylation reactions obtained in this work were then compared to those found in literature, as presented in Table 4.1.

It is clear from Table 4.1 that in the presence of the rhodium complex, **$HRh(CO)(PPh_3)_3$**, mainly linear aldehydes, i.e. 1-nonanal in the case of 1-octene as substrate, are formed with, on average, total aldehyde yields greater than 90 mol% and *n*/*iso* ratios of greater than 2.5. Literature reports similar observations of increased selectivity toward linear products at higher temperatures but also warns of excessive temperatures leading to higher isomerization rates [7,8]. Moreover, the results obtained are comparable to those published by Buhling *et al.* [6] with an average experimental error for product yields of *ca.* 3%. It is also clear from Table 4.1 that in the presence of the cobalt complex,

$Co(C_5H_7O_2)_3$, mainly linear aldehydes, i.e. 1-undecanal in the case of 1-decene as substrate, are formed at more severe conditions with, on average, total aldehyde yields greater than 85.0 mol% and *n*/*iso* ratios of greater than 2.3. Moreover, the results obtained are comparable to those published in literature [9].

Table 4.1: Product yield of olefin hydroformylation using homogeneous catalysts

Solvent	**Catalyst**	**Product Yield**			
1-Octene	**$HRh(CO)(PPh_3)_3$**	**This work**	[6]	[10]	[11]
n-Aldehyde (mol%)		66.3 ± 2.8	72.6	53.3	43.6
iso-Aldehyde (mol%)		25.7 ± 2.7	25.9	26.7	48.4
n/*iso* (mol.mol^{-1})		2.58 ± 0.2	2.80	2.00	0.90
Isomers (mol%)		7.01 ± 1.9	1.50	n.d.[a]	8.00
1-Decene	**$Co(C_5H_7O_2)_3$**	**This work**	[9]	[12]	[13]
n-Aldehyde (mol%)		58.1	61.0	47.0	80.0
iso-Aldehyde (mol%)		25.0	19.0	17.0	20.0
n/*iso* (mol.mol^{-1})		2.32	3.21	2.80	4.00
Isomers (mol%)		15.9	18.0	n.d.	n.d.

[a] Not disclosed.

Herewith, confirmation is afforded to the approximation illustrated in Figure 4.4 that the post-reaction mixtures consist mainly of linear products from olefin feedstock and the OSN experiments can proceed.

4.2.4 Concluding remarks

In this section, the product distribution of the 1-octene and 1-decene hydroformylation reaction in the presence of **$HRh(CO)(PPH_3)_3$** and **$Co(C_5H_7O_2)_3$**, respectively, was investigated. Literature results could be successfully reproduced with an average repeatability of *ca.* 7% for the olefin hydroformylation reaction [6]. It was found that using the homogeneous rhodium- and cobalt-based hydroformylation catalysts, mainly linear aldehydes were formed, i.e. 1-nonanal and 1-undecanal, with *n*/*iso* ratios of greater than 2. It was also evident that the cobalt-based system required severe conditions to provide catalyst activities comparable to that of the rhodium-based complex.

4.3 Recovery of homogeneous catalysts with OSN

4.3.1 Introduction

When introducing a catalyst into the feed, **$HRh(CO)(PPh_3)_3$**, it is desired that the STARMEM^{TM} 240 (ST-240) membrane should completely reject the homogeneous catalyst (>99.9%) so that it may be recycled and re-used for subsequent reactions. In this section, the capability of the ST-240 membrane in terms of catalyst recovery is investigated according to the procedures described in Section 3.4.4 and using Equation 4.1.

$$R = \left(1 - \frac{C_P}{C_F}\right) \times 100\% \qquad (4.1)$$

where

R parameter characterising membrane rejection performance (%)

C_P catalyst concentration in the permeate (mg.L^{-1})

C_F catalyst concentration in the feed (mg.L^{-1})

Manipulated variables include applied pressure and catalyst feed concentration in the presence of different solvents and its effect on the membrane's catalyst recovery performance presented and discussed. The effect of two different hydroformylation catalysts will also be investigated and compared in terms of catalyst recovery.

4.3.2 Experimental results

The experimental results for the ST-240 membrane performance in terms of catalyst recovery are presented in Table 4.2. An experimental error of approximately 1.8% was determined for the catalyst recovery studies.

Table 4.2: Recovery performance of the ST-240 membrane for **$HRh(CO)(PPh_3)_3$** and **$Co(C_5H_7O_2)_3$** recovery performance for the different reaction systems

Solvent	Catalyst	Pressure (bar)	Catalyst feed concentration (ppm)	Rejection
1-Octene	**$HRh(CO)(PPh_3)_3$**	10, 20, 30, 40	200	>98.0%[a]
	$HRh(CO)(PPh_3)_3$	10, 20, 30, 40	500	>98.0%[a]
	$Co(C_5H_7O_2)_3$	30	500	87.9%
1-Decene	**$HRh(CO)(PPh_3)_3$**	10, 20, 30, 40	200	>98.0%[a]
	$Co(C_5H_7O_2)_3$	30	500	87.9%
1-Nonanal	**$HRh(CO)(PPh_3)_3$**	30	200	>98.0%[a]
1-Undecanal	**$HRh(CO)(PPh_3)_3$**	30	200	>98.0%[a]
1-Nonanol	**$HRh(CO)(PPh_3)_3$**	30	200	>98.0%[a]
1-Undecanol	**$HRh(CO)(PPh_3)_3$**	30	200	>98.0%[a]

[a] Rejection limited by the AAS rhodium- and cobalt catalyst detection lower limit, 5 ppm and 3 ppm, respectively. All rhodium concentrations in the permeate were <5 ppm.

From Table 4.2, it can be observed that the ST-240 membrane performed extremely well in terms of recovering **$HRh(CO)(PPh_3)_3$**, for all organic solvents considered, achieving recoveries of >98.0%. For the recovery of **$Co(C_5H_7O_2)_3$** on the other hand, the ST-240 membrane achieved moderate recoveries of 87.9%. This is expected due to the smaller molecular size of latter (~350 $g.mol^{-1}$) relative to its rhodium counterpart (~920 $g.mol^{-1}$) and the ST-240 membrane's MWCO (400 $g.mol^{-1}$). Furthermore, previous studies have shown that a strong correlation exists between the molecular shape of a solute and its apparent permeance through the membrane, e.g. comparing branched to unbranched molecules, both Zheng *et al.* [14,15] and White [16] found higher recoveries and subsequently lower permeability for the branched molecules due to a larger steric presence. This correlates well the findings observed in this study, as a higher rejection for the larger **$HRh(CO)(PPh_3)_3$** relative to **$Co(C_5H_7O_2)_3$** can be attributed to the bulkier structure of the former.

It is apparent from Table 4.2 that catalyst recovery remains independent of the catalyst loading for the operating conditions considered in this study. This is in agreement with the observations made previously by the corresponding authors for the metathesis reaction system. Although studies were found which suggested otherwise, e.g. Razak *et al*. [17], it was previously shown by Whu *et al.* [18] that the catalyst loading only influences its recovery during the initial transient period of operation, where after a steady-state value

was reached once the membrane has successfully been broken-in and achieved steady-state conditions. In terms of applied pressure, no effect could be observed on catalyst recovery. This is in agreement with the observations made previously by the Livingston group [19,20] who observed that the influence of applied pressure on catalyst recovery becomes insignificant at higher pressures and in the presence of some organic solvents. Furthermore, it can be observed that the solvent systems considered in this study have no apparent influence on the catalyst recovery, as determined in previous work [1]. It was however apparent from past publications of the Livingston group that catalyst recovery was only minimally effected by the solvent for the STARMEM^{TM} series of membranes and varied only between 3 – 4% for different solvent systems. The same solvents had a more pronounced effect on other membranes, e.g. MPF, Duramem®, etc. [20–22]. This was later corroborated by Ormerod *et al*. [23].

Therefore, within the reaction network illustrated in Figure 4.2 and for the conditions considered in this study, OSN proved successful in the recovery of homogeneous catalysts from metathesis, hydroformylation and hydrogenations reaction systems, independent of the applied pressure and catalyst loading.

4.3.3 Concluding remarks

Catalyst rejections >98.0%% could be achieved for the rhodium-based catalyst, **$HRh(CO)(PPh_3)_3$**, for all reaction systems while a lower recovery for **$Co(C_5H_7O_2)_3$**, 87.9%, was achieved due, predominantly, to its smaller molecular size relative to the MWCO of the ST-240 membrane. Moreover, catalyst recovery was observed to remain unabated by variations in catalyst loading and applied pressure.

4.4 Reusability of homogeneous catalysts post OSN recovery

4.4.1 Introduction

The overarching aim of this investigation was to recover the homogeneous catalyst from a post-reaction mixture in a reusable form for recycle, as illustrated in Figure 4.5.

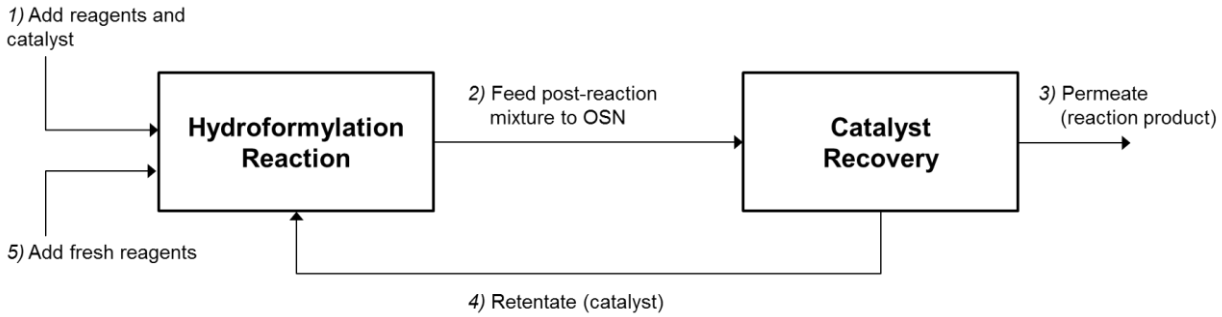

Figure 4.5: Schematic illustration of proposed consecutive reaction-recovery process

It was previously shown in this work that the homogeneous catalyst, **$HRh(CO)(PPh_3)_3$**, can be successfully recovered (>98.0%) from hydroformylation and hydrogenation post-reaction mixtures using the ST-240 membrane at catalyst concentrations of 200 and 500 ppm and applied pressures ranging between 10 and 40 bar. Moreover, catalyst concentration in the permeate could be reduced to less than 5 ppm. In this section the reusability of the recovered rhodium-based catalyst was tested by performing three consecutive reactions (two filtrations) and compared the *n*-aldehyde product yield before and after recovery. The cobalt-based catalyst, **$Co(C_5H_7O_2)_3$**, was disregarded from the reusability studies due to moderate recovery using the ST-240 membrane.

The hydroformylation of 1-octene will be used as model reaction for this investigation at conditions: 20 bar applied syngas (CO/H_2, 1:1) pressure, 80 °C operating temperature, 500 ppm catalyst concentration, 2 hours (120 minutes) total reaction time. During filtration, most of the solvent was allowed to permeate and the catalyst recovered as a highly concentrated solution. The catalyst deposit on the membrane surface was also recovered for reuse. Samples were taken upon completion of the reaction.

4.4.2 Experimental results

The consecutive reaction-recovery process was performed and the catalyst performance compared for each consecutive reaction. Results are summarised in Figure 4.6.

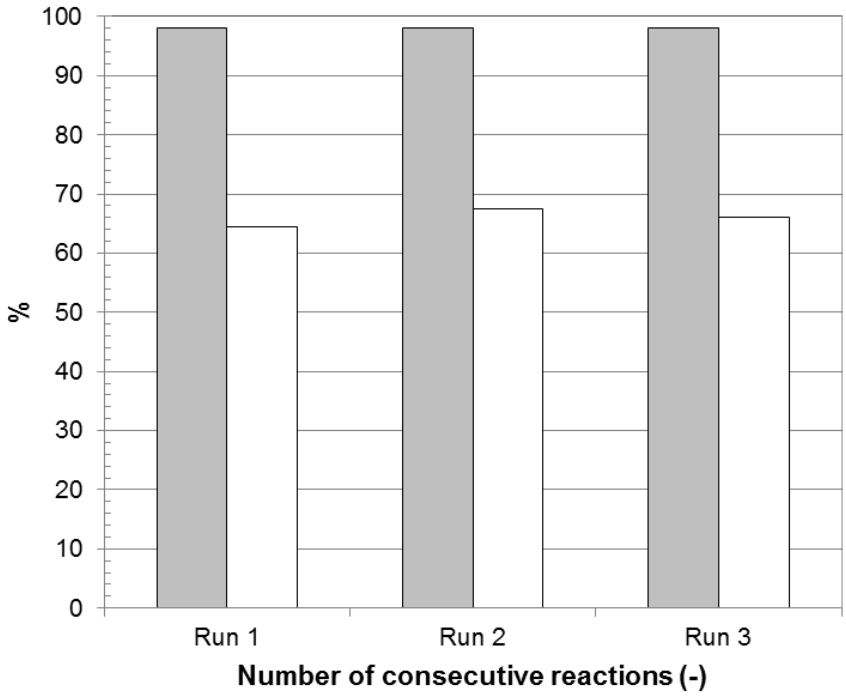

Figure 4.6: Consecutive reuse of **$HRh(CO)(PPh_3)_3$** after OSN recovery (catalyst recovered ▢; *n*-aldehyde product yield ☐)

It is clear from Figure 4.6 that the catalyst remains active even after two recovery cycles with comparable *n*-aldehyde product yields of approximately 65 mol% for each consecutive reaction. Moreover, the coupled reaction-recovery managed to increase the reaction turnover number, TON, from 2620 from a single-pass reaction to 3470 after three reactions.

Therefore, this study has successfully demonstrated that OSN can be used to recover a homogeneous catalyst in sufficient amounts from a post-reaction mixture for immediate reuse.

4.5 OSN cost and energy evaluation

4.5.1 Introduction

It is well known in literature that OSN is a lower energy and cost alternative to conventional separation units yet few present qualitative literature data to support this statement [24–28]. The few papers that did perform cost analyses and comparisons focussed mainly on solvent separation [29–31]. Therefore, there is a gap in the literature which clarifies the cost and energy benefits over that of conventional homogeneous catalyst recovery methods. The Livingston group [32] recently published a comprehensive study in which the sustainability of OSN is assessed while a few years prior, the group of Vankelecom [33] provided an energy usage breakdown of each industrial sector which incorporated OSN.

Based on the promising observations of previous OSN research groups, this section provides a simple comparison between the cost and energy consumption of OSN and distillation systems for the recovery of homogeneous catalysts from a hydroformylation post-reaction mixture. Aspen Plus™ simulation software was used to simulate the homogeneous catalyst recovery process from the different reaction mixtures (1-octene and 1-decene hydroformylation and 1-nonanal hydrogenation) considered in this investigation using a RadFrac distillation simulation approach similar to literature [30,31]. An economic evaluation was then performed in terms of energy usage and total operating costs. According to the shortcut economic analysis as described in Schmidt *et al.* [34], the total operating costs of an OSN process can be approximated as a function of the overall catalyst rejection and the membrane permeance (see Appendices F and G for raw data and sample calculations, respectively).

This chapter describes in detail the approach and assumptions used in the basic economic evaluation of recovery of homogeneous catalysts using distillation and OSN after which results are presented and discussed.

4.5.2 Design base

A summary of the design assumptions used for the cost and energy evaluation of the OSN and distillation systems is presented in Table 4.3.

A relatively small scale production capacity of 100 $kg.h^{-1}$ (876 $t.a^{-1}$) was approximated with an average yearly operational time of 8150 $h.a^{-1}$ [35,36]. A membrane price of \$270.$m^{-2}.a^{-1}$, i.e. representing a membrane unit lifetime of two years, was assumed [34]. The cost of the **$HRh(CO)(PPh_3)_3$** catalyst was approximated by a fifteen year average of the rhodium metal price, i.e. \$77,500.kg^{-1}, due to the relatively negligible cost of the ligand [37]. Solvent mass permeance, required to calculate membrane operating cost, are given in Table 4.3 for each solvent (Note: solvent permeance is discussed in Chapter 5).

Table 4.3: Summary of design assumptions used

Currency used	American Dollar (\$)
Operating time (t_{op})	8150 $h.a^{-1}$
Feed stream	
Total mass flow rate ($\dot{m}_{prod}$)	100 $kg.h^{-1}$
Catalyst concentration (C_F)	200 ppm
Catalyst type	**$HRh(CO)(PPh_3)_3$**
Solvents	1-octene, 1-decene, 1-nonanal, 1-undecanal, 1-nonanol, 1-undecanol
Temperature	20 °C
Pressure (ΔP)	30 bar
Costs	
$HRh(CO)(PPh_3)_3$ (c_{cat})	\$77,500.kg^{-1}
Membrane (c_{mem})	\$27.$m^{-2}.a^{-1}$
Solvent Mass Permeance ($P_{i,mem}$)	
1-octene	2.97 $kg.m^{-2}.h^{-1}.bar^{-1}$
1-decene	1.20 $kg.m^{-2}.h^{-1}.bar^{-1}$
1-nonanal	0.60 $kg.m^{-2}.h^{-1}.bar^{-1}$
1-undecanal	0.32 $kg.m^{-2}.h^{-1}.bar^{-1}$
1-nonanol	0.12 $kg.m^{-2}.h^{-1}.bar^{-1}$
1-undecanol	0.05 $kg.m^{-2}.h^{-1}.bar^{-1}$
Design objective and separation target	
Overall catalyst recovery	99.9%

Furthermore, in order for the reaction systems to be economically feasible, an overall catalyst recovery of 99.9% is required to maintain negligible catalyst losses. Therefore, to standardise the comparison, both systems were optimised to achieve an overall catalyst recovery of 99.9% [34].

Simulations were performed at operating conditions similar to the OSN permeation experiments, i.e. 20 °C, 200 ppm and 30 bar. Solvent permeance was calculated based on the average permeation rate of the solvent through the ST-240 membrane as determined experimentally divided by the applied pressure. See Appendices E and F for raw data and sample calculations, respectively.

4.5.3 Design methods

4.5.3.1 Catalyst recovery by distillation

Aspen Plus™ was used to simulate the catalyst recovery process from the organic species considered in this investigation using a multistage distillation process simulated using the RadFrac approach. In a typical catalyst recovery via distillation process, as illustrated in Figure 4.7, the post-reaction mixture (POST-RXN) was fed to a heat exchanger (HEATER) which preheats the mixture (FEED1) to the necessary operating temperature prior to entering the cascade distillation system (COLUMN1, COLUMN2 and COLUMN3).

The assumption was made that no pump is required as the POST-RXN stream exited the hydroformylation reactor at the separation operating pressure, i.e. 30 bar. In most cases, more than one distillation column was needed to achieve the desired 99.9% catalyst recovery for recycle and to deem the process economically viable through minimal catalyst losses. A mixer (MIXER) was added to collect the concentrated catalyst bottom product (BOTTOM1, BOTTOM2 and BOTTOM3) of the various stages to be recycled back to the reactor (CATALYST). The condensed reaction products (PRODUCT) were collected and sent for further species purification. Unit specifications are summarised in Table 4.4.

The total operating costs of distillation columns, TOC_{dist}, were calculated using the bare module cost method, based on the Chemical Engineering Plant Cost Index, as described in Turton *et al*. [35] according to approximate sizes and capacities as determined using methods described in Coulson and Richardson [38] at an operating pressure of 30 bar. The energy usages of the columns, $\dot{Q}_{dist}$, were approximated using Aspen Plus™ simulations.

Firstly, the purchased cost of the equipment, C_p^0, at standard conditions of atmospheric operating pressure and carbon steel material of construction was calculated as a function of equipment capacity, A_c, and design constants found in literature, K_i, according to Equation 4.2 [35]:

$$log_{10}C_p^0 = K_1 + K_2 log_{10}(A_c) + K_3[log_{10}(A_c)]^2 \quad (4.2)$$

The purchased cost was then used to calculate the total operating cost, TOC_{dist}, as a function of bare module factors, including a pressure factor, F_P, and a material factor, F_M and then inflation was accounted for by using the Chemical Engineering Plant Cost Index (CEPCI) [35].

$$TOC_{dist,2015} = [C_p^0 \times (B_1 + B_2 F_P F_M)] \times \frac{I_{2015}}{I_{2001}} \quad (4.3)$$

For pressure vessels, i.e. distillation columns, the pressure factor was determined based on the operating pressure, P, as well as the vessel diameter, D_c, and shell thickness, t_c [35].

$$F_p = \frac{\frac{(P)D_C}{2[850-0.6(P)]} + 0.00315}{t_c} \quad (4.4)$$

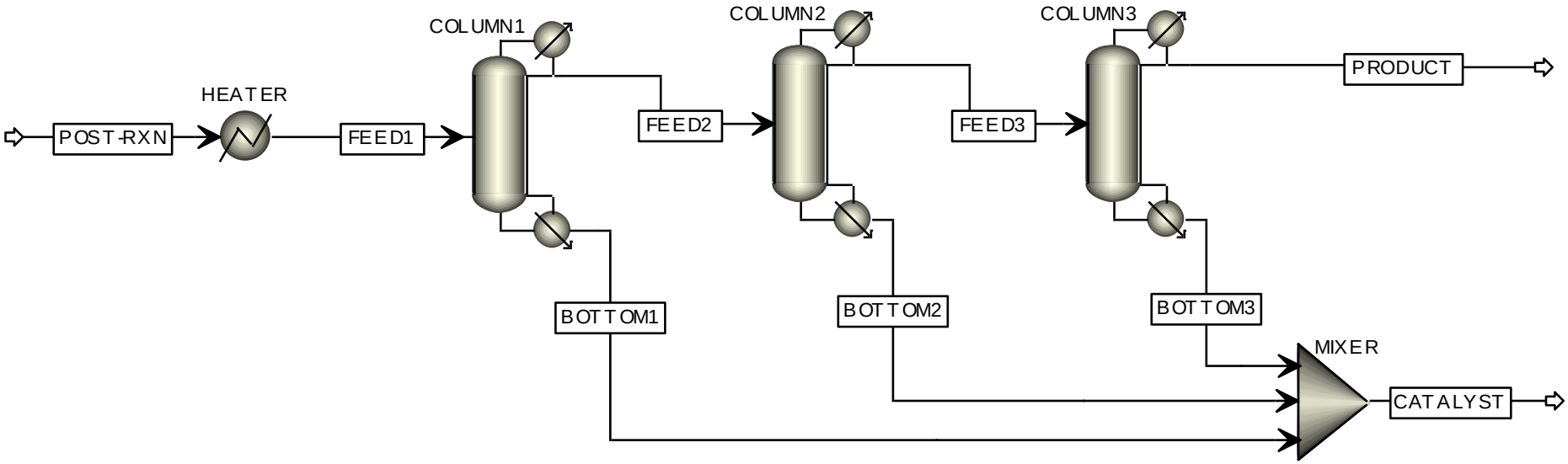

Figure 4.7: Aspen Plus™ flowsheet of a typical multistage distillation process for the recovery of homogeneous catalysts from post-reaction mixtures

Table 4.4: Unit specifications of multistage distillation Aspen Plus™ process

	HEATER[a]	DISTIL1	DISTIL2	DISTIL3
1-Octene				
Temperature (°C)	290	290	302	-
Pressure (bar)	30.0	30.0	30.0	-
Feed ($kg.h^{-1}$)	0.107	100	99.9	-
Duty (kW)	23.3	3.43	5.5E-4	-
1-Decene				
Temperature (°C)	340	340	-	-
Pressure (bar)	30.0	30.0	-	-
Feed ($kg.h^{-1}$)	0.126	100	-	-
Duty (kW)	27.6	3.80	-	-
1-Nonanal				
Temperature (°C)	384	384	-	-
Pressure (bar)	30.0	30.0	-	-
Feed ($kg.h^{-1}$)	0.140	100	-	-
Duty (kW)	30.6	2.56	-	-
1-Undecanal				
Temperature (°C)	415	415	-	-
Pressure (bar)	30.0	30.0	-	-
Feed ($kg.h^{-1}$)	0.153	100	-	-
Duty (kW)	33.4	3.03	-	-
1-Nonanol				
Temperature (°C)	408	408	-	-
Pressure (bar)	30.0	30.0	-	-
Feed ($kg.h^{-1}$)	0.181	100	-	-
Duty (kW)	39.6	0.262	-	-
1-Undecanal				
Temperature (°C)	445	445	455	455
Pressure (bar)	30.0	30.0	30.0	30.0
Feed ($kg.h^{-1}$)	0.192	100	99.8	99.7
Duty (kW)	41.9	0.833	1.7E-4	0.69E-4

[a] Feed given for heat exchangers are for the heating fluid mass flow (temperature in: 70 °C, temperature out: 18 °C).

4.5.3.2 Catalyst recovery by OSN

In terms of total OSN energy usage, $\dot{Q}_M$, the main energy contributor is the pressure pump, needed to provide the necessary transmembrane pressure, ΔP, to give a feed flow, F_F, and the recirculation pump, used to recirculate feed, F_r, over membrane to reduce concentration polarisation, and can be calculated using Equation 4.5:

$$\dot{Q}_M = \frac{F_F \Delta P}{\eta_P} + \frac{F_r \Delta P_D}{\eta_P} \tag{4.5}$$

where an overall pump efficiency, η_P, of 0.3, a recirculation stream five times the magnitude of the feed flow (5 x F_F), and a membrane module pressure drop, ΔP_D, of 0.5 bar is assumed similar to those used by the groups of Livingston [29] and Van der Bruggen [30]. Figure 4.8 presents an illustration of the flowsheet for a typical OSN catalyst recovery process.

In Figure 4.8, the post-reaction mixture (POST-RXN) is fed to the OSN membrane via a pressure pump (PUMPFEED) and contacts a fraction of the recycle stream (RECYCLE2). The OSN feed stream (FEED1) is then split into a permeate stream (PRODUCT), containing the solvent, unconverted substrate and products, and a retentate stream (CATALYST), containing the catalyst dissolved in the solvent. The retentate stream is then fed via a recycle pump (PUMPREC) split via a splitter (SPLITTER) into two recycle streams, with 80 – 85% of RECYCLE1 recycled back to the reactor for reuse (RECYCLE2) and 15 – 20% sent away for treatment. This allows for a recycle to feed ratio of approximately 4.5 – 5 in order to minimise membrane concentration polarisation [30].

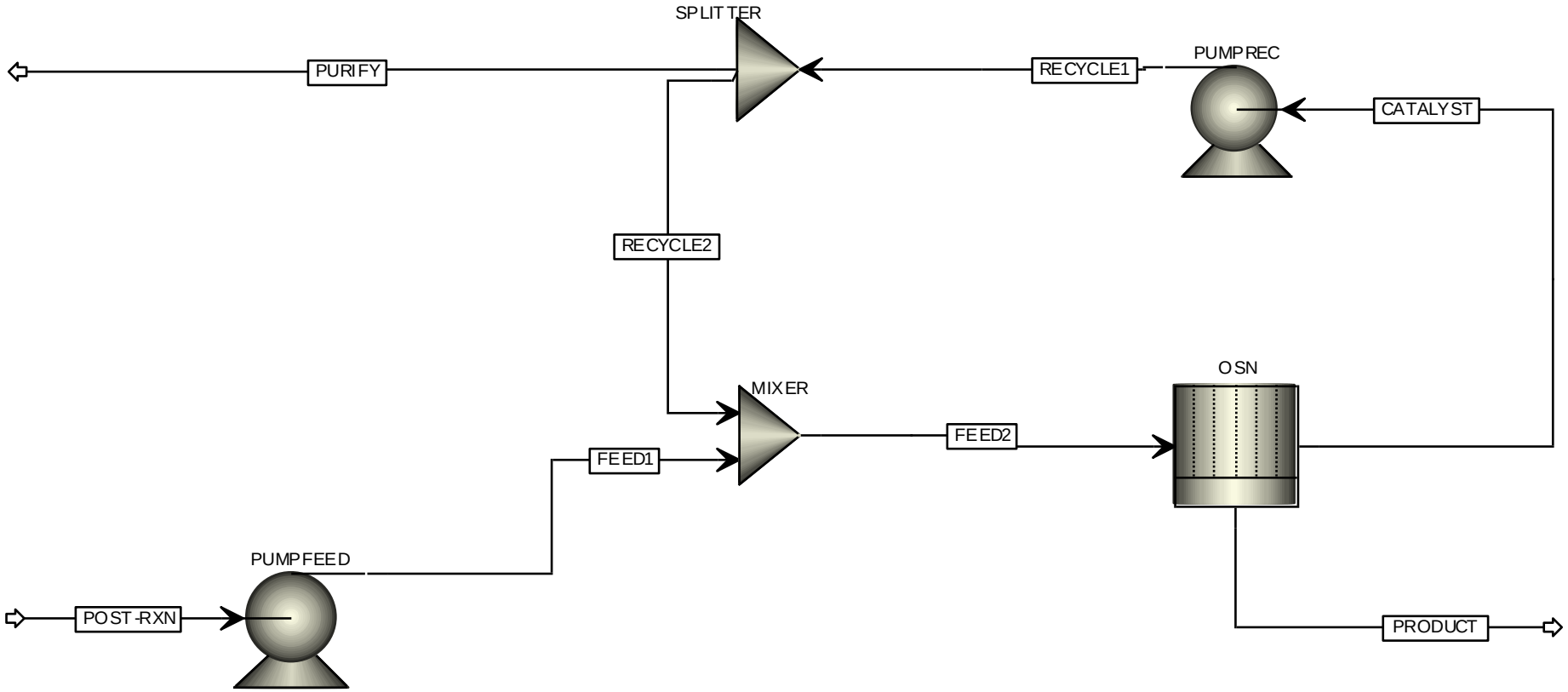

Figure 4.8: Aspen Plus™ flowsheet of a typical OSN process for the recovery of homogeneous catalysts from post-reaction mixtures

The total operating costs of the membranes, TOC_M, were calculated based on the catalyst lost in the permeate stream, $1 - R_{cat,overall}$, the permeability solvent i through the membrane, $P_{i,M}$, and the cost of the membranes themselves, c_M, as shown in Equation 4.6 (adapted from [34]):

$$TOC_M = \left(1 - R_{cat,overall}\right)\dot{m}_{prod}c_{cat}C_{cat} + \frac{\dot{m}_{prod}c_M}{\Delta P t_{op} P_{i,M}} \quad (4.6)$$

where $\dot{m}_{prod}$ is the production capacity, c_{cat} the cost of the catalyst, C_{cat} the catalyst concentration and t_{op} the annual processing time.

Schmidt *et al.* [34] previously noticed that the influence of overall catalyst recovery on the OSN total operating costs is much larger than the membrane permeance [34]. It is clear that a single ST-240 membrane stage is sufficient to reduce the concentration of the rhodium-based catalyst in the permeate to less than 5 ppm. However, a single ST-240 membrane may not always be capable of reaching the desired catalyst recovery. In this case, using the single-stage ST-240 membrane performance as determined experimentally, the number of membrane stages necessary to achieve an overall recovery of 99.9% can be calculated from Equation 4.7 (adapted from [34]).

$$R_{cat,overall} = \sum_{i=1}^{N_{stages}} R_{stage}\left(1 - R_{stage}\right)^{i-1} \quad (4.7)$$

where R_{stage} refers to the catalyst recovery capacity of a single membrane stage and N_{stages} the number of membrane stages needed to reach an overall catalyst recovery of 99.9%.

4.5.4 Results and discCDussion

In this section, the energy and cost efficiency of OSN and distillation for the recovery of **$HRh(CO)(PPh_3)_3$** from 1-octene and 1-decene hydroformylation post-reaction mixtures are compared. Table 4.5 summarises the total operating costs and energy usages of the OSN and distillation catalyst recovery systems for different solvent systems.

Based on the results presented in Table 4.5, it can be observed that the overall energy consumption remains consistently 99% lower for the multistage OSN system compared to the distillation process for all cases considered. This validates the energy benefits of membrane systems for homogeneous catalyst recovery. Moreover, it can also be observed from Table 4.5 that for the recovery of homogeneous catalysts, OSN systems

require *ca*. 90% less operational expenditure per annum than distillation processes. This clearly elucidates the cost benefits of OSN systems over classic separation units.

Table 4.5: Cost- and energy efficiency of OSN and distillation for **$HRh(CO)(PPh_3)_3$** recovery[a]

	OSN		Distillation	
	$\dot{Q}_M$ (kW)	TOC_M (Rx10^3)	$\dot{Q}_{dist}$ (kW)	TOC_{dist} (Rx10^3)
1-Octene	0.426	340	26.8	3,406
1-Decene	0.407	352	31.4	1,926
1-Nonanal	0.369	372	33.2	2,319
1-Undecanal	0.369	407	36.4	2,404
1-Nonanol	0.370	527	39.9	2,623
1-Undecanol	0.367	789	42.7	5,932

[a] All values determined on a 100 $kg.h^{-1}$ feed flow basis.

However, it should be noted that when the energy costs are excluded from the cost analysis, total operating costs for OSN is more than that required for distillation. This is due to the relatively large initial investment necessary for OSN operating and the regular maintenance, even replacement, of OSN systems. Distillation systems are also already in place at most industrial scale plants, significantly reducing its initial cost input. Unfortunately, there are more limitations to the OSN system. Firstly, separation is limited by the solubility of catalyst in the solvent and should be maintained to prevent the catalyst from settling out and potentially damaging the membrane. Secondly, large numbers of membrane modules is required in order to meet the volume capacity of distillation systems and requires increased investment and maintenance costs [29].

4.6 Concluding remarks on catalyst recovery

The reusability of the homogeneous rhodium-based catalyst, **$HRh(CO)(PPh_3)_3$**, was investigated after being subjected to OSN processing. Firstly, the STARMEM^{TM} 240 membrane proved successful in recovering the rhodium-based catalyst (>98.0%) from different reaction species. Furthermore, the recovered catalyst was shown to maintain its catalytic activity for at least three consecutive hydroformylation reaction cycles, thereby improving upon its overall TON. Therefore, OSN is capable of recovering the catalyst in a form not requiring additional costly and intrusive reactivation and separation methods.

Moreover, an economic and energy evaluation of OSN for the recovery of **$HRh(CO)(PPh_3)_3$** from reaction systems (1-octene/1-nonanal, 1-decene/1-undecanal and 1-nonanal/1-nonanol) was performed and compared against distillation in terms of energy and cost expenditures. Based on the evaluation, it was determined that energy and cost savings of up to 99% and 90%, respectively, can be achieved, thereby confirming the vast potential of OSN as an alternative to conventional downstream recovery processes. It should however be emphasised that, although promising, the cost and energy comparisons made are approximate and a complete economic analysis for continuous OSN systems still remains necessary to evaluate parameters such as payback periods, net present values, etc.

.

4.7 References

[1] P. Van der Gryp, A. Barnard, J.P. Cronje, D. de Vlieger, S. Marx, H.C.M. Vosloo, *J. Memb. Sci.* **353** (2010) 70–77.

[2] A. Peschel, B. Hentschel, H. Freund, K. Sundmacher, *Comput. Aided Process Eng*. (2011) 1247.

[3] J.K. MacDougall, D.J. Cole-hamilton, *J. Chem. Soc*. (1990) 165–167.

[4] J.L. Paul, W.L. Pieper, L.E. Wade, **Reduction of Catalyst Deactivation in Processes for Hydroformylation of Olefins with Rhodium Complex Catalysts**, US4,151,209, 1979.

[5] D. Evans, T.A. Osborn, G. Wilkinson, *J. Chem. Soc*. **11** (1968) 3133–3142.

[6] A. Buhling, P.C.J. Kamer, P.W.N.M. Van Leeuwen, *J. Mol. Catal. A Chem.* **98** (1995) 69–80.

[7] M. Haumann, H. Yildiz, H. Koch, R. Schomäcker, *Appl. Catal. A Gen*. **236** (2002) 173–178.

[8] R.M. Deshpande, S.S. Divekar, *J. Mol. Catal.* **67** (1991) 333–338.

[9] G. Achonduh, Q. Yang, H. Alper, *Tetrahedron*. **71** (2015) 1241–1246.

[10] J. Tijani, B. El Ali, *J. Organomet. Chem*. **692** (2007) 3492–3497.

[11] N.C. Antonels, J.R. Moss, G.S. Smith, *J. Organomet. Chem*. **696** (2011) 2003–2007.

[12] A.A. Dabbawala, J.N. Parmar, R. V Jasra, H.C. Bajaj, E. Monflier, *Catal. Commun*. **10** (2009) 1808–1812.

[13] A. Behr, P. Neubert, **Applied Homogeneous Catalysis**, Wiley VCH, Germany, 2012.

[14] F. Zheng, Z. Zhang, C. Li, Q. Yuan, *J. Memb. Sci.* **332** (2009) 13–23.

[15] F. Zheng, C. Li, Q. Yuan, F. Vriesekoop, *J. Memb. Sci*. **318** (2008) 114–122.

[16] L.S. White, *J. Memb. Sci.* **205** (2002) 191–202.

[17] N.S.A. Razak, M.S. Shaharun, H. Mukhtar, M.F. Taha, *Sains Malaysiana*. **42** (2013) 515–520.

[18] J.A. Whu, B.C. Baltzis, K.K. Sirkar, *J. Memb. Sci.* **170** (2000) 159–172.

[19] L.G. Peeva, E. Gibbins, S.S. Luthra, L.S. White, R.P. Stateva, A.G. Livingston, *J. Memb. Sci*. **236** (2004) 121–136.

[20] J.T. Scarpello, D. Nair, L.M. Freitas Dos Santos, L.S. White, A.G. Livingston, *J. Memb. Sci.* **203** (2002) 71–85.

[21] H. Wong, Y.H. See-Toh, F.C. Ferreira, R. Crook, A.G. Livingston, *Chem. Commun. (Camb).* (2006) 2063–2065.

[22] D. Nair, J.T. Scarpello, L.S. White, L.M. Freitas Dos Santos, I.F.J. Vankelecom, A.G. Livingston, *Tetrahedron Lett*. **42** (2001) 8219–8222.

[23] D. Ormerod, B. Sledsens, G. Vercammen, D. Van Gool, T. Linsen, A. Buekenhoudt, B. Bongers, *Sep. Purif. Technol*. **115** (2013) 158–162.

[24] M.G. Buonomenna, J. Bae, *Sep. Purif. Rev.* **44** (2015) 157–182.

[25] L. Hesse, J. Mićović, P. Schmidt, A. Górak, G. Sadowski, *J. Memb. Sci.* **428** (2013) 554–561.

[26] A.P.B. Ribeiro, J.M.L.N. de Moura, L.A.G. Goncalves, J.C.C.P. Petrus, L.A. Viotto, *J. Memb. Sci.* **282** (2006) 328–336.

[27] D. Bhanushali, D. Bhattacharyya, Ann. New York Acad. Sci. **177** (2003) 159–177.

[28] N. Ochoa, C. Pagliero, J. Marchese, M. Mattea, *Sep. Purif. Technol*. **22-23** (2001) 417–422.

[29] E.M. Rundquist, C.J. Pink, A.G. Livingston, *Green Chem.* **14** (2012) 2197–2205.

[30] S. Darvishmanesh, L. Firoozpour, J. Vanneste, P. Luis, J. Degrève, B. Van der Bruggen, *Green Chem.* **13** (2011) 3476–3483.

[31] J. Geens, B. De Witte, B. Van der Bruggen, *Sep. Sci. Technol.* **42** (2007) 2435–2449.

[32] G. Székely, M.F. Jimenez-Solomon, P. Marchetti, J.F. Kim, A.G. Livingston, *Green Chem.* (2014).

[33] P. Vandezande, L.E.M. Gevers, I.F.J. Vankelecom, *Chem. Soc. Rev*. **37** (2008) 365–405.

[34] P. Schmidt, E.L. Bednarz, P. Lutze, A. Górak, *Chem. Eng. Sci.* **115** (2014) 115–126.

[35] R. Turton, R.C. Bailie, W.B. Whiting, J.A. Schaeiwitz, **Analysis, Synthesis, and Design of Chemical Processes**, 3rd Ed., Prentice Hall, Boston, 2009.

[36] J.M. Douglas, **Conceptual Design of Chemical Processes**, McGraw-Hill, 1988.

[37] [Online], (2015). www.kitco.com. Date accessed: 20 July 2015.

[38] R.K. Sinnot, **Coulson & Richardson's Chemical Engineering Design**, 4th Ed., Butterworth-Heinemann, Oxford, 2005.

CHAPTER 5: Results and Discussion – OSN Characterisation and Modelling

5.1 Overview

Knowledge of membrane performance in terms of permeance and separation is crucial for application on industrial scale due to its effect on downstream processes. The aim of this chapter therefore is to characterise the STARMEM^{TM} 240 (ST-240) membrane in terms of flux and separation for application in homogeneous catalysis, considering the hydroformylation and subsequent hydrogenation of 1-octene and 1-decene as prototype reactions. Furthermore, the effects of applied pressure, solvent type and catalyst loading on membrane performance is quantified and discussed.

This chapter can be divided into five sections. Section 5.2 characterises the ST-240 membrane with respect to 1) reproducibility, repeatability and steady-state conditions, 2) flux performance of pure solvents, 3) permeance and solvent separation performance of binary mixtures, and, 4) catalyst permeation performance of solvent mixtures. Section 5.3 quantifies the degree of membrane-species interaction in terms of sorption while in Section 5.4 the experimental data is compared to literature transport models. This chapter is then concluded with Section 5.5 with some final remarks regarding OSN performance characterisation and modelling.

5.2 Permeance and separation performance of the ST-240 membrane

5.2.1 Introduction

The permeation and separation performance of the commercially available polyimide ST-240 membrane was characterised for the hydroformylation reaction system in terms of species flux, catalyst recovery, species separation and degree of membrane-species sorption (swelling). Parameters that were varied during the course of characterisation include feed pressure, solvent type and feed concentration as well as catalyst type and catalyst feed concentration.

5.2.2 Steady-state verification

The repeatability and reproducibility of the experimental dead-end setup used and procedure followed, and therefore the experimental results obtained, were tested and are presented in this section. Furthermore, the characterisation of steady-state conditions is also given.

The confirmation of steady-state, characterised by constant flux and separation values with time, is required as it serves as a true reflection of the OSN performance at the conditions under investigation. The membrane conditioning procedure, as described in Section 3.4.3, is required to alleviate the initial stages of membrane compaction and

serves as pretreatment for the achievement of steady-state conditions. A typical observation regarding the achievement of steady-state permeate flux is presented in Figure 5.1 for 1-nonanal at 30 bar. For this specific experiment, the cell was reloaded five times and the filtration process repeated until an approximate steady-state flux of 15.0 ± 3.2 $L.m^{-2}.h^{-1}$ was confirmed.

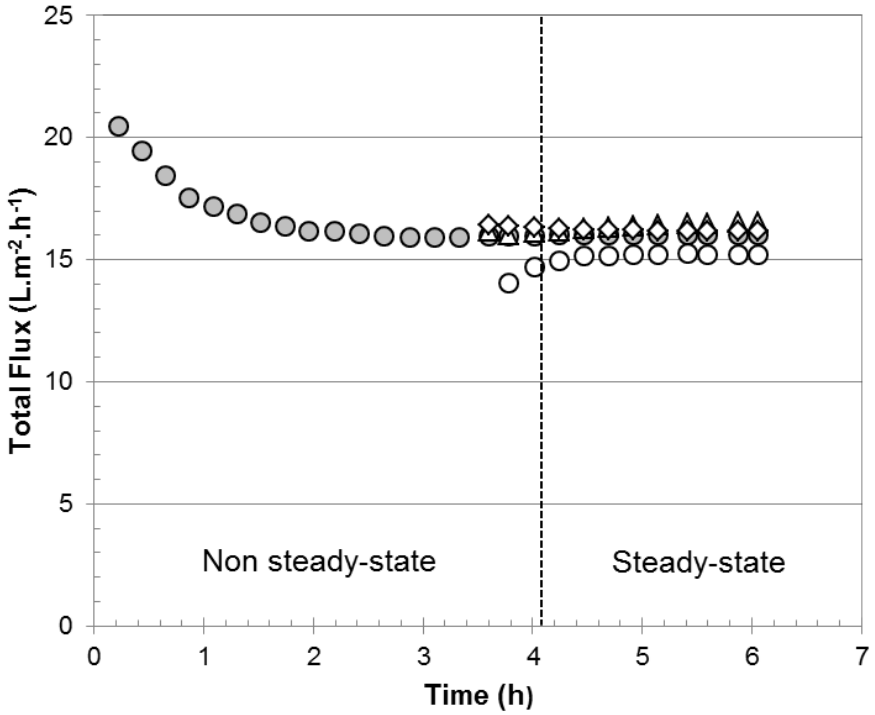

Figure 5.1: Typical flux measurement depicting the characterisation of steady-state for 1-nonanal at 30 bar (●) with three repeatable runs (○, △ and ◇)

It is clear from Figure 5.1 that steady-state conditions were acquired *ca.* 4 hours into each experimental run at which point flux stabilises to a constant value. Furthermore, the flux was highest initially and decreases as the experiment continues by nearly 30% which indicates membrane compaction. Adam *et al.* reassured that the flux decline caused by compaction should not influence the membrane's separation capacity unless significant morphological alterations occur to the membrane's active layer [1]. Moreover, Whu *et al.* [2] previously observed that compaction and its effects on membrane performance lasted only while the membrane was under pressure. They characterised compaction as a decline in flux caused partly due to the shrinkage of membrane pore size and/or reduction of the membrane thickness.

5.2.3 Experimental repeatability and reproducibility

The experimental error of the OSN experimental methodology and setup was tested in order to confirm its reliability and dependability. This was done by performing at least three repeated experiments under similar operating conditions at different times. The results obtained for the repeated runs are compared through statistical analysis and observations are made in terms of variance, deviation and percentage error. This was done for pure and binary species systems. A summary of the experimental errors, considering the case of pure 1-octene as feed, at different pressures is given in Table 5.1.

Table 5.1: Repeatability results of pure species fluxes

Pressure (bar)	Flux ($kg.m^{-2}.h^{-1}$)	Standard deviation (-)	Error (%)
1-Octene			
10	29.3	1.02	0.590
20	58.0	4.13	2.38
30	96.7	8.98	5.19
40	110	6.18	3.57
1-Decene			
30	32.3	2.19	1.27
1-Nonanal			
30	12.4	3.21	1.61
1-Undecanal			
30	7.91	3.38	1.95
1-Nonanol			
30	2.32	1.19	0.530
1-Undecanol			
30	1.38	0.840	0.420

In order to illustrate the repeatability of the binary systems, 1-octene/1-nonanal at 30 bar was considered as feed at different organic species concentration and five experimental repeats were performed. A summary of experimental errors are presented in Table 5.2.

Table 5.2: Repeatability results of binary mixtures fluxes

1-Octene volume fraction (-)	Flux (kg.m^{-2}.h^{-1})	Standard deviation (-)	Error (%)
0.0	12.4	3.21	1.61
0.2	13.8	5.59	2.79
0.4	16.1	3.22	1.61
0.6	19.5	2.63	1.52
0.8	23.6	6.48	3.24
1.0	96.7	8.98	5.19

Based on these findings, the flux values of the pure and binary mixture systems can be approximated within an average experimental error of approximately 3.0% which compares well with literature [3].

5.2.4 Pure species permeation

5.2.4.1 Introduction

Species separation is achieved based on the difference in the rate at which species permeate through the membrane. With this mind, the permeation rates for pure species representative of the 1-octene and 1-decene hydroformylation reactions were evaluated with respect to variations in applied pressure and species properties.

5.2.4.2 Effect of applied pressure

The pure species fluxes achieved with the ST-240 membrane at different pressures (10 - 40 bar), constant stirrer speed (500 rpm) and room temperature (20 ± 2 °C) are presented in Figure 5.2.

It can be observed from Figure 5.2 that the pure species flux increased in the applied pressure range of 10 – 40 bar. In decreasing order, the pure fluxes can be arranged in the order 1-octene > 1-decene > 1-nonanal > 1-undecanal > 1-nonanol > 1-undecanol. Moreover, Figure 5.2 demonstrates the linear dependence of flux on applied pressure which can be described by the Spiegler-Kedem equation [4]:

$$J_V = L_P(\Delta P - \sigma\Delta\pi) \qquad (5.1)$$

where J_V is the species volume flux, ΔP the transmembrane pressure, $\Delta\pi$ transmembrane osmotic pressure, σ the reflection coefficient and L_P is the membrane permeance.

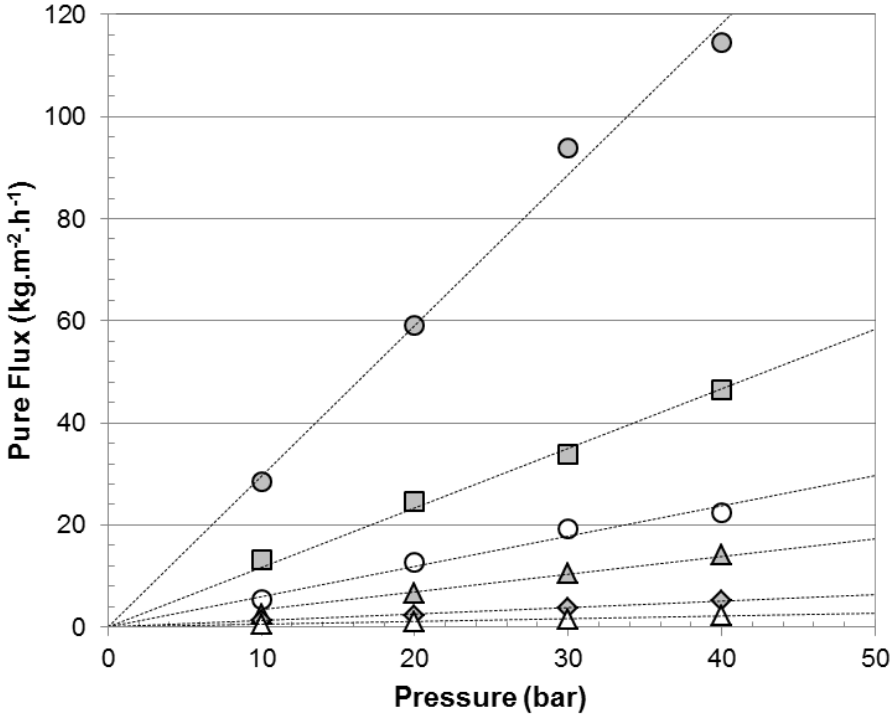

Figure 5.2: Effect of applied pressure on pure species flux.
[○1-octene;□ 1-decene; ○ 1-nonanal;△ 1-undecanal;◇ 1-nonanol;
△ 1-undecanol]

Each of the species has a unique L_P value, as listed in Table 5.3, and describes its permeance, i.e. ease of passage, through the membrane.

Table 5.3: Permeance of pure species used in this study

Species	Mass Permeance ($kg.m^{-2}.h^{-1}.bar^{-1}$)
1-Octene	2.97 ± 0.102
1-Decene	1.20 ± 0.065
1-Nonanal	0.600 ± 0.043
1-Undecanal	0.322 ± 0.039
1-Nonanol	0.123 ± 0.004
1-Undecanol	0.0520 ± 0.002

Equation 5.1 describes the transport of species across a membrane and states that in the absence of osmotic pressure (i.e. $\Delta\pi \cong 0$), volume flux, J_V, will be linearly dependent on the transmembrane pressure, ΔP. This is true for pure species as the zero intercepts, as shown in Figure 5.2, reflect the absence of solutes in the feed. This linear flux-pressure

relationship as observed in Figure 5.2 can be corroborated with the findings of previous researchers [5–8].

5.2.4.3 Effect of species properties

In order to emphasise the influence of solvent properties on membrane permeation, some of the properties of the chemicals used in this investigation are listed in Table 5.4.

As observed in Figure 5.2, the large difference between the olefin flux through the ST-240 membrane relative to that of the alcohols was expected due to the differences in molecular size, viscosity and polarity. Relative to the membrane MWCO (400 $g.mol^{-1}$), the molecular weights of 1-nonanol (144 $g.mol^{-1}$) and 1-undecanol (172 $g.mol^{-1}$) were the closest and therefore were anticipated to have the lowest fluxes as it was most affected by steric hindrance. As for the olefins (112 $g.mol^{-1}$ for 1-octene and 140 $g.mol^{-1}$ for 1-decene), their molecular weights were furthest away from the MWCO of ST-240, indicating that their small size relative to the membrane pore size allow for easy permeation. Therefore, the olefins were anticipated to have the highest fluxes. However, when the species are arranged in order of increasing molecular weight 1-octene < 1-decene < 1-nonanal < **1-nonanol** < **1-undecanal** < 1-undecanol, no clear correlation can be observed between its apparent permeate flux. This indicates that molecular size (molecular weight, molar volume, etc.) alone is not sufficient in describing species transport across the membrane. Darvishmanesh *et al.* reported that the apparent molecular size is significantly influenced by the presence of organic solvents due to a combination of solvation and hydration effects, thereby clarifying the inability of MWCO and size parameters as a predictive measure for membrane performance across all solvents [9].

In terms of molecular shape, per definition, it refers to the geometrical conformation of a given molecular based on the distribution of its mass [10]. Chen *et al.* [11] observed that solute rejection is greater influenced by molecular length than compared to its width. Molecular shape is in general difficult to predict due to various reasons, including 1) the large number of geometric conformations that a molecule may exhibit, and 2) molecular shape is strongly influenced by the nature of the surrounding solvent due to inter- and intramolecular interactions. Previous studies have shown that branched molecules exhibit a higher rejection, i.e. a lower flux, than its analogous linear counterpart [10,12,13].

Table 5.4: Summary of properties of the species used in this investigation [14–18]

	Structure	Molecular Weight (MW)	Molar Volume (V_m)	Viscosity (η)	Dipole Moment (μ_D)	Polarity	Solubility Parameter (δ)
1-Octene		112	157	0.452	0.340	Non-polar	15.6
1-Decene		140	187	0.748	0.420	Non-polar	16.0
1-Nonanal	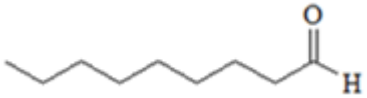	142	172	1.35	2.84	Moderately polar	19.0
1-Undecanal	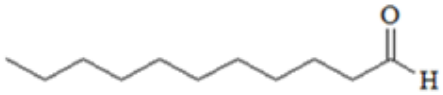	170	206	1.73	2.50	Moderately polar	18.7
1-Nonanol	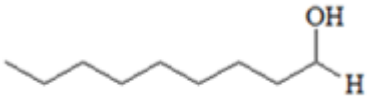	144	174	9.32	1.61	Polar	20.7
1-Undecanol	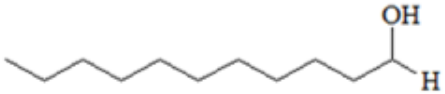	172	208	15.5	1.62	Polar	20.3

Parameters are needed to describe not only the structural properties of the species but also those that are able to relate the chemical properties of the solvent to properties of the membrane.

The viscosity of pure species perfectly reflects the pure species fluxes observed, when arranged in the order 1-octene < 1-decene < 1-nonanal < 1-undecanal < 1-nonanol < 1-undecanol. This shows that the viscosity of the species is inversely proportional to its flux through the membrane, as demonstrated in Figure 5.3, with a Pearson correlation, a measure of the linear dependence of two variables, of approximately 99.3%. The direct dependence of species permeation on properties such as viscosity demonstrates the convective nature of species transport across the membrane, i.e. species transport is dominated by diffusive properties.

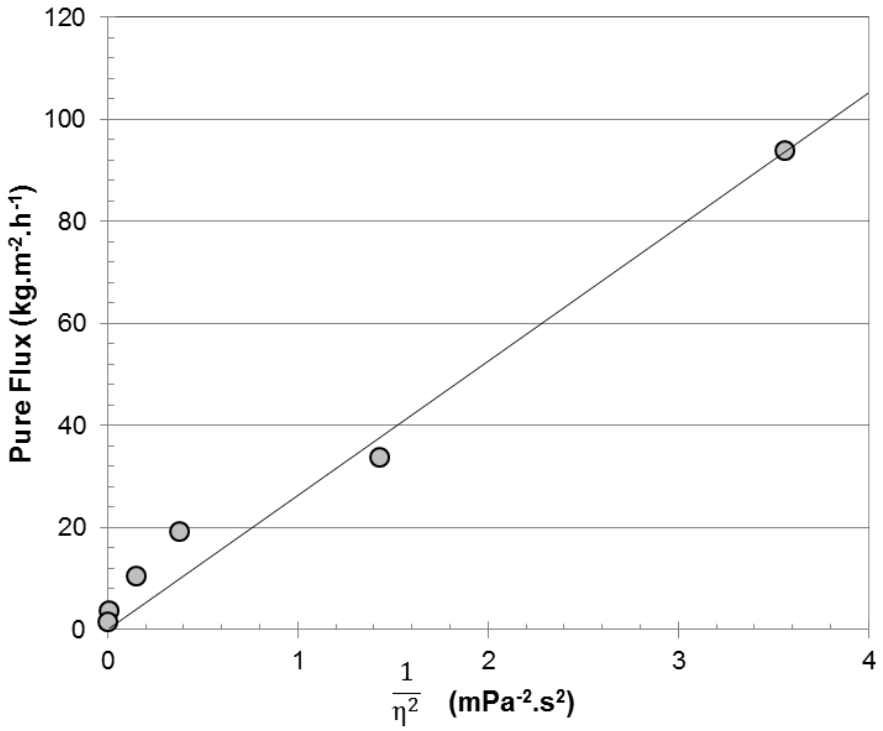

Figure 5.3: Correlation between the inverse of pure species viscosity and their corresponding flux

Previous studies have shown that the fluxes of polymeric membranes are inversely proportional to the viscosity of the permeating component indicating the importance of viscosity in membrane permeation [8,20–22]. However, Geens *et al.* [23] stated that although nearly every flux prediction model includes the reciprocal of viscosity, it alone cannot sufficiently describe the flux of organic mixtures. Therefore, to broaden the

dimensionality of the models, additional parameters are required to encompass a much wider range of properties representative of the permeating component.

When ranked in terms of increasing species dipole moment, the order is presented as 1-octene < 1-decene < **1-nonanol** < **1-undecanol** < **1-nonanal** < **1-undecanal**. From this arrangement, it can be seen that the aldehydes and alcohols swapped places when comparing it to the order of increasing fluxes. This is as a result of the large dipole moment for the aldehyde species due to the presence of the carbonyl group. However, when comparing the dipole moment of species of the same functional group, a correlation can be observed with flux, i.e. for the olefins, flux decreases with increasing dipole moment. Therefore, dipole moment, as a representative of polarity, is unable to predict the flux of organic solvents across different functional groups and therefore another polarity parameter is required for this purpose. When considering the electronegativity, χ_P, of atoms as demonstrated by the Pauling scale, i.e. Hydrogen 2.20, Carbon 2.55 and Oxygen 3.44, the bond polarity, δ_B, can be determined for the C-H, O=C and O-H bonds corresponding to the olefins, aldehydes and alcohols, as 0.35, 0.89 and 1.24, respectively [24]. Refer to Appendix G for sample calculations.

Based on the bond polarity values as determined using Pauling's scale, the polarity of the olefins, aldehydes and alcohols can be approximated as non-polar, moderately polar and polar, respectively, as presented in Table 5.4. When ranked in terms of increasing bond polarity, e.g. olefins < aldehydes < alcohols, it provides a better reflection of the different pure species fluxes. It can be seen from Figure 5.2 that the non-polar olefins, i.e. 1-octene and 1-decene, has the highest flux while the highly polar alcohols, i.e. 1-nonanol and 1-undecanol, exhibited the lowest flux. This confirms the hydrophobic nature of the ST-240 membrane as it restricts the permeation of polar species and attracts the non-polar species. The aldehydes are considered moderately polar and therefore achieved a flux less than that of the olefins but greater than the alcohols. Therefore, it is proven that for the hydrophobic ST-240 membrane, polarity can be used to provide a general indication of pure fluxes. Similar observations were made by previous researchers [25–28].

The Van der Bruggen group [12,29] previously reported on an interesting effect of dipole moment, stating that the molecule's orientation relative to the membrane surface is altered based on its polarity. For linear molecules, a perpendicular orientation relative to the membrane surface can decrease its apparent size and allow for a reduction in rejection.

The difference in solubility parameter, $\Delta\delta$, as shown in Equation 5.2, can be estimated using the group contribution method and has previously been used by researchers to characterise the affinity of two species (i.e. solvent, solute, membrane) toward each other, giving an indication of species miscibility and degree of membrane swelling [9,12,27,30–32].

$$\Delta\delta = |\delta_i - \delta_M| \tag{5.2}$$

where δ_i is the solubility parameter of species i and δ_M the solubility parameter of the membrane material, i.e. Matrimid 5218 with 23.2 $MPa^{0.5}$ [33].

The solubility parameter of the olefins, i.e. 1-octene and 1-decene, is furthest away from that of the membrane material with an absolute difference of approximately 7.5 $MPa^{0.5}$. The olefins are followed by the aldehydes and then the alcohols, with absolute solubility differences of approximately 4.3 $MPa^{0.5}$ and 2.7 $MPa^{0.5}$, respectively. This indicates the larger the absolute difference between the solubility parameter of the species and the membrane, the higher the flux.

However, contradicting results are reported regarding the relationship between permeance and solubility parameter. Literature has shown that, generally, the closer the solubility parameters of two species, i.e. the smaller the difference between the solubility parameter of the species, the stronger the interaction forces between the two which translate into a higher flux. Robinson *et al.* [32] stated that a higher solubility parameter, i.e. closer to that of the membrane, will result in higher fluxes. Yet, in the same breath, they claim that the relationship in question may be misleading as they reported low permeance for species with very large $|\delta_i - \delta_M|$ values. Similar contradicting results were reported by the Van der Bruggen group [9] although recognising the importance of solubility parameter especially in membrane separation. For their study, using the ST-122 membrane (23.2 $MPa^{0.5}$), they recorded methyl ethyl ketone (9.3 $MPa^{0.5}$) as having the highest permeance (8.51 $L.m^{-2}.h^{-1}.bar^{-1}$). However, they also recorded the permeance of methanol (14.5 $MPa^{0.5}$) as 5.48 $L.m^{-2}.h^{-1}.bar^{-1}$, indicating that the larger the $|\delta_i - \delta_M|$ value, the higher the flux.

In summary, confirmation is afforded to the inherent influence that molecular size, viscosity and the interaction between the membrane and solvent (solubility and polarity), respectively, have on the flux of components through a membrane. Various other parameters have also been reported to influence the flux of species through membranes,

including surface tension [23,34–36]. Comprehensive studies by research groups such as those of Van der Bruggen [9,12] and Vandecasteele [29] afforded confirmation of the influence of this and other parameters on membrane performance. However, on its own, either of these parameters mentioned fail to predict membrane performance across all functional groups and membrane types. Geens *et al.* [23] and Bhanushali *et al.* [8] went on to describe their interpretation of a good flux model, with successful results, to include a combination of solvent properties such as viscosity, molecular size and a parameter which will account for the membrane-solvent affinity (i.e. surface tension, polarity, etc.) and would take the form as presented in Equation 5.3:

$$Permeability \propto \left(\frac{molecular\ size}{1}\right) \times \left(\frac{1}{viscosity}\right) \times \left(\frac{1}{affinity}\right) \quad (5.3)$$

The model proposed by Bhanushali, consisting of the elements shown in Equation 5.3 provides a good correlation with the experimental fluxes obtained for each of the species considered, as presented in Figure 5.4, with a Pearson correlation of approximately 98.0%. This confirms the significant influence of viscosity, molecular size and membrane-solvent affinity on membrane permeation performance.

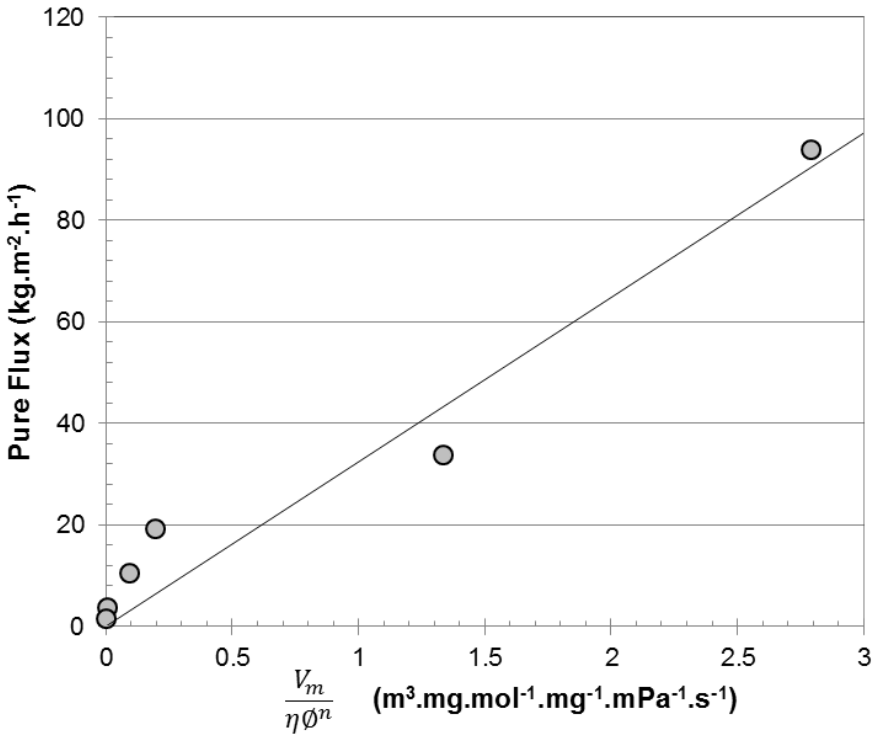

Figure 5.4: Confirmation of influence of viscosity, molecular size and membrane-solvent affinity on membrane permeation performance for different reaction species

In order to study the effect of catalyst load on the membrane performance, the **$HRh(CO)(PPh_3)_3$** concentration in 1-octene was varied and the pressure held constant at 30 bar. A comparison of the membrane permeation performance in the absence and presence of **$HRh(CO)(PPh_3)_3$** is given in Figure 5.5.

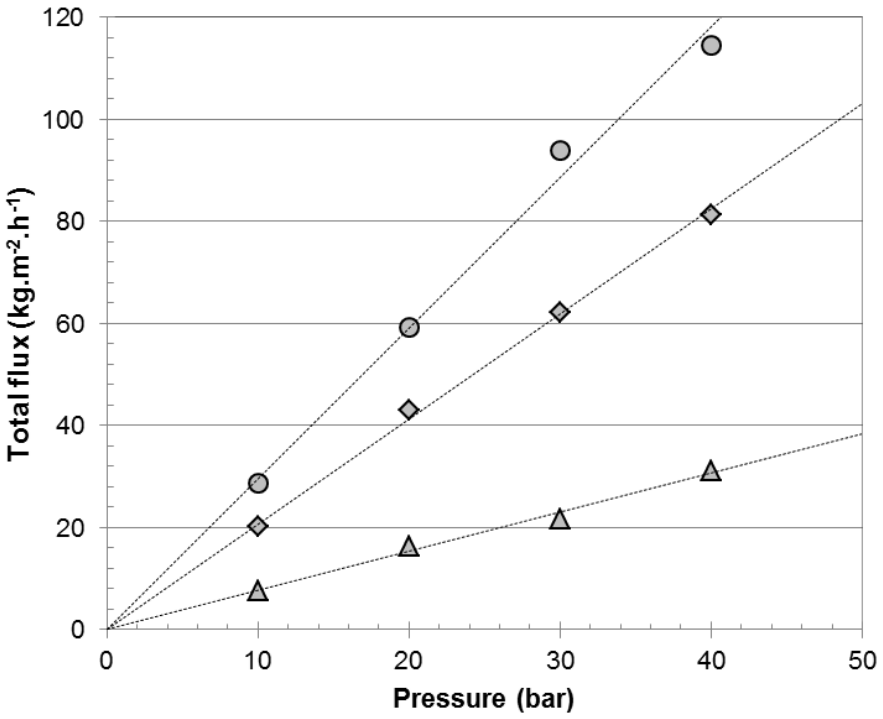

Figure 5.5: Total flux of 1-octene at **$HRh(CO)(PPh_3)_3$** concentrations of 0 ppm (●), 200 ppm (◆) and 500 ppm (▲)

In terms of flux, the addition of the catalyst significantly degraded the species flux and this effect became more pronounced at higher catalyst loadings, as demonstrated in Figure 5.5. Literature has previously shown that an increase in the catalyst feed concentration will lead to a significant reduction in membrane permeance and has been attributed to possible fouling or concentration polarisation mechanisms [37]. Per definition, these phenomena are caused by the deposition of solid particulate onto the membrane surface and the blockage of membrane pores. In terms of catalyst deposition, a photograph of a new fresh membrane was compared to that of a membrane that has been repeatedly used for catalyst recovery and is presented in Figure 5.6.

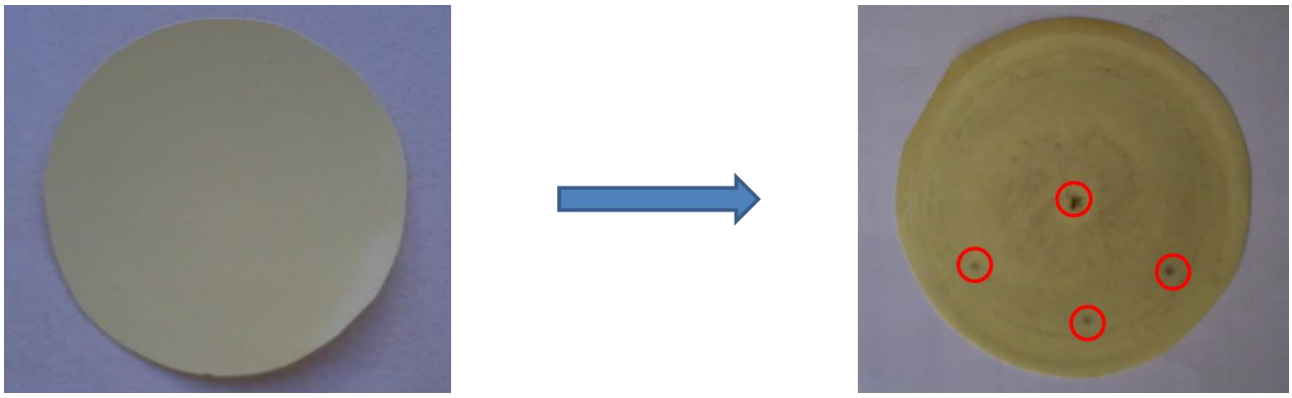

Figure 5.6: Observation of catalyst deposition onto ST-240 membrane surface

Figure 5.6 clearly demonstrates that small amounts of dark solids deposited on the membrane surface, also noticed previously by Rabiller-Baudry *et al.* [38], which could be the cause of the flux reduction observed. The solvent fluxes are then compared, shown in Figure 5.7, upon the addition of the cobalt-catalyst, **$Co(C_5H_7O_2)_3$**, to that observed for the rhodium-based catalyst, **$HRh(CO)(PPh_3)_3$**, at similar operating conditions of feed concentration (500 ppm) and applied pressure (30 bar).

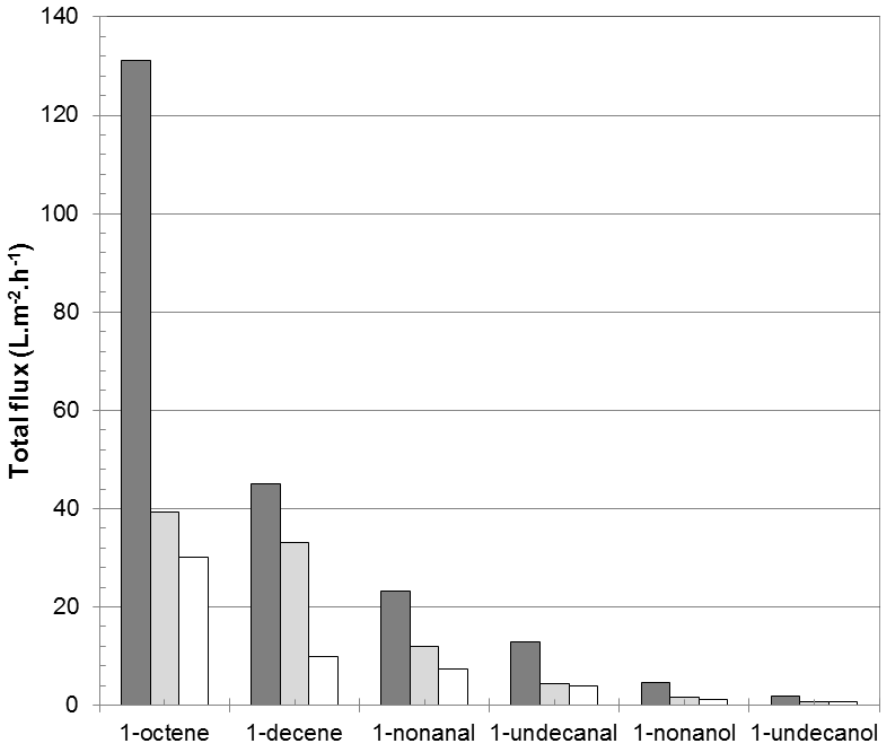

Figure 5.7: Effect of **$HRh(CO)(PPh_3)_3$** (▒) and **$Co(C_5H_7O_2)_3$** (□) addition relative to pure species flux (■) at 30 bar

It is clear from Figure 5.7 that a higher solvent flux is observed in the presence of the rhodium-based catalyst than compared to its cobalt counterpart at similar concentrations. It was discovered that due to the large and bulky nature of the rhodium catalyst, it can be easily rejected by the membrane. Therefore, within the membrane pores, it can be argued that the solvent molecules pass through with minimal resistance. However, in the case of the cobalt catalyst, as reported previously, it had a recovery of 88%, indicating that some of the catalyst has passed through the membrane. It can therefore be argued that in the presence of cobalt catalyst, the solvent molecules are competing with the cobalt catalyst for passage through the membrane, resulting in a lower solvent flux.

5.2.5 Binary species mixture permeation and separation

5.2.5.1 Introduction

The species permeation and separation performance of the ST-240 membrane for binary species mixtures are presented in this section. The pressure was maintained constant at 30 bar while the concentration of the binary mixtures was varied between 0 and 100 vol%. Binary mixtures considered were 1-octene/1-nonanal and 1-decene/1-undecanal (representative of the hydroformylation reaction) as well as 1-nonanal/1-nonanol (representative of hydrogenation side-reaction).

5.2.5.2 Experimental results

The experimental results obtained for the total flux of binary mixtures 1-octene/1-nonanal, 1-decene/1-undecanal and 1-nonanal/1-nonanol at an applied pressure of 30 bar and room temperature (20 ± 2 °C) are presented in Figure 5.8 as a function of feed concentration.

With respect to the total flux of binary mixtures, it can be observed from Figure 5.8 to increase exponentially with increasing feed concentration of the lower volatility component (LVC) in the respective binary mixtures, i.e. 1-octene, 1-decene and 1-nonanal. Similar trends were observed by the Wessling [39] and Livingston [36] groups for binary mixtures of isopropanol-toluene and methanol-water, respectively. Moreover, up until 60 vol% of the lighter volatility component (LVC) in each of the respective binary mixtures, the total flux appeared to have a slight linear dependence on the feed volume fraction but increased exponentially as the concentration of the LVC increased. Adam *et al.* attributed this flux behaviour to flow coupling effects between the species involved in the mixture and these effects tend to increase at higher pressures [1]. Dijkstra *et al*. [21] also noticed that same behaviour with their binary systems (pentane/decane and pentane/dodecane) using a PDMS membrane and suggested that a change occurs in the mechanism through which

these species pass across the membrane [21]. Increasing the feed concentration of the species which preferentially sorbs into the membrane will result in a reduction in the percentage diffusive transport and subsequently increase the viscous transport.

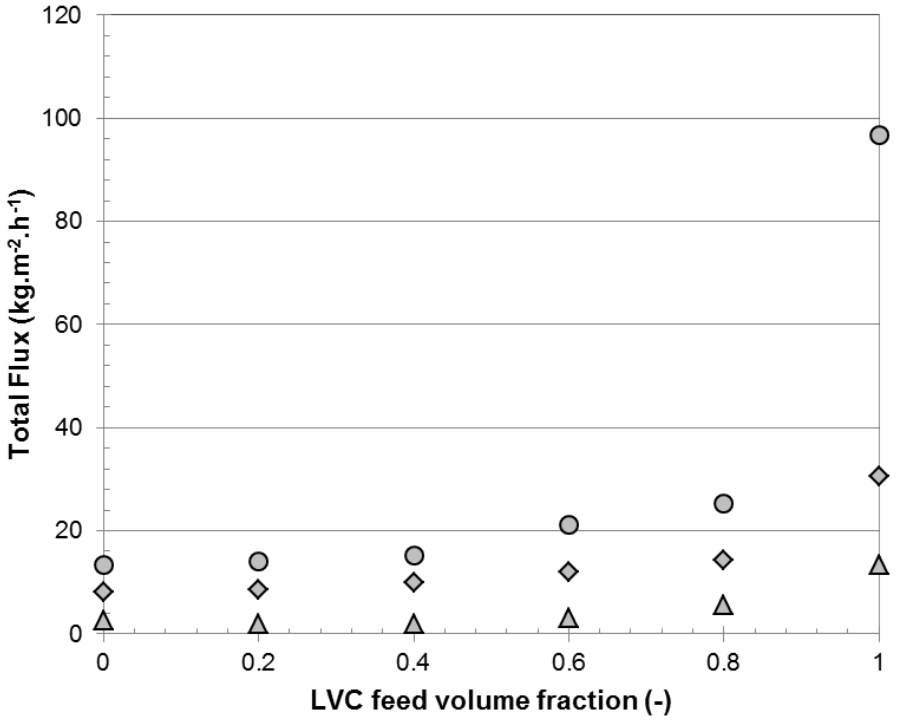

Figure 5.8: Total flux for the binary mixtures of 1-octene/1-nonanal (●), 1-decene/1-undecanal (◆) and 1-nonanol/1-nonanal (▲)

With respect to the separation of binary mixtures, results are given in Figure 5.9 in which the solvent concentration in the feed and permeate streams are compared. It should be noted that Figure 5.9 is expressed in terms of the concentration of the solvent in the binary mixture which preferentially permeates through the membrane relative to the other, i.e. 1-nonanal in the case of 1-octene/1-nonanal mixture, 1-decene for the 1-decene/1-undecanal mixture and 1-nonanol for the 1-nonanal/1-nonanol mixture.

The degree of species separation, α_i, achieved by the ST-240 membrane is determined by allowing the system to proceed until steady-state and thereafter, analysing the concentration of a solvent in the permeate using GC. The degree of separation refers to the ratio of the resulting permeate concentration, C_P, of solvent i to that present in the feed, C_F, as shown in Equation 5.4.

$$\alpha_i = \frac{C_{P,i}}{C_{F,i}} \tag{5.4}$$

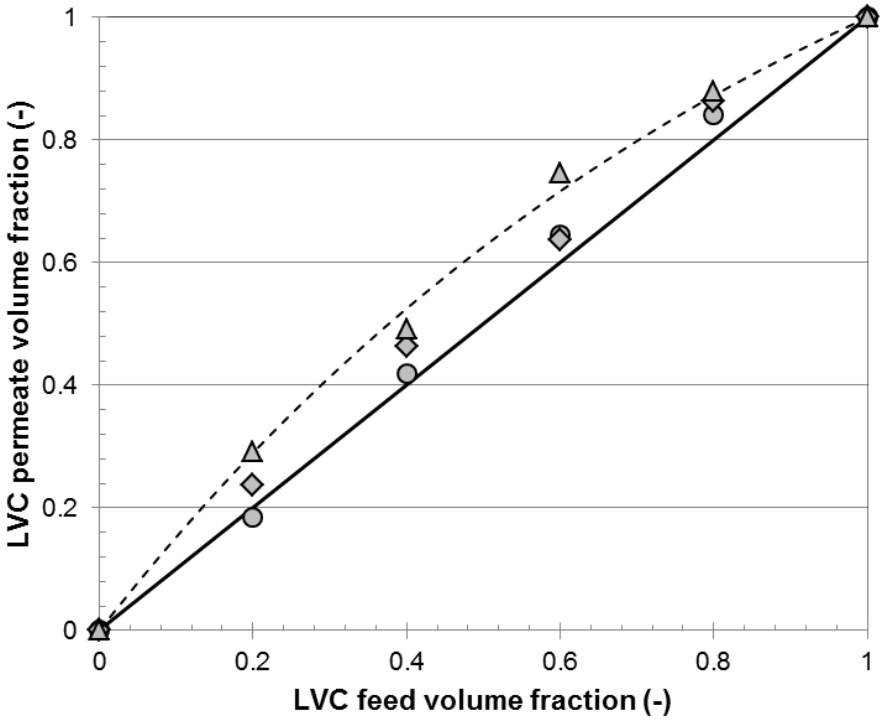

Figure 5.9: Degree of binary solvent separation for 1-octene/1-nonanal (●), 1-decene/1-undecanal (◆) and 1-nonanol/1-nonanal (Experimental ▲, VLE – – –)

It is clear from Figure 5.9 that the concentrations in the feed and permeate are fairly similar which indicate a degree of separation close to one for both the hydroformylation mixtures of 1-octene/1-nonanal and 1-decene/1-undecanal. Consequently, this shows that no separation is achieved between the species and the conclusion can be drawn that these two hydroformylation reaction systems act as quasi-single species when permeating through the ST-240 membrane. A similar conclusion was made by the Van der Bruggen group [9], suggesting that the inability of solvent separation using OSN could either be due to 1) coupled diffusion of species, or 2) the competitive permeation of species. Adam *et al*. [1] also realised that, in extreme cases, flow coupling might degrade separation, causing species to be dragged against its chemical potential gradient. For the STARMEM^{TM} membranes, similar reports of non-separation were made for the metathesis reaction system of 1-octene/7-tetradecene [40]. Previous studies also reported similar observations of non-separation for solvent mixtures of methanol/toluene, acetone/alcohols, acetone/paraffins, etc. [19,41].

Interestingly, the ST-240 membrane shows moderate separation for the hydrogenation reaction system, i.e. 1-nonanal/1-nonanol, and is comparable to the vapour-liquid

equilibrium data implemented for distillation processes, as illustrated in Figure 5.9. This indicates that for the 1-nonanal hydrogenation reaction system, OSN should be able to provide a similar separation performance as conventional distillation systems.

5.2.5.3 Concluding remarks

The permeation and species separation performance of the ST-240 membrane for the different reaction mixtures were characterised in this section. Results showed that pure species flux exhibited a linear and direct proportional relationship with applied pressure while the flux of binary species changed exponentially with increasing feed concentration. It was observed that a multitude of parameters representative of the solvent and membrane properties, *inter alia* molecular size, viscosity, polarity, influences flux. Moreover, it was discovered that the 1-octene and 1-decene hydroformylation reaction mixtures permeated through the ST-240 membrane as pseudo-single species with a degree of separation of approximately one while the hydrogenation reaction mixture, i.e. 1-nonanal/1-nonanol, exhibited moderate separation, comparable to that achieved by distillation processes.

5.3 Characterisation of membrane sorption

5.3.1 Introduction

The degree of membrane-solvent interaction, i.e. membrane sorption, observed between the ST-240 membrane and the species considered in this investigation is presented in this section. This is done by determining the amount of pure olefins (1-octene and 1-decene), aldehydes (1-nonanal and 1-undecanal) and alcohols (1-nonanol and 1-undecanol) that absorbed into the membrane when immersed in these organic reaction species.

5.3.2 Experimental results

The swelling degree, SD, is a parameter used to describe the membrane-solvent interaction of polymeric membranes and is defined as the increase in membrane mass or the amount of solvent absorbed, $M_{wet} - M_{dry}$,relative to the initial dry mass of the membrane, M_{dry},as shown in Equation 5.5.

$$SD = \left(\frac{M_{wet} - M_{dry}}{M_{dry}}\right) \times 100\% \qquad (5.5)$$

The swelling degrees for the olefins, the aldehydes and the alcohols, measured as described in Section 3.6 and calculated according to Equation 5.5, were determined to be 20%, 33% and 30%, respectively. This indicates that the ST-240 membrane swells to a greater extent when contacted with the polar species such as the aldehydes and alcohols

than compared to nonpolar olefins and suggests that the membrane has a higher affinity towards the former. This difference in membrane-species interaction between the olefins, aldehydes and alcohols with the membrane has a significant effect on the observed pure species flux, as observed in Figure 5.2. In other words, the greater the affinity between the membrane and the solvent, the lower the species flux will be.

5.4 Modelling of species transport through the ST-240 membrane

5.4.1 Introduction

Wang *et al.* [42] quoted the following regarding the state of OSN modelling:

"The possibilities (of OSN) are seemingly endless, but effective material tailoring (and implementation) requires some degree of priori knowledge. This intuition is difficult to gain due to the lack of predictive models… and a less efficient trial-and-error approach is often taken."

In light of the comment made, this section aims to contribute to the modelling database of OSN membranes by describing the transport of pure and binary mixtures of species representative of the hydroformylation and hydrogenation reactions through the ST-240 membrane. Firstly, classical pore-flow and solution-diffusion models, described in Section 2.5 and presented in Equations 5.6 and 5.7, respectively, are used to verify the porous nature of the membrane. These models have been dubbed to be the most encompassing due to its consideration of the physical and chemical properties of the membrane and the permeating species [43]. Thereafter, modifications of these models with increased interdependency and complexity are considered in an attempt to increase the prediction capacity for the reaction systems under investigation.

$$J_V = \frac{\varepsilon {d_{pore}}^2}{32 l \tau} \times \frac{P_o - P_z}{\eta} \tag{5.6}$$

where ε is the membrane surface porosity, τ the membrane tortuosity, d_p the membrane pore size and η the solution viscosity.

$$J_{V,1} = \frac{D_1 K_1}{l}\left[v_{1,f} - \frac{J_{V,1}}{J_{V,1}+J_{V,2}} \exp\left(-\frac{V_{m,1}\Delta P}{RT}\right)\right] \tag{5.7a}$$

$$J_{V,2} = \frac{D_2 K_2}{l}\left[v_{2,f} - \frac{J_{V,1}}{J_{V,1}+J_{V,2}} \exp\left(-\frac{V_{m,2}\Delta P}{RT}\right)\right] \tag{5.7b}$$

where $J_{V,i}$ is the volume flux of component i, v_i the weight fraction of component i, D_i the diffusion coefficient of species i, K_i the membrane sorption coefficient for species i, l the

membrane thickness, $V_{m,i}$ the molar volume of species i, ΔP is the transmembrane pressure, R the universal gas constant and T the temperature.

5.4.2 Pore-flow models

Before the Hagen-Poiseuille pore flow model, PF-1, can be used to model the reaction systems, it can be observed from Equation 5.6 that parameters representative of the membrane properties, namely pore size, tortuosity, porosity and thickness, are required. However, these parameters have not been determined experimentally. Silva *et al*. [41] describes using pure species flux data in PF-1 to calculate these parameters as a single lumped parameter named the pore flow permeance term, as shown in Equation 5.8:

$$P_i^{PF} = \left(\frac{\varepsilon {d_{pore}}^2}{32 l \tau}\right)_i \tag{5.8}$$

The P_i^{PF} of each of the reaction species used in this study are listed in Table 5.5 with sample calculations provided in Appendix G.

Table 5.5: Pore-flow permeance values for reaction species used

	P_i^{PF} x 10^{-15} (m)
1-Octene	6.36
1-Decene	3.44
1-Nonanal	3.47
1-Undecanal	3.03
1-Nonanol	4.28
1-Undecanol	2.54

The assumption is made that the membrane geometry, ST-240 in this study, remained constant, i.e. absence of membrane compaction or swelling. Therefore, this term should be independent of solvent mixtures and should describe all solvents. Although the derived pore flow permeance values for the pure species are in fact different, when considering mixtures in PF-1, the total flux of a binary mixture can be estimated using an arithmetic average permeance of the species involved, $\left(\frac{\varepsilon {d_{pore}}^2}{32 l \tau}\right)_{mix}$, with viscosity being the only composition dependent parameter.

$$J_V = \left(\frac{\varepsilon {d_{pore}}^2}{32 l \tau}\right)_{mix} \times \frac{\Delta P}{\eta_{mix}} \tag{5.9}$$

where η_{mix} is the viscosity of the binary mixture. Silva *et al.* [41] also proposed a two-term Hagen-Poiseuille model, PF-2, which incorporates the change in membrane properties due to membrane-solvent interactions, i.e. swelling. For this approach, instead of using a specific permeance term representing a mixture, a concentration average of the pure species is considered assuming no viscosity selectivity and a linear pressure profile inside the membrane, shown in Equation 5.10, and using parameters representative of the pure species to estimate the total flux of a binary mixture:

$$J_V = \frac{\Delta P}{\eta_{mix}}\left(\bar{V}_{m,1}C_1\left(\frac{\varepsilon {d_{pore}}^2}{32\tau l}\right)_1 + \bar{V}_{m,2}C_2\left(\frac{\varepsilon {d_{pore}}^2}{32\tau l}\right)_2\right) \tag{5.10}$$

where $\bar{V}_{m,i}$ is the partial molar volume of species i and C_i is the concentration of species i in the membrane. The estimated total flux values for the 1-octene reaction system when using the two pore-flow models, PF-1 and PF-2, are compared to experimental flux values in Figure 5.10.

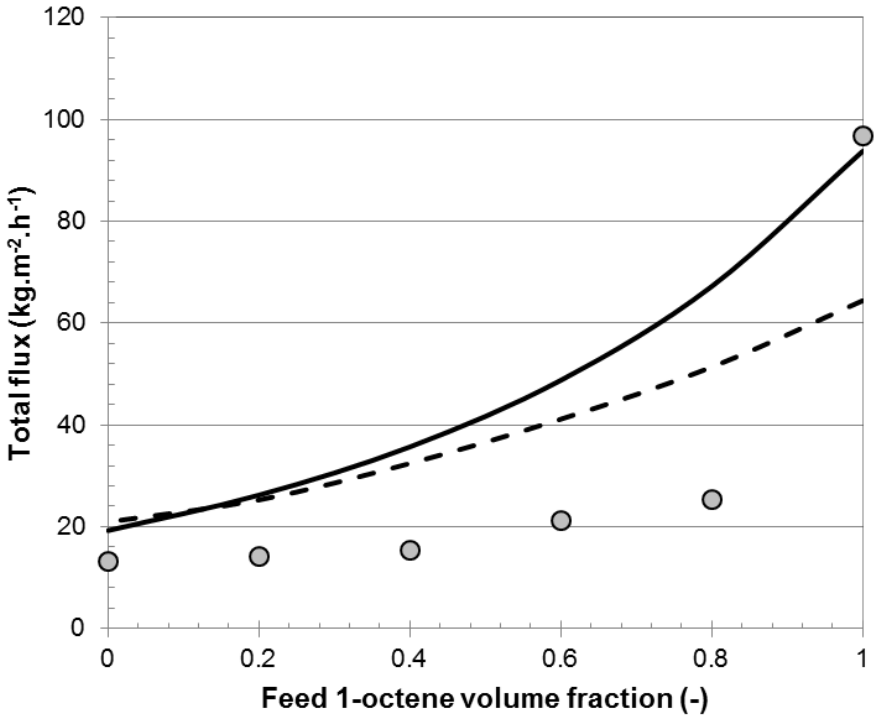

Figure 5.10: Comparison between experimental flux (●) for 1-octene/1-nonanal system through ST-240 (at 30 bar and 20°C) and the calculated values for PF-1 (-----) and PF-2 (——)

It is clear from Figure 5.10 that both the one-term and two-term Hagen-Poiseuille pore-flow models, PF-1 and PF-2, fit the experimental binary flux data of the 1-octene hydroformylation reaction poorly. The reason for the predictive failure of PF-1 is that this

model ignores the presence of membrane and solvent interaction, i.e. swelling, by the use of a constant permeance term and relies mainly on viscosity for flux prediction. This is an incorrect approximation as the STARMEM^{TM} membranes has been proven to swell in the organic reaction species used in this study. The predictive failure of PF-1 gives further indication, concurring to experimental observations, that viscosity is not the only determining factor in species transport across OSN membranes. Although PF-2 accounts for the membrane-solvent interaction, i.e. swelling of the membrane polymer matrix in the model, thereby providing a relatively better fit to the data than the PF-1 model, it still falls short in sufficient predictive capacity as the solute-solvent interactions, i.e. flow coupling effects between species, are ignored. Similar observations were made for the binary mixtures of 1-decene/1-undecanal and 1-nonanal/1-nonanol as shown in Figures 5.11 and 5.12. The presence of flow coupling effects in the reaction systems investigated, i.e. 1-octene/1-nonanal, 1-decene/1-undecanal and 1-nonanal/1-nonanol, have been experimentally elucidated and have previously been reported in literature [1].

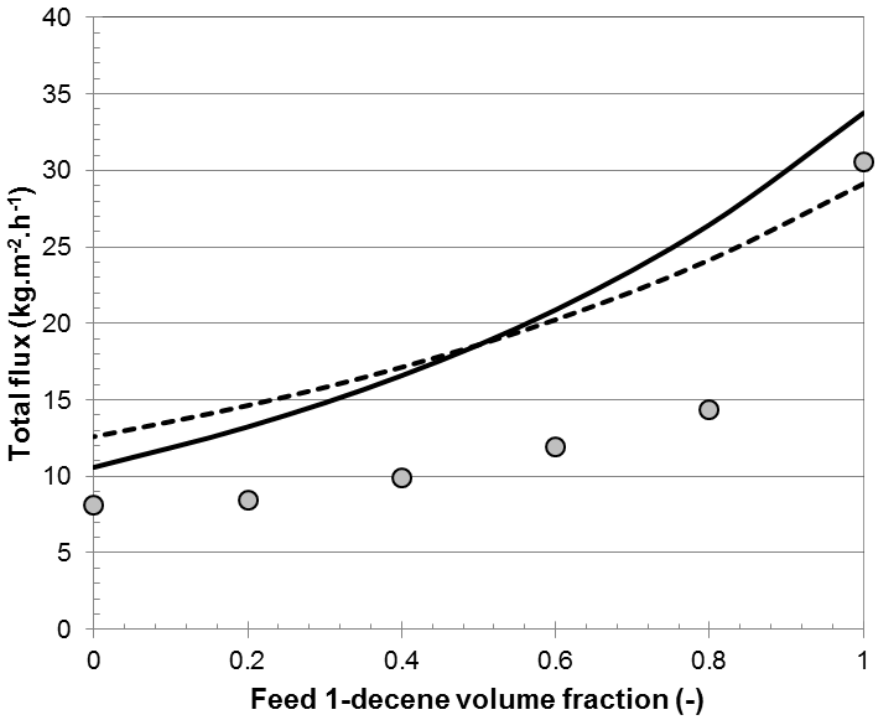

Figure 5.11: Comparison between experimental flux (●) for 1-decene/1-undecanal system through ST-240 (at 30 bar and 20°C) and the calculated values for PF-1 (-----) and PF-2 (——)

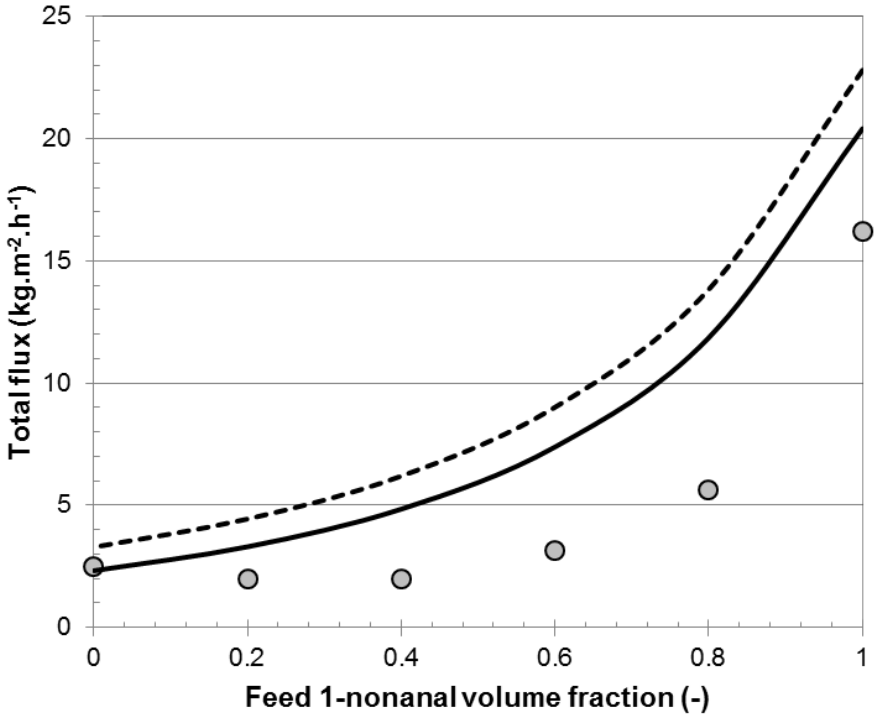

Figure 5.12: Comparison between experimental flux (●) for 1-nonanal/1-nonanol system through ST-240 (at 30 bar and 20°C) and the calculated values for PF-1 (-----) and PF-2 (——)

5.4.3 Solution-diffusion models

Similar to the pore-flow models, a permeance term is required before the classic solution-diffusion model, SD-1, can be used to model the reaction systems. In this case, the permeance gives measure to species diffusive capabilities and represents the unknown parameters of species diffusion, membrane thickness and a value reflecting the membrane sorption capacity, as given in Equation 5.11:

$$P_i^{SD} = \frac{D_i K_i}{l} \tag{5.11}$$

The solution-diffusion permeance values, assumed independent of composition, can be approximated by using partial flux data and are listed in Table 5.6 for each of the species considered in this study.

Table 5.6: Solution-diffusion permeance values for reaction species used

	P_i^{SD} x 10^{-15} (kg.m^{-2}.s^{-1})
1-octene	0.149
1-decene	0.046
1-nonanal	0.028
1-undecanal	0.013
1-nonanol	0.005
1-undecanol	0.002

It is clear from Equations 5.7a and 5.7b that SD-1 is basically also a two-term model as the flux and concentration of each of the species involved in the mixture are used for flux estimation. Moreover, the partial fluxes for the species involved in the mixture are required to estimate the total flux, as shown in Equation 5.12.

$$J_n = J_{n,1} + J_{n,2} \tag{5.12}$$

The empirical SD-based model proposed by Bhanushali *et al.* [8], given in Equation 5.13, uses four parameters, i.e. viscosity, molar volume (representative of molecular size), surface tension of the membrane material and a sorption value (indication of membrane-solvent interaction) and has previously been shown in this study to correlate well with species flux, as shown in Figure 5.2 [8].

$$J \sim \frac{V_m}{\eta} \frac{1}{\emptyset^n \gamma_m} \tag{5.13}$$

By combining the Bhanushali model with the PF-2 model, the SD-2 model is proposed as shown in Equation 5.14 [40]:

$$J_V = \frac{\Delta P}{\eta_{mix} \emptyset^n} \left(\bar{V}_1 c_{1,m} \left(\frac{\varepsilon {d_{pore}}^2}{32\tau l} \right)_1 + \bar{V}_2 c_{2,m} \left(\frac{\varepsilon {d_{pore}}^2}{32\tau l} \right)_2 \right) \tag{5.14}$$

The SD-1 and SD-2 model values for total flux are compared to experimental binary flux data of the 1-octene/1-nonanal mixture in Figure 5.13.

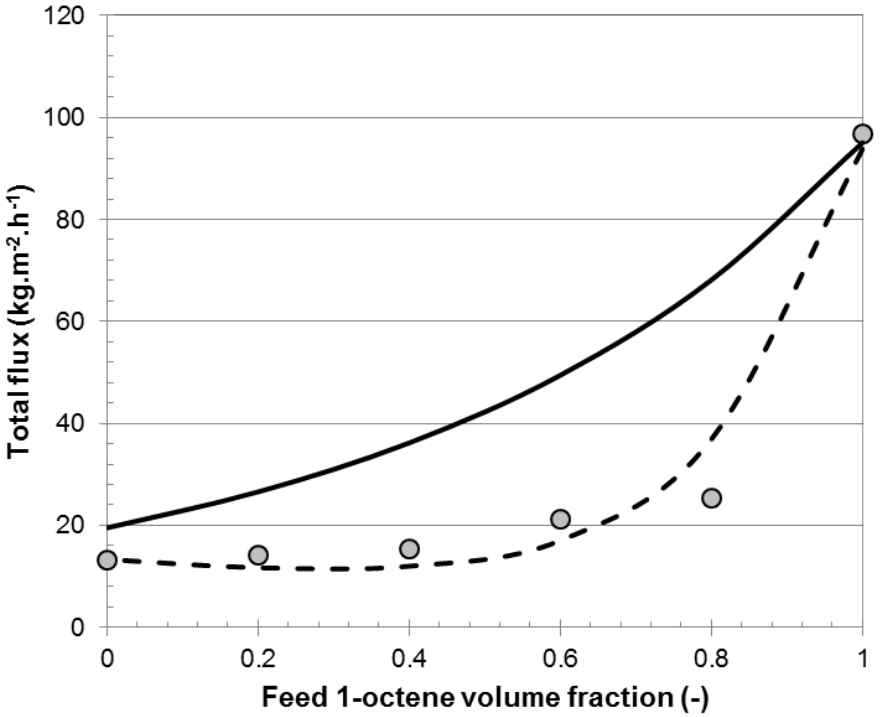

Figure 5.13: Comparison between experimental flux (●) for 1-octene/1-nonanal system through ST-240 (at 30 bar and 20 °C) and the calculated values for SD-1 (– – –) and SD-2 (——)

It is clear from Figure 5.13 that the classic solution-diffusion model, SD-1, provides a better prediction of binary fluxes of 1-octene/1-nonanal as it fits well to the experimental flux data. Similar observations were made for the binary mixtures of 1-decene/1-undecanal and 1-nonanal/1-nonanol as shown in Figures 5.14 and 5.15. A possible explanation for the improved predictive capacity of SD-1 for the transport of 1-octene/1-nonanal through ST-240 is that it is able to account for flow coupling effects as the partial fluxes of each species involved in the mixture is needed to determine the total flux. Previous publications noted that one of the advantages of the Maxwell-Stefan equations, from which the solution-diffusion models can be derived, considers the diffusional coupling between all species present, i.e. the membrane, solvent, and solute [44–48]. SD-2 on the other hand severely overestimates the binary flux data for all the reaction species considered which can be attributed to the dominant contribution of the PF-2 model instead of Bhanushali's proposed solution-diffusion based model. This observation provides even further affirmation of the importance of including solute-solvent interaction parameters in the prediction of membrane performance. Darvishmanesh *et al.* [9] claimed that although membrane-solvent effect dominating for separation, solute-solvent effects take precedence for membrane permeance.

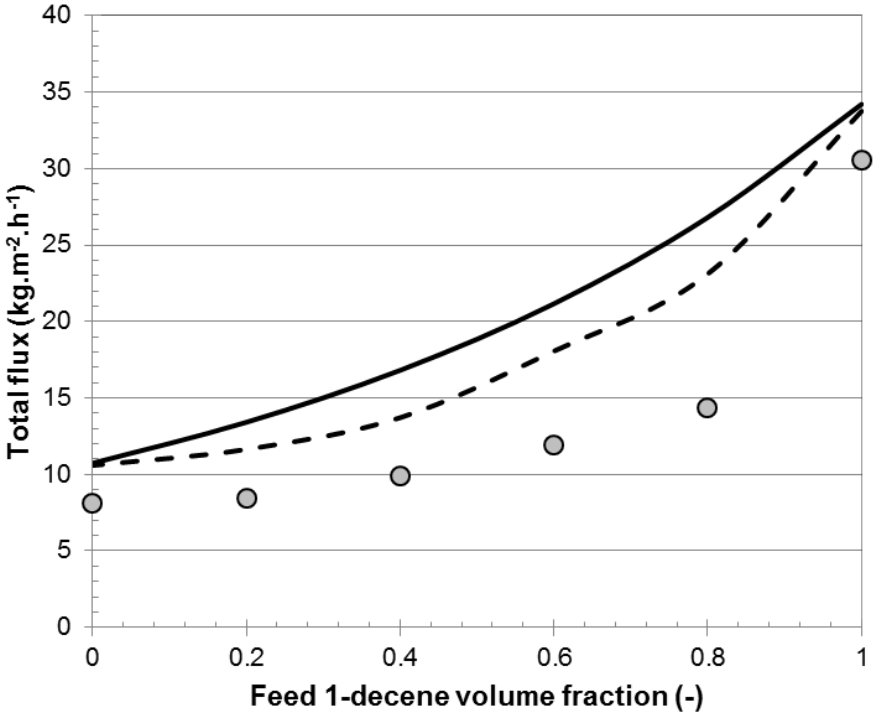

Figure 5.14: Comparison between experimental flux (●) for 1-decene/1-undecanal system through ST-240 (at 30 bar and 20 °C) and the calculated values for SD-1 (– – –) and SD-2 (——)

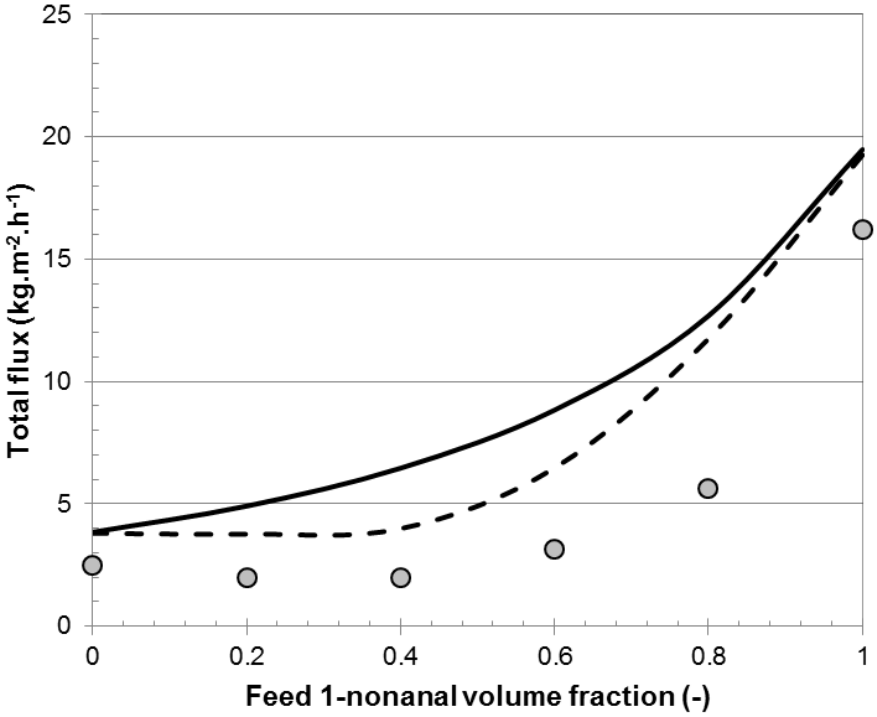

Figure 5.15: Comparison between experimental flux (●) for 1-nonanal/1-nonanol system through ST-240 (at 30 bar and 20 °C) and the calculated values for SD-1 (– – –) and SD-2 (——)

5.4.4 Modification of solution-diffusion model

It is shown in Section 4.6 that the solution-diffusion model, SD-1, which takes into account solute-solvent interactions describe the different reaction systems considered in this study, i.e. 1-octene/1-nonanal, 1-decene/1-undecanal and 1-nonanal/1-nonanol, the best. Since this model neglects to consider membrane-solvent interactions, it is proposed that a parameter describing the relative affinity between the membrane and the reaction species be incorporated in SD-1 through an additional solubility fraction, δ_{SD}. Darvishmanesh *et al*. [9] concluded that when both species in a binary mixture have an affinity toward the membrane, competitive permeation between the species occurs, thereby hindering their respective movement toward the membrane, i.e. changing the partial flux of the respective species. It is suggested that δ_{SD} will account for this competitive hindrance and adjust the respective partial fluxes of the species involved in the mixture accordingly. The solubility fraction is approximated as the ratio between the difference in solubility parameters of the species involved in the mixture and the membrane, as expressed in Equation 5.15:

$$\delta_{SD,i} = \frac{(\delta_M - \delta_i)^2}{x_i.(\delta_M - \delta_i)^2 + x_j.(\delta_M - \delta_j)^2} \tag{5.15}$$

where x_i and x_j are the molar fractions of species i and j.

By incorporating the solubility fraction into SD-1, the model becomes:

$$J_{n,1} = \frac{P_1^{SD}}{\delta_{SD,1}}\left[w_{1,f} - \frac{J_{n,1}}{J_{n,1}+J_{n,2}}\exp\left(-\frac{V_{m,1}\Delta P}{RT}\right)\right] \tag{5.16a}$$

$$J_{n,2} = \frac{P_2^{SD}}{\delta_{SD,2}}\left[w_{2,f} - \frac{J_{n,2}}{J_{n,1}+J_{n,2}}\exp\left(-\frac{V_{m,2}\Delta P}{RT}\right)\right] \tag{5.16b}$$

with the total remaining as:

$$J_n = J_{n,1} + J_{n,2} \tag{5.12}$$

The newly proposed solution-diffusion model, named SD-3, are compared to experimental binary flux data for the 1-octene/1-nonanal mixture as presented in Figure 5.16.

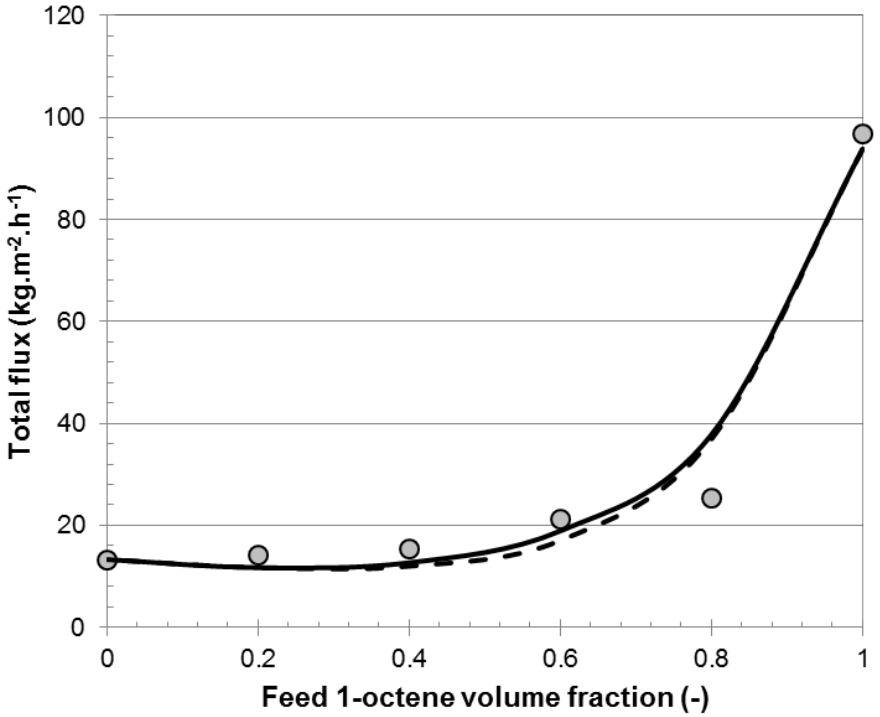

Figure 5.16: Comparison between experimental flux (●) for 1-octene/1-nonanal system through ST-240 (at 30 bar and 20 °C) and the calculated values for SD-1 (– – –) and SD-3 (——)

It can be observed from Figure 5.16 that for the 1-octene/1-nonanal reaction system, the introduction of the solubility fraction (SD-3) provides a slight improvement in predictive capacity compared to SD-1. However, when considering the binary mixtures of 1-decene/1-undecanal and 1-nonanal/1-nonanol, as presented in Figures 5.17 and 5.18, the inclusion of a parameter representative of the membrane-species interactions, the SD-3 model provides an increase in predictive capacity of approximately 3% compared to the SD-1 model.

5.4.5 Concluding remarks

Five transport models commonly used in literature were used to describe the transport of binary mixtures of 1-octene/1-nonanal, 1-decene/1-undecanal and 1-nonanal/1-nonanol, representative of the 1-octene hydroformylation, 1-decene hydroformylation and 1-nonanal hydrogenation reaction systems, respectively, through the ST-240 membrane. These include two Hagen-Poiseuille pore-flow models, PF-1 and PF-2, two solution-diffusion models, SD-1 and SD-2, and a newly proposed model based on the classic solution-diffusion model, SD-3. Pearson correlations were determined for each of the models considered for predicting the membrane permeation performance of each of the binary mixtures and are presented in Table 5.7.

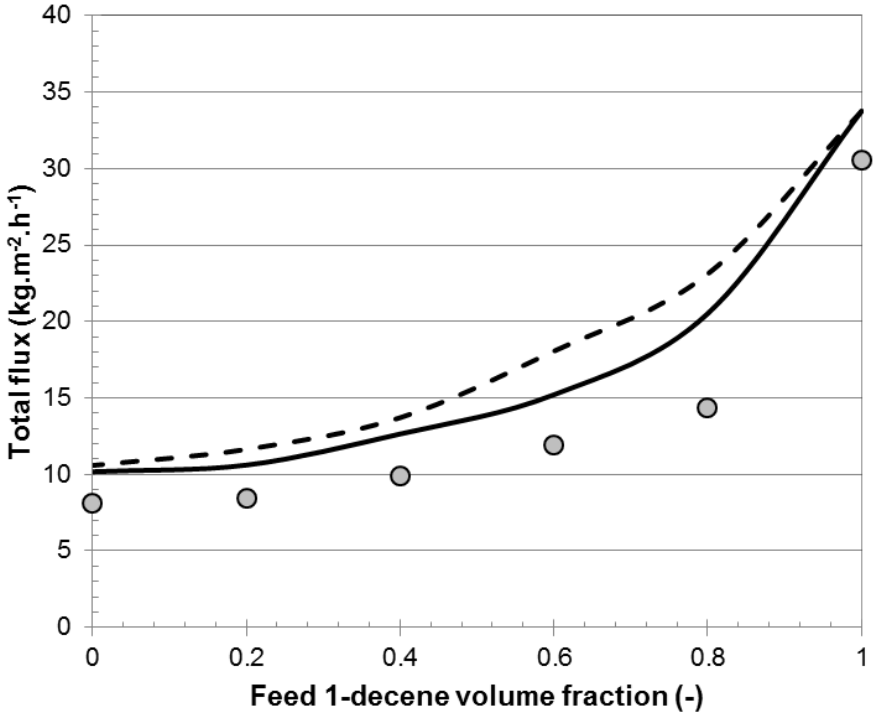

Figure 5.17: Comparison between experimental flux (●) for 1-decene/1-undecanal system through ST-240 (at 30 bar and 20 °C) and the calculated values for SD-1 (– – –) and SD-3 (——)

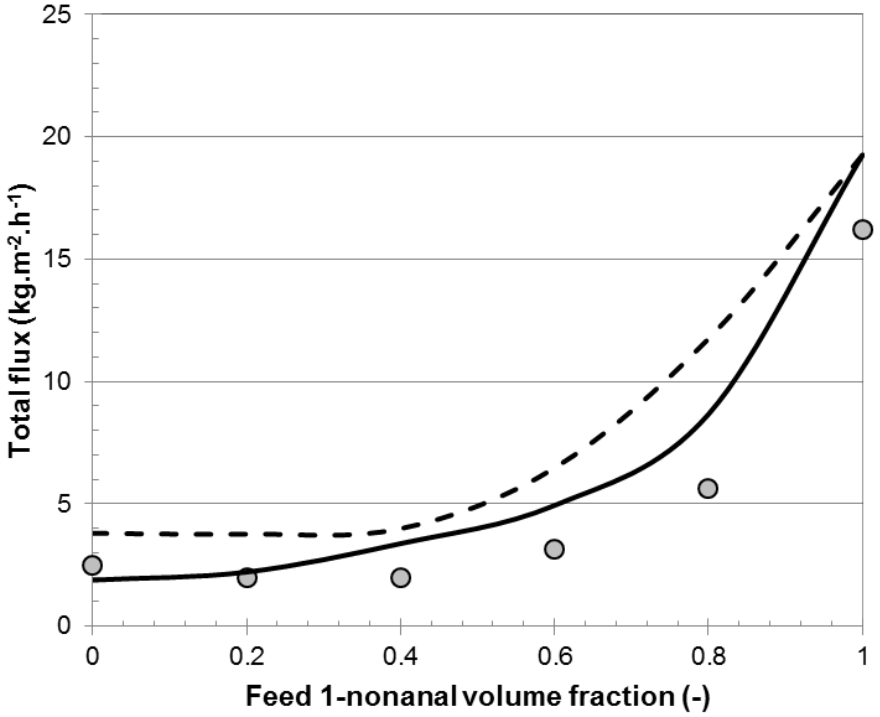

Figure 5.18: Comparison between experimental flux (●) for 1-nonanal/1-nonanol system through ST-240 (at 30 bar and 20 °C) and the calculated values for SD-1 (– – –) and SD-3 (——)

Table 5.7: Summary of different transport models used and their predictive capacity towards binary flux data (Pearson correlation)

Reaction system	PF-1	PF-2	SD-1	SD-2	SD-3
1-octene/1-nonanal	0.833	0.870	0.983	0.870	0.998
1-decene/1-undecanal	0.900	0.908	0.962	0.908	0.986
1-nonanal/1-nonanol	0.947	0.952	0.963	0.936	0.986

Results showed that, of the four literature-based models investigated, the newly proposed model based on the classic solution-diffusion model, SD-1, provided the best fit to experimental data as it is able to account for the membrane-solvent as well as solute-solvent interactions. Moreover, with the SD-1 model, it is possible to predict the permeation of the different reaction systems with an accuracy of >96%. The introduction of a parameter representative of the membrane-solvent interactions increased the model's predictive accuracy by approximately 3%. Herewith, further conclusive evidence is provided that the transport mechanism of the ST-240 membrane is dominated by convective rather than steric effects. The one-term and two-term Hagen-Poiseuille pore-flow models, PF-1 and PF-2, severely overestimated the binary flux data due to the unaccountability of interactions between the membrane and the solvent and the interspecies interactions in these pore-flow models.

5.5 Concluding remarks on OSN characterisation and modelling

In this chapter, the OSN performance for the hydroformylation reaction system was characterised in terms of pure species and binary mixture permeation and the effects of applied pressure and species properties elucidated. Moreover, the potential for species separation using the ST-240 membrane was investigated and modelled using literature-based transport models.

The ST-240 membrane was found to provide suitable permeation performance for the 1-octene and 1-decene hydroformylation reaction systems, resulting in a wide range of permeation rates that ranged from 1.66 to 138 $kg.m^{-2}.h^{-1}$. It was observed that the olefins attained the highest permeation rates while the alcohols had the lowest. This is due to the larger size, higher viscosity and higher polarity of the alcohols relative to that of the olefins. The aldehydes exhibited moderate fluxes compared to the olefins and the alcohols. It was found that applied pressure has a linear effect on permeate flux while solvent properties such as molecular size, viscosity and membrane interaction, greatly influences its apparent flux.

The ST-240 membrane was found to attain minimal species separation, indicating that the reaction systems permeate as a pseudo-single species through the membrane. Furthermore, the alcohols and aldehydes were found to preferentially absorb into the ST-240 membrane relative to the olefins.

Four literature-based transport models, two pore-flow models (PF-1 and PF-2) and two solution-diffusion models (SD-1 and SD-2), were used to describe the transport of binary mixtures of 1-octene/1-nonanal, 1-decene/1-undecanal and 1-nonanal/1-nonanol through the ST-240 membrane. It was found that of the literature-based models used, the classic solution-diffusion model (SD-1) provided the best fit to experimental data, with a predictive accuracy of >96% due to it being able to account for membrane-solvent interactions. Both pore-flow models severely overestimated the binary flux data due to the unaccountability of interactions between the membrane and the solvent as well as the interspecies interactions. Furthermore, by incorporating an additional term based on the differences in solubility parameters of the species and the membrane, the predictive accuracy of the SD-1 model can be improved by approximately 3%.

5.6 References

[1] W.J. Adam, B. Luke, P. Meares, *J. Memb. Sci.* **13** (1983) 127–149.

[2] J.A. Whu, B.C. Baltzis, K.K. Sirkar, *J. Memb. Sci.* **170** (2000) 159–172.

[3] P. Van der Gryp, H.C.M. Vosloo, S. Marx, **Separation of Grubbs-based catalysts with nanofiltration**, Potchefstroom, 2008.

[4] K.S. Spiegler, O. Kedem, *Desalination.* **1** (1966) 311–326.

[5] S. Darvishmanesh, L. Firoozpour, J. Vanneste, P. Luis, J. Degrève, B. Van der Bruggen, *Green Chem.* **13** (2011) 3476–3483.

[6] J.T. Scarpello, D. Nair, L.M. Freitas Dos Santos, L.S. White, A.G. Livingston, *J. Memb. Sci.* **203** (2002) 71–85.

[7] E. Gibbins, M. D'Antonio, D. Nair, L.S. White, L.M. Freitas dos Santos, I.F.J. Vankelecom, A.G. Livingston, *Desalination.* **147** (2002) 307–313.

[8] D. Bhanushali, S. Kloos, C. Kurth, D. Bhattacharyya, *J. Memb. Sci.* **189** (2001) 1–21.

[9] S. Darvishmanesh, J. Degrève, B. Van der Bruggen, *Phys. Chem. Chem. Phys.* **12** (2010) 13333–13342.

[10] F. Zheng, C. Li, Q. Yuan, F. Vriesekoop, *J. Memb. Sci.* **318** (2008) 114–122.

[11] S. Chen, J.S. Taylor, L.A. Mulford, C.D. Norris, *Desalination*. **160** (2004) 103–111.

[12] S. Darvishmanesh, J. Vanneste, E. Tocci, J. Jansen, F. Tasseli, J. Degrève, E. Drioli, B. Van der Bruggen, *J. Phys. Chem. B*. **115** (2011) 14507–14517.

[13] L.S. White, *J. Memb. Sci*. **205** (2002) 191–202.

[14] C.L. Yaws, **Thermophysical Properties of Chemicals and Hydrocarbons**, 2nd Ed., Elsevier, Oxford, 2014.

[15] D. Van Krevelen, K. te Nijenhuis, **Properties of Polymers: their correlation with chemical structure; their numerical estimation and prediction from additive group contributions**, Elsevier, 2009.

[16] H. Djojoputro, S. Ismadji, *J. Chem. Eng. Data*. **50** (2005) 2003–2007.

[17] R.F. Fedors, *Polym. Eng. Sci.* **14** (2004) 147–154.

[18] R.H. Perry, D.W. Green, **Perry's Chemical Engineers' Handbook**, 7th Ed., McGraw-Hill, Kansas, 1999.

[19] R. Machado, D. Hasson, R. Semiat, *J. Memb. Sci.* **163** (1999) 93–102.

[20] S. Aerts, A. Buekenhoudt, H. Weyten, L.E.M. Gevers, I.F.J. Vankelecom, P.A. Jacobs, *J. Memb. Sci*. **280** (2006) 245–252.

[21] M.F.J. Dijkstra, S. Bach, K. Ebert, *J. Memb. Sci.* **286** (2006) 60–68.

[22] S. Zeidler, U. Kätzel, P. Kreis, *J. Memb. Sci.* **429** (2013) 295–303.

[23] J. Geens, B. Van der Bruggen, C. Vandecasteele, *Sep. Purif. Technol*. **48** (2006) 255–263.

[24] K.L. Barbalace, Periodic Table of Elements, Sorted by Electronegativity (Pauling). [Online], (2007).

[25] J. Shirley, S. Mandale, V. Kochkodan, *Desalination.* **344** (2014) 116–122.

[26] D.F. Stamatialis, N. Stafie, K. Buadu, M. Hempenius, M. Wessling, *J. Memb. Sci.* **279** (2006) 424–433.

[27] E.S. Tarleton, J.P. Robinson, C.R. Millington, A. Nijmeijer, M.L. Taylor, *J. Memb. Sci.* **278** (2006) 318–327.

[28] Y. Kiso, Y. Sugiura, T. Kitao, K. Nishimura, *J. Memb. Sci.* **192** (2001) 1–10.

[29] B. Van der Bruggen, J. Schaep, D. Wilms, C. Vandecasteele, *J. Memb. Sci.* **156** (1999) 29–41.

[30] A. Miyagi, H. Nabetani, M. Nakajima, *Sep. Purif. Technol.* **88** (2012) 216–226.

[31] E.S. Tarleton, J.P. Robinson, S.J. Smith, J.J.W. Na, *J. Memb. Sci*. **261** (2005) 129-135.

[32] J.P. Robinson, E.S. Tarleton, C.. R. Millington, A. Nijmeijer, *J. Memb. Sci.* **230** (2004) 29–37.

[33] Y.H. See Toh, F.W. Lim, A.G. Livingston, *J. Memb. Sci.* **301** (2007) 3–10.

[34] S. Darvishmanesh, A. Buekenhoudt, J. Degrève, B. Van der Bruggen, *J. Memb. Sci*. **334** (2009) 43–49.

[35] I. Kim, J. Jegal, K. Lee, *J. Polym. Sci. Part B Polym. Phys.* **40** (2002) 2151–2163.

[36] X.J. Yang, A.G. Livingston, L. Freitas Dos Santos, Experimental observations of nanofiltration with organic solvents, J. Memb. Sci. 190 (2001) 45–55.

[37] L.G. Peeva, E. Gibbins, S.S. Luthra, L.S. White, R.P. Stateva, A.G. Livingston, *J. Memb. Sci.* **236** (2004) 121–136.

[38] M. Rabiller-Baudry, G. Nasser, T. Renouard, D. Delaunay, M. Camus, *Sep. Purif. Technol.* **116** (2013) 46–60.

[39] S. Postel, S. Wessel, T. Keil, P. Eiselt, M. Wessling, *J. Memb. Sci*. **466** (2014) 361-369.

[40] P. Van der Gryp, A. Barnard, J.P. Cronje, D. de Vlieger, S. Marx, H.C.M. Vosloo, *J. Memb. Sci*. **353** (2010) 70–77.

[41] P. Silva, S. Han, A.G. Livingston, *J. Memb. Sci.* **262** (2005) 49–59.

[42] J. Wang, D.S. Dlamini, A.K. Mishra, M.T.M. Pendergast, M.C.Y. Wong, B.B. Mamba, V. Freger, A.R.D. Verliefde, E.M.V. Hoek, *J. Memb. Sci.* **454** (2014) 516–537.

[43] S. Sobana, R.C. Panda, *Sep. Sci. Technol*. **46** (2011) 551–560.

[44] L. Hesse, J. Mićović, P. Schmidt, A. Górak, G. Sadowski, *J. Memb. Sci*. **428** (2013) 554–561.

[45] P. Izák, L. Bartovská, K. Friess, P. Uchytil, *J. Memb. Sci.* **214** (2003) 293–309.

[46] P. Izak, L. Bartovska, K. Friess, M. Sipek, P. Uchytil, *Polymer (Guildf).* **44** (2003) 2679–2687.

[47] A. Heintz, W. Stephan, *J. Memb. Sci.* **89** (1994) 143–151.

[48] A. Heintz, W. Stephan, *J. Memb. Sci.* **89** (1994) 153–169.

CHAPTER 6: Conclusions and Recommendations

6.1 Introduction

The work done in this study is three-fold: 1) the hydroformylation reaction of olefins, 2) OSN performance in terms of permeation and separation and 3) an economic and energy evaluation between OSN and a conventional separation technique for the recovery of homogeneous catalysts.

This chapter aims to highlight the contributions made in this study for the recovery of homogeneous catalysts from hydroformylation and hydrogenation post-reaction mixtures in a reusable and active form. Furthermore, recommendations are made for possible future work

6.2 Major study contributions

The contributions made in this study are two-fold:

Firstly, it was demonstrated that the commercially available OSN membrane, STARMEM^{TM} 240 (ST-240), successfully recovered the homogeneous catalysts, **$HRh(CO)(PPh_3)_3$** and **$Co(C_5H_7O2)_3$**, from different reaction systems, i.e. hydroformylation and hydrogenation, as illustrated in Figure 6.1. Moreover, it was shown that the catalyst concentrations in the permeate can be reduced to less than 5 ppm, indicative of a >99% recovery.

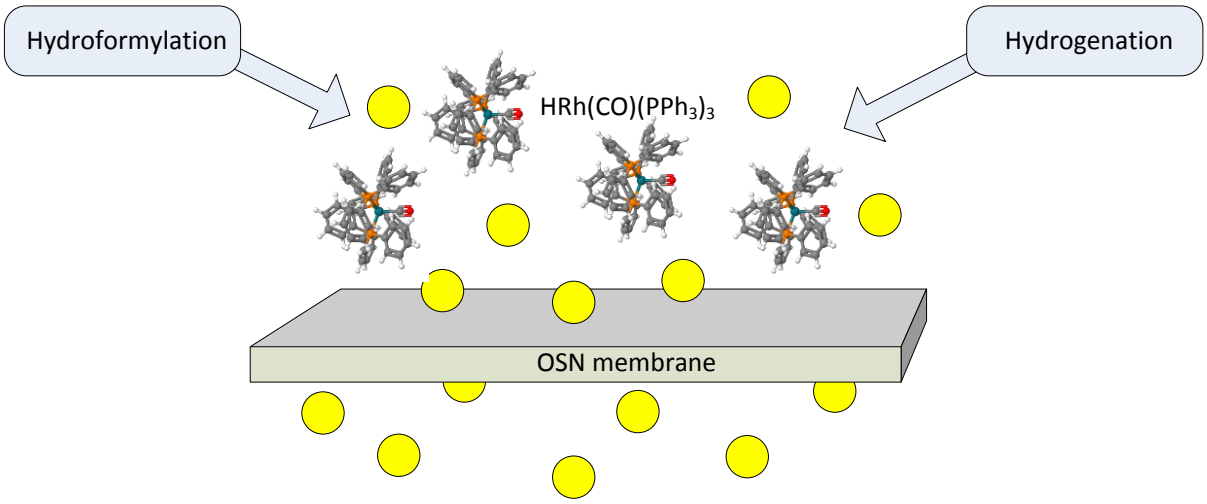

Figure 6.1: Depiction of major contribution of study: successful recovery of homogeneous catalyst from different reaction mixtures
[● representing all organic species, i.e. solvent, reagent and product]

Secondly, it was proven that **$HRh(CO)(PPh_3)_3$** could be successfully recovered in a reusable form for at least three consecutive hydroformylation reaction cycles, as presented in Figure 6.2.

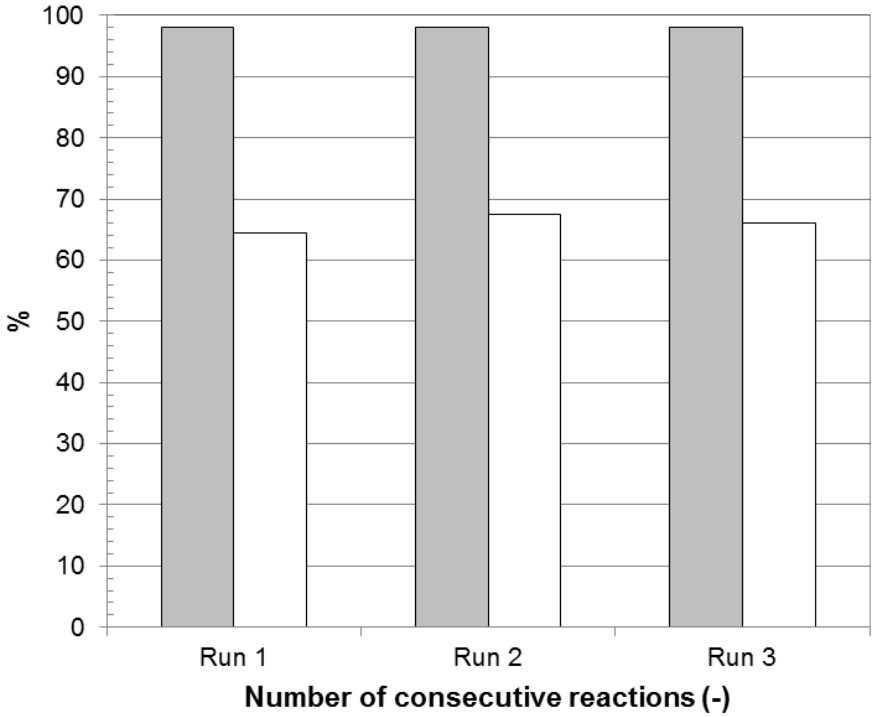

Figure 6.2: Graphical interpretation of study main objective depicting the successful recycle and reuse of **HRh(CO)(PPh$_3$)** for at least three consecutive 1-octene hydroformylation reaction cycles
[☐ catalyst recovery in wt%; ☐ *n*-aldehyde product yield in mol%]

6.3 Conclusions

6.3.1 Hydroformylation of olefins

The 1-octene hydroformylation was performed at the reaction conditions: solvent toluene = 21 mL, substrate 1-octene = 3.3 mL, ligand **PPh$_3$** = 22 mg, transition metal **HRh(CO)(PPh$_3$)$_3$** = 4 mg with a ligand to rhodium and substrate to rhodium molar ratios of 20:1 and 4940:1, respectively at 20 bar and 80 °C.

As expected, a mixture of products formed during the hydroformylation of 1-octene in the presence of **HRh(CO)(PPh$_3$)$_3$**, including isomeric octenes, octane as well as aldehydes, both linear and branched. The isomeric octenes and octane are formed, in minimal amounts, due to the unwanted side reactions, isomerisation reaction and olefin hydrogenation, respectively.

It was found that **HRh(CO)(PPh$_3$)$_3$** resulted in a high regioselectivity toward the linear aldehyde, *n*-nonanal, with a yield of *ca*. 66 mol% with linear to branched (*n*/*iso*) ratio of greater than 2. Previous studies have reported similar findings [1].

6.3.2 Organic Solvent Nanofiltration (OSN)

6.3.2.1 General conclusions

Experimental work was done using three different polyimide membranes (Duramem® 150, Duramem® 200 and STARMEM^{TM} 240) with six different organic species (1-octene, 1-decene, 1-nonanal, 1-undecanal, 1-nonanol, 1-undecanol) representative of the hydroformylation and hydrogenation reactions. Screening tests confirmed that the ST-240 provided the best performance in terms of flux and rejection and was hereafter used for further investigation. The ST-240 membrane was subjected to characterisation tests and it was found that:

- Pure species flux observed a linear and directly proportional dependence on applied pressure.
- Parameters reflecting the solvent molecular size (molecular weight, molecular size, molecular shape, etc.), solvent viscosity and membrane-solvent and solute-solvent interactions (polarity, solubility, surface tension, etc.) greatly influenced the permeation rate of the solvent. Yet, on their own, they were incapable of providing an accurate prediction of membrane performance and can merely be used to reflect trends within a homologous series with common functional groups. When used in combination however, as proposed by Bhanushali *et al.* [2] and Geens *et al.* [3], membrane permeation performance of pure species can be estimated with an accuracy of 98% (Pearson correlation).

6.3.2.2 Species separation

Binary mixtures of 1-octene/1-nonanal, 1-decene/1-undecanal and 1-nonanal/1-nonanol were considered at concentrations ranging between 0 – 100 vol% at 30 bar applied pressure. It was found that:

- Total flux of the binary mixtures increased exponentially with increasing feed concentration. This exponential behaviour can be attributed to interspecies interaction, i.e. flow coupling, where the respective species compete for permeation through the membrane and in the process, significantly reduce their respective partial fluxes.
- The ST-240 membrane achieved minimal separation between 1-octene and 1-nonanal as well as 1-decene and 1-undecanal. This indicates that the aforementioned binary mixtures permeate through the ST-240 membrane as a pseudo-single component. On the other hand, the binary mixture of 1-nonanal and 1-nonanol experienced a moderate separation with the ST-240 with a degree of

separation resembling that of the VLE data for this mixture used in distillation principles.

6.3.2.3 Catalyst recovery

The catalyst recovery capability of the ST-240 was tested in the presence of the six organic species previously mentioned at catalyst feed concentrations of 200 and 500 ppm at 30 bar applied pressure. The homogeneous rhodium-based catalyst, **$HRh(CO)(PPh_3)_3$**, was used as the catalyst of interest as it is commonly used in literature to catalyse the hydroformylation reaction [4–9] and is close to 100 times more than its closest competitor [10,11]. The performance of the rhodium-based catalyst in terms of recovery and flux were also compared to another typical homogeneous hydroformylation catalyst, **$Co(C_5H_7O_2)_3$** [12–15]. From the results presented, it was concluded that:

- The ST-240 membrane performed extremely well in terms of **$HRh(CO)(PPh_3)_3$** recovery for all reaction systems considered, achieving recoveries >98.0%. Catalyst concentrations in the permeate were reduced to less than 5 ppm.
- The recovered catalyst was shown to maintain its catalytic activity after being subjected to OSN for at least three consecutive hydroformylation reaction cycles, thereby improving its overall turnover number, TON, from 2620 in a single-pass reaction to 3470 after three reactions.
- For **$Co(C_5H_7O_2)_3$**, the ST-240 membrane achieved moderate recoveries of 87.9%. This was expected due to the smaller size of the cobalt-based catalyst (356 $g.mol^{-1}$) relative to that of the rhodium-based catalyst (920 $g.mol^{-1}$) and the membrane's MWCO (400 $g.mol^{-1}$).
- Catalyst loadings and applied pressure exerted no influence on the ST-240 membrane's catalyst recovery capacity.
- The addition of a catalyst in the feed severely degraded the species flux through the membrane relative to pure feed conditions. Thereby confirming that flux decreased with increasing catalyst feed concentration. The effect of **$HRh(CO)(PPh_3)_3$** addition on permeation rate is more pronounced than compared to the addition of **$Co(C_5H_7O_2)_3$**.
- Energy and cost savings of up to 99% and 90%, respectively, can be attained upon using OSN systems for homogeneous catalyst recovery as compared to conventional distillation systems.

6.3.2.4 Membrane sorption

The degree of membrane-solvent interaction was characterised using sorption tests and it was found that:

- The ST-240 membrane swelled to a greater extent in the polar aldehyde and alcohol species compared to the nonpolar olefins.

6.3.2.5 OSN modelling

Four literature-based transport models, i.e. classic solution-diffusion model (SD-1), modified solution-diffusion model (SD-2), one-term Hagen-Poiseuille pore-flow model (PF-1) and a two-term Hagen-Poiseuille pore-flow model (PF-2), and a newly proposed model based on the classic solution-diffusion model with the introduction of a parameter reflective of the solute-solvent interactions were compared to experimental binary flux data. It was found that:

- A combination of parameters reflecting solvent molecular size and solvent viscosity as well as membrane-solvent and solute-solvent interactions are essential for providing accurate predictive capacities to transport models. The relationship between the aforementioned parameters and membrane permeation rate can be described as:

$$Permeability \propto \left(\frac{molecular\ size}{1}\right) \times \left(\frac{1}{viscosity}\right) \times \left(\frac{1}{affinity}\right) \tag{6.1}$$

- The Hagen-Poiseullie pore-flow models, PF-1 and PF-2, poorly fitted the experimental data due to the unaccountability of interaction parameters.
- SD-1 provided the best fit relative to the four literature-based models as its derivation stems from the Maxwell-Stefan equations which considers solute-solvent interactions, and observed a predictive accuracy of >96%.
- The newly proposed SD-3 model, incorporating an additional solubility term, improved the predictive capacity of the SD-1 model by approximately 3% and thereby provided the best fit relative to all other transport model investigated.

$$J_{V,1} = \frac{P_1^{SD}}{\delta_{SD,1}}\left[v_{1,f} - \frac{J_{V,1}}{J_{V,1}+J_{V,2}}\exp\left(-\frac{V_{m,1}\Delta P}{RT}\right)\right] \tag{6.2a}$$

$$J_{V,2} = \frac{P_2^{SD}}{\delta_{SD,2}}\left[v_{2,f} - \frac{J_{V,2}}{J_{V,1}+J_{V,2}}\exp\left(-\frac{V_{m,2}\Delta P}{RT}\right)\right] \tag{6.2b}$$

with the total flux given as:

$$J_V = J_{V,1} + J_{V,2} \quad (6.2c)$$

6.4 Recommendations for future work

This work shows that the use of OSN for homogeneous catalyst recovery is both technically and economically viable. However, there are still many issues that need to be addressed. From the conclusions drawn in this study, recommendations for future endeavours are thus forth:

- The use of dead-end OSN operation, although sufficient for proof of concept, provides an incorrect reflection of typical industrial conditions, e.g. build-up of solids, batch-wise operation, etc. Therefore, it is recommended that continuous cross-flow OSN systems be used for the recovery of homogeneous catalysts from post-reaction mixtures.
- In this study, binary mixtures were considered as the different prototype reaction systems used were approximated to attain perfect selectivity toward the linear product. In future, the author recommends using multicomponent mixtures, i.e. ternary, quaternary, etc. including also branched species to provide a better reflection of typical industrial conditions and to test the OSN potential for solvent and catalyst separation to a greater extent.
- Different homogeneous catalysts should be investigated to further extend the scope of OSN for catalyst recovery
- This work provides a brief economic and energy evaluation to support the beneficial claims of OSN in terms of costs and energy usage commonly alluded to in literature. However, a full economic study is yet to be performed, considering the entire life cycle of an OSN membrane from fabrication to disposal. This warrants a further full sustainability assessment of OSN membranes not previously performed.

6.5 Contributions and awards from this study

From this study, the following contributions were made to the field of OSN and to the research community:

- First prize winner for the best oral presentation at the Postgraduate Research Day 2014 hosted at the University of Stellenbosch
- Waylin Peddie, Hermanus Vosloo, and Percy van der Gryp. Recovery and reuse of tris(triphenylphosphine)rhodium carbonyl hydride from a hydroformylation product stream. Conference Proceedings of CATSA, Pretoria, South Africa, November 2014.
- Waylin Peddie, Hermanus Vosloo, and Percy van der Gryp. Evaluation of membrane technology as an alternative to conventional downstream separation units. Conference Proceedings of the 2nd International Syngas Convention, Cape Town, South Africa, March 2015
- Percy van der Gryp, Waylin Peddie, and Hermanus Vosloo. OSN application in beneficiation of lower value olefins to high value surfactants. Conference Proceedings of Euromembrane, Aachen, Germany, September 2015.
- Waylin Peddie, Hermanus Vosloo, and Percy van der Gryp. Application of Organic Solvent Nanofiltration in Homogeneous Catalysis. Conference Proceedings of CATSA, Kleinmond, South Africa, November 2015.

6.6 References

[1] A. Buhling, P.C.J. Kamer, P.W.N.M. Van Leeuwen, *J. Mol. Catal. A Chem*. **98** (1995) 69–80.

[2] D. Bhanushali, S. Kloos, C. Kurth, D. Bhattacharyya, *J. Memb. Sci.* **189** (2001) 1-21.

[3] J. Geens, K. Boussu, C. Vandecasteele, B. Van Der Bruggen, *J. Memb. Sci.* **281 (**2006) 139–148.

[4] P.J. Baricelli, E. Lujano, M. Modrona, A.C. Marrero, Y.M. Garcia, A. Fuentes, R.A. Sànchez-Delgado, *J. Organomet. Chem.* **689** (2004) 3782–3792.

[5] D. He, D. Pang, T. Wang, Y. Chen, Y. Lui, J. Lui, Q. Zhu, *J. Mol. Catal. A Chem*. **174** (2001) 21–28.

[6] B.M. Bhanage, S.S. Divekar, R.M. Deshpande, R.V. *J. Mol. Catal. A Chem*. **115** (1997) 247–257.

[7] S.S. Divekar, R.M. Bhanage, R.M. Deshpande, R. V. Gholap, R. V. Chaudhari, *J. Mol. Catal.* **91** (1994) L1–L6.

[8] R.M. Deshpande, B.M. Bhanage, S.S. Divekar, R. V. Chaudhari, *J. Mol. Catal*. **78** (1993).

[9] C.K. Brown, G. Wilkinson, *J. Chem. Soc*. (1970).

[10] [Online], (2015). www.sigmaaldrich.com. Date accessed: 20 July 2015.

[11] [Online], (2015). www.kitco.com. Date accessed: 20 July 2015.

[12] F. Hebrard, P. Kalck, *Chem. Rev.* **109** (2009) 4272–4282.

[13] T. Zeelie, **Rhodium and Cobalt Catalysts in the Heterogeneous Hydroformylation of Ethene, Propene and 1-Hexene,** Helsinki, 2007.

[14] L.B. Backman, A. Rautiainen, A.O.I. Krause, M. Lindblad, *Catal. Today*. **43** (1998) 11–19.

[15] T.A. Kainulainen, M.K. Niemelä, A.O.I. Krause, *Catalysis Lett*. **53** (1998) 97-101.

APPENDIX A: Additional Detailed Literature

A.1 Introduction

In this section, additional literature is provided regarding the literature reviewed as described in Chapter 2.

A.2 Hydroformylation

A.2.1 Historical background

Hydroformylation, also known as the 'oxo'-process, is one of the oldest and most widely used applications of homogeneous catalysis used for the catalytic conversion of olefins. Interestingly, this reaction was accidentally discovered by the German scientist, Otto Roelen, in 1938 during his investigation of the Fischer-Tropsch reaction using a catalyst consisting of cobalt, thorium and magnesium oxide. Upon further investigation, Roelen speculated that the active species of this catalyst was cobalt tetracarbonyl hydride, **$HCo(CO)_4$**, depicted also in Figure A.1, and was verified four years later by Walter Hieber [1]. This unmodified cobalt-carbonyl catalyst was identified as the first-generation in hydroformylation catalysts.

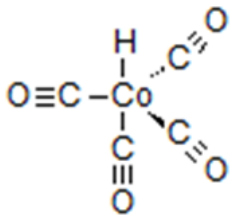

Figure A.1: First-generation homogeneous unmodified cobalt-based catalyst introduced by Otto Roelen

During the 1950's, Enjay Chemical, BASF and Exxon developed and successfully implemented the first industrial-scale application of the hydroformylation reaction using the first-generation hydroformylation catalyst to produce mainly *n*-aldehydes [2]. However, this process had the significant disadvantage of requiring relatively severe reaction conditions (270 – 300 bar and 120 – 180 °C) which were, at the time, difficult and costly to achieve due to the technological impairments. The extremely high pressures were crucial to counteract the low reactivity of the cobalt-based catalyst. Additionally, large amounts of cobalt-containing waste were produced [3]. Interestingly, this was not the first attempt at implementing hydroformylation industrially.

In 1945, Ruhrchemie/Rhône-Poulenc (RCH/RP) in Germany attempted this endeavour but due to the economic instabilities brought forth by the Second World War, this plant never made it out of the start-up phase [2].

Upon entering the 1960's, Shell introduced phosphine ligands to these cobalt catalysts to produce the active complex **$HCo(CO)_3(PPh_3)_3$**, illustrated in Figure A.2, which was able to operate under milder reaction conditions (40 – 80 bar and 150 – 180 °C) compared to its predecessor. However, this process was also not without its faults. By introducing the ligands, the product selectivity shifted from the preferred aldehydes to alcohols as the majority product. Furthermore, the catalytic activity was reduced due to the increased stability brought on by the ligand [2]. Nonetheless, this sparked the emergence, and eventual dominance, of what was known as the second-generation of hydroformylation ligand-modified catalysts.

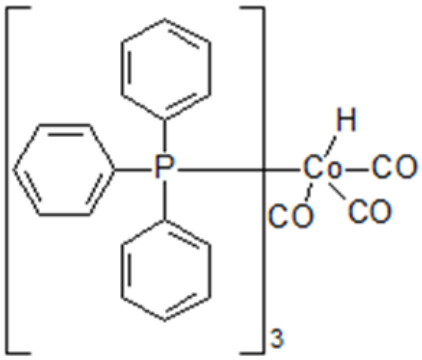

Figure A.2: Second-generation homogeneous phosphine modified cobalt-based catalyst introduced by Shell

Following the success of the phosphine ligand, various other ligands emerged, including phosphites, bidentate ligands and diphosphines, each with its own set of advantages and disadvantages. In the 1970's, a ground-breaking discovery was made when it was found that rhodium can replace cobalt as the active metal species in the form of tris(triphenylphosphine)rhodium carbonyl hydride, **$HRh(CO)(PPh_3)_3$**, as illustrated in Figure A.3. This project was spearheaded by the Union Carbide Company in 1974 which operated at very mild conditions (15 – 18 bar and 85 – 95 °C) producing mainly *n*-aldehydes [3,4].

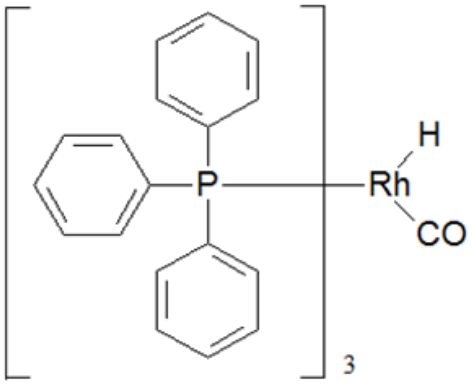

Figure A.3: Second-generation homogeneous phosphine modified rhodium-based catalyst introduced by Union Carbide

The prominent **$HRh(CO)(PPh_3)_3$** catalyst was first discovered by Lauri Vaska in 1963 [5]. However, Professor Sir Geoffrey Wilkinson (rewarded with a Nobel Prize for Chemistry in 1973) and his team, funded by Johnson Matthey and Davy Process Technology, were the first to realise its vast potential to act as catalyst for the hydroformylation reaction just a few years later and published reproducible results which complemented the findings of Union Carbide [6]. Rhodium-based catalysts not only provided higher catalytic activities, approximately 2 – 4 times greater than cobalt, as well as the ability to operate under much milder conditions and are also more atom-efficient, i.e. capable of effectively using the feed to a greater extent for increased process efficiency. For these reasons, the chemical industry shifted its attention towards the use of rhodium-based catalysts around the mid 1970's. However, cobalt-based catalysts still remain at the forefront of industrial-scale hydroformylation reactions due to its low cost and ease of separation compared to rhodium complexes [2].

The need for improved catalyst recovery prompted the third-generation of hydroformylation catalysts which shifted from conventional homogeneous catalysis to a technique known as biphasic catalysis. This technique makes use of a "homogeneous" two-phase reaction system catalysed by a water-soluble catalyst. These water-soluble complexes first appeared in 1984 when the sodium salt of triphenyl phosphine trisulfonic acid (**TPPTS**) was combined with rhodium metal, replacing the phosphine ligand shown in Figure A.4, to give the easily synthesised active complex **$HRh(CO)(TPPTS)_3$**. This catalyst was introduced in the RCH/RP process which was characterised by moderate reaction conditions (50 bar and

120 °C). Although delivering outstanding performance, its use was restricted to short chain hydrocarbons due to its lack of solubility in those with longer carbon chains [3].

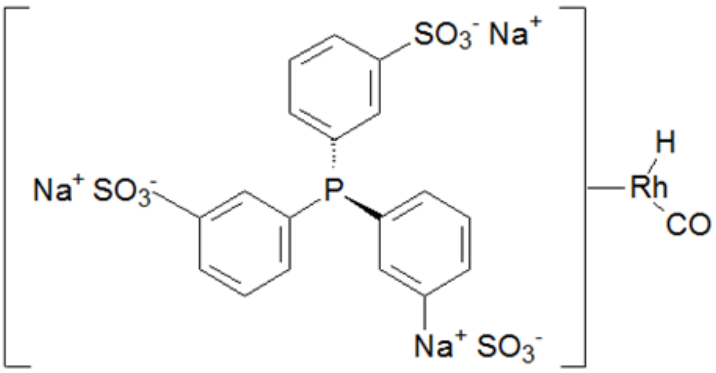

Figure A.4: Third-generation biphasic phosphine modified rhodium-based catalyst introduced by Ruhrchemie/Rhône-Poulenc

Some of the significant breakthroughs are summarised in Table A.1.

Table A.1: Significant breakthroughs of in the field of hydroformylation

1938	Hydroformylation reaction discovered by Otto Roelen upon studying the Fischer-Tropsch reaction using cobalt tetracarbonyl hydride, **$HCo(CO)_4$**
1945	Ruhrchemie/Rhône-Poulenc attempted to implement hydroformylation on industrial scale but failed due to economic instabilities caused by WW II.
1950's	Enjay Chemical, BASF and Exxon successfully implemented hydroformylation on industrial scale using unmodified cobalt-carbonyl catalyst (270 – 300 bar and 120 – 180 °C)
1960's	Heck and Breslow propose the mechanism for the ligand-free cobalt-catalysed hydroformylation reaction Shell introduce the phosphine-modified cobalt-catalyst, **$HCo(CO)_3(PR_3)$** (40 – 80 bar and 150 – 180 °C)
1963	Lauri Vaska and Wilkinson and co-workers discover tris(triphenylphosphine) rhodium carbonyl hydride, **$HRh(CO)(PPh_3)_3$**
1974	Union Carbide Company successfully implement **$HRh(CO)(PPh_3)_3$** on industrial scale (15 – 18 bar and 85 – 95 °C)
1984	Ruhrchemie/Rhône-Poulenc introduce water-soluble ligand triphenyl phosphine trisulfonic acid (**TPPTS**) to give the active complex **$HRh(CO)(TPPTS)_3$**

A.1.2 Hydroformylation reaction pathways

The first indication of the reaction mechanism involved in the ligand-free cobalt-catalysed hydroformylation reaction was given by Heck and Breslow in the 1960's and was later reviewed by Orchin and Rupilius [2]. Figure A.5 illustrates the catalytic cycle involved in the aforementioned reaction with R = C_nH_{2n+1}.

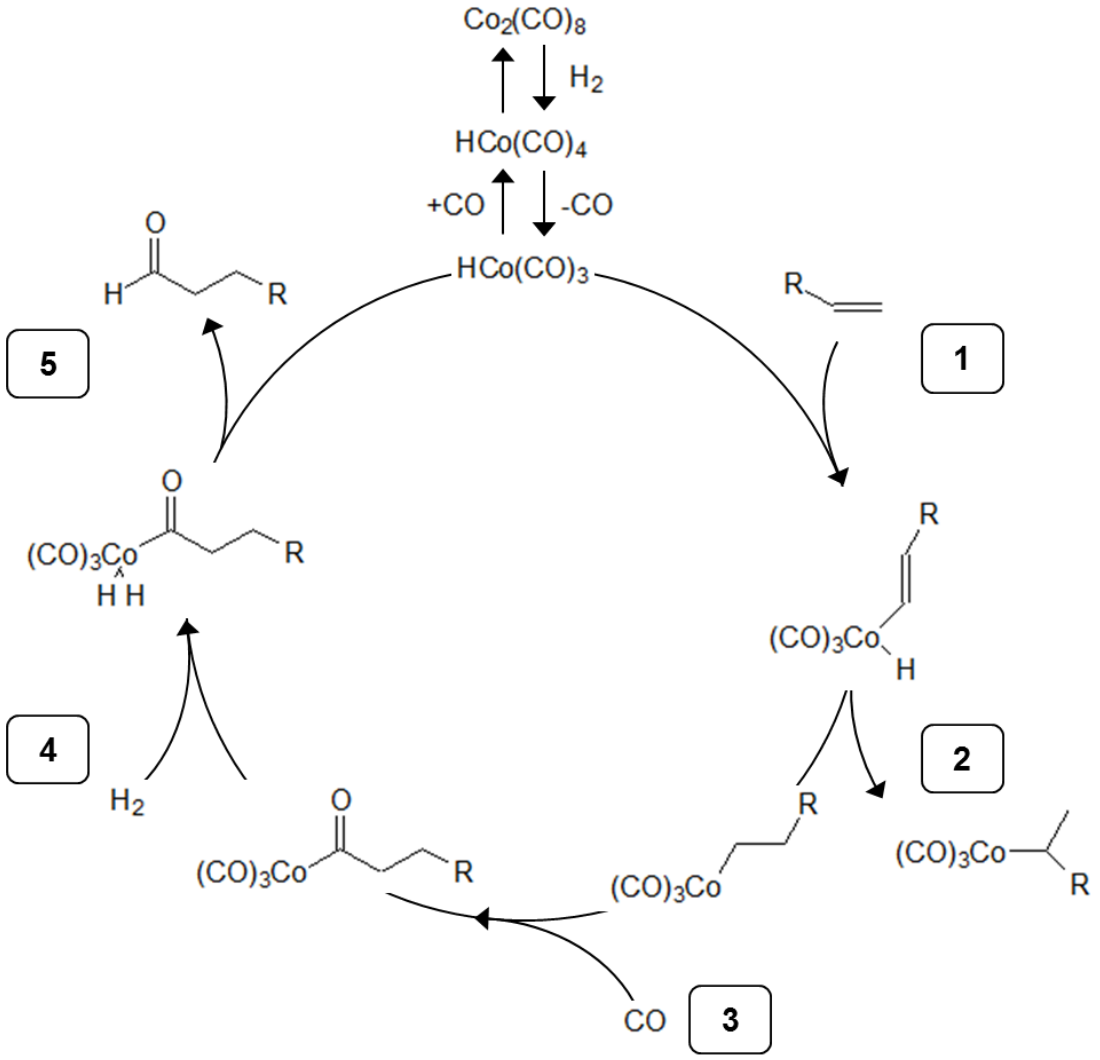

Figure A.5: Reaction mechanism for the cobalt-catalysed hydroformylation of olefins

The reaction mechanism can be broken down into five principles steps:

1. Olefin association
2. Alkyl complex formation
3. Carbon monoxide association
4. Oxidative addition of hydrogen
5. Reductive elimination of the aldehyde product

The reaction mechanism kicks off with the replacement of carbon monoxide by the olefin which is then followed by the migration of the hydride to give an either linear or branched alkyl complex depending on the olefin isomer involved in the reaction. The next step comprises the migration of the alkyl complex to the coordinated carbon monoxide. Lastly, the alkyl complex reacts with the hydrogen to form the aldehyde which then dissociates. This results in the regeneration the active complex and the subsequent restart of the catalytic cycle [7].

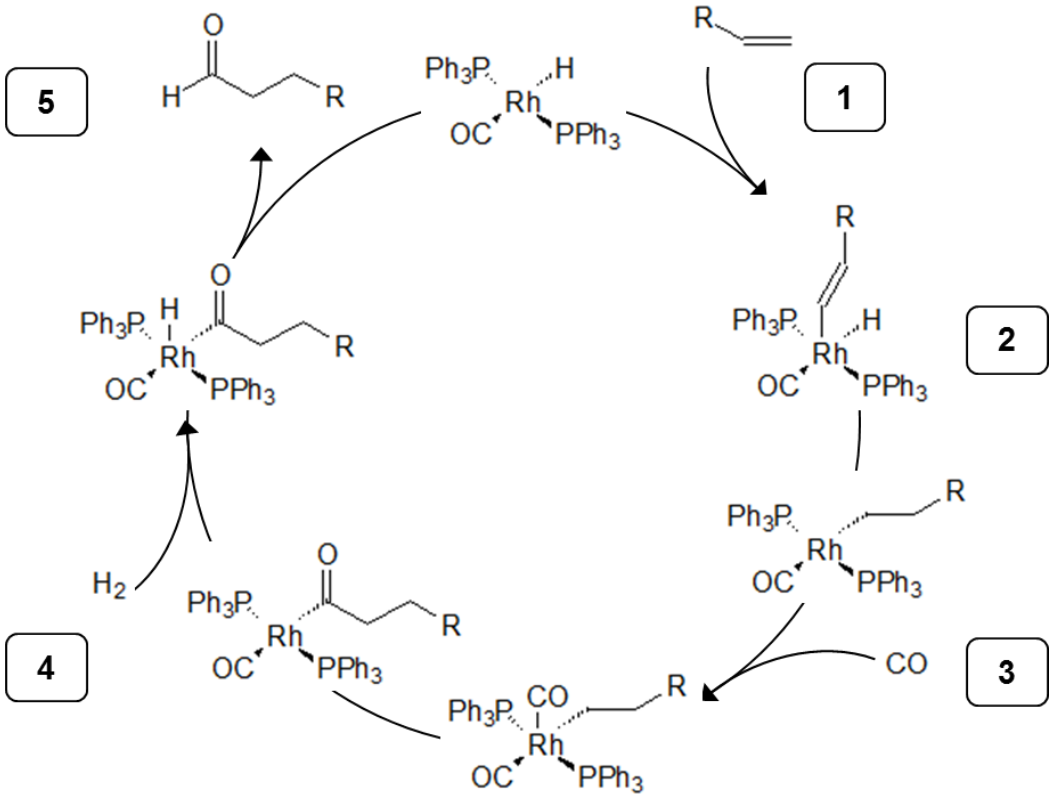

Figure A.6: Reaction mechanism for the rhodium-catalysed hydroformylation of olefins

It has been reported by Sir Geoffrey Wilkinson that the mechanism describing the hydroformylation reaction in the presence of phosphine modified rhodium complexes proceeds in a similar fashion to that proposed by Heck and Breslow [3]. Therefore, the catalytic cycle involved in the rhodium-catalysed hydroformylation reaction has been proposed as shown in Figure A.6.

A.2 OSN

A.2.1 Historical background

The origins of membranes can be traced back to early 18th century scientists such as Abbè Noblet who experimented with the permeation of water through a diaphragm in 1748. Through the 19th and early 20th centuries, membranes were only used on small scale to develop physical and chemical theories including the Van't Hoff equation and Maxwell's kinetic theory of gases. These researchers, among many others at the time, used any available material as membranes including pig bladders and animal intestines. The reproducibility of these natural materials soon was questioned which led to a shift to initially nitrocellulose and eventually to the polymer, cellulose acetate. Near the conclusion of World War 1 (~1918) is where membranes enjoyed its first substantial application as a means to test the purity of drinking water in Germany and Europe. This application was then converted by a US company, Millipore, into a lucrative business which is still recognised as a noteworthy producer of MF membranes. By 1960, although only for a few very small and specialised applications, membranes made its breakthrough onto the industrial scale. The 50 years after was spent on intensive research and development which focused mainly on eliminating performance and cost shortfalls associated with membrane use [8].

A few prominent discoveries made in this period include that by Loeb and Sourirajan in the early 1960's, who developed a membrane which can provide 10 times higher flux than any available membrane at the time and also Alex Affaroni who, in 1966, perfected the use of membranes in medical applications such as artificial organs and controlled drug delivery systems [8]. Back in the mid 1960's, Sourirajan and his co-workers [9] piqued interest in the field of non-aqueous nanofiltration systems who studied the separation of hydrocarbons through porous membranes. A few years later, Paul and his team [10–12] built on the foundation laid out by Sourirajan and published a range of articles that contributed significantly. Influential also were the various publications and patents ranging from the 1970's to the late 1990's, such as those by Linder *et al*. [13] and Ward *et al*. [14], investigating the possibility of using different membrane materials for a wide range of applications.

Initial NF membranes, due to its lack of chemical resistance, could not be used in the presence of organic solvents. However, during the last 15 years, extensive research has been dedicated to the development of solvent resistant membranes, aptly known

today as OSN. Making its breakthrough in the 20th century, OSN can no longer be considered as new but its relevance, even today, remains fully intact, achieving renown across various industries, including oil [15–17], food [18–23], biological [24,25], pharmaceutical [26–28] and fine chemical [29]. Vandezande *et al*. [30] foresaw that increases in the energy price and the ever-growing concern regarding ecological sustainability will only accelerate the industrial application of OSN membranes. Although strongly arguing the vast potential which the field of OSN membranes hold, they still noted to the fact that room for improvement still exist including further enhanced stability and robustness, higher capacities and longer operational lifetimes [30].

Koch Membrane Systems, situated in USA, was the first company to commercialise OSN membranes in the late 1990's through its MPF-50, MPF-60 (both these products are now discontinued) and MPF-44 membranes [31]. W. R. Grace-Davidson, also established in the USA, then pioneered the development of the most important OSN membranes of its era, named the STARMEM^{TM} series including STARMEM^{TM}-120, ST-122, ST-228 and ST-240 [32]. SolSep only recently became a contender in the OSN market introducing five of its membranes with nominal MWCO ranging between 300 and 750 g.mol^{-1} [33]. Some membranes intended for aqueous applications may be applied in organic environments such as the Desal membrane series introduced by Osmonics, The Netherlands [34]. Although these membranes are known to have a high stability toward organic solvents, performance monitoring is warranted for various applications.

A key moment in the field of OSN came in the 1990's when Exxon Mobil applied for several patents relating to the development of polyimide membranes to be used for the separation of lube oil from dewaxing solvents [35–38]. This research then culminated in the first industrial-scale application of OSN in 1998 at the Exxon Mobil refinery, MAX-DEWAX, in Beaumont, Texas which has a capacity of approximately 300 million litres per year [39].

The earliest documented application of membranes for homogeneous catalyst recovery can be dated back to the early 1970's where Goldup and his group at British Petroleum (BP) Co. Ltd. patented their findings regarding the separation of phosphine modified rhodium complexes from a hydroformylation post-reaction mixture using a silicon-based membrane [40]. Publications by Gosser *et al.* [41]

extended the work by Goldup and reported that polyimide RO membranes can successfully be used to recover homogeneous catalysts based on various transition metals. Catalyst recoveries ranging between 60 - 99% were reported and in the process, the potential of OSN membranes in homogeneous catalysis was highlighted. Gosser *et al.* [42] went on to patent their work in 1974. It is worth mentioning that during this time, various other researchers followed suit, including Shuey and Wan [43], Anderson [44] and White *et al*. [45], further strengthening the field of OSN through publications and patent applications, especially in the oil processing industry.

Some of the major milestones in the development of OSN membranes are summarised in Table A.2.

Table A.2: Significant breakthrough in the field of OSN

1748	Origin of membranes; Abbè Noblet uses a diaphragm to permeate water
1800's	Van't hoff and Maxwell use membranes on small-scale to develop the Van't Hoff equation and the kinetic theory of gases, respectively
1918	Membranes used during World War 1 to test quality of drinking water
Early 1900's	Millipore adopt membranes to create a lucrative business
1960's	Industrial-scale breakthrough of membranes
	Loeb-Sourirajan develop a membrane capable of achieving a flux 10 times higher than its predecessor
	Sourirajan and co-workers investigate use of OSN membranes in the purification of hydrocarbons
1966	Alex Affaroni expands membrane application to the medical industry and perfects use of membranes as artificial organs and for controlled drug delivery systems
1970's	Goldup and co-workers at BP successfully implement OSN on industrial scale for the recovery of homogeneous catalysts
	Lawrence Gosser investigate the use of polyimide RO membranes for catalyst recovery
	Paul and co-workers publish various articles and patents regarding OSN membranes

Table A.2: Significant breakthrough in the field of OSN (*cont.*)

	Ward and co-workers investigate the potential of silicon/polycarbonate materials for OSN membranes
1974	Gosser patents work regarding catalyst recovery via OSN
1983	Anderson uses UF membrane for dewaxing application
1985	Shuey and Wan uses OSN membranes for the purification of organic liquids
1990's	Commercialisation of OSN membranes by Koch Membrane Systems through their MPF-series membranes
	W. R. Grace-Davidson introduces the STARMEM series membranes
1993	White investigates the use of OSN membranes for solvent recovery from lube oil
1996	Linder co-workers investigate the possibility of using silicon-derived materials for OSN membranes
1998	Exxon Mobil in Beaumont, Texas successfully implement OSN on industrial scale

A.3 OSN modelling

A.3.1 Theoretical overview of OSN modelling

The driving force that causes the transport of species across the membrane is due to a gradient in chemical potential across said membrane. Therefore, the flux of the permeating species, J, can be related to this chemical potential gradient, μ, through a factor known as the membrane permeance constant, L, as shown in Equation A.1.

$$J = -L\nabla\mu \tag{A.1}$$

By considering the membrane as an infinite sheet of polymer, the abovementioned equation can be simplified to its one-dimensional form given in Equation A.2.

$$J = -L\frac{d\mu}{dz} \tag{A.2}$$

where

z z-direction perpendicular to the membrane surface (m)

The chemical potential given in Equations A.1 and A.2 represents any of the driving forces, i.e. pressure, concentration, electric potential, etc., and can be reformed to suit a specific application. In terms of pressure and concentration gradients alone, chemical potential can be expressed as shown Equation A.3.

$$d\mu = RT \times dln(\gamma C) + V_m \times dP \quad \text{(A.3)}$$

where

γ activity coefficient relating concentration to activity (-)

C species concentration (mol.m^{-3})

V_m molar volume (m^3.mol^{-1})

P applied pressure (Pa)

R universal gas constant (J.mol^{-1}.K^{-1})

T applied temperature (K)

For incompressible fluids, such as liquids or solids, the volume does not change significantly with pressure. This allows for the integration of Equation A.3 with respect to constant volume to give:

$$\mu = \mu^0 + RT \times \ln(\gamma C) + V_m \times (P - P^{sat}) \quad \text{(A.4)}$$

where

μ^0 pure component chemical potential (J.mol^{-1})

P^{sat} saturation vapour pressure (Pa)

In the case of compressible fluids, such as gases, where the pressure changes have significant effects of the phase volume, Equation A.4 is integrated with respect to variable volume to give:

$$\mu = \mu^0 + RT \times \ln(\gamma C) + RT \times \ln\left(\frac{P}{P^{sat}}\right) \quad \text{(A.5)}$$

The general assumptions made by Wijmans and Baker [46] which govern the transport of species across nanofiltration membranes are:

- The phases on either side of the membrane is in equilibrium with the material of the membrane

$$\mu_{i,FM} = \mu_{i,MF} \quad \text{Feed side} \quad \text{(A.6)}$$

$$\mu_{i,P} = \mu_{i,MP} \quad \text{Permeate side} \quad \text{(A.7)}$$

- The rate at which species adsorb and desorb from the membrane surface is much higher in relation to the rate of diffusion through the membrane material

A.3.2 Origins, principles and derivation of solution-diffusion model

The solution-diffusion model, developed by Lonsdale and Merten in 1965 [47], and later reviewed by Wijmans and Baker in 1995 [46], describes the transport of species through dense “nonporous” polymer membranes in three principle steps, as shown in Figure A.7. These steps consist of: 1) the sorption of species from the feed phase onto the membrane surface facing the feed side, 2) the diffusion of species through the membrane, and finally, 3) the desorption of species from the membrane surface facing the permeate side into the permeate phase. Since it can be considered that the adsorption and desorption rates of species are equal, separation of species occurs mainly due to differences in the species diffusion rates, i.e. step 2 as described previously. The assumptions associated with the solution-diffusion model include [48]:

- Chemical potential of species on either side of the membrane is in equilibrium with the membrane surfaces
- The dissolution and diffusion onto and into the homogeneous, non-porous membrane occurs due to a concentration gradient across the membrane
- No pressure gradient exists within the membrane
- Constant activity coefficient for permeating species within the membrane
- Concentration polarisation is non-existent

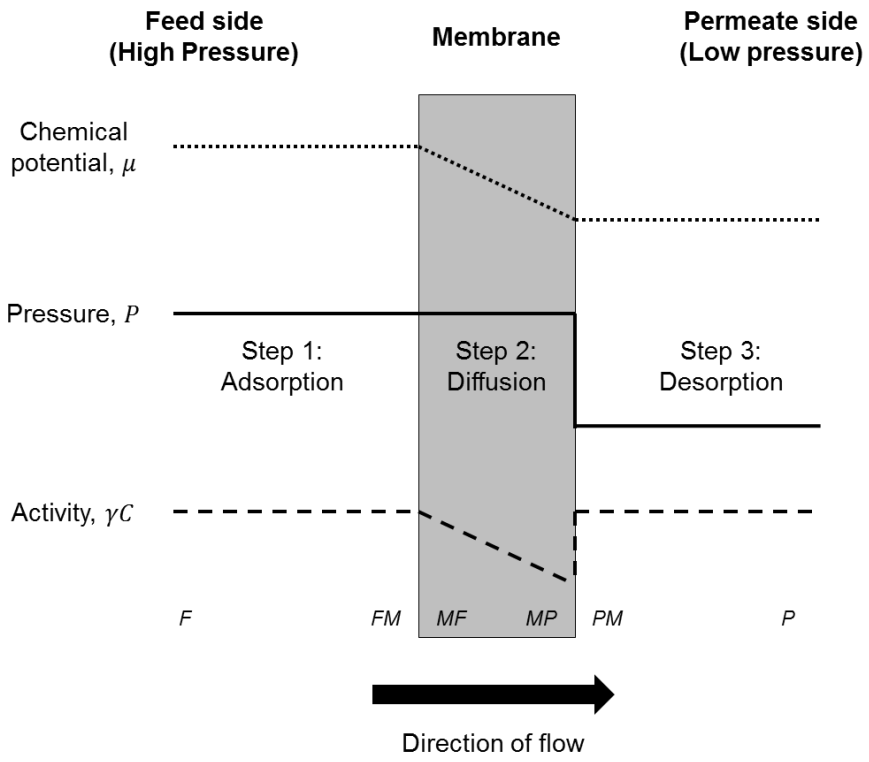

Figure A.7: Schematic illustration of solution-diffusion model (adapted from [46])

The term “nonporous” may provide some misconception as pores do in fact exist within the structure of the dense membrane albeit on a molecular level. Mulder states that a better classification of these pores is free volume elements formed within the free volume theory in mind. The free volume approach states that the flux of a molecule depends on the probability of it finding sufficient free volume through which it can displace [49].

The discontinuous drop in pressure on the permeate (support) side of the membrane observed in Figure A.7 has been clarified by Paul who claimed that the membrane is too weak to hold a pressure gradient. As a result of this approximation, a concentration gradient exists between the feed and permeate sides of the membrane and subsequently, flux is regarded as a result of diffusion across this concentration gradient [50].

Literature commonly equates the classic solution-diffusion model to a form similar to Fick’s law of diffusion [46]. However, recent reports by the groups of Gorak [51] and Wessling [52] have confirmed that this is only true for rubbery polymeric membranes and that the predictions based on the solution-diffusion model for glassy swollen polymers are less straightforward. This was attributed to the different equilibrium

states of the solvent and the membrane polymer matrix. In the same breath, the Wessling group [52,53] successfully managed to provide validity to the assumptions of the solution-diffusion model through ellipsometry measurements comparing static pressure and non-equilibrium measurements with hexane permeation through a rubbery PDMS membrane. The ST-240 membrane was used in this study, forming part of the STARMEM^{TM} series, consists of the polyimides Matrimid 5218 and Lenzing P84 which have glass transition temperatures of approximately 306 °C and 311 °C. Thus, the ST-240 membrane is in the glassy state at moderate temperatures. The Gorak group further reported that the polyimides, Matrimid 5218 and Lenzing P84, appear to exhibit non-Fickian behaviour at 25 °C and suggests that the derivation of the solution-diffusion model, at moderate temperatures, should be based on the Maxwell-Stefan diffusion equation rather than Fick's law [51]. As separation processes occur at a wide range of temperatures, consideration is given to membranes in both the rubbery and glassy state. Therefore, derivations for the solution-diffusion model based on both the Fickian and Maxwell-Stefan approach will be presented.

Starting with Fick's law, considering Fickian polymers in the rubbery state, the assumption of the chemical potential of species on either side of the membrane being in equilibrium can be equated using chemical potential expression given in Equation A.8.

$$J_{n,i} = -D_{i,M}\frac{dC_i}{dz} \tag{A.8}$$

where

$J_{n,i}$ partial molar flux of species i (mol.m^{-2}.s^{-1})

$D_{i,M}$ diffusion of species i through the membrane M (m^2.s^{-1})

The *feed side* is represented by Equation A.6a and substituted into Equation A.8 gives:

$$\mu_{i,F}^{o} + RT \times \ln\left(\gamma_{i,FM}C_{i,FM}\right) + V_{m,i} \times (P_{FM} - P_i^{sat}) = \mu_{i,F}^{o} + RT \times \ln\left(\gamma_{i,MF}C_{i,MF}\right) + V_{m,i} \times (P_{MF} - P_i^{sat}) \tag{A.9}$$

Rearranging Equation A.9 and considering a constant pressure gradient across the membrane, $P_{FM} = P_{MF}$, simplifies to the expression:

$$C_{i,MF} = K_i C_{i,FM} \tag{A.10}$$

where K_i is the sorption coefficient (-) and is equal to $\frac{\gamma_{i,FM}}{\gamma_{i,MF}}$. Subscripts MF and FM refer to the position of the species, i.e. in bulk feed solution, in membrane, in bulk permeate solution, etc., as indicated in Figure A.12.

The *permeate side* is represented by Equation A.6b and substituted into Equation A.8 gives:

$$\mu_{i,P}^{o} + RT \times \ln\left(\gamma_{i,P} C_{i,P}\right) + V_{m,i} \times (P_P - P_i^{sat}) = \mu_{i,P}^{o} + RT \times \ln\left(\gamma_{i,MP} C_{i,MP}\right) + V_{m,i} \times (P_{MP} - P_i^{sat}) \tag{A.11}$$

Similar to Equation A.9, except in this case $P_P \neq P_{MP}$ due to the discontinuity in pressure which exits at the permeate side inherent to the solution-diffusion model, as illustrated in Figure A.12, rearranging for concentration gives:

$$C_{i,MP} = \frac{\gamma_{i,P}}{\gamma_{i,MP}} C_{i,P} \exp\left(\frac{-V_{m,i}(P_{MP} - P_P)}{RT}\right) \tag{A.12}$$

$$\therefore\ C_{i,MP} = \frac{\gamma_{i,MF}}{\gamma_{i,MF}} \frac{\gamma_{i,FM}}{\gamma_{i,FM}} \frac{\gamma_{i,P}}{\gamma_{i,MP}} C_{i,P} \exp\left(\frac{-V_{m,i}(P_{MP} - P_P)}{RT}\right) \tag{A.13}$$

Assuming the solvent activity is in equilibrium on either side of the membrane, i.e. $\frac{\gamma_{i,MF}}{\gamma_{i,FM}}$, Equation A.13 can be expressed as:

$$C_{i,MP} = K_i \frac{\gamma_{i,P}}{\gamma_{i,MP}} C_{i,P} \exp\left(\frac{-V_{m,i}(P_{MP} - P_P)}{RT}\right) \tag{A.14}$$

At this point, the expressions derived for concentration, Equations A.10 and A.14, can be substituted into Fick's law, Equation A.9, resulting in the classic solution-diffusion model:

$$J_{n,i} = \frac{D_i K_i}{l}\left[C_{i,FM} - C_{i,P} \frac{\gamma_{i,P}}{\gamma_{i,MP}} \exp\left(-\frac{V_{m,i} \times (P_{MP} - P_P)}{RT}\right)\right] \tag{A.15}$$

Wijmans and Baker [46] derived the solution-diffusion model based on the assumption of equal activity coefficients ($\gamma_{i,P} = \gamma_{i,MP}$), but the Livingston research group [54] proposed the use of partial molar fluxes of a binary mixture of i and j rather than their concentrations, shown in Equations A.16 and A.17, respectively:

$$J_{n,i} = \frac{D_i K_i}{l}\left[C_{i,FM} - C_{i,P} \exp\left(-\frac{V_{m,i} \times (P_{MP} - P_P)}{RT}\right)\right] \tag{A.16}$$

$$J_{n,i} = \frac{D_i K_i}{l}\left[C_{i,FM} - \frac{J_{n,i}}{J_{n,i}+J_{n,j}}\frac{\gamma_{i,P}}{\gamma_{i,MP}}\exp\left(-\frac{V_{m,i}\times(P_{MP}-P_P)}{RT}\right)\right] \quad \text{(A.17)}$$

When incorporating the definition of osmotic pressure and using the Taylor approximation series, the above expressions can be simplified to [55]:

$$J_i = A_i(\Delta P - \Delta\pi) \quad \text{(A.18)}$$

where the solute molar permeance of species i is denoted by A_i (mol.m^{-2}.s^{-1}.Pa^{-1}) and is equal to $\frac{D_i K_i C_{i,0} V_{m,i}}{lRT}$.

For the case of polymers in its glassy state, i.e. the polyimides Matrimid 5218 and Lenzing P84, at moderate temperatures, Silva *et al.* used the Maxwell-Stefan equation to derive the solution-diffusion model [56]. The general Maxwell-Stefan equation states that the driving force, F_i, exerted on species i is equal to the sum of the dimensionless friction forces, ξ, between itself and other species, including the membrane, and can be expressed in terms of molar fluxes, as shown in Equation A.19 [57–59]:

$$F_i = \sum_{\substack{j=i \\ i\neq j}}^{n}\left[x_j\xi_{ij}\left(J_{n,i} - J_{n,j}\right)\right] \quad \text{(A.19)}$$

where

x_j molar fraction of species j (mol.mol^{-1})

In this work, the driving force is the difference in chemical potential across the membrane. With no pressure gradient across the membrane, the Maxwell-Stefan equation simplifies to the expression shown in Equation A.20:

$$-x_{i,M}\nabla_{T,P}\mu_i = \sum_k\left(\xi_{i,k}\frac{x_{k,M}J_{n,i} - x_{i,M}J_{n,k}}{C_{t,M}} + \xi_{i,M}\frac{x_M J_{n,i}}{C_{t,M}}\right) \quad \text{(A.20)}$$

Additional assumptions include negligible interspecies friction and constant activity coefficient of permeating species inside the membrane, and integrating over the membrane thickness gives [54]:

$$J_{n,i} = \frac{D_i K_i}{l}\left[x_{i,FM} - x_{i,P}\frac{\gamma_{i,P}}{\gamma_{i,FM}}\exp\left(-\frac{\bar{V}_{m,i}\times(P_{MP}-P_P)}{RT}\right)\right] \quad \text{(A.21)}$$

It is clear that the model derived through the Maxwell-Stefan equation, Equation A.21, is similar to classic solution-diffusion model derived in Equation A.15, except for the latter being expressed in molar fractions. The Wessling group [57] later noted that the solution-diffusion model derived from Maxwell-Stefan and Fick's law both were in good agreement with experimental data. Moreover, they stated that the Maxwell-Stefan equation is used by researchers only to avoid simplifying assumptions inherent to Fick's law and that it gave more realistic results. Paul [60] provides another excellent representation of the derivation of the solution-diffusion model.

A.3.3 Origins, principles and derivations of pore-flow model

The pore-flow model, developed by Okada and Matsuura in 1985 [30], describes the transport of species through a porous membrane where the flow thereof is dependent solely on physical properties such as viscosity, molecular size and membrane pore diameter. The assumptions made during the derivation of this model, which can be depicted schematically as shown in Figure A.8, include [56]:

- Driving force for permeation is based solely on a pressure gradient across the membrane.
- Solute and solvent concentration remains constant throughout the membrane (i.e. no concentration gradient exists within the membrane)
- Membrane pores are rigid and constant in size and shape (straight cylindrical pores).

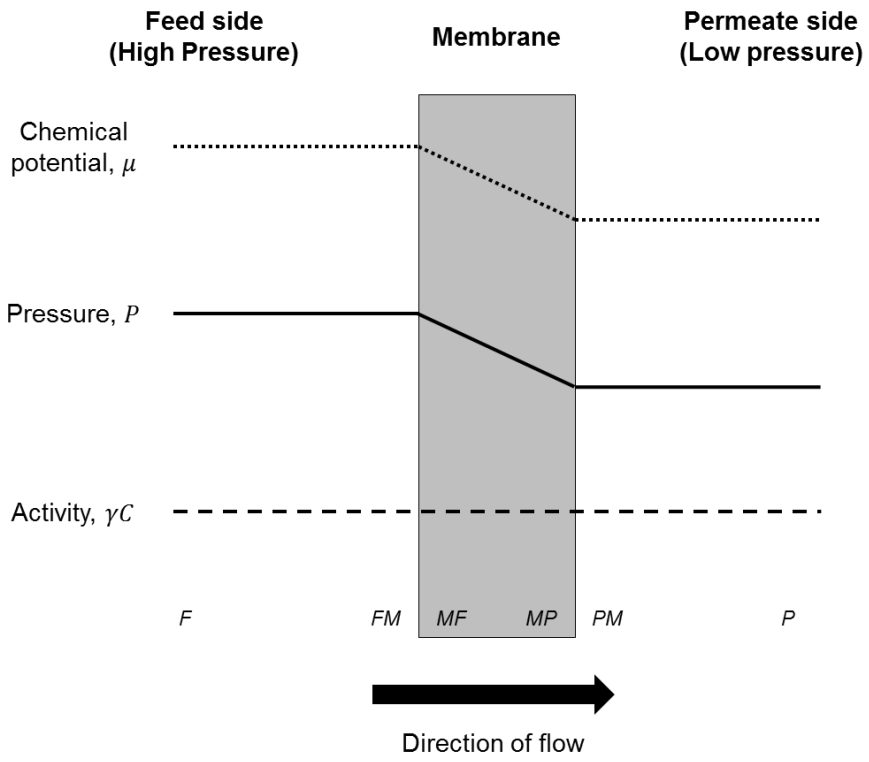

Figure A.8: Schematic illustration of pore-flow model (adapted from [46])

Based on these approximations, the transport of species through porous membranes, characteristic of the MF and UF membranes consisting of pores roughly in the size range 2 nm – 10 µm [49], can be mathematically described by Darcy's law, as shown in Equation 2.28, which takes into consideration the physical properties of the membrane, including pore size, surface porosity, tortuosity, etc.

$$J = K_D \times \frac{P_o - P_z}{l} \qquad \text{(A.22)}$$

where

K_D Darcy's law permeance coefficient

P_o Upstream / feed side pressure (Pa)

P_z Downstream / permeate side pressure (Pa)

l membrane thickness (m)

By combining Equations A.3 and A.5, at a negligible concentration gradient, also gives Darcy's law with K_D being equal to Lv.

In the presence of organic solvents, membranes may experience a change in pore size due to swelling. Therefore, Darcy's law can be modified to include solvent viscosity to account for this phenomenon. The modified correlation is termed the Hagen-Poiseuille equation and expressed as shown in Equation A.23.

$$J_V = \frac{\varepsilon {d_{pore}}^2}{32l\tau} \times \frac{P_o - P_z}{\eta} \qquad \text{(A.23)}$$

where

ε membrane surface porosity (-)

τ membrane tortuosity (-)

d_p membrane pore size (m)

η solvent viscosity (Pa.s)

A.3.4 Combination of solution-diffusion and pore-flow models

The key difference between the solution-diffusion and pore-flow models are in the way these models express the chemical potential gradient within the membrane. The solution-diffusion model assumes that the pressure remains uniform throughout the membrane and that chemical potential can be expressed in terms of a concentration gradient alone. In the case of pore-flow models, the concentration gradient is assumed negligible and equates the pressure gradient to the chemical potential driving force.

Wijmans and Baker [46] further claimed that the difference in these two models can be based on the relative permanence of the membrane pores in each case. Pores larger in size is said to be "more permanent" and therefore will adhere to the pore-flow model's definition to being more rigid and constant in terms of its size, orientation and shape. A contrasting argument can be made for pores smaller in size. Vandezande *et al*. [30] defined the pores of membrane adhering to the solution-diffusion model as:

"*…free volume elements that are present as statistical fluctuations that appear and disappear in about the same time scale as the motions of the permeants that pass the membrane*."

Therefore, according to the definition given, smaller pores are considered “non-permanent” which are not fixed in terms of size and shape. Baker [8] further goes on to suggest that, as a rule of thumb, membrane pore diameters less than 0.5 nm, the flow through it can be considered as solution-diffusion while pores larger than 1 nm will be pore-flow in nature. Wijmans and Baker [46] determined that in the pore diameter range 0.5 – 1 nm, the two definitions of pores given becomes blurred. Therefore, to address the confusion by many researchers when considering membranes pores in this diameter range, the pore-flow and solution-diffusion models were combined to birth two new models which reconcile the pore definitions adopted by the parent models. These models are known as the resistance-in-series model and the solution-diffusion-with-imperfections model, as shown in Equations A.24 and A.25, respectively [61,62]:

$$J_V = \frac{\Delta P}{\emptyset[(\gamma_c - \gamma_l) + f_{1,n}] + f_{2,n}} \tag{A.24a}$$

with

$$f_1 = \frac{k_M^1}{k_M^0} \tag{A.24b}$$

$$f_2 = \frac{k_M^2}{\left(d_{pore}^2\right)^2} \tag{A.24c}$$

$$\emptyset = \frac{k_M^0}{\left(d_{pore}^1\right)^2} \tag{A.24d}$$

where

f parameter describing the nanofiltration sublayers independent of the solvent

$\emptyset$ solvent dependent parameter (-)

γ_c critical surface tension of membrane material (-)

γ_l critical surface tension of solvent (-)

$$J_V = \frac{C_{i,M} D_{i,M} V_{m,i}}{RTl} \Delta P + \frac{C_{i,M} B_o}{\eta l} \Delta P \tag{A.25}$$

where B_o is a hydraulic parameter indicating the membrane openness (-).

Both these models were proposed with the purpose of addressing the limitations in their parent models.

In the case of the resistance-in-series model, as shown in Equation A.24, Machado *et al.* [61] included terms in order to account for solvent-membrane interactions governed by viscous and surface effects. These additional terms related the flux of a solvent mixture with easily measurable solvent and membrane properties which were found previously by the authors to significantly influence membrane performance, i.e. viscosity, surface tension, membrane hydrophobicity [63].

In the case of the solution-diffusion-with-imperfections model, as shown in Equation A.25, Mason and Lonsdale noted that flux not only occurs through the pores of porous membranes but also through imperfections (i.e. channels, pores, surface inconsistencies, etc.), that when large enough, may allow the passage of species [62,64]. The proposed model was purposefully constructed to account for the extra flux. Sherwood *et al*., [65] prior to the proposition of the solution-diffusion-with-imperfections model, published experimental findings which verified the solution-diffusion-with-imperfections model as being capable of describing solvent transport in terms of both diffusive transport and viscous transport that may occur due to imperfections or defects present within the membrane. This is due to the addition of viscous term to the classic solution-diffusion model. Excellent reviews of this model was published by Fierro et al. [66] and Yaroschuk [67,68].

A.3.5 Phenomenological models

Prior to the solution-diffusion and pore-flow models, early membrane transport models, such as the Kedem-Katchalsky and Spiegler-Kedem models, were based on the principle of irreversible thermodynamics which describes transport in terms of phenomenological relationships and considers the membrane as a “black box”. The Kedem-Katchalsky model is defined as shown in Equation A.26:

$$J_w = A(\Delta P - \sigma \Delta \pi) \tag{A.26}$$

For binary systems, the transport of solvents are defined as shown in Equation A.26 but that for solutes are defined in Equation A.27 [69–72]:

$$J_s = B\Delta \pi + (1 - \sigma) C_{avg} J_w \tag{A.27}$$

The key parameters are defined as,

$$A = \left(\frac{J_w}{\Delta P}\right)_{\Delta\pi=0} \quad \text{(A.28)}$$

$$B = \left(\frac{J_s}{\Delta\pi}\right)_{J_w=0} \quad \text{(A.29)}$$

$$\sigma = \left(\frac{\Delta P}{\Delta\pi}\right)_{J_w=0} \quad \text{(A.30)}$$

Another problem is immediately apparent as a distinction has to be made between the solute and the solvent. This is in fact difficult to do so as Adam *et al.* [73] claimed that the conventional distinction between solutes and solvents loses its significance when organic liquids are considered. Wijmans and Baker [46] defined the reflection coefficient, σ, as an interaction parameter to characterise interactions between the solvent and solute passing through a membrane channel. They further stated that for σ < 1 the membrane is considered semi-permeable while σ = 1 indicates an impermeable solute (solute completely rejected). The problem with Kedem-Katchalsky model is its dependency on concentration where if large concentration differences exist across the membrane, the linearity approximation within the irreversible thermodynamics becomes invalid [64,74]. Spiegler and Kedem [75] observed this problem and proposed a modified version of the model rooted from irreversible dynamics, based on two parameters, solute permeance, B, and reflection coefficient, which has no concentration dependence. J_w is defined the same as for the Kedem-Katchalsky model, but J_s is defined as shown in Equation A.31 [76]:

$$J_s = B\Delta x\frac{dC}{dx} + (1-\sigma)J_w C_{avg} \quad \text{(A.31)}$$

Integration of the differential form of Equation A.31 results in the expression for real rejection as given in Equation A.32:

$$R_{real} = \frac{\sigma(1-F)}{1-\sigma F} \quad \text{(A.32)}$$

with

$$F = \exp\left(-\frac{1-\sigma}{B}J_w\right) \quad \text{(A.33)}$$

These phenomenological equations are typically used to describe the rejection of uncharged molecules in aqueous solutions, combining both convective and diffusive transport. From this stems different models to predict the reflection coefficient,

communal in their assumption that rejection takes place mainly through size exclusion and differing in the definition of exclusion forces, namely the Steric Hindrance Pore (SHP) [77], Ferry [78], Verniory [79] and lognormal model [80], as shown in Equations A.34 – A.37, respectively:

$$\sigma = 1 - H_F S_F \tag{A.34a}$$

with

$$H_F = 1 + \frac{16}{9}a^2 \tag{A.34b}$$

$$S_F = (1-a)^2\left(2-(1-a)\right)^2 \tag{A.34c}$$

$$a = \frac{d_{ij}}{d_{pore}} \tag{A.34d}$$

$$\sigma = 1 - 2(1-a)^2 - (1-a)^4 \tag{A.35}$$

$$\sigma = 1 - g(a)S_F \tag{A.36a}$$

$$g(a) = \frac{1-0.67a^2-0.25a^5}{1-0.76a^5} \tag{A.36b}$$

$$\sigma = \int_0^{r_c} \frac{1}{S_P\sqrt{2\pi}} \frac{1}{r} \exp\left(-\frac{(ln(r)-ln(\bar{r}))^2}{2S_P^2}\right) dr \tag{A.37}$$

where H_F is the membrane pore wall correction factor, S_F the steric hindrance factor, d_{ij} the effective diameter of species i in solvent j, r_{pore} the membrane pore radius and S_P the standard deviation of the lognormal distribution.

Slight variations of these reflection coefficient models also include those proposed by Haberman and Sayre [81], Zeman and Wales [82], Bohlin [83] and Li *et al.* [84].

A.4 References

[1] G.D. Frey, *J. Organomet. Chem*. **754** (2014) 5–7.

[2] P.W.N.M. Van Leeuwen, **Rhodium Catalyzed Hydroformylation: Catalysis by Metal Complexes**, Volume 22, Kluwer Academic Publishers, The Netherlands, 2000.

[3] A. Behr, P. Neubert, **Applied Homogeneous Catalysis**, Wiley VCH, Germany, 2012.

[4] R.L. Pruett, J.A. Smith, **Hydroformylation Process**, US3,527,809, 1970.

[5] S.S. Bath, L. Vaska, *Commun. to Ed.* (1963) 3501.

[6] G. Wilkinson, **Improvements in Catalytic Hydrogenation and Hydroformylation**, British 1,219,763, 1971.

[7] P.W.N.M. Van Leeuwen, **Homogeneous Catalysis - Understanding the art**, Kluwer Academic Publishers, The Netherlands, 2004.

[8] R.W. Baker, **Membrane Technology and Applications**, 2nd Ed., John Wiley & Sons, Ltd., England, 2004.

[9] S. Sourirajan, *Nature.* **203** (1964) 1348–1349.

[10] O.M. Ebra-Lima, D.R. Paul, *J. Appl. Polym. Sci.* **19** (1975) 1381–1386.

[11] D.R. Paul, J.D. Paciotti, O.M. Ebra-Lima, *J. Appl. Polym. Sci.* **19** (1975) 1837–1845.

[12] D.R. Paul, O.M. Ebra-Lima, *J. Appl. Polym. Sci.* **19** (1975).

[13] C. Linder, M. Nemas, M. Perry, R. Katraro, **Silicon-Derived Solvent Stable Membranes,** US5,265,734, 1993.

[14] W.J. Ward, W.R. Browall, R.M. Salemme, *J. Memb. Sci*. **1** (1976) 99–108.

[15] E.S. Tarleton, J.P. Robinson, J.S. Low, *Chem. Eng. Res. Des*. **87** (2009) 271–279.

[16] R. Subramanian, K.S.M.S. Raghavarao, H. Nabetani, M. Nakajima, T. Kimura, T. Maekawa, *J. Memb. Sci.* **187** (2001) 57–69.

[17] L.S. White, A.R. Nitsch, *J. Memb. Sci.* **179** (2000) 267–274.

[18] G. Cocchi, M.G. De Angelis, F. Doghieri, *J. Memb. Sci*. (2015) 1–47.

[19] O. Akin, F. Temelli, S. Köseoglu, *Crit. Rev. Food Sci. Nutr.* **52** (2012) 347–371.

[20] I. Sereewatthanawut, I.I.R. Baptista, A.T. Boam, A. Hodgson, A.G. Livingston, *J. Food Eng.* **102** (2011) 16–24.

[21] D. Peshev, L.G. Peeva, G. Peev, I.I.R. Baptista, A.T. Boam, *Chem. Eng. Res. Des.* **89** (2010) 318–327.

[22] A.P.B. Ribeiro, J.M.L.N. de Moura, L.A.G. Goncalves, J.C.C.P. Petrus, L.A. Viotto, *J. Memb. Sci*. **282** (2006) 328–336.

[23] F.P. Cuperus, H.H. Nijhuis, *Trends Food Sci. Technol*. **4** (1993) 277–282.

[24] M.L. Gerardo, D.L. Oatley-Radcliffe, R.W. Lovitt, *J. Memb. Sci.* **464** (2014) 86–99.

[25] C. Abels, F. Carstensen, M. Wessling, *J. Memb. Sci.* **444** (2013) 285–317.

[26] D. Ormerod, B. Sledsens, G. Vercammen, D. Van Gool, T. Linsen, A. Buekenhoudt, B. Bongers, *Sep. Purif. Technol*. **115** (2013) 158–162.

[27] M. Brito Martinez, B. Van der Bruggen, Z.R. Negrin, P.L. Alconero, *J. Ind. Eng. Chem.* **18** (2012) 1635–1641.

[28] G. Székely, J. Bandarra, W. Heggie, B. Sellergren, F. Castelo, *J. Memb. Sci*. **381** (2011) 21–33.

[29] J. Wöltinger, K. Drauz, A.S. Bommarius, *Appl. Catal. A Gen.* **221** (2001) 171–185.

[30] P. Vandezande, L.E.M. Gevers, I.F.J. Vankelecom, *Chem. Soc. Rev.* **37** (2008) 365–405.

[31] Koch Membrane Systems Inc., United Kingdom. [Online], (2015). http://kochmembrane.com/. [Date accessed: 9 July 2015].

[32] Evonik Industries AG, Germany. [Online], (2015). http://corporate.evonik.com/.

[33] SolSep BV, The Netherlands. [Online], (2014). http://solsep.com/. [Date accessed: 9 July 2015].

[34] GE Osmonics Desal membranes, Delft. [Online], (2015). http://lenntech.com/products/membrane/osmonics/. [Date accessed: 9 July 2015].

[35] K.J. Smith, **Upgrading Heavy Oil by Ultrafiltration Using Ceramic Membrane**, CA2,185,264 A1, 1998.

[36] A. Welmers, L.E. Black, **Solvent Extraction Process Involving Membrane Separation of Extract Phase and/or Intermediate Zone Phase**, US5,435,918, 1995.

[37] T. Chen, **Separation of Hydrocarbon Dewaxing and Deasphalting Solvent From Dewaxed and/or Deasphalted Oil Using Interfacially Polymerized Membrane**, US5,182,024, 1993.

[38] L.E. Black, **Interfacially polymerized membranes for the reverse osmosis separation of organic solvent solutions**, US5,173,191, 1992.

[39] R.M. Gould, L.S. White, C.R. Wildemuth, *Environ. Prog.* **20** (2001) 12–16.

[40] A. Goldup, M.T. Westaway, G. Walker, **Separation of Metal Compounds**, US3,645,891, 1972.

[41] L.W. Gosser, W.H. Knoth, G.W. Parshall, *J. Mol. Catal*. **2** (1977) 253–263.

[42] L.W. Gosser, **Membrane separation of homogeneous catalysts from nitrile solutions**, US3,853,754, 1974.

[43] H.F. Shuey, W. Wan, **Asymmetric Polyimide Reverse Osmosis Membrane, Method for Preparation of Same and Use Thereof For Organic Liquid Separations**, US4,532,041, 1985.

[44] B.P. Anderson, **Ultrafiltration Polyimide Membrane and Its Use For Recovery of Dewaxing**, US4,963,303, 1989.

[45] L.S. White, I.F. Wang, B.S. Minhas, **Polyimide Membrane For Separation of Solvents From Lube Oil**, US5,264,166, 1993.

[46] J.G. Wijmans, R.W. Baker, *J. Memb. Sci.* **107** (1995) 1–21.

[47] H.K. Lonsdale, *J. Memb. Sci.* **10** (1982) 81–181.

[48] M.F.J. Dijkstra, S. Bach, K. Ebert, A transport model for organophilic nanofiltration, J. Memb. Sci. 286 (2006) 60–68.

[49] M. Mulder, **Basic Principles of Membrane Technology**, Kluwer Academic Publishers, The Netherlands, 1991.

[50] D.R. Paul, *J. Appl. Polym. Sci.* **16** (1972) 771–782.

[51] L. Hesse, J. Mićović, P. Schmidt, A. Górak, G. Sadowski, *J. Memb. Sci.* **428** (2013) 554–561.

[52] W. Ogieglo, L. Upadhyaya, M. Wessling, A. Nijmeijer, N.E. Benes, *J. Memb. Sci*. **464** (2014) 80–85.

[53] W. Ogieglo, H. Van der Werf, K. Tempelman, H. Wormeester, M. Wessling, A. Nijmeijer, N.E. Benes, *J. Memb. Sci*. **437** (2013) 313–323.

[54] L.G. Peeva, E. Gibbins, S.S. Luthra, L.S. White, R.P. Stateva, A.G. Livingston, *J. Memb. Sci*. **236** (2004) 121–136.

[55] D. Bhanushali, S. Kloos, C. Kurth, D. Bhattacharyya, *J. Memb. Sci.* **189** (2001) 1–21.

[56] P. Silva, S. Han, A.G. Livingston, *J. Memb. Sci*. **262** (2005) 49–59.

[57] S. Postel, S. Wessel, T. Keil, P. Eiselt, M. Wessling, *J. Memb. Sci*. **466** (2014) 361-369.

[58] J.A. Wesselingh, R. Krishna, **Mass Transfer in Multicomponent Mixtures**, Delft University Press, The Netherlands, 2000.

[59] R. Krishna, J.A. Wesselingh, *Chem. Eng. Sci*. **52** (1997) 861–911.

[60] D.R. Paul, *J. Memb. Sci*. **241** (2004) 371–386.

[61] R. Machado, D. Hasson, R. Semiat, *J. Memb. Sci*. **166** (2000) 63–69.

[62] E.A. Mason, H.K. Lonsdale, *J. Memb. Sci*. (1990) 1–81.

[63] R. Machado, D. Hasson, R. Semiat, *J. Memb. Sci.* **163** (1999) 93–102.

[64] M. Soltanieh, W.N. Gill, *Chem. Eng. Commun.* **12** (1981) 279.

[65] T.K. Sherwood, P.L.T. Brian, R.E. Fischer, *Ind. Eng. Chem. Fundam*. **5** (1968) 120-121.

[66] D. Fierro, A. Boschetti-de-Fierro, V. Abetz, *J. Memb. Sci*. **413-414** (2012) 91–101.

[67] A.E. Yaroshchuk, *J. Memb. Sci*. **239** (2004) 9–15.

[68] A.E. Yaroshchuk, *J. Memb. Sci.* **101** (1995) 83–87.

[69] G. Suchanek, *Gen. Physiol. Biophys*. **25** (2006) 53–63.

[70] G. Suchanek, *Gen. Physiol. Biophys.* **24** (2005) 247–258.

[71] S. Koter, *J. Memb. Sci*. **246** (2005) 109–111.

[72] A. Kargol, *J. Memb. Sci.* **191** (2001) 61–69.

[73] W.J. Adam, B. Luke, P. Meares, *J. Memb. Sci.* **13** (1983) 127–149.

[74] S. Koter, *Desalination.* **198** (2006) 335–345.

[75] K.S. Spiegler, O. Kedem, *Desalination*. **1** (1966) 311–326.

[76] G.H. Koops, S. Yamada, S.I. Nakao, *J. Memb. Sci.* **189** (2001) 241–254.

[77] S.I. Nakao, S. Kimura, *J. Chem. Eng. Japan*. **15** (1982) 200–205.

[78] J.D. Ferry, *Chem. Rev. - Am. Chem. Soc*. (1936) 373–455.

[79] A. Verniory, R. Dubois, P. Decoodt, J.P. Gassee, P.P. Lambert, *J. Gen. Physiol*. **62** (1973) 489–507.

[80] B. Van der Bruggen, J. Schaep, D. Wilms, C. Vandecasteele, *Sep. Sci. Technol*. **35** (2000) 169–182.

[81] W. Haberman, R.M. Sayre, **Motion of rigid and fluid spheres in stationary and moving liquids inside cylindrical tubes**, 1958.

[82] L. Zeman, M. Wales, *Sep. Sci. Technol*. **16** (1981) 275–290.

[83] J. Geens, K. Boussu, C. Vandecasteele, B. Van Der Bruggen, *J. Memb. Sci*. **281** (2006) 139–148.

[84] W. Li, J. Li, T. Chen, Z. Zhao, C. Chen, *J. Memb. Sci*. **258** (2005) 8–15.

APPENDIX B: Detailed Experimental Procedures

B.1 Stepwise procedure for the hydroformylation reactions

1. Clean the inside of the reactor prior to starting the reaction using acetone.
2. Preheat a bath filled with glycerol so that it reaches the desired temperature (80 °C).
3. Load the substrate (alkene, 3.13 mL) and internal standard (n-dodecane, 0.7 mL) into the Teflon sleeve of the reactor.
4. Charge the reactor with 200 ppm solution of **$HRh(CO)(PPh_3)_3$** (4 mg, 0.00435 mmol) in 21 mL toluene to give a substrate to rhodium molar ratio of 4940:1.
5. Add additional ligand (**PPh_3**, 22 mg) to give a ligand to rhodium molar ratio of 20:1.
6. Add a magnetic stirrer bar into the reactor to stir the reaction mixture (500 rpm).
7. Seal the reactor and connect it to the syngas cylinder via a pipeline fitted to the top flange of the reactor.
8. Connect the thermocouple to the reactor in order to monitor the temperature inside the reactor.
9. Submerge the reactor in the fluid in order to attain a uniform temperature throughout the reactor (Note: submerge reactor up until the bottom of the top flange).
10. Place a thermometer into the glycerol filled tank in order to monitor the glycerol temperature (Note: wait for the contents of the reactor to attain the desired temperature before proceeding with the reaction).
11. Connect the reactor to the syngas cylinder and flush the reactor three times with syngas in order to purge the system (Note: take care not to let the pressure inside the reactor drop to less than atmospheric).
12. After purging, pressuring reactor to the desired syngas pressure (20 bar, CO/H_2 1:1).
13. Proceed with the reaction for 2 hours.
14. Withdraw a 1.5 mL sample upon completion of the reaction (Note: use a filter syringe to extract the sample so as to prevent any catalyst therein which would possible harm the GC internals).
15. Analyse the samples using GC.
16. While in the bath, depressurise the reactor and slowly vent the gases.
17. Clean the reactor and prepare for the succeeding reaction.

B.2 Stepwise procedure for OSN experiments

B.2.1 Membrane pretreatment, conditioning and steady-state characterisation

1. Load filtration cell with 250 mL toluene.
2. Secure top flange to cell body by fastening bolts.
3. Once sealed, place cell on a magnetic stirrer and adjust stirrer to 500 rpm.
4. Direct the permeate drainage pipe toward a permeate 200 mL collection flask.
5. Place the collection flask on an electronic scale.
6. Connect the nitrogen cylinder gas line to the cell gas inlet.
7. Pressurise cell to 30 bar (follow pressurisation valve sequencing).
8. Allow 50 mL of the initial feed volume to permeate out into the collection flask and discard the flask contents (This will contain preservation oil).
9. Once 50 mL has permeate, depressurise cell (follow depressurisation valve sequencing), open cell and add 50 mL fresh toluene.
10. Close and pressurise the cell.
11. Allow two thirds (150 mL) of the initial feed volume to permeate .
12. During permeation, measure the flux as mass or volume of permeate collected per unit time and membrane active area. If a constant flux has been attained, the pretreatment has completed and the cell can be depressurised (follow depressurisation valve sequencing). If not, the cell depressurised, opened and the permeate is added back to the cell.
13. Repeat steps 10 – 12 until a steady-state flux is achieved.

B.2.2 Reaction species separation

1. Make up a synthetic binary solution of concentration 0 – 100 wt%.
2. Load filtration cell with 150 mL of synthetic binary solution.
3. Secure top flange to cell body by fastening bolts.
4. Once sealed, place cell on a magnetic stirrer and adjust stirrer to 500 rpm.
5. Direct the permeate drainage pipe toward a permeate 200 mL collection flask.
6. Place the collection flask on an electronic scale.
7. Connect the nitrogen cylinder gas line to the cell gas inlet.
8. Pressurise cell to 30 bar.
9. Allow 40% (60 mL) of the initial feed volume to permeate.
10. During permeation, measure the flux as mass or volume of permeate collected per unit time and membrane active area. If a constant flux has been attained, the pretreatment has completed and the cell can be depressurised

(follow depressurisation valve sequencing). If not, the cell depressurised, opened and permeate is added back to the cell.

11. Repeat steps 3 – 10 until a steady-state flux is achieved.
12. Once steady-state is confirmed, depressurise, open and the permeate added back to the cell. The cell is then sealed and pressurised. Allow 10% (15 mL) of the initial feed volume to permeate into the collection flask. At this point, take a sample (1 x 4 mL) of the bulk permeate solution.
13. Depressurise and open cell.
14. Take a sample (1 x 4 mL) of the retentate (remainder in cell).
15. Analyse sample with GC.

B.2.3 Catalyst recovery

1. Make up a synthetic catalyst feed solution of 200 or 500 ppm.
2. Load filtration cell with 150 mL of catalyst feed solution.
3. Secure top flange to cell body by fastening bolts.
4. Once sealed, place cell on a magnetic stirrer and adjust stirrer to 500 rpm.
5. Direct the permeate drainage pipe toward a permeate 200 mL collection flask.
6. Place the collection flask on an electronic scale.
7. Connect the nitrogen cylinder gas line to the cell gas inlet.
8. Pressurise cell to 30 bar.
9. Allow 40% (60 mL) of the initial feed volume to permeate.
10. During permeation, measure the flux as mass or volume of permeate collected per unit time and membrane active area. If a constant flux has been attained, the pretreatment has completed and the cell can be depressurised (follow depressurisation valve sequencing). If not, the cell depressurised, opened and permeate is added back to the cell.
11. Repeat steps 3 – 10 until a steady-state flux is achieved.
12. Once steady-state is confirmed, depressurise, open and the permeate added back to the cell. The cell is then sealed and pressurised. Allow 10% (15 mL) of the initial feed volume to permeate into the collection flask. At this point, take a sample (1 x 5 mL) of the bulk permeate solution.
13. Depressurise and open cell.
14. Take a sample (1 x 5 mL) of the retentate (remainder in cell).
15. Analyse sample with FAAS.

B.2.4 Valve sequencing

Pressurisation

1. Keep all valves (V-01 through V-04, as shown in Figure A.1) in the close position.
2. Open the nitrogen gas cylinder (V-01). The pressure on the cylinder pressure gauge to immediately increase.
3. Open the gas isolation and inlet valve (V-03) located on the filtration cell.
4. Adjust the nitrogen gas regulator (V-02) to the desired pressure (Note: use both the gas line and cell pressure gauges).

Depressurisation

1. At this point, all valves are open, except the filtration cell pressure release valve (V-04).
2. Close the nitrogen gas cylinder valve (V-01).
3. Close the gas isolation and inlet valve (V-03) located on the cell.
4. Slowly open the nitrogen gas regulator (V-02) to vent the pressure in the gas line (Note: the pressure will drop on the gas line gauge). Once the pressure in the gas line has dropped completely, close the nitrogen regulator valve (V-02).
5. Slowly open the cell pressure release valve (V-04).
6. Open the gas isolation valve (V-03) to ensure all gases have been vented.
7. At this point, V-01 and V-02 should be closed and V-03 and V-04 should be open.

Figure B.1: Valves used for pressurisation and depressurisation procedures

APPENDIX C: Membrane Screening Results

C.1 Introduction

In this section, commercially available OSN membranes are assessed based on stability, permeance and rejection for suitability for the recovery of homogeneous catalysts from different post-reaction solvent mixtures.

C.2 Screening criterion and experimental methodology

From literature, it is evident that polymeric membranes are preferred for OSN applications due to their strong tolerance to organic solvents. Although the use of these OSN membranes dates back many years, only a few successful commercially available OSN membranes exist, including the STARMEM™ series, the SolSep series as well as the Duramem® and Puramem® series and to some extent the MPF, Nadir and Desal series. These membranes with their respective suppliers and specifications are summarised in Table C.1.

All OSN membranes listed in Table C.1 are good candidates based on their strong tolerance against organic solvents due to their polymeric nature. Polyimide (PI) membranes have been reported to be stable in a wide range of organic solvents and are relatively easily manufactured [1–5]. The Livingston research group has extensively studied the fabrication process of PI membranes typically used for OSN application has been extensively studied and investigates the effects of PI characteristics and solvent exposure on membrane performance [6–9]. Polydimethylsiloxane (PDMS) membranes, although similar in solvent resistance strength to PI, are known to swell severely in apolar solvents, potentially resulting in the peeling off of the selective layer and causing a reduction in selective capacity [10,11]. Reports have been made that PDMS membranes could potentially experience a 170% increase in its thickness after swelling without applied pressure [12]. Other polymeric membranes, i.e. polyamide (PA) and polyethersulfone (PES), are known to swell significantly in polar solvents [13–16]. Henceforward, attention is shifted toward PI based membranes, i.e. STARMEM™, Duramem® and Puramem®, as literature has shown that it should provide the best performance in the presence of organic solvents and using flux and rejection as exclusionary criteria.

Table C.1: Summary of commercially available OSN membranes [13,17–22]

Supplier	Trade name	Series	MWCO ($g.mol^{-1}$)	Material	Stable in	Permeance ($L.m^{-2}.h^{-1}.bar^{-1}$)	Rejection (%)
Evonik	STARMEM™	ST-120	200	PI	Alcohols, paraffins, aromatics, EA, DCM, THF, ketones, esters	2.5	>99.4%
		ST-122	220	PI		4.3	>96.0%
		ST-228	280	PI			>90.0%
		ST-240	400	PI		5.0	>85.0%
	Duramem®	DM-150	150	PI		0.3	>99.9%
		DM-200	200	PI	Alcohols, paraffins, esters, EA	1.2	>99.9%
		DM-300	300	PI		1.3	>99.0%
		DM-500	500	PI		1.5	>96.0%
	Puramem®	PM-280	280	PI	Alcohols, paraffins, esters, EA	0.6 – 1.0	>96.7%
SolSep BV	SolSep	030306/F	500	n.d.	Alcohols, EA, DMF, THF, DMSO	<0.01	n.d.
		030705/F	500	n.d.		0.2	n.d.
Koch	SelRO	MPF-34/44	200 – 250	PDMS	Alcohols, chlorinated solvents, DCM, DE, EA, aromatics, THF	0.5	>80.0%
		MPF-50	700	PDMS		>3	>93.4%
		MPF-60	400	PDMS			>97.0%
Microdyn	Nadir	N30F/NF-PES-10	400 – 1000	PES	Paraffins, IPA, DE	1 – 10	>8.0%
Osmonics	Desal	Desal DL/DK	150 – 300	PA	Alcohols, EA, DCM	0.1 – 2	>88.6%

The primary focus of this investigation was to successfully recovery the rhodium-based catalyst, **$HRh(CO)(PPH_3)_3$**, with a molecular weight of *ca.* 920 $g.mol^{-1}$. Therefore, a membrane with a MWCO less 800 $g.mol^{-1}$ will be able to successfully reject this catalyst. From Table C.1, it can be observed that most of the OSN membranes listed, excluding NF-PES-10 from the Nadir series, have MWCO values less than 800 $g.mol^{-1}$ and therefore would provide high catalyst recoveries and subsequently be suitable for inclusion in this study.

However, low catalyst recoveries have been previously reported in literature when using the Desal membranes including Zhao *et al.* [23] with recoveries of 12 – 68% for the crystal violet catalyst (408 $g.mol^{-1}$), Aerts *et al.* [22] with <25% recovery values for the Jacobsen catalyst (622 $g.mol^{-1}$), and Luthra *et al.* [24] who reported a recovery of 48% for the TOABr catalyst (547 $g.mol^{-1}$). Furthermore, very low fluxes have been observed for the Desal membranes in the order of 5 $L.m^{-2}.h^{-1}$. Similarly for the Nadir membranes, Aerts *et al.* reported low recoveries in the range 25 – 40% for the Jacobsen catalyst with low to moderate fluxes ranging 10 – 80 $L.m^{-2}.h^{-1}$. Therefore, based on the literature, the Nadir and Desal membranes should provide moderate catalyst recoveries and can be excluded from further screening.

In the case of the MPF series, although high catalyst recoveries have been reported in literature including Zhao *et al*. [23] (83 – 94% for crystal violet) and De Smet *et al.* [25] (>98% for Ru-BINAP [849 $g.mol^{-1}$]) , these membranes are known to have very low fluxes ranging from 1 – 36 $L.m^{-2}.h^{-1}$ depending on the solvent. Therefore, due to relative low flux for organic solvents compared to the other membranes, the MPF membranes can be removed from contention for inclusion in this study.

Considering the STARMEM™ series, literature shows a definitive trend of the successful use of STARMEM™ membranes to recover catalysts with molecular weights ranging between 200 – 950 $g.mol^{-1}$ based on metals such as palladium, rhodium and ruthenium in the range 75 – 99.95% coupled with high solvent fluxes in the range 50 - 125 $L.m^{-2}.h^{-1}$ [26–31]. Furthermore, White stated in his concluding remarks that polyimide membranes, i.e. STARMEM™, Duramem® and Puramem® series, are favourable in OSN applications due to its viability in alternative solvents, i.e. hydrocarbons, alcohols, ketones, etc., good flux rates and high solute rejections [32]. Therefore, it can be anticipated that the polyimide Duramem® and Puramem® series should also provide good catalyst recoveries similar to that reported for STARMEM™ membranes. Ormerod *et al.* [33] reported high catalyst recoveries

(99.95%) for the first-generation Hoveyda-Grubbs metathesis catalyst (601 $g.mol^{-1}$) using a membrane from the Duramem series. Schmidt *et al.* [34] used the Puramem® 280 membrane for the recovery of triphenylphosphine from a 1-pentene hydroformylation post-reaction mixture with successful results (>96.7%, 1.5 $L.m^{-2}.h^{-1}.bar^{-1}$). The proven success of the polyimide STARMEM™, Duramem® and Puramem® membranes warrant their inclusion in this investigation for the purpose of homogeneous catalyst recovery.

C.3 Experimental validation of selected OSN membranes

Membrane compatibility tests, as described in Section 3.4.2, were performed using the selected STARMEM™ (ST-240) and Duramem® (DM-150 and DM-200) membranes to determine which of these three membranes would be best suited for further participation in this study. These membranes were subjected to species representative of the 1-octene and 1-decene hydroformylation as well as the 1-nonanal hydrogenation reaction systems. The physical and permeation compatibility of the membrane with the species were then evaluated by observing any change to the active layer of the membrane and measuring the solvent fluxes, respectively. A membrane was classified as unstable if any discoloration or disintegration occurs on the top active layer during prolonged exposure to the reaction species. Moreover, it was desired that a flux of >1 $L.m^{-2}.h^{-1}$ be achievable at a pressure of 30 bar. However, the membrane was considered incompatible if fluxes below 1 $L.m^{-2}.h^{-1}$ were achieved and subsequently rejected from the study.

For the visual tests, no discoloration or damage to the top active layer was observed which correlates well with the specifications provided by the manufacturer. However, the absence of any visual defects does not mean the membrane's properties remain intact. Van der Bruggen *et al.* [35] recently did a study to determine the effects of membrane exposure to organic solvents and found that the characteristics of the membrane changes after contact, ranging from slight (small change in flux) to significant (complete loss of selectivity). In this study, the STARMEM™ and Duramem® membranes curled when exposed to the organic solvents, caused by the shrinkage and swelling of different surfaces of a membrane, which can result in significant changes in solvent flux.

Prior to the permeation compatibility tests, the membranes used were first conditioned using a predetermined pretreatment solvent. The results of the screening experiments are summarised in Table C.2.

Table C.2: Screening tests with different polymeric OSN membranes

	Duramem®		STARMEM™
	DM-150	**DM-200**	**ST-240**
Species Permeance ($x10^{-3}$ $m^3.m^{-2}.h^{-1}.bar^{-1}$)			
Toluene	0.25	0.45	2.00
1-Octene	0.03	0.07	4.50
1-Decene	<0.03	0.15	1.50
1-Nonanal	<0.01	<0.01	0.80
1-Undecanal	<0.01	<0.01	0.45
1-Nonanol	<0.01	<0.01	0.15
1-Undecanol	<0.01	<0.01	0.06
Catalyst Rejection (%)			
$HRh(CO)(PPH_3)_3$	>99.0%	>99.0%	>99.0%
$Co(C_5H_7O_2)_3$	>99.4%	>99.4%	87.9%

It can be observed from Table C.2, that ST-240, the membrane with the highest MWCO (400 $g.mol^{-1}$) compared to the DM-150 (150 $g.mol^{-1}$) and DM-200 ($g.mol^{-1}$) also gave the highest flux for all reaction species. Coupled with catalyst recoveries >99.0% for **$HRh(CO)(PPH_3)_3$**, the ST-240 was deemed favourable for further characterisation.

The relative fluxes for the different membranes increased as follows: DM-150 < DM-200 < ST-240. Very low permeabilities were expected for the DM-150 membrane due to its very tight structure and can therefore be excluded from this investigation. Minimal olefin permeation (~0 $L.m^{-2}.h^{-1}$) was observed for the Duramem® membranes which can be attributed due to its hydrophilic and dense nature. The opposite was observed for the hydrophobic STARMEM™ membranes which gave high olefin permeation. Based on these results, the ST-240 membrane was selected for inclusion in this investigation and was used for further testing.

C.4 References

[1] K. Vanherck, A. Cano-Odena, G. Koeckelberghs, T. Dedroog, I. Vankelecom, *J. Memb. Sci.* **353** (2010) 135–143.

[2] L. Shao, L. Liu, S. Cheng, Y. Huang, J. Ma, *J. Memb. Sci.* **312** (2008) 174–185.

[3] Y.H. See-Toh, M. Silva, A. Livingston, *J. Mater. Chem.* **324** (2008) 220–232.

[4] Y.H. See Toh, F.W. Lim, A.G. Livingston, *J. Memb. Sci.* **301** (2007) 3–10.

[5] L. Shao, T. Chung, S. Hong, K. Pallathadka, *J. Memb. Sci.* **238** (2004) 153–163.

[6] I. Soroko, M.P. Lopes, A.G. Livingston, *J. Memb. Sci.* **381** (2011) 152–162.

[7] I. Soroko, M. Makowski, F. Spill, A.G. Livingston, *J. Memb. Sci.* **381** (2011) 163–171.

[8] I. Soroko, M. Sairam, A.G. Livingston, *J. Memb. Sci*. **381** (2011) 172–182.

[9] Y.H. See-Toh, F.C. Ferreira, A.G. Livingston, *J. Memb. Sci*. **299** (2007) 236–250.

[10] B. Soltane, D. Roizard, E. Favre, *J. Memb. Sci.* **435** (2013) 110–119.

[11] K. Ebert, J. Koll, M.F.J. Dijkstra, M. Eggers, *J. Memb. Sci*. *285* (2006) 75–80.

[12] E.S. Tarleton, J.P. Robinson, M. Salman, *J. Memb. Sci.* **280** (2006) 442–451.

[13] X.Q. Cheng, Y.L. Zhang, Z.X. Wang, Z.H. Guo, Y.P. Bai, L. Shao, *Adv. Polym. Technol.* (2014) 1–24.

[14] S. Roy, S. Addo, S. Mitra, K.K. Sirkar, *J. Memb. Sci.* **375** (2011) 81–87.

[15] P.B. Kosaraju, K.K. Sirkar, *J. Memb. Sci.* **321** (2008) 155–161.

[16] I. Kim, J. Jegal, K. Lee, *J. Polym. Sci. Part B Polym. Phys.* **40** (2002) 2151–2163.

[17] Evonik Industries AG, Germany. [Online], (2015). http://corporate.evonik.com/.

[18] SolSep BV, The Netherlands. [Online], (2014). http://solsep.com/. [Date accessed: 9 July 2015].

[19] Koch Membrane Systems Inc., United Kingdom. [Online], (2015). http://kochmembrane.com/. [Date accessed: 9 July 2015].

[20] Microdyn-Nadir, Germany. [Online], (2015).

[21] GE Osmonics Desal membranes, Delft. [Online], (2015). http://lenntech.com/products/membrane/osmonics/. [Date accessed: 9 July 2015].

[22] S. Aerts, A. Buekenhoudt, H. Weyten, L.E.M. Gevers, I.F.J. Vankelecom, P.A. Jacobs, *J. Memb. Sci.* **280** (2006) 245–252.

[23] Y. Zhao, Q. Yuan, *J. Memb. Sci*. **279** (2006) 453–458.

[24] S.S. Luthra, X. Yang, L.M. Freitas Dos Santos, L.S. White, A.G. Livingston, *J. Memb. Sci*. **201** (2002) 65–75.

[25] K. De Smet, S. Aerts, E. Ceulemans, I.F.J. Vankelecom, P.A. Jacobs, *Chem. Commun.* (2001) 597–598.

[26] J. Fang, R. Jana, J.A. Tunge, B. Subramaniam, *Appl. Catal. A Gen.* **393** (2011) 294–301.

[27] P. Van der Gryp, A. Barnard, J.P. Cronje, D. de Vlieger, S. Marx, H.C.M. Vosloo, *J. Memb. Sci.* **353** (2010) 70–77.

[28] M. Priske, K.D. Wiese, M. Kraume, C. Baumgarten, *J. Memb. Sci.* **360** (2010) 77–83.

[29] P. Silva, S. Han, A.G. Livingston, *J. Memb. Sci*. **262** (2005) 49–59.

[30] J.T. Scarpello, D. Nair, L.M. Freitas Dos Santos, L.S. White, A.G. Livingston, *J. Memb. Sci*. **203** (2002) 71–85.

[31] D. Nair, S.S. Luthra, J.T. Scarpello, L.S. White, L.M. Freitas Dos Santos, A.G. Livingston, *Desalination*. **147** (2002) 301–306.

[32] L.S. White, *J. Memb. Sci*. **205** (2002) 191–202.

[33] D. Ormerod, B. Sledsens, G. Vercammen, D. Van Gool, T. Linsen, A. Buekenhoudt, B. Bongers, *Sep. Purif. Technol*. **115** (2013) 158–162.

[34] P. Schmidt, E.L. Bednarz, P. Lutze, A. Górak, *Chem. Eng. Sci.* **115** (2014) 115–126.

[35] B. Van der Bruggen, J. Geens, C. Vandecasteele, *Sep. Sci. Technol*. **37** (2007) 783–797.

APPENDIX D: Equipment Drawings

D.1 Membrane pressure cell (exploded view)

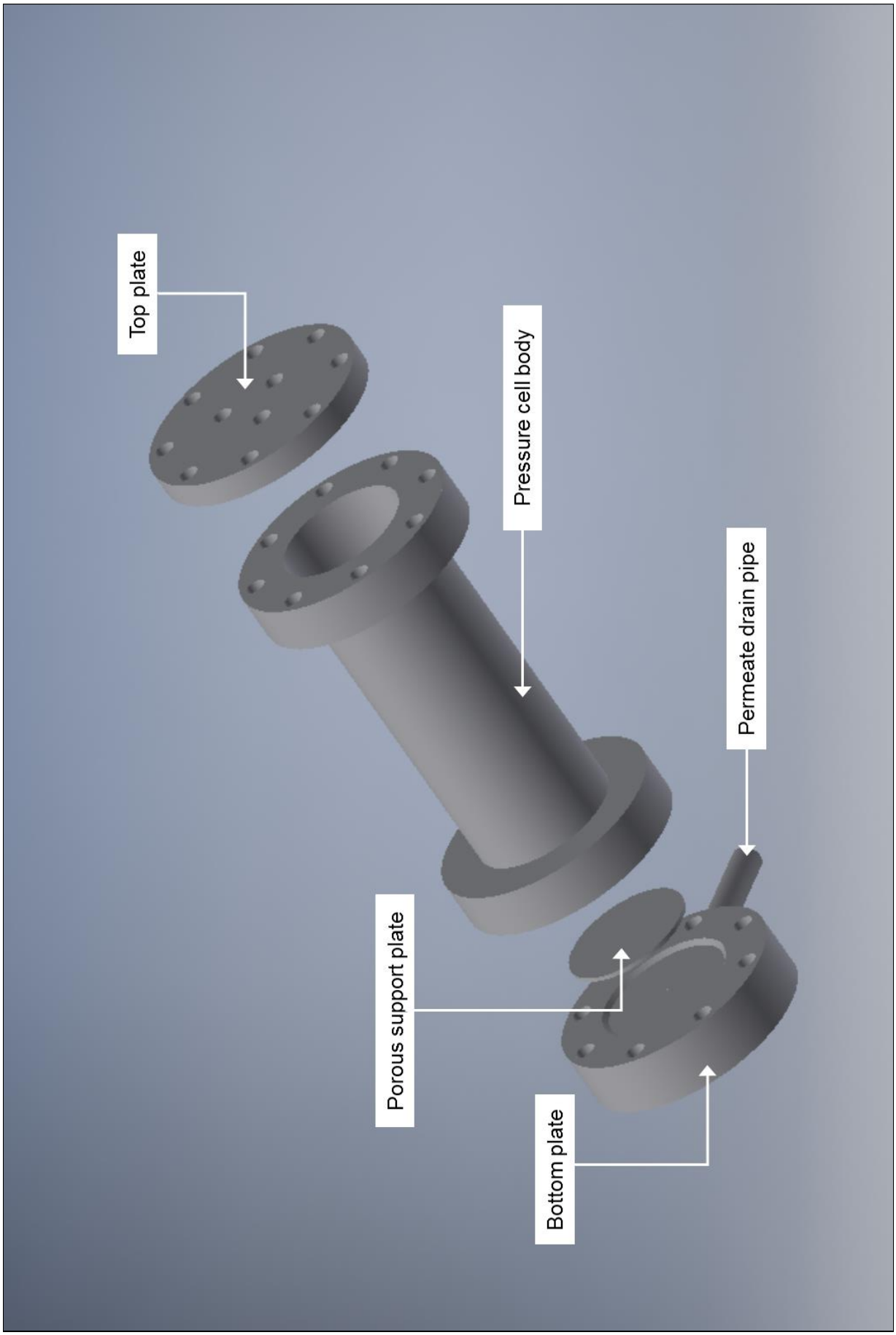

D.2 Membrane pressure cell (main body - annotated view)

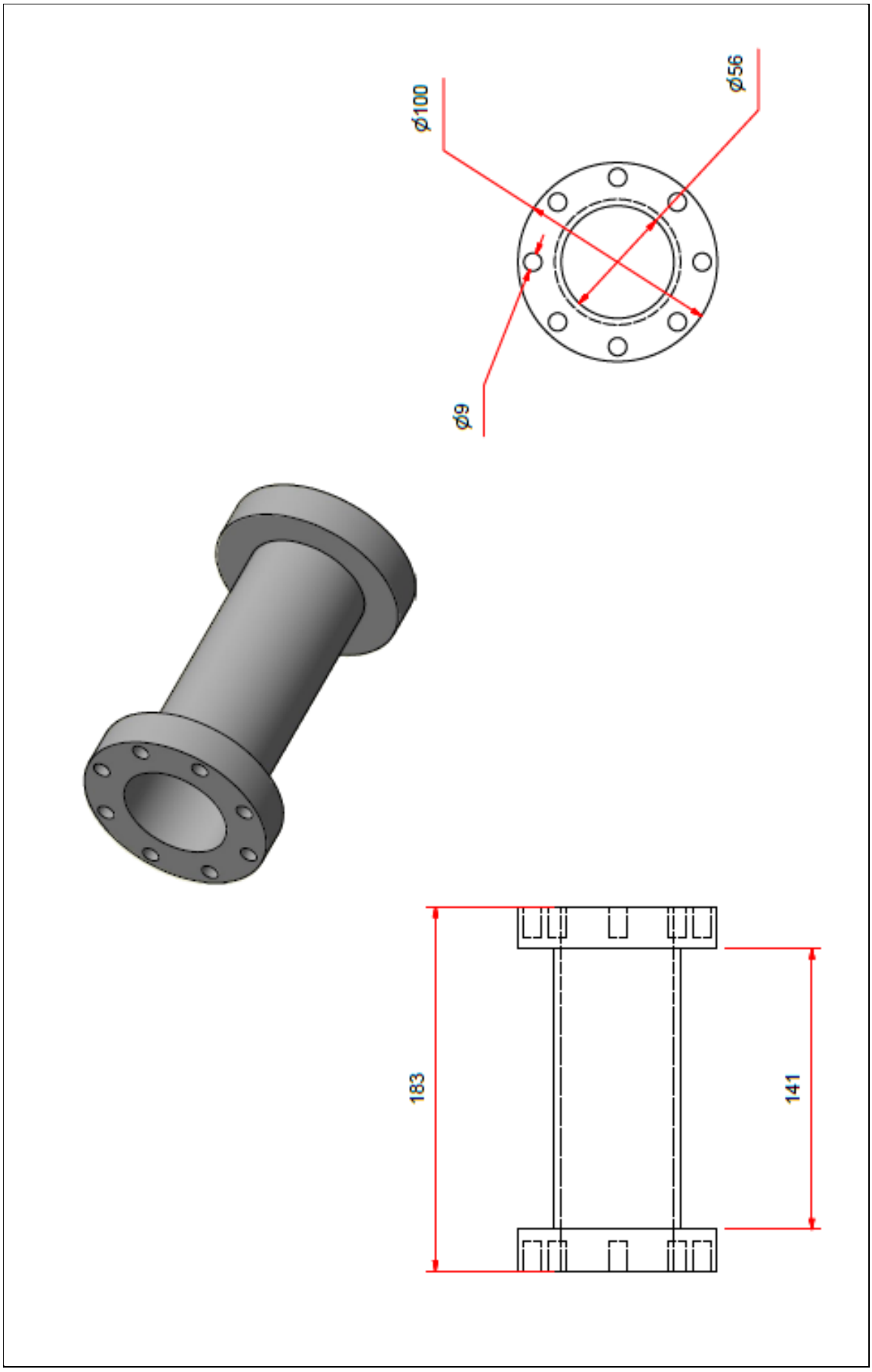

D.3 Membrane pressure cell (support plate – annotated view)

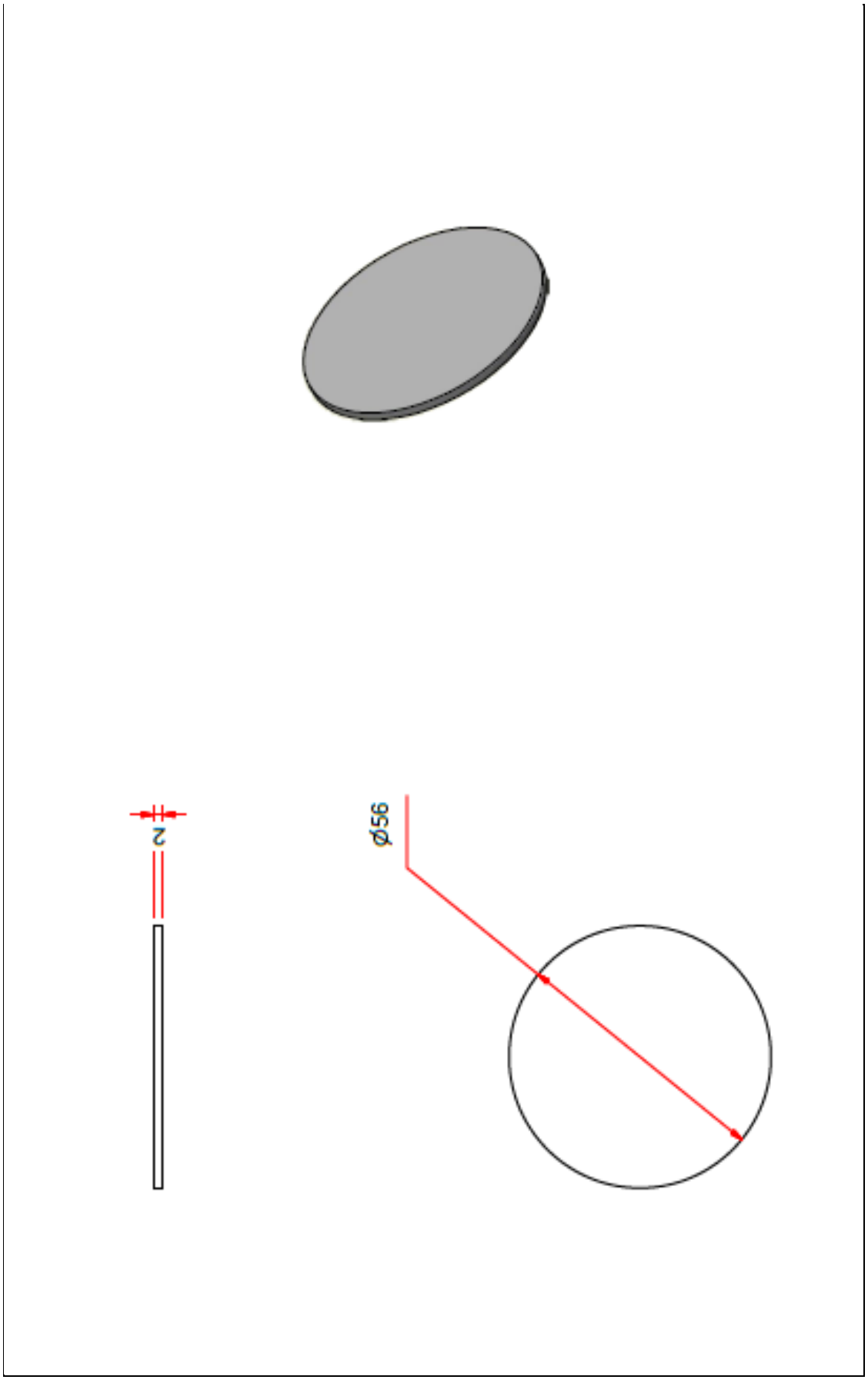

APPENDIX E: Analytical Procedures and Calibrations

E.1 Gas chromatography (GC)

E.1.1 Start-up, operational and shutdown procedures

Start-up

1. Open the Air and Hydrogen valves against the wall (Note: Make sure that the correct pressures are attained, i.e. 46 psi for Air and 40 psi for Hydrogen)
2. Open the Air cylinder in the parking area located below the building
3. Open the valve of the Helium cylinder to attain a pressure of ± 500 kPa and open the tap which allows the gas to be directed to the GC instrument
4. Do not adjust any of the regulators
5. Once all the correct valves are opened, turn on the GC using the switch located at the back of the GC instrument to the left and close the oven door
6. Make sure that the flow through the column is at a pressure of 15 psi (if not, adjust the flow using the correctly labelled gas needle valve
7. Determine the split flow by using a simple bubble flow meter attached to the split flow outlet located at the left hand side of the GC instrument (if not correct, adjust the split flow knob labelled “Front” to set the split flow as desired)
8. Switch on the oven using the “Col Oven On” button
9. While column is in the progress of heating, select and modify the GC method to be used for analysis. Press “Build/Modify” then “Method 1”. Enter the method settings as shown below (press “Enter” after each setting to continue):
    a. Initial column temperature: 50 °C
    b. Initial column hold time: 1 minute
    c. Program final column temperature: 250 °C
    d. Program column rate in °C.min^{-1}: 5 °C.min^{-1}
    e. Program hold time: 10 minutes
    f. Injector temperature: 250 °C
    g. Detector temperature: 270 °C
10. Load the method by pressing “Activate” then “Method 1”
11. To display the current column, injector and detector temperatures, press the “Status” button
12. Before the FID detector can be ignited, carefully open the gas needle valves on the GC instrument in the following order:
    a. Hydrogen (Front)
    b. Air (Front)

c. Make-up (Rear)

13. Wait for the detector to reach its desired temperature
14. Once the selected detector temperature has been reached, the flame can be ignited using the “Start” button. A pop sound will be heard signalling the ignition of the FID flame (Note: test if the flame is indeed burning by holding a cold steel spatula at the mouth of the flame opening)
15. A run will start after pressing the “Start” button. Press “Reset” to end this run
16. Once all the selected temperatures have been reached, a green light under “Ready” will show indicating that the GC is ready for use

Operational Procedure

1. Start the computer
2. Open the GC software from the desktop
3. Create and save a method (obtain software method settings from Mrs Botha)
4. From the start page of the software, select “Run” followed by “Method” then select “Channel 2” for the Varian 3400 GC instrument
5. Run a blank by creating a run named for example “Blank” and wait for the screen which indicates the GC is waiting for a sample
6. Gently tap the sample inject port, located at the top of the GC instrument, to simulate the injection of a sample. This will initiate the blank run. Allow the run to continue for its full duration and allow all residual components to be removed from the column
7. Repeat steps 4 and 6 for a second time for increased reliability
8. Once blank runs have been completed, sample analysis can now continue
9. Prepare the sample as indicated in the Section C.1.2
10. Before injecting the prepared sample, wash the 5 µL injection needle with toluene by sucking up pure toluene (Note: Repeat five times)
11. Rinse the inside of the needle with the sample (Note: Repeat five times)
12. Suck up the sample using the needle and before pushing it out, wipe the tip of the needle to remove any residual components. Then adjust the needle so that only 0.3 µL remain within the needle (Note: When adjusting needle, secure the end of the needle to avoid the end to accidentally fall in and push out the sample)
13. Carefully and speedily inject the sample into the GC sample injection port
14. The “Status” button on the GC instrument can be used to monitor the elapsed analysis time and the current column, detector and injector temperatures

15. The screen on the computer will indicate that an analysis is now being recorded
16. Once the run has been completed, the software will save and print a copy of the resulting GC chromatograms

Shutdown

1. Press “Build/Modify” and set the initial column temperature to 40 °C
2. Allow the column to cool down. When cooled, switch the oven off by pressing “Shift” and “Col Oven On” (Note: Open the oven door to allow the column to cool faster)
3. Press “Build/Modify” and set both the injector and detector temperatures to 100 °C
4. If the GC will be used within a week, the instrument may be left on. However, if the GC will not be used for a week or more, it is recommended that the instrument be switched off
5. Close the Hydrogen, Air and Make-up needle valves
6. Close the Hydrogen and Air valves against the wall. Also close the valve on the Air cylinder in the parking area. Lastly, close the Helium cylinder valve as well as the tap directing the gas to the GC instrument (Note: If another GC is in operation, do not close any of these valves)

E.1.2 Calibration curves and data

Preparing standards and samples

1. Prepare five standards each containing 10, 20, 40, 80 and 100 µL of each species to be used in the investigation. Weigh each the contribution of each specie using an electronic scale with an accuracy of 0.0001 g (Note: Tare the scale to neglect the weight of the sample bottle)
2. Add 30 µL n-dodecane to each of the standards and similarly weigh its contribution
3. Dissolve each of the standards in pure Methanol (use about 1.5 – 2.0 mL toluene)
4. Prepare three replicates of the standards to ensure repeatability
5. Place all the standards in an ultrasonic bath to further dissolve any suspended solids

6. Once all solids have been dissolved and the standards are confirmed as a clear liquid, the standards are now injected into the GC instrument and used to determine the calibration curve (see Operational Procedure above)

GC calibration curves and data for the reaction species used are presented in Figures E.1 through E.7 and Table E.1.

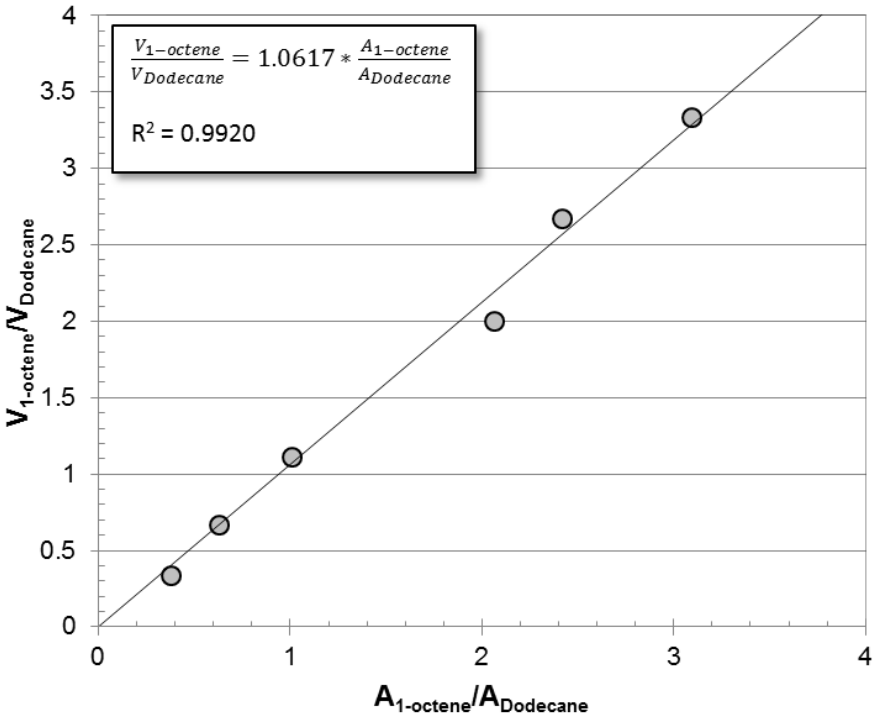

Figure E.1: GC calibration curve for 1-octene

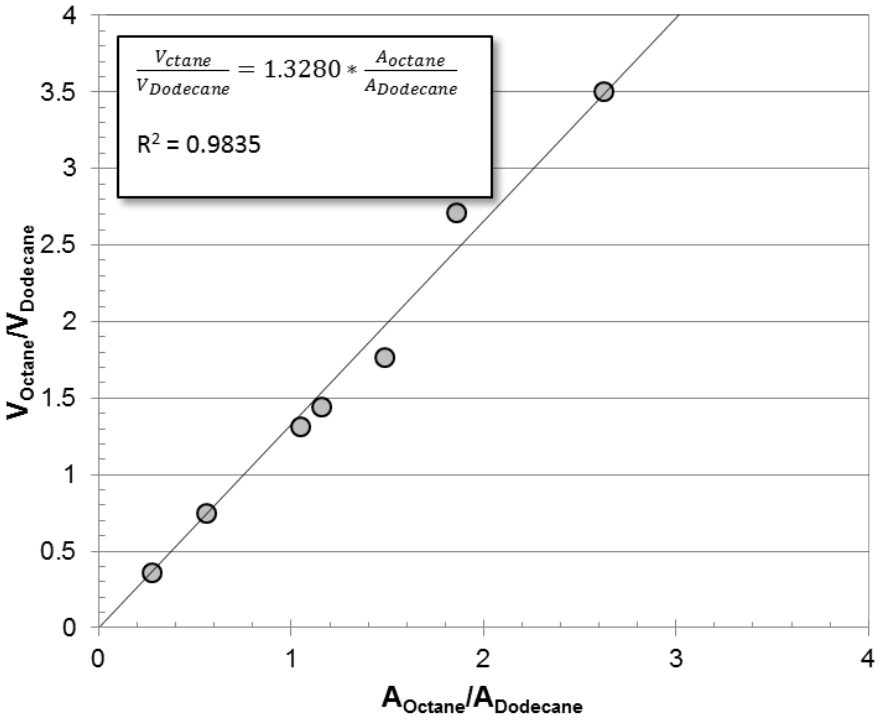

Figure E.2: GC calibration curve for octane

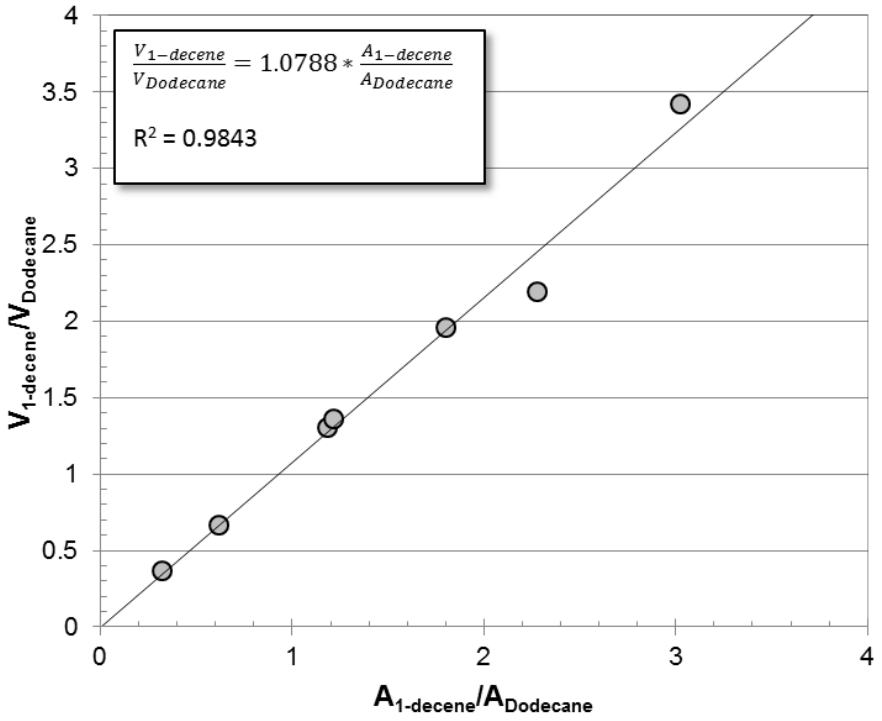

Figure E.3: GC calibration curve for 1-decene

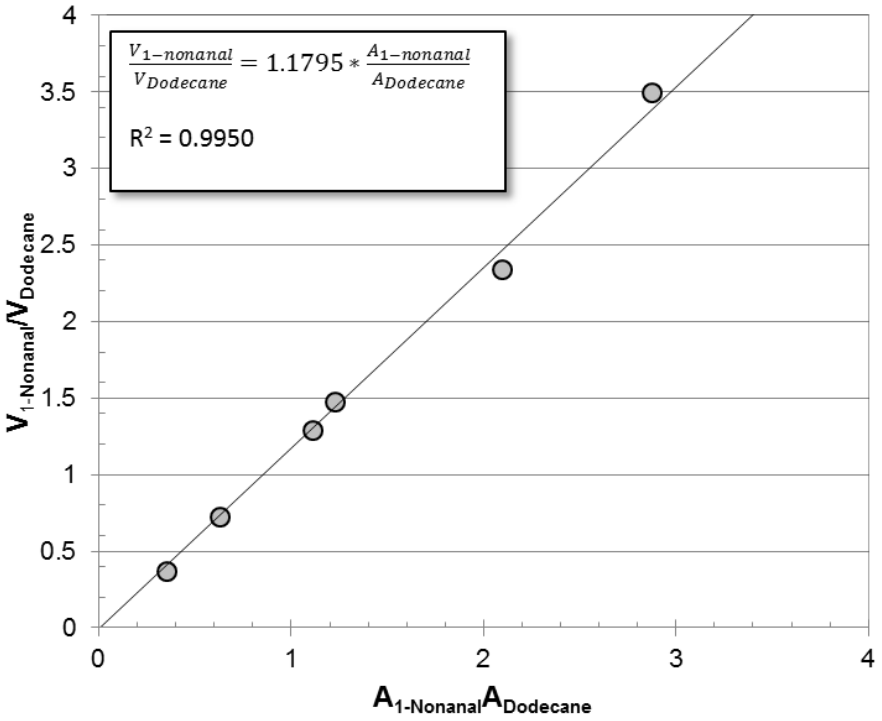

Figure E.4: GC calibration curve for 1-nonanal

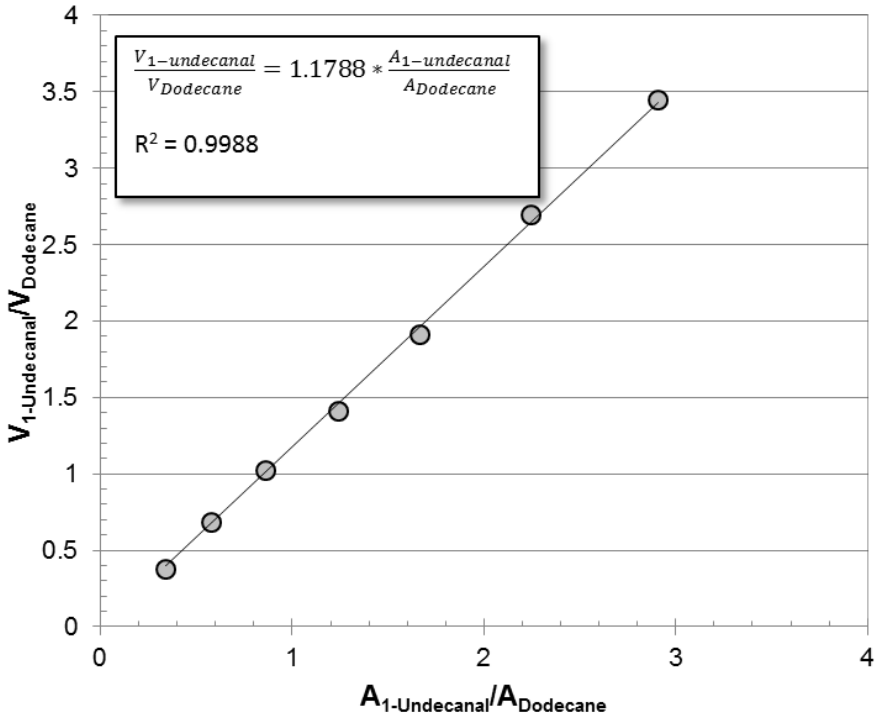

Figure E.5: GC calibration curve for 1-undecanal

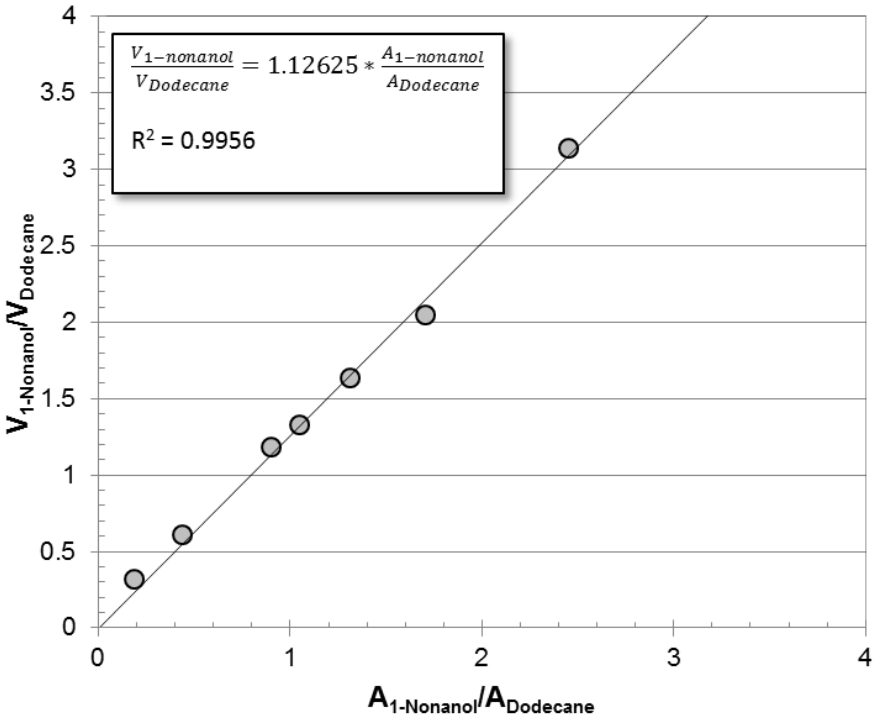

Figure E.6: GC calibration curve for 1-nonanol

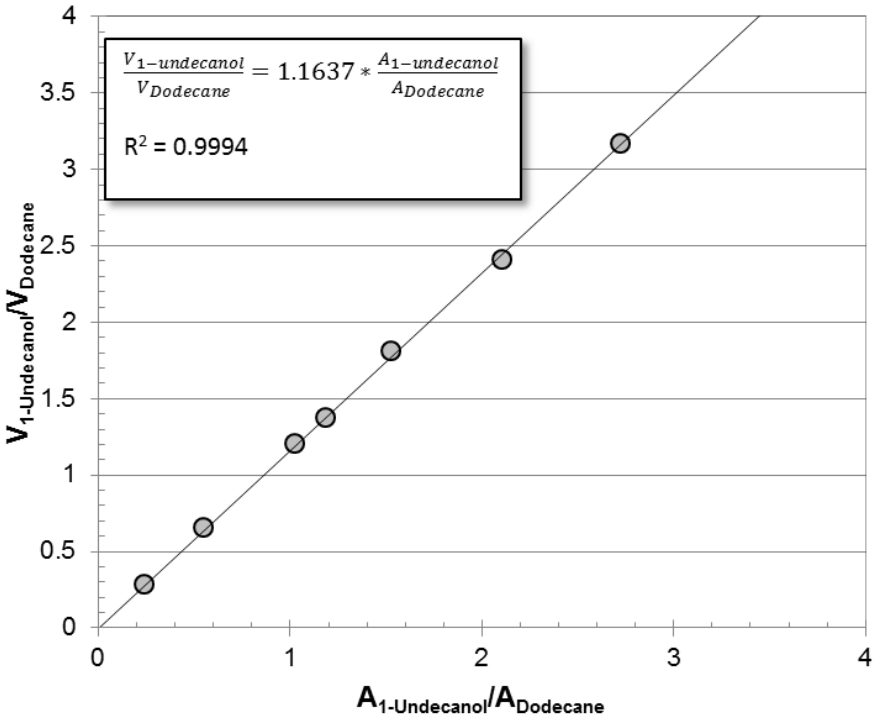

Figure E.7: GC calibration curve for 1-undecanol

Table E.1: Raw experimental data for GC calibration

	Octane	1-Octene	1-Decene	1-Nonanal	1-Nonanol	1-Undecanal	1-Undecanol	Dodecane
				GC peak areas (A_i)				
10 µL	475232	42312.0	549551	603449	325618	582867	409840	1719380
20 µL	819597	602113	910403	926575	644751	849450	802523	1470710
40 µL	1352750	867145	1521070	1436030	1160620	1111970	1317080	1286930
60 µL	1725590	1668870	2093390	3119280	1523750	1932810	1772070	1162040
80 µL	1137450	1674280	1071620	1074170	882194	1265570	1120570	1265570
100 µL	1647870	1737150	1897460	1804060	1538640	1826950	1710210	627761
				Peak area ratios ($A_i/A_{Dodecane}$)				
10 µL	0.276397	0.380000	0.319621	0.350968	0.189381	0.338998	0.238364	1.00000
20 µL	0.557279	0.630947	0.619021	0.630017	0.438394	0.577577	0.545669	1.00000
40 µL	1.05115	1.00726	1.18194	1.11586	0.901852	0.864051	1.02343	1.00000
60 µL	1.48496	2.06536	1.80147	-	1.31126	1.66328	1.52496	1.00000
80 µL	1.85647	2.41805	2.27593	2.09785	1.70377	2.24419	2.10223	1.00000
100 µL	2.62500	3.09587	3.02258	2.87380	2.45100	2.91027	2.72431	1.00000

E.2 Flame atomic absorption spectroscopy (FAAS)

E.1.1 Start-up, operational and shutdown procedures

Start-up

1. Switch on the extractor fan above the AAS machine (switch located at the entrance of the lab) to remove any potentially toxic vapours that may be released during analysis
2. Regulate the supply of air and acetylene gas to sufficient ratio's using the valves located next to the AAS machine (Note: Acetylene gas is preferred as it provides a stable flame)
3. Check that the gas supply pressures does not fall outside the range of 600 – 700 kPa
4. Clean the suction pipe by gently removing it from the AAS machine and carefully inserting a guitar string through the pipe
5. Once cleaned, place the suction pipe in a glass beaker containing fresh distilled water (Note: Distilled water will act as blank during calibration)
6. Remove any unwanted residues within the burner casing by sliding a piece of carton along the grooves of the burner
7. Ensure that the waste container (located at the bottom of the AAS machine) is not full before starting with the analysis. If the container is full, empty its contents in a predetermined located
8. Switch on the AAS machine and the computer screen

Operational Procedure

1. Once the AAS machine is turned on, gently secure the lamp (representing the metal to be analysed) in the casing
2. Select the metal under consideration as prompted by the AAS software
3. Follow AAS software instructions to proceed through method development and input the following specifications:
    a. Lamp position: As indicated within the casing
    b. Lamp current (mA): 4
    c. Wavelength (nm): 304.4 for Cobalt and 343.5 for Rhodium
    d. Flame: Air – Acetylene
    e. Sample Introduction: Manual
    f. Replicates: 3
    g. Measurement time (sec): 2

h. Delay time (sec): 1

4. Optimise the lamp alignment to provide accurate results using the two knobs located on the lamp holder (Note: AAS software will provide assistance in attaining the optimum lamp alignment)
5. Press ‘Ignite’ on the AAS machine to ignite the flame
6. Check the consistency of the flame to ensure accurate measurements and prevent any operational problems (Note: The flame should have a thin and uniform blue streak at the bottom)
7. Zero the AAS machine using distilled water as the blank
8. Prepare five standard (or stock) solutions each with a different concentration of the same metal
9. Analyse the standard solutions by removing the suction pipe from the distilled water and placing it in the beaker containing the standard solution to calibrate the AAS (Note: When removing the suction pipe from a solution, gently wipe the end of the pipe using the operator’s fingers. DO NOT USE PAPER!)
10. Plot the calibration curve using the absorbance values obtained from AAS for each metal considered
11. Once the calibration curve is sufficient, the AAS machine is now ready to measure the metal concentrations of the actual samples
12. Press ‘F6’ to display the screen which prompts for sample analysis
13. Place the suction pipe in the sample and press ‘F9’ to allow the AAS machine to measure the metal concentration
14. If a different metal is to be use, repeat steps 1 – 13

Shutdown

1. Extinguish the flame by pressing ‘Flame off’
2. Switch off the AAS machine as well as the computer screen
3. Close the air and acetylene supply valves
4. Switch off the extractor fan
5.

FAAS calibration curves and data for the reaction species used are presented in Figure E.8 and Table E.2.

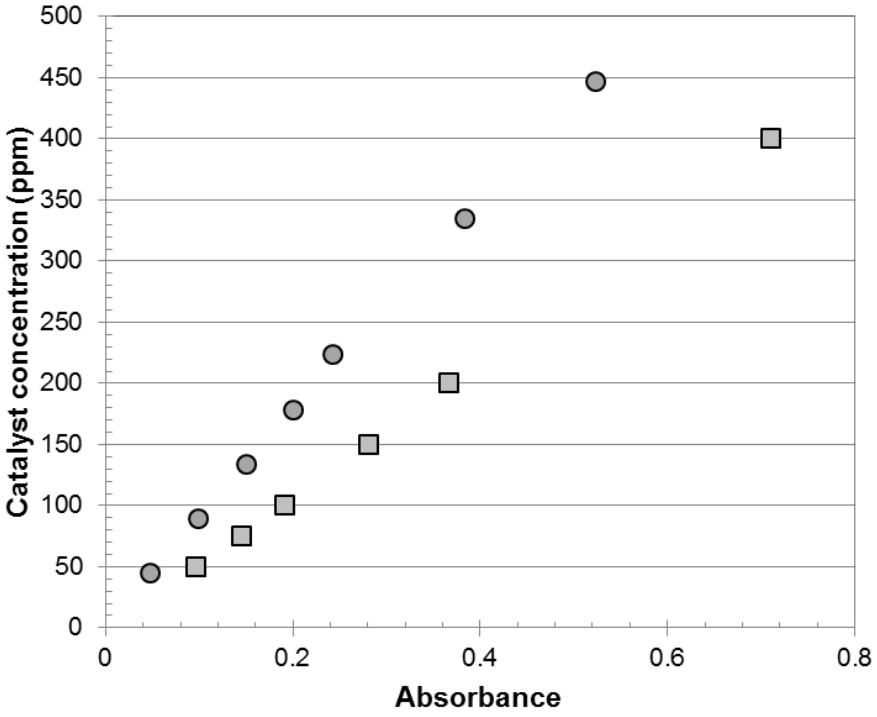

Figure E.8: FAAS calibration curve for **$HRh(CO)(PPh_3)_3$** (●) and **$Co(C_5H_7O_2)_3$** (■)

Table E.2: Standards of catalysts used for FAAS calibration

Catalyst concentration (ppm)	RSD (%)	Mean absorption (-)
Rhodium-based		
45	1.4	0.048
89	0.9	0.099
134	1.1	0.150
179	1.6	0.201
223	2.0	0.243
335	0.8	0.383
446	0.9	0.523
Cobalt-based		
50	1.1	0.096
75	1.8	0.145
100	1.2	0.191
150	1.0	0.281
200	0.5	0.367

APPENDIX F: Raw Experimental Data

F.1 Hydroformylation of olefins

The results for the hydroformylation reaction of 1-octene is summarised in Table F.1 at conditions: 20 bar, 80 °C, [P]/[Rh] molar ratio 20:1, [C_8]/[Rh] molar ratio 4940:1 and for 1-decene catalyzed by co at 20 bar and 110 °C summarised in Table F.2.

Table F.1: Post-reaction product distribution in mmol after 120 minutes

	A_i	A_i/A_{n-doc}	$RF \times (A_i/A_{n-dod})$	V_i (mL)	m_i (g)	n_i (mol)
			Reaction 1			
1-Octene	7786000	9.30100	9.992	1.998	1.429	12.73
Octane	121800	0.1455	0.1932	0.03865	0.0271	0.2380
Iso-Octenes	27610	0.03298	0.03543	0.00709	0.0051	0.0452
1-Nonanal	6947000	8.299	9.790	1.958	1.619	11.38
2-Methyloctanal	3584000	4.281	5.049	1.010	0.8352	5.876
2-Ethylheptanal	75830	0.09059	0.1069	0.02137	0.0177	0.1240
Dodecane	837000	1.000	-	-	-	-
			Reaction 2			
1-Octene	3495000	10.42	11.19	2.239	1.601	14.27
Octane	453800	1.353	1.797	0.3590	0.2530	2.210
Iso-Octenes	27890	0.08300	0.08900	0.01800	0.0130	0.1140
1-Nonanal	3281300	9.784	11.54	2.308	1.909	13.42
2-Methyloctanal	1329400	3.964	4.675	0.9350	0.7730	5.440
2-Ethylheptanal	50240	0.1500	0.1770	0.03500	0.0290	0.2060
Dodecane	335400	1.000	-	-	-	-
			Reaction 3			
1-Octene	6828500	10.42	11.19	2.238	1.600	14.26
Octane	360500	0.5499	0.7303	0.1461	0.1027	0.8990
Iso-Octenes	37690	0.05750	0.06180	0.01240	0.0088	0.0787
1-Nonanal	7213000	11.00	12.98	2.596	2.147	15.09
2-Methyloctanal	459100	7.003	8.259	1.652	1.366	9.610
2-Ethylheptanal	18930	0.02890	0.03410	0.0068	0.0056	0.0396
Dodecane	655500	1.0000	-	-	-	-

Table F.2: Post-reaction product distribution in mmol after 300 minutes

	A_i	A_i/A_{n-dod}	$RF \times (A_i/A_{n-dod})$	V_i (mL)	m_i (g)	n_i (mol)
1-Decene	3832000	2.178	2.3404	1.638	1.171	0.0104
Decane	21170	0.01203	0.01597	0.0111	0.0078	6E-05
Iso-Decenes	426300	0.2423	0.2603	0.1822	0.1302	0.0011
1-Undecanal	155500	0.8835	1.042	0.7297	0.6035	0.0042
2-Methyldecanal	572300	0.3253	0.3837	0.2686	0.2221	0.0015
2-Ethylnonanal	96430	0.05481	0.0646	0.0452	0.0374	0.0002
Dodecane	1759000	1.000	-	-	-	-

F.2 Pure species flux

F.2.1 1-Octene pure flux data

Table F.3: 1-Octene dynamics and steady-state flux data at 10 bar

Membrane	ST-240				
Conditions	**10 bar**, 19 °C, 500 rpm				
	Raw data			Calculated data	
m (g)	Δm (g)	time (s)	Δt (s)	Dynamic flux ($kg.m^{-2}.h^{-1}$)	Steady-state flux ($kg.m^{-2}.h^{-1}$)
103	5	7243	360	30.80	-
108	5	7604	361	30.77	30.00
113	5	7962	358	30.74	30.12
118	5	8322	360	30.71	30.11
123	5	8688	366	30.66	29.98
128	5	9054	366	30.62	29.90

Table F.4: 1-Octene dynamics and steady-state flux data at 20 bar

Membrane	ST-240				
Conditions	**20 bar**, 19 °C, 500 rpm				
	Raw data			Calculated data	
m (g)	Δm (g)	time (s)	Δt (s)	Dynamic flux ($kg.m^{-2}.h^{-1}$)	Steady-state flux ($kg.m^{-2}.h^{-1}$)
93.95	10	3358	358	60.60	-
103.95	10	3717	359	60.58	-
113.95	10	4077	360	60.54	60.17
123.95	10	4437	360	60.51	60.17
134.45	10.5	4816	379	60.47	60.11
139.45	5	4997	181	60.45	60.07

Table F.5: 1-Octene dynamics and steady-state flux data at 30 bar

Membrane	ST-240				
Conditions	**30 bar**, 20 °C, 500 rpm				
	Raw data			Calculated data	
m (g)	Δm (g)	time (s)	Δt (s)	Dynamic flux ($kg.m^{-2}.h^{-1}$)	Steady-state flux ($kg.m^{-2}.h^{-1}$)
253.5	10.5	5752	237	95.46	-
268	14.5	6076	324	95.54	-
283	15	6412	336	95.60	96.94
298	15	6747	335	95.67	96.82
313	15	7083	336	95.72	96.87
323	10	7307	224	95.75	96.83

Table F.6: 1-Octene dynamics and steady-state flux data at 40 bar

Membrane	ST-240				
Conditions	**40 bar**, 20 °C, 500 rpm				
	Raw data			Calculated data	
m (g)	Δm (g)	time (s)	Δt (s)	Dynamic flux ($kg.m^{-2}.h^{-1}$)	Steady-state flux ($kg.m^{-2}.h^{-1}$)
19.5	19.5	371	371	113.8	-
39.5	20	749	378	114.2	114.6
59.5	20	1130	378	114.3	114.6
79.5	20	1510	378	114.4	114.6
89.5	10	1690	190	114.3	114.5

F.2.2 1-Decene pure flux data

Table F.7: 1-Decene dynamic and steady-state flux data at 10 bar

Membrane	ST-240				
Conditions	**10 bar**, 21 °C, 500 rpm				
	Raw data			Calculated data	
m (g)	Δm (g)	time (s)	Δt (s)	Dynamic flux ($kg.m^{-2}.h^{-1}$)	Steady-state flux ($kg.m^{-2}.h^{-1}$)
59.5	4.9	14600	1230	8.814	-
65.5	6	16200	1530	8.782	8.647
69.5	4	17100	1010	8.768	8.639
75.5	6	18700	1510	8.752	8.633
79.6	4.1	19700	1040	8.742	8.628
84.5	4.9	20900	1240	8.733	8.626

Table F.8: 1-Decene dynamic and steady-state flux data at 20 bar

Membrane	ST-240				
Conditions	**20 bar**, 19 °C, 500 rpm				
	Raw data			Calculated data	
m (g)	Δm (g)	time (s)	Δt (s)	Dynamic flux ($kg.m^{-2}.h^{-1}$)	Steady-state flux ($kg.m^{-2}.h^{-1}$)
109.9	10.9	9870	971	32.14	-
118.4	8.5	10600	756	32.16	-
128.4	10	11500	879	32.21	24.64
138.4	10	12400	882	32.25	24.60
148.4	10	13200	879	32.29	24.61
158.4	10	14200	879	32.32	24.62

Table F.9: 1-Decene dynamic and steady-state flux data at 30 bar

Membrane	ST-240				
Conditions	**30 bar**, 25 °C, 500 rpm				
	Raw data			Calculated data	
m (g)	Δm (g)	time (s)	Δt (s)	Dynamic flux ($kg.m^{-2}.h^{-1}$)	Steady-state flux ($kg.m^{-2}.h^{-1}$)
199	99.5	12700	6400	33.85	-
218.5	19.5	13900	1260	33.84	33.66
238.5	20	15200	1270	33.85	33.72
258.5	20	16500	1260	33.88	33.79
279	20.5	17800	1290	33.91	33.85
298.5	19.5	19100	1230	33.94	33.90

Table F.10: 1-Decene dynamic and steady-state flux data at 40 bar

Membrane	ST-240				
Conditions	**40 bar**, 20 °C, 500 rpm				
	Raw data			Calculated data	
m (g)	Δm (g)	time (s)	Δt (s)	Dynamic flux ($kg.m^{-2}.h^{-1}$)	Steady-state flux ($kg.m^{-2}.h^{-1}$)
138.75	19.25	6540	890	45.92	-
158.75	20	7450	910	46.13	46.85
178.75	20	8390	942	46.11	47.23
198.75	20	9350	960	46.01	46.80
218.75	20	10300	978	45.85	46.37
238.75	20	11300	976	45.72	45.93

F.2.3 1-Nonanal pure flux data

Table F.11: 1-Nonanal dynamic and steady-state flux data at 10 bar

Membrane	ST-240				
Conditions	**10 bar**, 26 °C, 500 rpm				
	Raw data			Calculated data	
m (g)	Δm (g)	time (s)	Δt (s)	Dynamic flux ($kg.m^{-2}.h^{-1}$)	Steady-state flux ($kg.m^{-2}.h^{-1}$)
2.5	2.5	936	936	5.785	-
5	2.5	1940	1000	5.571	5.372
7.5	2.5	2960	1020	5.479	5.338
10.1	2.6	3980	1020	5.495	5.406
12.5	2.4	4930	951	5.490	5.420

Table F.12: 1-Nonanal dynamic and steady-state flux data at 20 bar

Membrane	ST-240				
Conditions	**20 bar**, 23 °C, 500 rpm				
	Raw data			Calculated data	
m (g)	Δm (g)	time (s)	Δt (s)	Dynamic flux ($kg.m^{-2}.h^{-1}$)	Steady-state flux ($kg.m^{-2}.h^{-1}$)
17.25	5	3130	885	11.93	-
22.25	5	4030	906	11.93	12.06
27.25	5	4940	908	11.93	12.03
32.25	5	5850	912	11.92	12.00
37.25	5	6770	913	11.91	11.98
42.25	5	7670	909	11.91	11.97

Table F.13: 1-Nonanal dynamic and steady-state flux data at 30 bar

Membrane	ST-240				
Conditions	**30 bar**, 25 °C, 500 rpm				
	Raw data			Calculated data	
m (g)	Δm (g)	time (s)	Δt (s)	Dynamic flux ($kg.m^{-2}.h^{-1}$)	Steady-state flux ($kg.m^{-2}.h^{-1}$)
94.5	5	12600	696	16.28	-
99.5	5	13300	716	16.22	15.49
104	4.5	13900	599	16.22	15.63
109	5	14600	686	16.20	15.65
114	5	15300	694	16.18	15.65
119	5	15900	680	16.16	15.68

Table F.14: 1-Nonanal dynamic and steady-state flux data at 40 bar

Membrane	ST-240				
Conditions	**40 bar**, 24 °C, 500 rpm				
	Raw data			Calculated data	
m (g)	Δm (g)	time (s)	Δt (s)	Dynamic flux ($kg.m^{-2}.h^{-1}$)	Steady-state flux ($kg.m^{-2}.h^{-1}$)
59.5	10	5790	1010	22.24	-
69	9.5	6730	933	22.22	22.14
79	10	7710	987	22.18	22.12
89	10	8710	990	22.15	22.08
99	10	9710	999	22.10	22.04
109	10	10700	1030	22.01	21.94

F.2.4 1-Undecanal pure flux data

Table F.15: 1-Undecanal dynamic and steady-state flux data at 20 bar

Membrane	ST-240				
Conditions	**20 bar**, 27 °C, 500 rpm				
	Raw data			Calculated data	
m (g)	Δm (g)	time (s)	Δt (s)	Dynamic flux ($kg.m^{-2}.h^{-1}$)	Steady-state flux ($kg.m^{-2}.h^{-1}$)
5	2.5	1690	860	6.386	-
7.5	2.5	2560	867	6.338	6.297
10	2.5	3450	888	6.276	6.271
12.5	2.5	4320	868	6.269	6.212
15	2.5	5180	863	6.270	6.219
17.5	2.5	6020	841	6.293	6.230

Table F.16: 1-Undecanal dynamic and steady-state flux data at 30 bar

Membrane	ST-240				
Conditions	**30 bar**, 27 °C, 500 rpm				
	Raw data			Calculated data	
m (g)	Δm (g)	time (s)	Δt (s)	Dynamic flux ($kg.m^{-2}.h^{-1}$)	Steady-state flux ($kg.m^{-2}.h^{-1}$)
5.5	5.5	1070	1070	13.48	-
9	3.5	1860	792	12.68	-
14	5	2880	1020	12.74	10.60
19.3	5.3	3960	1080	12.79	10.63
24	4.7	4940	976	12.76	10.57
29	5	5950	1020	12.78	10.58

Table F.17: 1-Undecanal dynamic and steady-state flux data at 40 bar

Membrane	ST-240				
Conditions	**40 bar**, 24 °C, 500 rpm				
	Raw data			Calculated data	
m (g)	Δm (g)	time (s)	Δt (s)	Dynamic flux ($kg.m^{-2}.h^{-1}$)	Steady-state flux ($kg.m^{-2}.h^{-1}$)
87	5	1360	773	13.83	-
92	5	14400	778	13.84	14.05
97	5	15100	775	13.85	14.04
102	5	15900	776	13.85	14.03
107	5	16700	784	13.85	14.00
112	5	17500	794	13.84	13.96

F.2.5 1-Nonanol pure flux data

Table F.18: 1-Undecanal dynamic and steady-state flux data at 10 bar

Membrane	ST-240				
Conditions	**10 bar**, 26 °C, 500 rpm				
	Raw data			Calculated data	
m (g)	Δm (g)	time (s)	Δt (s)	Dynamic flux ($kg.m^{-2}.h^{-1}$)	Steady-state flux ($kg.m^{-2}.h^{-1}$)
0.95	0.5	1630	890	1.264	-
1.45	0.5	2730	1100	1.148	1.085
1.95	0.5	3480	750	1.212	1.183
2.45	0.5	4220	735	1.257	1.244
2.95	0.5	4990	772	1.280	1.273

Table F.19: 1-Undecanal dynamic and steady-state flux data at 20 bar

Membrane	ST-240				
Conditions	**20 bar**, 27 °C, 500 rpm				
	Raw data			Calculated data	
m (g)	Δm (g)	time (s)	Δt (s)	Dynamic flux ($kg.m^{-2}.h^{-1}$)	Steady-state flux ($kg.m^{-2}.h^{-1}$)
1	1	1010	1000	2.149	-
2	1	1950	947	2.216	2.287
3	1	2810	860	2.308	2.397
4	1	3770	956	2.297	2.352
5	1	4670	902	2.317	2.364
6	1	5620	953	2.310	2.345

Table F.20: 1-Undecanal dynamic and steady-state flux data at 30 bar

Membrane	ST-240				
Conditions	**30 bar**, 29 °C, 500 rpm				
	Raw data			Calculated data	
m (g)	Δm (g)	time (s)	Δt (s)	Dynamic flux ($kg.m^{-2}.h^{-1}$)	Steady-state flux ($kg.m^{-2}.h^{-1}$)
4.54	1.54	2570	835	3.822	-
6	1.46	3420	849	3.798	3.787
7.5	1.5	4270	848	3.804	3.798
9	1.5	5160	894	3.775	3.764
10.5	1.5	6110	943	3.724	3.707
12	1.5	6710	604	3.873	3.879

Table F.21: 1-Undecanal dynamic and steady-state flux data at 40 bar

Membrane	ST-240				
Conditions	**40 bar**, 25 °C, 500 rpm				
	Raw data			Calculated data	
m (g)	Δm (g)	time (s)	Δt (s)	Dynamic flux ($kg.m^{-2}.h^{-1}$)	Steady-state flux ($kg.m^{-2}.h^{-1}$)
2.5	2.5	1050	1050	5.172	-
5	2.5	2090	1040	5.192	5.212
7.05	2.05	2980	899	5.116	5.085
10	2.95	4210	1230	5.145	5.136
12.05	2.05	5080	873	5.135	5.125
15	2.95	6310	1230	5.146	5.140

F.2.6 1-Undecanol pure flux data

Table F.22: 1-Undecanal dynamic and steady-state flux data at 10 bar

Membrane	ST-240				
Conditions	**10 bar**, 26 °C, 500 rpm				
	Raw data			Calculated data	
m (g)	Δm (g)	time (s)	Δt (s)	Dynamic flux ($kg.m^{-2}.h^{-1}$)	Steady-state flux ($kg.m^{-2}.h^{-1}$)
0.25	0.25	890	890	0.6084	-
1.45	1.2	5780	4890	0.5432	0.5313
1.75	0.3	7370	1590	0.5144	0.5013
2	0.25	8220	855	0.5267	0.5168
2.25	0.25	9370	1150	0.5198	0.5105
2.5	0.25	10300	896	0.5272	0.5195

Table F.23: 1-Undecanal dynamic and steady-state flux data at 20 bar

Membrane	ST-240				
Conditions	**20 bar**, 26 °C, 500 rpm				
	Raw data			Calculated data	
m (g)	Δm (g)	time (s)	Δt (s)	Dynamic flux ($kg.m^{-2}.h^{-1}$)	Steady-state flux ($kg.m^{-2}.h^{-1}$)
0.98	0.38	1750	636	1.213	-
1.48	0.5	2850	1110	1.122	-
1.98	0.5	3830	974	1.1195	1.112
2.48	0.5	5090	1250	1.056	0.9713
2.98	0.5	6150	1060	1.049	0.9864
3.48	0.5	7240	1080	1.041	0.9889

Table F.24: 1-Undecanal dynamic and steady-state flux data at 30 bar

Membrane	ST-240				
Conditions	**30 bar**, 26 °C, 500 rpm				
	Raw data			Calculated data	
m (g)	Δm (g)	time (s)	Δt (s)	Dynamic flux ($kg.m^{-2}.h^{-1}$)	Steady-state flux ($kg.m^{-2}.h^{-1}$)
0.5	0.5	715	715	1.514	-
0.95	0.45	1260	542	1.637	-
1.45	0.5	1920	666	1.633	-
1.95	0.5	2760	836	1.531	-
3.45	1.5	4860	2110	1.536	1.544
3.95	0.5	5630	770	1.518	1.507

Table F.25: 1-Undecanal dynamic and steady-state flux data at 40 bar

Membrane	ST-240				
Conditions	**40 bar**, 25 °C, 500 rpm				
	Raw data			Calculated data	
m (g)	Δm (g)	time (s)	Δt (s)	Dynamic flux ($kg.m^{-2}.h^{-1}$)	Steady-state flux ($kg.m^{-2}.h^{-1}$)
0.97	0.97	961	961	2.186	-
1.97	1	1920	965	2.215	2.244
2.97	1	2900	977	2.216	2.230
3.97	1	3870	963	2.224	2.237
4.97	1	4850	983	2.220	2.228
5.97	1	5850	996	2.212	2.217

F.3 Pure species permeance

Table F.26: Permeance of pure species

	10 bar	20 bar	30 bar	40 bar
Flux ($kg.m^{-2}.h^{-1}$)				
1-Octene	29.3	58.0	96.7	110
1-Decene	13.1	24.6	32.3	46.5
1-Nonanal	5.38	12.7	12.4	22.3
1-Undecanal	2.48	6.60	7.91	14.0
1-Nonanol	1.21	2.35	2.32	5.14
1-Undecanol	0.517	1.01	1.38	2.23
Mass Permeance ($kg.m^{-2}.h^{-1}.bar^{-1}$)				
1-Octene	2.86	2.96	3.13	2.87
1-Decene	1.31	1.23	1.13	1.16
1-Nonanal	0.538	0.637	0.642	0.558
1-Undecanal	0.248	0.330	0.353	0.351
1-Nonanol	0.121	0.117	0.127	0.129
1-Undecanol	0.0517	0.0507	0.0507	0.0557

F.4 Binary species separation

F.4.1 Binary mixture of 1-octene and 1-nonanal total flux data

Table F.27: Total flux data of 80:20 1-octene and 1-nonanal mixture

Membrane	ST-240				
Concentration	**80 vol%** 1-octene, **20 vol%** 1-nonanal				
Conditions	30 bar, 21 °C, 500 rpm				
	Raw data			Calculated data	
m (g)	Δm (g)	time (s)	Δt (s)	Dynamic flux ($kg.m^{-2}.h^{-1}$)	Steady-state flux ($kg.m^{-2}.h^{-1}$)
35	2.5	3310	250	22.89	-
37.5	2.5	3560	248	22.82	21.74
40	2.5	3810	254	22.72	21.60
42.5	2.5	4070	256	22.62	21.49
45	2.5	4330	264	22.49	21.28
47.5	2.5	4590	255	22.42	21.27

Table F.28: Total flux data of 60:40 1-octene and 1-nonanal mixture

Membrane	ST-240				
Concentration	**60 vol%** 1-octene, **40 vol%** 1-nonanal				
Conditions	30 bar, 19 °C, 500 rpm				
	Raw data			Calculated data	
m (g)	Δm (g)	time (s)	Δt (s)	Dynamic flux ($kg.m^{-2}.h^{-1}$)	Steady-state flux ($kg.m^{-2}.h^{-1}$)
104	15.5	5790	856	38.89	-
118	14	6580	789	38.84	38.76
133.5	15.5	7440	858	38.87	38.84

147.5	14	8230	788	38.83	38.78
167.1	19.6	9320	1090	38.84	38.80
182	14.9	10200	844	38.79	38.73

Table F.29: Total flux data of 20:80 1-octene and 1-nonanal mixture

Membrane	ST-240
Concentration	**20 vol%** 1-octene, **80 vol%** 1-nonanal
Conditions	30 bar, 20 °C, 500 rpm

Raw data				Calculated data	
m (g)	Δm (g)	time (s)	Δt (s)	Dynamic flux ($kg.m^{-2}.h^{-1}$)	Steady-state flux ($kg.m^{-2}.h^{-1}$)
49	2.5	7270	394	14.60	-
51.5	2.5	7660	387	14.56	14.12
54	2.5	8040	388	14.54	14.10
56.5	2.5	8420	383	14.52	14.10
59	2.5	8810	386	14.50	14.09
61.5	2.5	9210	398	14.46	14.05

F.4.2 Binary mixture of 1-decene and 1-undecanal total flux data

Table F.30: Total flux data of 80:20 1-decene and 1-undecanal mixture

Membrane	ST-240
Concentration	**80 vol%** 1-decene, **20 vol%** 1-undecanal
Conditions	30 bar, 24 °C, 500 rpm

Raw data				Calculated data	
m (g)	Δm (g)	time (s)	Δt (s)	Dynamic flux ($kg.m^{-2}.h^{-1}$)	Steady-state flux ($kg.m^{-2}.h^{-1}$)
57	5	8750	733	14.11	-
62	5	9510	763	14.12	14.39
67	5	10300	770	14.11	14.34
72	5	11100	780	14.10	14.28
81.5	9.5	12500	1438	14.12	14.29
85.5	4	13100	630	14.10	14.25

Table F.31: Total flux data of 60:40 1-decene and 1-undecanal mixture

Membrane	ST-240
Concentration	**60 vol%** 1-decene, **40 vol%** 1-undecanal
Conditions	30 bar, 24 °C, 500 rpm

Raw data				Calculated data	
m (g)	Δm (g)	time (s)	Δt (s)	Dynamic flux ($kg.m^{-2}.h^{-1}$)	Steady-state flux ($kg.m^{-2}.h^{-1}$)
44	5	7710	907	12.35	-
49	5	8640	934	12.27	11.76
53.5	4.5	9440	792	12.27	11.92
58.5	5	10300	907	12.24	11.93
61	2.5	10800	451	12.23	11.94

63.5	2.5	11300	494	12.18	11.83

Table F.32: Total flux data of 40:60 1-decene and 1-undecanal mixture

Membrane	ST-240
Concentration	**40 vol%** 1-decene, **60 vol%** 1-undecanal
Conditions	30 bar, 23 °C, 500 rpm

Raw data				Calculated data	
m (g)	Δm (g)	time (s)	Δt (s)	Dynamic flux ($kg.m^{-2}.h^{-1}$)	Steady-state flux ($kg.m^{-2}.h^{-1}$)
7.5	2.5	2000	677	8.098	-
10	2.5	2690	687	8.043	7.940
12.5	2.5	3260	569	8.300	8.404
15	2.5	3840	581	8.455	8.616
17.5	2.5	4440	597	8.537	8.703
19.5	2	4910	476	8.592	8.756

Table F.33: Total flux data of 20:80 1-decene and 1-undecanal mixture

Membrane	ST-240
Concentration	**20 vol%** 1-decene, **80 vol%** 1-undecanal
Conditions	30 bar, 23 °C, 500 rpm

Raw data				Calculated data	
m (g)	Δm (g)	time (s)	Δt (s)	Dynamic flux ($kg.m^{-2}.h^{-1}$)	Steady-state flux ($kg.m^{-2}.h^{-1}$)
34	5	8650	1220	8.514	-
39	5	9900	1250	8.530	8.513
44	5	11200	1280	8.520	8.505
49	5	12500	1310	8.499	8.484
51	2	12900	472	8.524	8.511
53	2	13400	483	8.540	8.529

F.4.3 Binary mixture of 1-nonanal and 1-nonanol total flux data

Table F.34: Total flux data of 80:20 1-nonanal and 1-nonanol mixture

Membrane	ST-240
Concentration	**80 vol%** 1-nonanal, **20 vol%** 1-nonanol
Conditions	30 bar, 26 °C, 500 rpm

Raw data				Calculated data	
m (g)	Δm (g)	time (s)	Δt (s)	Dynamic flux ($kg.m^{-2}.h^{-1}$)	Steady-state flux ($kg.m^{-2}.h^{-1}$)
26.9	2.1	10200	771	5.686	-
29.3	2.4	11100	885	5.701	5.631
31.8	2.5	12000	868	5.739	5.748
34.5	2.7	13000	1047	5.727	5.717
36.8	2.3	13900	886	5.720	5.704
39.3	2.5	15000	1075	5.672	5.609

Table F.35: Total flux data of 60:40 1-nonanal and 1-nonanol mixture

Membrane	ST-240				
Concentration	**60 vol%** 1-nonanal, **40 vol%** 1-nonanol				
Conditions	30 bar, 24 °C, 500 rpm				
	Raw data			Calculated data	
m (g)	Δm (g)	time (s)	Δt (s)	Dynamic flux ($kg.m^{-2}.h^{-1}$)	Steady-state flux ($kg.m^{-2}.h^{-1}$)
22.7	1	16300	659	3.025	-
23.1	0.4	16500	314	3.020	3.173
23.6	0.5	16900	317	3.027	3.184
25.1	1.5	17900	1005	3.039	3.190
25.6	0.5	18200	338	3.042	3.191
26.1	0.5	18500	319	3.048	3.199

Table F.36: Total flux data of 40:60 1-nonanal and 1-nonanol mixture

Membrane	ST-240				
Concentration	**40 vol%** 1-nonanal, **60 vol%** 1-nonanol				
Conditions	30 bar, 23 °C, 500 rpm				
	Raw data			Calculated data	
m (g)	Δm (g)	time (s)	Δt (s)	Dynamic flux ($kg.m^{-2}.h^{-1}$)	Steady-state flux ($kg.m^{-2}.h^{-1}$)
5.2	1	5630	1070	2.001	-
6.2	1	6750	1120	1.988	1.980
7.2	1	7820	1070	1.992	1.986
8.2	1	8930	1100	1.988	1.983
9.2	1	10000	1080	1.990	1.985
10.2	1	11100	1100	1.987	1.983

Table F.37: Total flux data of 20:80 1-nonanal and 1-nonanol mixture

Membrane	ST-240				
Concentration	**20 vol%** 1-nonanal, **80 vol%** 1-nonanol				
Conditions	30 bar, 27 °C, 500 rpm				
	Raw data			Calculated data	
m (g)	Δm (g)	time (s)	Δt (s)	Dynamic flux ($kg.m^{-2}.h^{-1}$)	Steady-state flux ($kg.m^{-2}.h^{-1}$)
8.25	1	908	1100	1.967	-
9.25	1	10200	1160	1.955	1.956
10.25	1	11300	1060	1.963	1.967
11.25	1	12400	1110	1.961	1.964
12.25	1	13500	1070	1.966	1.970
12.8	0.55	14000	547	1.974	1.981

F.5 Homogeneous catalyst recovery data using ST-240

Table F.38: Catalyst recovery data

Pressure (bar)	Catalyst	Membrane	Feed (ppm)	Permeate (ppm)	Retentate (ppm)	Rejection
1-Octene						
10	Rh	ST-240	200	5.00	-	98.0%
10	Rh	ST-240	500	5.00	-	99.0%
20	Rh	ST-240	200	5.00	-	98.0%
20	Rh	ST-240	500	5.00	446	99.0%
30	Rh	ST-240	200	5.00	-	98.0%
30	Rh	ST-240	200	5.00	357	98.0%
30	Rh	ST-240	200	5.00	268	98.0%
30	Rh	ST-240	500	5.00	446	99.0%
40	Rh	ST-240	200	5.00	268	98.0%
40	Rh	ST-240	500	5.00	536	99.0%
30	Rh	DM-200	500	5.00	-	99.0%
30	Co	DM-200	500	3.00	-	99.4%
30	Co	ST-240	500	60.45	514	87.9%
1-Decene						
10	Rh	ST-240	200	5.00	-	98.0%
20	Rh	ST-240	200	5.00	-	98.0%
30	Rh	ST-240	200	5.00	-	98.0%
30	Co	ST-240	500	60.45	544.1	87.9%
30	Co	ST-240	500	90.68	-	81.9%
40	Rh	ST-240	200	5.00	-	98.0%
1-Nonanal						
10	Rh	ST-240	200	5.00	-	98.0%
20	Rh	ST-240	200	5.00	267.9	98.0%
30	Rh	ST-240	200	5.00	267.9	98.0%
30	Co	ST-240	500	3.00	544.1	99.4%
40	Rh	ST-240	200	5.00	357.2	98.0%
1-Undecanal						
10	Rh	ST-240	200	5.00	-	98.0%
30	Rh	ST-240	200	5.00	-	98.0%
30	Co	ST-240	500	3.00	-	98.0%
30	Rh	ST-240	200	5.00	-	98.0%
40	Rh	ST-240	200	5.00	-	98.0%
1-Nonanol						
10	Rh	ST-240	200	5.00	-	98.0%
20	Rh	ST-240	200	5.00	-	98.0%
30	Rh	ST-240	200	5.00	-	98.0%
30	Co	ST-240	500	5.00	-	98.6%
1-Undecanol						
30	Rh	ST-240	200	5.00	-	98.0%
30	Co	ST-240	500	6.00	-	98.8%
30	Rh	ST-240	200	5.00	-	98.0%

F.6 OSN modelling

F.6.1 Flux estimation data using pore-flow based transport models

Table F.39: Total flux estimation data for binary mixture 1-octene and 1-nonanal

$P^{PF}_{1-octene} = 3.87E-12\ kg.m^{-2}.h^{-1}$

$P^{PF}_{1-nonanal} = 2.67E-12\ kg.m^{-2}.h^{-1}$

$P^{PF}_{average} = 3.12E-12\ kg.m^{-2}.h^{-1}$

1-Octene (mL.mL^{-1})	1-Nonanal (mL.mL^{-1})	$J_{m,PF-1}$ (kg.m^{-2}.h^{-1})	$J_{m,PF-2}$ (kg.m^{-2}.h^{-1})
1.0	0.0	64.43	93.81
0.8	0.2	51.36	67.23
0.6	0.4	41.14	48.78
0.4	0.6	32.44	35.69
0.2	0.8	25.27	26.22
0.0	1.0	20.93	19.26

Table F.40: Total flux estimation data for binary mixture 1-decene and 1-undecanal

$P^{PF}_{1-decene} = 2.31E-12\ kg.m^{-2}.h^{-1}$

$P^{PF}_{1-undecanal} = 1.67E-12\ kg.m^{-2}.h^{-1}$

$P^{PF}_{average} = 1.99E-12\ kg.m^{-2}.h^{-1}$

1-Decene (mL.mL^{-1})	1-Undecanal (mL.mL^{-1})	$J_{m,PF-1}$ (kg.m^{-2}.h^{-1})	$J_{m,PF-2}$ (kg.m^{-2}.h^{-1})
1.0	0.0	64.43	93.81
0.8	0.2	51.36	67.23
0.6	0.4	41.14	48.78
0.4	0.6	32.44	35.69
0.2	0.8	25.27	26.22
0.0	1.0	20.93	19.26

Table F.41: Total flux estimation data for binary mixture 1-nonanal and 1-nonanol

$P^{PF}_{1-nonanal} = 2.37E-12\ kg.m^{-2}.h^{-1}$

$P^{PF}_{1-nonanol} = 3.24E-12\ kg.m^{-2}.h^{-1}$

$P^{PF}_{average} = 2.80E-12\ kg.m^{-2}.h^{-1}$

1-Nonanal (mL.mL^{-1})	1-Nonanol (mL.mL^{-1})	$J_{m,PF-1}$ (kg.m^{-2}.h^{-1})	$J_{m,PF-2}$ (kg.m^{-2}.h^{-1})
1.0	0.0	22.81	20.42
0.8	0.2	13.83	11.86
0.6	0.4	9.016	7.391
0.4	0.6	6.198	4.847
0.2	0.8	4.442	3.306
0.0	1.0	3.291	2.325

F.6.2 Flux estimation data using solution-diffusion based transport models

Table F.42: Total flux estimation data for binary mixture 1-octene and 1-nonanal

$P^{SD}_{1-octene} = 0.1488\ kg.m^{-2}.s^{-1}$

$P^{SD}_{1-nonanal} = 0.02812\ kg.m^{-2}.s^{-1}$

1-Octene (mL.mL^{-1})	1-Nonanal (mL.mL^{-1})	$J_{m,1-octene}$ (kg.m^{-2}.h^{-1})	$J_{m,1-nonanal}$ (kg.m^{-2}.h^{-1})	$J_{m,SD-1}$ (kg.m^{-2}.h^{-1})	$J_{m,SD-2}$ (kg.m^{-2}.h^{-1})
1.0	0.0	93.81	0	93.81	95.06
0.8	0.2	41.24	5.068	46.31	68.13
0.6	0.4	17.96	7.437	25.40	49.43
0.4	0.6	10.03	10.95	20.99	36.17
0.2	0.8	4.650	14.61	19.26	26.57
0.0	1.0	0	19.26	19.26	19.51

Table F.43: Total flux estimation data for binary mixture 1-decene and 1-undecanal

$P^{SD}_{1-decene} = 0.04573\ kg.m^{-2}.s^{-1}$

$P^{SD}_{1-undecanal} = 0.001315\ kg.m^{-2}.s^{-1}$

1-Decene (mL.mL^{-1})	Undecanal (mL.mL^{-1})	$J_{m,1-decene}$ (kg.m^{-2}.h^{-1})	$J_{m,1-undecanal}$ (kg.m^{-2}.h^{-1})	$J_{m,SD-1}$ (kg.m^{-2}.h^{-1})	$J_{m,SD-2}$ (kg.m^{-2}.h^{-1})
1.0	0.0	33.76	0	33.76	34.21
0.8	0.2	19.97	3.146	23.11	26.80
0.6	0.4	12.07	5.993	18.06	21.16
0.4	0.6	6.382	7.334	13.71	16.81
0.2	0.8	2.772	8.871	11.64	13.41
0.0	1.0	0	10.59	10.59	10.73

Table F.44: Total flux estimation data for binary mixture 1-nonanal and 1-nonanol

$P^{SD}_{1-nonanal} = 0.02812\ kg.m^{-2}.s^{-1}$

$P^{SD}_{1-nonanol} = 0.005484\ kg.m^{-2}.s^{-1}$

Nonanal (mL.mL^{-1})	Nonanol (mL.mL^{-1})	$J_{m,1-nonanal}$ (kg.m^{-2}.h^{-1})	$J_{m,1-nonanol}$ (kg.m^{-2}.h^{-1})	$J_{m,SD-1}$ (kg.m^{-2}.h^{-1})	$J_{m,SD-2}$ (kg.m^{-2}.h^{-1})
1.0	0.0	19.26	0	19.26	19.48
0.8	0.2	10.18	1.564	11.75	12.69
0.6	0.4	4.529	1.940	6.470	8.837
0.4	0.6	1.958	2.032	3.991	6.465
0.2	0.8	0.9328	2.836	3.769	4.913
0.0	1.0	0	3.804	3.804	3.848

F.6.3 Flux estimation data using a modified solution-diffusion transport model

Table F.45: Total flux estimation data for binary mixture 1-octene and 1-nonanal

$\delta_M - \delta_{1-octene} = 7.586\ MPa^{0.5}$

$\delta_M - \delta_{1-nonanal} = 4.229\ MPa^{0.5}$

1-Octene (mL.mL^{-1})	1-Nonanal (mL.mL^{-1})	$\delta_{SD-3,1-octene}$ (MPa$^{0.5}$)	$\delta_{SD-3,1-nonanal}$ (MPa$^{0.5}$)	$J_{m,SD-3}$ (kg.m^{-2}.h^{-1})
1.0	0.0	1	0.3108	93.81
0.8	0.2	1.159	0.3604	37.78
0.6	0.4	1.380	0.4290	18.90
0.4	0.6	1.705	0.5299	12.67
0.2	0.8	2.228	0.6927	11.69
0.0	1.0	3.217	1	13.30

Table F.46: Total flux estimation data for binary mixture 1-decene and 1-undecanal

$\delta_M - \delta_{1-decene} = 7.245 MPa^{0.5}$

$\delta_M - \delta_{1-undecanal} = 4.455\ MPa^{0.5}$

1-Decene (mL.mL^{-1})	1-Undecanal (mL.mL^{-1})	$\delta_{SD-3,1-decene}$ (MPa$^{0.5}$)	$\delta_{SD-3,1-undecanal}$ (MPa$^{0.5}$)	$J_{m,SD-3}$ (kg.m^{-2}.h^{-1})
1.0	0.0	1	0.3781	33.76
0.8	0.2	1.142	0.4318	20.52
0.6	0.4	1.331	0.5033	15.21
0.4	0.6	1.595	0.6032	12.65
0.2	0.8	1.989	0.7525	10.61
0.0	1.0	2.640	1	10.17

Table F.47: Total flux estimation data for binary mixture 1-nonanal and 1-nonanol

$\delta_M - \delta_{1-nonanal} = 4.229 MPa^{0.5}$

$\delta_M - \delta_{1-nonanol} = 2.472\ MPa^{0.5}$

1-Nonanal (mL.mL^{-1})	1-Nonanol (mL.mL^{-1})	$\delta_{SD-3,1-nonanal}$ (MPa$^{0.5}$)	$\delta_{SD-3,1-nonanol}$ (MPa$^{0.5}$)	$J_{m,SD-3}$ (kg.m^{-2}.h^{-1})
1.0	0.0	1	0.3415	19.26
0.8	0.2	1.151	0.3939	8.671
0.6	0.4	1.357	0.4632	0.9417
0.4	0.6	1.653	0.5646	3.382
0.2	0.8	2.110	0.7217	2.210
0.0	1.0	2.927	1	1.888

F.7 Total operating costs calculation data

Table F.48: Distillation column data

	Column costs (R.a^{-1})	Tray costs (R.a^{-1})	Total costs (R.a^{-1})	Total costs (R.(kg fed)$^{-1}$)
1-Octene	R 324 400.00	R 3 081 000.00	R 3 405 700.00	3.87
1-Decene	R 183 700.00	R 1 742 100.00	R 1 925 700.00	2.18
1-Nonanal	R 169 900.00	R 2 149 200.00	R 2 319 200.00	2.63
1-Undecanal	R 194 500.00	R 2 209 300.00	R 2 403 800.00	2.73
1-Nonanol	R 187 200.00	R 2 435 300.00	R 2 622 500.00	2.98
1-Undecanol	R 612 500.40	R 5 319 100.00	R 5 931 500.00	6.74

Table F.49: OSN data

	L_p (kg.m^{-2}.h^{-1}.bar^{-1})	TOC_M (R.a^{-1})	TOC_M (R.(kg fed)$^{-1}$)
1-Octene	2.968	R 169 900.00	0.19
1-Decene	1.202	R 175 400.00	0.20
1-Nonanal	0.6003	R 184 600.00	0.21
1-Undecanal	0.3223	R 200 600.00	0.23
1-Nonanol	0.1232	R 256 200.00	0.29
1-Undecanol	0.05243	R 377 800.00	0.43

F.8 Energy usage calculation data

Table F.50: OSN data

	F_F (m^3.h^{-1})	F_r (m^3.h^{-1})	$Q_{M,F}$ (kW)	$Q_{M,r}$ (kW)	Q_M (kWh.(kg fed)$^{-1}$)
1-Octene	0.139	0.699	0.393	0.0328	0.00426
1-Decene	0.133	0.666	0.375	0.0318	0.00406
1-Nonanal	0.120	0.604	0.340	0.0283	0.00368
1-Undecanal	0.120	0.604	0.340	0.0283	0.00368
1-Nonanol	0.121	0.606	0.341	0.0284	0.00369
1-Undecanol	0.120	0.602	0.339	0.0282	0.00367

APPENDIX G: Sample Calculations

G.1 Solubility parameter

The molecular structures of the organic species used in this study are displayed in Figure G.1:

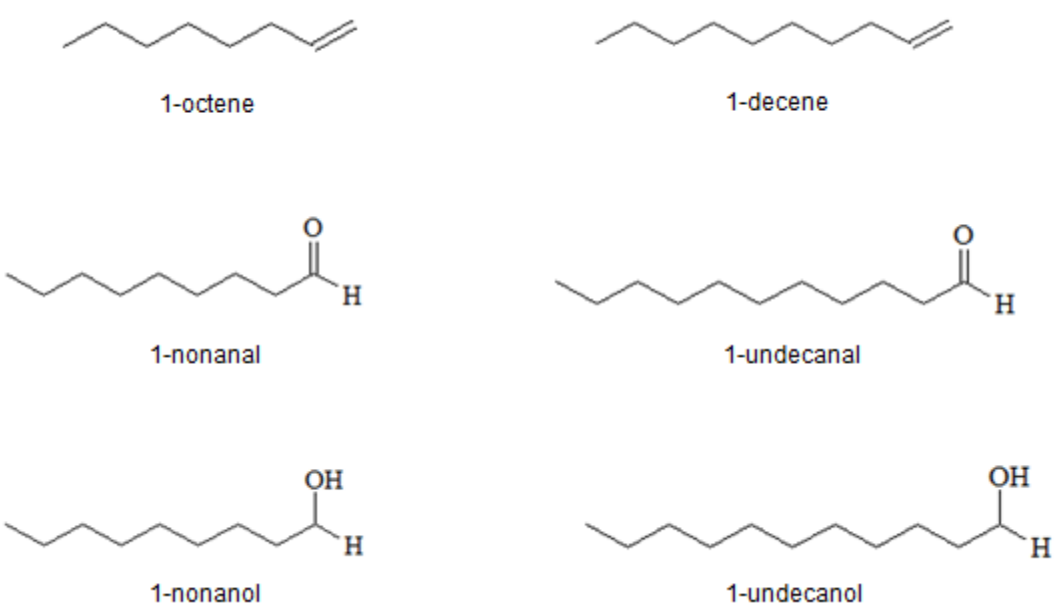

Figure G.1: Molecular structures of organic species used in this study

The solubility parameters of these organic species, δ, were estimated using the group contribution method, a widely accepted method of calculating solubility parameters of solvents and polymers as described by Van Krevelen [1]. Calculations are based on the cohesive energy, E_{coh}, and molar volume, V_m, of functional groups at 25 °C as obtained from Fedors [2] and Hansen [3].

$$\delta_i = \sqrt{\frac{\sum E_{coh,i}}{\sum V_{m,i}}} \qquad \text{(G.1)}$$

Approximated values of E_{coh} and V_m of functional groups have been reported to be accurate within 10% [2] and are presented in Table G.1.

Table G.1: Functional group cohesive energies and molar volumes

	E_{coh} (J.mol^{-1})	V_m x 10^{-6} (m^3.mol^{-1})
$-CH_3$	4710	33.5
$-CH_2-$	4940	16.1
$-CH_3$	4310	28.5
$=CH_2$	4310	13.5
$=CH-$	21350	22.3
$-CH=O$	29800	10.0
$-OH$	31940	71.4

Table G.2 presents the solubility parameters as calculated using Equation F.1.

Table G.2: Solubility parameters of organic species used in this study

	$\sum E_{coh}$ (J.mol^{-1})	$\sum V_m$ x 10^{-6} (m^3.mol^{-1})	δ [(MPa)$^{0.5}$]
1-Octene	38030	156	15.6
1-Decene	47910	188	16.0
1-Nonanal	60640	169	19.0
1-Undecanal	70520	201	18.8
1-Nonanol	74030	172	20.7
1-Undecanol	83910	205	20.3

G.2 Hydroformylation of 1-octene product yields

The hydroformylation of 1-octene was performed at the reaction conditions: 200 ppm solution of **$HRh(CO)(PPh_3)_3$** (4 mg, 0.00435 mmol), toluene (21 mL), n-dodecane (0.7 mL), 1-octene (3.3 mL, 21 mmol), additional **PPh_3** (22 mg, 0.085 mmol), 80 °C, 20 bar. Samples were withdrawn and analysed with GC. Using the areas from GC, the species concentrations in the sample relative to the known concentration of the internal standard can be determined.

GC peak areas:

$A_{n-dod} = 837094.8$

$A_{1-nonanal} = 6947265$

$A_{2-methyloct} = 3583546$

$A_{2-ethylhept} = 75831.9$

Species volumes were determined using the correlation as shown in Equation G.2:

$$\frac{V_i}{V_{n-dod}} = RF * \frac{A_i}{A_{n-dod}} \quad \text{(G.2)}$$

Species volumes:

$V_{n-dod} = 0.7\ mL$

$V_{1-nonanal} = 0.7 \times 1.18 \times \frac{6947265}{837094.8} = 1.958\ mL$

$V_{2-methyloct} = 0.7 \times 1.18 \times \frac{3583546}{837094.8} = 1.010\ mL$

$V_{2-ethylhept} = 0.7 \times 1.18 \times \frac{75831.9}{837094.8} = 0.02137\ mL$

Species moles:

$n_{1-nonanal} = \frac{V_{1-nonanal} \times \rho_{1-nonanal}}{MW_{1-nonanal}} = \frac{1.958\ mL \times 0.827\ g.mL^{-1}}{142\ g.mol^{-1}} = 0.01138\ mol$

$n_{2-methyloct} = \frac{1.010\ mL \times 0.827\ g.mL^{-1}}{142\ g.mol^{-1}} = 0.005876\ mol$

$n_{2-ethylhept} = \frac{0.02137\ mL \times 0.827\ g.mL^{-1}}{142\ g.mol^{-1}} = 0.000124\ mol$

Product yields:

$Y_{b-ald} = \frac{Y_{n-ald}}{Y_{n-ald} + Y_{b-ald} + Y_{iso-olefin} + Y_{paraffin}}$

$\therefore Y_{n-ald} = \frac{0.01138}{0.01138 + (0.005876 + 0.000124) + 4.25E-05 + 0.000238} = 0.6443\ (64.43\ mol\%)$

$Y_{b-ald} = \frac{Y_{b-ald}}{Y_{n-ald} + Y_{b-ald} + Y_{iso-olefin} + Y_{paraffin}}$

$\therefore Y_{b-ald} = \frac{0.005876 + 0.000124}{0.01138 + (0.005876 + 0.000124) + 4.25E-05 + 0.000238} = 0.3397\ (34.00\ mol\%)$

$\therefore {}^{n}/_{b} = \frac{0.644}{0.339} = 1.897$

G.3 Permeate flux

The active membrane area required for the flux calculation can be determined by measuring the inner diameter of the filtration membrane cell (46 cm):

$$A = \frac{\pi}{4} {D_M}^2 = \frac{\pi}{4}(46\ cm)^2 = 16.6\ cm^2\ (or\ 0.00166\ m^2)$$

Based on cumulative mass and time data, the dynamic mass flux of 1-octene can be calculated at 30 bar,

$$J_{m,1} = \frac{0.268\ kg}{0.00166\ m^2 \times 6076\ min \div 60\ h.min^{-1}} = 95.55\ kg.m^{-2}.h^{-1}$$

$$J_{m,2} = \frac{0.283\ kg}{0.00166\ m^2 \times 6412\ min \times 60\ h.min^{-1}} = 95.61\ kg.m^{-2}.h^{-1}$$

When dynamic fluxes are observed to remain near constant, the steady-state mass flux can be calculated,

$$J_{m,ss} = \frac{0.283 - 0.268\ kg}{0.00166\ m^2 \times (6412 - 6076) min \div 60\ h.min^{-1}} = 96.71\ kg.m^{-2}.h^{-1}$$

The permeance of 1-octene can be calculated at 30 bar,

$$P_m = \frac{96.71\ kg.m^{-2}.h^{-1}}{30\ bar} = 3.22 kg.m^{-2}.h^{-1}.bar^{-1}$$

G.4 Bond polarity

To calculate the bond polarity, the electronegativity of each atom in the molecule is determined, as presented in Figure G.2.

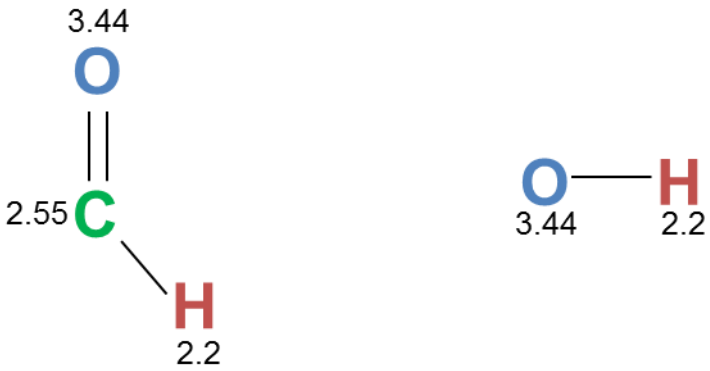

Figure G.2: Electronegativity of atoms

Based on these electronegativity values, the bond polarity can be calculated.

Figure G.3: Bond polarity of molecules

G.5 Catalyst recovery

The feed and permeate catalyst concentration was measured using FAAS as 200 ppm and 5 ppm. The recovery can then be calculated,

$$R = \left(1 - \frac{C_P}{C_F}\right) \times 100\% \qquad \text{(G.3)}$$

$$\therefore R = \left(1 - \frac{5}{200}\right) \times 100\% = 97.5\%$$

G.6 Membrane swelling degree

Measure the weight of the dry piece of membrane,

$$M_{dry} = 0.015\ g$$

Submerge the piece of membrane in the solvent, i.e. 1-octene. After the specified waiting period, the membrane is re-weighed,

$$M_{wet} = 0.018\ g$$

The swelling degree, i.e. sorption, can then be calculated based on the dry and wet weights of the membrane.

$$SD = \left(\frac{M_{wet} - M_{dry}}{M_{dry}}\right) \times 100\% \qquad \text{(G.4)}$$

$$\therefore SD = \left(\frac{0.018\ g - 0.015\ g}{0.015\ g}\right) \times 100\% = 20\%$$

G.7 Pore-flow and solution-diffusion modelling

G.7.1 Pore-flow transport models

Pore-flow permeance for 1-octene,

$$P^{PF} = \frac{J_{m,ss} \times \eta}{\Delta P} \quad \text{(G.5)}$$

$$\therefore P^{PF} = \frac{96.71\ kg.m^{-2}.h^{-1} \times 0.452E{-}03\ Pa.s}{30\ bar \times 101325\ Pa.bar^{-1} \times 3600\ s.h^{-1}} = 3.995E-12\ kg.m^{-2}\ (= 5.587E-12\ m)$$

Considering the Hagen-Poiseuille equation, as shown in Equation G.6, for a binary mixture of 80 vol% 1-octene and 20 vol% 1-nonanal at 30 bar, the total flux can be estimated,

$$J_V = P^{PF}_{average} \times \left(\frac{\Delta P}{\eta_{mix}}\right) \quad \text{(G.6)}$$

The average permeance was determined based on the relative permeance of the respective species in the binary mixture.

$$P^{PF}_{average} = PF^{PF}_{1-octene} + PF^{PF}_{1-nonanal}$$

$$\therefore P^{PF}_{average} = 0.5 \times (3.995E-12\ kg.m^{-2} + 2.367E-12\ kg.m^{-2}) = 3E-12\ kg.m^{-2}$$

and,

$$\eta_{mix} = (v_{1-octene}.(\eta_{1-octene})^{1/3} + v_{1-nonanal}.(\eta_{1-nonanal})^{1/3})^3$$

$$\therefore \eta_{mix} = 0.8 \times (0.452\ mPa.s)^{1/3} + 0.2 \times (1.345\ mPa.s)^{1/3} = 0.5816\ mPa.s$$

Therefore,

$$J_V = 3E-12\ kg.m^{-2} \times \left(\frac{30\ bar \times 101325\ Pa.bar^{-1}}{0.8985E{-}03\ Pa.s}\right) = 51.36\ kg.m^{-2}.h^{-1}$$

F.7.2 Solution-diffusion transport model

Solution-diffusion permeance for 1-octene

$$P^{SD} = \frac{J_{m,ss}}{\left(1-\exp\left(-\frac{V_m \Delta P}{RT}\right)\right)} \quad \text{(G.7)}$$

$$\therefore P^{SD} = \frac{96.71\ kg.m^{-2}.h^{-1} \div 3600}{\left(1-\exp\left(-\frac{0.0001569\ m^3.mol^{-3} \times 30\ bar \times 101325}{8.314\ J.mol^{-1}.K^{-1} \times 298K}\right)\right)} = 0.1488\ kg.m^{-2}.s^{-1}\ (= 2E-04\ m.s^{-1})$$

Considering the classic solution-diffusion equation, as shown in Equation G.6, for a binary mixture of 80 vol% 1-octene and 20 vol% 1-nonanal at 30 bar, the total flux can be estimated,

$$J_m = J_{m,1-octene} + J_{m,1-nonanal} \tag{G.8}$$

where

$$J_{m,1-octene} = P^{SD}_{1-octene}\left[v_{1-octene} - \frac{J_{n,1-octene}}{J_{n,1-octene}+J_{n,1-nonanal}}\exp\left(-\frac{V_{m,1-octene}\Delta P}{RT}\right)\right]$$

$$J_{m,1-nonanal} = P^{SD}_{1-octene}\left[v_{1-octene} - \frac{J_{n,1-nonanal}}{J_{n,1-octene}+J_{n,1-nonanal}}\exp\left(-\frac{V_{m,1-nonanal}\Delta P}{RT}\right)\right]$$

The above equations were solved simultaneously to determine the partial molar fluxes of 1-octene and 1-nonanal.

Considering a binary mixture of 80 vol% 1-octene and 20 vol% 1-nonanal at 30 bar, the total and partial fluxes were estimated as,

$$J_{m,1-octene} = 0.1488 \times \left[0.8 - \frac{41.24}{41.24+5.068}\exp\left(-\frac{0.0001569\times30\times101325}{8.314\times298}\right)\right] = 41.24\ kg.m^{-2}.h^{-1}$$

$$J_{m,1-nonanal} = 5.068\ kg.m^{-2}.h^{-1}$$

$$\therefore\ J_m = 41.24 + 5.068 = 46.31\ kg.m^{-2}.h^{-1}$$

G.7.3 Modified solution-diffusion model

It was proposed that the classic solution-diffusion model can be modified with an additional solubility parameter, as shown in Equation G.9, to improve predictive accuracy,

$$\delta_{SD,1-octene} = \frac{(\delta_M-\delta_{1-octene})^2}{x_{1-octene}.(\delta_M-\delta_{1-octene})^2+x_{1-nonanal}.(\delta_M-\delta_{1-nonanal})^2} \tag{G.9}$$

where,

$$\delta_M = 23.2\ MPa^{0.5}$$

$$\delta_{1-octene} = 15.6\ MPa^{0.5}$$

$$\delta_{1-nonanal} = 19.0\ MPa^{0.5}$$

$$\therefore\ \delta_{SD,1-octene} = \frac{(23.2-15.6)^2}{0.8.(23.2-15.6)^2+0.2.(23.2-19.0)^2} = 0.9588$$

$$J_{m,1-octene} = \frac{0.1488}{0.9588} \times \left[0.8 - \frac{33.82}{33.83+3.075} \exp\left(-\frac{0.0001569 \times 30 \times 101325}{8.314 \times 298}\right)\right] = 33.83\ kg.m^{-2}.h^{-1}$$

$$J_{m,1-nonanal} = 3.075 kg.m^{-2}.h^{-1}$$

$$\therefore\ J_m = 33.83 + 3.075 = 36.91\ kg.m^{-2}.h^{-1}$$

G.8 Total operating costs and energy usage

G.8.1 Distillation column

Columns were sized using Coulson's and Richardson's design methods. Considering the case with 1-octene as solvent and 200 ppm **$HRh(CO)(PPh_3)_3$**, cascade column volumes were determined as 0.0835 m^3 and 0.102 m^3.

The total operating costs of the column was determined according to the bare module cost approach based on the Chemical Engineering Plant Cost Index, as described in Turton *et al*. [4].

$$log_{10}C_p^0 = K_1 + K_2 log_{10}(A_c) + K_3[log_{10}(A_c)]^2 \qquad \text{(G.10)}$$

$$\therefore\ C_p^0 = 10^{3.4974+0.4485 log_{10}(0.102)+0.1074[log_{10}(0.102)]^2} = \$\ 1{,}438.73$$

$$TOC_{dist} = C_p^0 \times (B_1 + B_2 F_P F_M) \qquad \text{(G.11)}$$

$$\therefore TOC_{dist} = \$\ 1{,}438.73 \times (2.25 + 1.82 \times 3.15 \times 0.8978) = \$\ 10{,}642.43$$

This value can then be translated to 2015,

$$TOC_{dist,2015} = \frac{I_{2015}}{I_{2001}} TOC_{dist,2001} = \frac{584.6}{397} \$\ 10{,}642.43 = \$\ 15{,}671.44\ (= R\ 168{,}154.57)$$

This was for all columns required in the cascade to obtain the desired catalyst recovery of 99.9%. Therefore, in the case of 1-octene as solvent, the total operating costs were,

$$TOC_{dist,total} = R\ 168{,}154.57 + R\ 156{,}213.96 = R\ 324{,}368.53$$

Including the trays, the total unit cost for the 1-octene system surmounts to R 3,405,714.79 per annum.

From Aspen Plus™, the total energy usage for the cascade 1-octene system was determined as 26.75 kW.

G.8.2 OSN

The total operating costs for the OSN membrane system was approximated using the short-cut cost analysis method introduced by Schmidt *et al.* [5], presented in Equation G.12.

$$TOC_M = \left(1 - R_{cat,overall}\right)\dot{m}_{prod}c_{cat}C_{cat} + \frac{\dot{m}_{prod}c_M}{\Delta P t_{op} P_{i,M}} \quad \text{(G.12)}$$

$$\therefore TOC_M = (1 - 0.999) \times 876000 kg.a^{-1} \times 0.0002\ kg.kg^{-1} \times R\,948{,}264.kg^{-1} + \frac{876000\ kg.a^{-1} \times R3{,}345.m^{-2}.a^{-1} \times 2\ a}{30 \times 101325 \times 8150\ h.a^{-1} \times 2.97\ kg.m^{-2}.h^{-1}.bar^{-1}}$$

$$\therefore TOC_M = R\,340{,}345.53\ per\ annum$$

The energy usage of the OSN systems, can be calculated using Equation G.13.

$$\dot{Q}_M = \frac{F_F \Delta P}{\eta_P} + \frac{F_r \Delta P_D}{\eta_P} \quad \text{(G.13)}$$

$$\therefore \dot{Q}_M = \frac{100\ kg.h^{-1} \times \frac{1}{0.715}\ kg^{-1}.m^3 \times 30 \times 101325}{0.3} + \frac{5 \times 100 \times \frac{1}{0.715} \times 0.5 \times 101325}{0.3}$$

$$\therefore \dot{Q}_M = 0.4265\ kW$$

G.9 References

[1] D. Van Krevelen, K. te Nijenhuis, **Properties of Polymers: their correlation with chemical structure; their numerical estimation and prediction from additive group contributions**, Elsevier, 2009.

[2] R.F. Fedors, *Polym. Eng. Sci.* **14** (2004) 147–154.

[3] C.M. Hansen, **Hansen Solubility Parameters, A User's Handbook**, 2nd Ed., CRC Press, 2007.

[4] R. Turton, R.C. Bailie, W.B. Whiting, J.A. Schaeiwitz, **Analysis, Synthesis, and Design of Chemical Processes**, 3rd Ed., Prentice Hall, Boston, 2009.

[5] P. Schmidt, E.L. Bednarz, P. Lutze, A. Górak, *Chem. Eng. Sci.* **115** (2014) 115–126.